A Theoretical Study of Recycling Effects of rcDNA-containing Capsids on Hepatitis B Virus Infection

Rupchand Sutradhar

Department of Mathematics
Indian Institute of Technology Guwahati
Guwahati - 781039, India

January, 2025

A Theoretical Study of Recycling Effects of rcDNA-containing Capsids on Hepatitis B Virus Infection

A Thesis Submitted
in the Partial Fulfillment of the Requirements
for the Degree of
DOCTOR OF PHILOSOPHY

by

Rupchand Sutradhar
(Roll Number: 196123112)

Department of Mathematics
Indian Institute of Technology Guwahati
Guwahati - 781039, India

January, 2025

DECLARATION

It is certified that the work contained in this thesis titled **"A Theoretical Study of Recycling Effects of rcDNA-containing Capsids on Hepatitis B Virus Infection"** was completed by me, under the supervision of **Prof. Durga Charan Dalal, Department of Mathematics, Indian Institute of Technology Guwahati** for the award of the degree of Doctor of Philosophy and this work has not been submitted elsewhere for a degree.

January, 2025

Rupchand Sutradhar
(Roll No. 196123112)
Department of Mathematics
Indian Institute of Technology Guwahati

CERTIFICATE

It is certified that the work contained in this thesis titled **"A Theoretical Study of Recycling Effects of rcDNA-containing Capsids on Hepatitis B Virus Infection"** by **Rupchand Sutradhar**, a student of **Department of Mathematics, Indian Institute of Technology Guwahati**, for the award of the degree of Doctor of Philosophy has been carried out under my supervision and this work has not been submitted elsewhere for a degree.

January, 2025

Prof. Durga Charan Dalal
Professor
Department of Mathematics
Indian Institute of Technology Guwahati

Dedicated to

"My Father"

Late Arun Sutradhar,

"My Mother"

Mrs. Lakshmi Sutradhar,

and

"My Brothers"

Mr. Ashim Sutradhar,

Mr. Dipu Sutradhar

ACKNOWLEDGMENT

This doctoral thesis would never have been possible without the contributions of numerous people in various stages of my journey. Foremost, I would like to express my heartfelt gratitude to my thesis supervisor, Prof. Durga Charan Dalal, for his guidance and consistent encouragement to complete this thesis. He taught me how to do flawless Mathematics. I am deeply indebted to him for his support and inspiration throughout this degree. His expertise and suggestions have been invaluable to me, and I am grateful for his willingness to go above and beyond to help me succeed. I appreciate his generosity with his time. Outside the academic realm, he has been a pillar of support in many other aspects of my life. I learn from him the value of kindness and selflessness in one's professional life. It is truly impossible to express my feelings for him in just single paragraph. His impact on my life is so profound that if I were to write about him, words would flow endlessly, filling page after page, yet still falling short of expressing his kindness, wisdom, and unwavering support.

I would like to convey my heartfelt gratitude to my doctoral committee members, Prof. Swaroop Nandan Bora, Prof. Rajen Kumar Sinha and Prof. Bhupen Deka for their valuable feedback, timely suggestions and periodically review my research work. Their insights have helped me to improve my research and studies during the PhD tenure at IIT Guwahati. My sincere gratitude and thanks to Prof. Anjan Kumar Chakrabarty, Prof. Ayon Ganguly, Prof. Subhamay Saha, Prof. Arup Chattopadhyay and Prof. Siddhartha Pratim Chakrabarty for their kind help and potential support in various stage during my PhD life.

I am grateful to IIT Guwahati and Council of Scientific & Industrial Research, Govt. of India for providing me financial support for carrying out research in this PhD program. I am especially thankful to all the office staff of our department for their technical support and official help. I also acknowledge the support I have received from our Department staffs Santanu Da, Jayanta Da, Phatik Da, Pran Pratim Da, Pranab Jyoti Da, Trishna didi who helped me with the official and technical matters over the years.

I want to express my heartfelt gratitude to Supriya Mondal for being a special person in my life. Throughout my PhD journey, she continuously motivated me with strong mental support. Her constant presence and unwavering reassurance during the murky times are beyond compare. Despite the challenges, she has been stood by me through all the ups and downs, offering words of encouragement and helping me stay on track. She embraced me wholeheartedly at all times and in every form. I am deeply grateful for her patience, understanding, and unconditional love. I can't thank her enough.

I am forever indebted to my friends for their friendship and understanding during the whole journey. They have always been there to listen to me vent, celebrate my successes, and

offer me tremendous mental support during my difficult times. I am thankful to my friends Gopi Da, Madhab Da, Sirshendu, Shilpi, Mijanur, Ashish, Anjali, Devang, Debnarayan and Ramendra for intermittently productive conversations and sharing many cheerful memories at IIT Guwahati campus. I would like to take this opportunity to convey my gratitude to my seniors Dr. Nilay Mondal, Dr. Avijit Das, Dr. Mrityunjoy Barman, Dr. Shyam Swarup Mondal and Dr. Bichitra Kumar Lenka for their valuable suggestions at various times. The mental supports which I have received from my two dear seniors cum friends Dr. Chandan Pradhan and Dr. Soma Das during the tough times in my third year of PhD are something that I cannot put into words. They have accepted me as one of their own, treating me with the love and care of a blood-related dada and didi. I still cherish the memory of their enchanting company. I also thank my beloved seniors Sandip Da, Aniruddha Da, Abhijit Da, Sagar Da and juniors Tanay, Bikram, Alapan, Mousumi, Arindam, Bivakar, Aryan, Pankaj, Nayan, Anindita and others for sharing a great bond of affection in the Department. My two school friends Dr. Subrata Dey and Sourav Chowdhury deserve special appreciation in this note for their love and affection that helped me stay peaceful during the stressful days.

I owe a lot to one of my best teachers, Dr. Anirban Chattopadhyay who taught me to embrace mathematics with great care during my college days. I also remember the affection and unwavering support from two of my favorite tuition teachers, Parthapratim Mandal and Debabrata Mondal, during my school life.

Above all, those whose accomplishments are never-ending are my family members. I am grateful to my family for their support and encouragement. They have been there for me every step of the way, and I could not have done this without them. In particular, I would like to thank my father late Arun Sutradhar whose values are deeply ingrained in my heart and mind, even in his absence and my mother Lakshmi Sutradhar who always stood by me in every step of this journey. After my father left, I witnessed my mother's struggle firsthand, and it is something I will never forget. They have always believed in me, and their sacrifices have made this journey possible. I deeply appreciate my brothers, Ashim Sutradhar and Dipu Sutradhar for their constant support and inspiration during this endeavor. It might have been impossible for me to continue my studies if my these two elder brothers hadn't sacrificed their valuable childhood days after our father passed away. My elder brother, Ashim Sutradhar, has been a father figure to me. I would like to thank my sister-in-law Riya Sutradhar who helped me in many ways directly or indirectly to carry out this study. Overall, their unconditional love, concern, care, encouragement and blessing in my life are unbelievable, immeasurable and invaluable. I am truly delighted to have my youngest family member, my lovely and adorable nephew Aritra Sutradhar, be a part of my PhD journey. His presence brings an unparalleled sense of joy and warmth to my life.

I am truly grateful to all the people who have helped me and contributed to the completion of this thesis. Honestly, this thesis would not have been possible without them as well as their support. I apologize for not being able to mention them all individually.

January, 2025

(Rupchand Sutradhar)

Department of Mathematics

Indian Institute of Technology Guwahati

ABSTRACT

In this thesis, the dynamics of hepatitis B virus (HBV) infection are studied by incorporating several aspects, such as recycling of capsids, the effects of fractional-order derivative, the impacts of proliferation, the roles of sub-viral particles and antibodies. This dissertation begins by investigating the roles of cytoplasmic recycling of rcDNA-containing capsids in HBV infection. To this purpose, a novel four-compartmental (uninfected and infected hepatocyte, rcDNA-containing capsids and virus) ODE model is proposed to better understand this viral infection. This model demonstrates excellent agreement with the experimental data of two chimpanzees. The effects of three key parameters (recycling rate, virus production rate, and volume fraction of newly produced capsids in favour of virus production) are analyzed via numerical experiments. Furthermore, a comprehensive global sensitivity analysis is conducted using the widely-used technique Latin hypercube sampling–partial rank correlation coefficient. As a result, this study shows that the accumulation of rcDNA-containing capsids within the infected hepatocyte is a key factor contributing to the exacerbation of the disease. In other words, the cytoplasmic recycling of newly produced rcDNA-containing capsids acts as a positive feedback loop in the viral infection.

Next, the proposed model is extended by replacing the ordinary derivative with a fractional derivative, resulting in two nonlinear fractional-order HBV infection models based on the Caputo derivative. In the first model, the order of fractional derivatives is commensurate across all compartments, whereas in the second model, the orders are incommensurate. The existence and uniqueness of solutions for both models are established. The modified models are validated with experimental data. We numerically solve both fractional-order models using the predictor–corrector Adams–Bashforthm–Moulton method (for commensurate order) and implicit product integration of trapezoidal type method (for incommensurate order) with various choices of fractional orders and initial conditions. Stability analyses are conducted for both models. Additionally, the impacts of individual component of fractional derivatives in incommensurate-order model on infection dynamics are also explored. All the results are presented graphically, and it is observed that with the decrease in the order of fractional derivative, the peak level of infection or severity of the infection decreases, however, disease takes longer time to be cured.

Later, the temporal dynamics of this viral infection are investigated through two more intercellular mathematical models that incorporate the proliferation of both uninfected and infected hepatocytes, as well as the recycling of capsids. One model examines continuous proliferation, while the other one deals with discontinuous proliferation based on cellular volume of the liver. Both models are formulated on the basis of the following biological findings reported in the literature: mitosis of an infected hepatocytes yields in two uninfected progenies. After showing the identifiability of the model parameters, the values of the parameters are estimated based on the experimental data. The results of this study suggest that if the infected hepatocytes proliferate at a different rate that of uninfected hepatocytes, the proliferation of uninfected hepatocytes contributes to an increase in infection,

but the proliferation of infected hepatocytes acts to reduce the infection from the long-term perspective. The global sensitivity analysis also corroborates these findings. Furthermore, it is also observed that the differences between the outcomes of continuous and discontinuous proliferations are significant and noteworthy.

The subsequent work presents an updated mathematical model that incorporates the roles of sub-viral particles (SVPs) and roles of immune system, specifically antibodies. This model also accounts for the spatial mobility of capsids, viruses, SVPs, antibodies, and offers unique characteristics in the context of this viral infection. The study examines the changes in the infection dynamics considering both single-point and multi-point initial conditions. The findings suggest that SVPs significantly enhance the intracellular viral replication and gene expression by reducing the neutralization of virus particles by antibodies. Furthermore, the recycling of capsids substantially increases the concentration of SVPs. Experiments conducted with single-point and multi-point infection initial conditions show that if the liver is infected at multiple points, the infection spreads more rapidly.

The final work focuses on a comprehensive analysis of the intracellular dynamics of this viral infection. Considering the intracellular processes observed in the viral life cycle and can be targeted by the antiviral therapy, an intracellular HBV infection dynamics model is proposed. The well-known fourth-order highly accurate *Runge-Kutta* method is employed to numerically solve the proposed model. In order to identify the most influencing parameters, a global sensitivity analysis of the parameters is performed using partial rank correlation coefficients based on Latin hypercube sampling method. The effects of initial concentrations of cccDNAs, the roles of HBx proteins, dslDNA-containing intermediates and intracellular delay are explicitly discussed. Results indicate that HBx proteins show considerable influence on the course of infection, whereas intracellular delay and dslDNA-containing intermediates have negligible impacts on the disease dynamics. Furthermore, the study reveals that SVPs have potential to augment the infection.

ABBREVIATIONS

Biological Terms

HBV	Hepatitis B Virus
HDV	Hepatitis D Virus
HIV	Human Immunodeficiency Virus
WHO	World Health Organization
HCC	Hepatocellular Carcinoma
NTCP	NA(+)-taurocholate Co-transporting Polypeptide
HSPGs	Heparan Sulfate Proteoglycans
cccDNA	covalently closed circular DNA
rcDNA	relaxed circular DNA
RNP	Ribonucleoprotein
DNA	Deoxyribonucleic Acid
RNA	Ribonucleic Acid
pgRNA	pregenomic RNA
HBx	HBV X Proteins
mRNA	messenger RNA
ssDNA	single-stranded DNA
dsDNA	double-stranded DNA
dslDNA	double-stranded linear DNA
CTL	Cytotoxic T Lymphocyte
NK	Natural Killer
GE	Genome Equivalents
POIH	Proliferation of Infected Hepatocyte
SVPs	Sub-viral Particles

ALF	Acute Liver Failure
CLF	Chronic Liver Failure
CHB	Chronic Hepatitis B
HBsAg	Hepatitis B Surface Antigen

Mathematical Terms

ODE	Ordinary Differential Equation
PDE	Partial Differential Equation
FDE	Fractional Differential Equation
DDE	Delay Differential Equation
SSE	Sum of Squares Error
LHS	Latin Hypercube Sampling
CC	Correlation Coefficient
PRCC	Partial Rank Correlation Coefficient
LAS	Local Asymptotically Stable
GAS	Global Asymptotically Stable
LSA	Local Sensitivity Analysis
GSA	Global Sensitivity Analysis
BRN	Basic Reproduction Number
DFE	Disease-free Equilibrium
ABM	Adams–Bashforthm–Moulton
DAISY	Differential Algebra for Identifiability of System
MPS	Most Positively Sensitive
MNS	Most Negatively Sensitive
CCT	Cell-to-cell Transmission

Pharmaceutical Terms

CT	Combination Therapy
FDA	Food and Drug Administration
IFN-α	Interferon-alpha
PEG-IFN-α	Pegylated Interferon-α
NAs	Nucleoside Analogs
CAM	Capsid Assembly Modulator
ETV	Entecavir
LMV	Lamivudine
LDT	Telbivudine
ADV	Adefovir Dipivoxil
TDF	Tenofovir Disoproxil Fumarate
DAAs	Direct-acting Antivirals
CRISPR/Cas9	Clustered Regularly Inter-spaced Short Palindromic Repeats-associated 9
ZFNs	Zinc-finger Nucleases

NOMENCLATURES

$X(t)$	Uninfected hepatocytes
$Y(t)$	Infected hepatocytes
$U(t)$	rcDNA-containing capsids
$V(t)$	Viruses
T	Total number of cells in liver
$S_v(t)$	Sub-viral particles
$A(t)$	Antibodies
$R(t)$	rcDNA-containing capsids produced from upcoming viruses within an infected hepatocytes
$R_g(t)$	3.5 kb pgRNAs within an infected hepatocytes
$R_s(t)$	2.4 and 2.1 kb mRNAs within an infected hepatocytes
$R_h(t)$	0.7 kb mRNAs within an infected hepatocytes
$H(t)$	HBx proteins within an infected hepatocyte
$P(t)$	Polymerase within an infected hepatocytes
$Z(t)$	RNP complexes within an infected hepatocyte
$C_p(t)$	Core proteins within an infected hepatocyte
$P_g(t)$	pgRNA-containing capsids within an infected hepatocyte
$S_p(t)$	Surface proteins within an infected hepatocyte
$S(t)$	Single-stranded DNA-containing capsids within an infected hepatocytes
$D(t)$	Newly produced double-stranded DNA-containing capsids within an infected hepatocytes
$D_L(t)$	Double-stranded linear DNA-containing capsids within an infected hepatocytes
λ	Constant growth rate of uninfected hepatocytes
μ	Natural death rate of uninfected hepatocytes

k	Virus-to-cell infection rate
δ	Death rate of infected hepatocytes and capsids
a	Production rate of capsids from infected hepatocytes
γ	Capsid-to-capsid production rate or recycling rate of capsids
η	Volume fraction of capsids in favor of virus production
β	Production rate of viruses from capsids
δ_v	Death rate of viruses
α	Order of fractional derivative
α_1	Order of fractional derivative for uninfected hepatocytes
α_2	Order of fractional derivative for infected hepatocytes
α_3	Order of fractional derivative for rcDNA-containing capsids
α_4	Order of fractional derivative for virions
R_0	Basic reproduction number
r	Proliferation rate of uninfected hepatocytes
ρ	Proliferation rate of infected hepatocytes
θ	Fraction of liver cells that cannot be infected by HBV
b	Production rate of SVPs from infected hepatocytes
g_1	Binding rate of antibody and virus
g_2	Binding rate of antibody and SVPs
h	Production rate of antibodies
δ_s	Death rate of SVPs
δ_a	Death rate of antibodies
$\mathcal{D}_1$	Diffusion coefficient of capsids
$\mathcal{D}_2$	Diffusion coefficient of viruses
$\mathcal{D}_3$	Diffusion coefficient of SVPs
$\mathcal{D}_4$	Diffusion coefficient of antibodies

α_1^*	Production rate of rcDNA-containing capsids from viruses
α_2^*	Production rate of cccDNA from rcDNA-containing capsids
δ_r	Decay rate of rcDNA-containing capsids
λ_{rg}	Production rate of 3.5 kb pgRNAs from cccDNAs
μ_1	Interaction rate 3.5 kb pgRNAs and polymerases
δ_{r_g}	Decay rate of 3.5 kb pgRNAs
λ_{rh}	Production rate of 0.7 kb mRNAs from cccDNAs
δ_{r_h}	Decay rate of 0.7 kb mRNAs
λ_p	Production rate of polymerases from pgRNAs
δ_p	Decay rate of polymerases
λ_c	Production rate of core protein from pgRNAs
μ_2	Interaction rate RNP complexes and core proteins
δ_{c_p}	Decay rate of core proteins
λ_{S_p}	Production rate of surface proteins from 2.4 and 2.1 kb mRNAs
η_{S_p}	Exit rate of SVPs
δ_{S_p}	Decay rate of surface proteins
β_1	Production rate of pgRNA-containing capsids
β_2	Production rate of ssDNA-containing capsids and dslDNA-containing capsids
λ_{dsl}	Production rate of 2.4 and 2.1 kb mRNAs from dslDNA-containing capsids
δ_{d_L}	Decay rate of dslDNA-containing capsids
k_2	Binding rate of surface protein with rcDNA-containing capsids
δ_d	Decay rate of double-stranded DNA-containing capsids
δ_c	Decay rate of cccDNAs
λ_{rs}	Production rate of 2.4 and 2.1 kb mRNA from cccDNAs
δ_{r_s}	Decay rate of 2.4 and 2.1 kb mRNAs
λ_h	Production rate of HBx proteins from 0.7 kb mRNAs

δ_h	Decay rate of HBx proteins
δ_z	Decay rate of RNP complexes
δ_{P_g}	Decay rate of pgRNA-containing capsids
δ_s	Decay rate of ssDNA-containing capsids
δ_{sv}	Decay rate of SVPs
Λ^{-1}	Average level of surface proteins

List of Figures

List of Tables

Contents

CHAPTER 1

Introduction

"All models are wrong, but some are useful"

George E. P. Box

1.1 Introduction

Hepatitis B virus (HBV) causes the deadly liver disease hepatitis B. As reported by the World Health Organization (WHO), approximately 296 million people worldwide suffer from the chronic HBV infection, with 1.5 million new cases were found each year. It was estimated that 820,000 people died due to HBV infection in the year 2019 alone, and most of them had either cirrhosis or hepatocellular carcinoma (HCC) [1]. Naturally, there are two phases of HBV infection: acute and chronic. In the acute phase of infection, HBV DNA density may be as high as 10^{10} copies/ml. Acute infection typically lasts a few weeks or months and is eventually cured as a result of immune response [2, 3]. For the adult population, there is a clearance rate of 85-95% in acute infection. On the other hand, chronic infection which is a severe global health problem with high morbidity and mortality rates can last for many years and may result in terrible diseases, such as liver cirrhosis, HCC [4]. In general, chronic infection is a life-long incurable condition which affects the personal aspects of the patient's life, such as stigma-discrimination, anxiety about disease progression, and long-term health care costs. According to the literature and clinical findings, horizontal and vertical transmissions are the two main modes of HBV transmission in human population. Blood transfusions, unprotected intercourse, reusing syringes and blades, and the reusing of medical equipment during surgery are common examples of horizontal transmission. Vertical transmission of HBV occurs during the child's birth if the mother is already infected [5]. The common symptoms of HBV are abdominal pain, dark urine, fever, fatigue, loss of appetite, joint pain, nausea, vomiting, yellowing of the skin, and jaundice, etc.

1.1.1 Life cycle of the virus

HBV is a non-cytopathic DNA virus belonging to the family of Hepadnaviridae. The life cycle of HBV is unique and quite complex. At the onset of infection, virus particles first interact with heparan sulfate proteoglycans (HSPGs) receptors in a non-specific and low-affinity manner, and then these bind to NA(+)-taurocholate co-transporting polypeptide (NTCP) receptor with high affinity. Virus particles enter into the hepatocytes through clathrin-mediated endocytosis [6] and release relaxed circular DNA (rcDNA)-containing capsids (viral genome) into the cytoplasm. NTCP that localizes predominantly in the liver cells plays some key roles in the uptake of bile salts into the hepatocytes. This receptor has been identified as a crucial entry receptor for both HBV and hepatitis D virus (HDV) in the year 2012 [7]. The incoming nucleocapsid within the cytoplasm is steered toward the nucleus along with the microtubules [8]. Subsequently, it uncoats its rcDNA which is then delivered into the nucleus through the nuclear pore complex in an importin-dependent manner. In the nucleus, HBV genomic DNA is repaired by cellular factors and is converted into covalently closed circular DNAs (cccDNAs) by the host DNA repair mechanism [9,10]. These cccDNAs not only withstand antiviral interventions but also elude innate antiviral surveillance. Al-

though it is not clear how cccDNAs are maintained in the nucleus. cccDNAs are inherently stable, and function as a template for viral RNAs. RNA polymerase IIs (RNA Poly II) uses the cccDNAs to produce viral RNAs, such as pgRNA, L, S, PreC, X mRNAs. HBV X protein promotes the de-silencing of the cccDNAs and prevents its silencing throughout the course of infection. These viral proteins are synthesized by ribosomes through the translation of mRNAs. Polymerase and pgRNA form a 1:1 complex called a ribonucleoprotein (RNP) complex [11]. The encapsulation of this RNP complex by core proteins leads to the formation of new pgRNA-containing nucleocapsids, commonly referred to as immature nucleocapsids. The pgRNAs are reverse-transcribed by polymerases, resulting in the immature nucleocapsid being converted into a rcDNA-containing nucleocapsid, known as the mature nucleocapsid [12]. These newly produced rcDNA-containing nucleocapsids either return to the nucleus and maintain the cccDNA pool or are enveloped by surface proteins and released as a complete virus from infected hepatocytes [13]. Depending on the concentrations of surface proteins, a portion of these rcDNA-containing capsids is transported back to the nucleus and increases the amount of supercoiled cccDNA. It is known as recycling of rcDNA-containing capsids [11] and is considered as a significant factor in the intracellular dynamics of HBV replication. Besides the viruses, the infected hepatocytes release a large number of two types of non-infectious viral-like particles known as sub-viral particles (SVPs) which can take both spherical and filamentous forms. Some essential steps of the viral life cycle are shown in Figure 1.1.

1.1.2 Available therapy

Currently, two therapeutic approaches are available to treat the HBV-infected patients: (i) nucleotide analogues, and (ii) immune modulator drugs (standard or pegylated interferon alpha) [14, 15]. Among the oral antiviral drugs, tenofovir disoproxil, tenofovir alafenamide, and entecavir are considered as first-line treatments, while telbivudine, adefovir dipivoxil, and lamivudine are categorized as second-line options. Antiviral medications are designed to retard or block the virus reproduction whereas the immune modulator drugs enhance the capabilities of immune system to help in elimination of viruses. The choice between monotherapy and combination therapy (CT) in the treatment of HBV infection depends on several factors, including the patient's disease stage, viral load, liver function, etc. One of the major limitations of monotherapy is its vulnerability to the development of drug-resistant strains. Moreover, monotherapy is often insufficient for complete viral suppression, and there is a possibility of risk of relapsing the viral infection after discontinuation of therapy. On the other hand, CT can reduce the risk of resistance, enhance the efficacy of drugs, lead to more comprehensive and effective viral suppression compared to monotherapy because in CT, different drugs target different stages of the HBV life cycle. Despite the benefits of CT, it is important to inform of the significant challenges it presents, including drug-drug interactions, a higher pill burden, risk of toxicity and increased treatment costs, etc. For patients with high

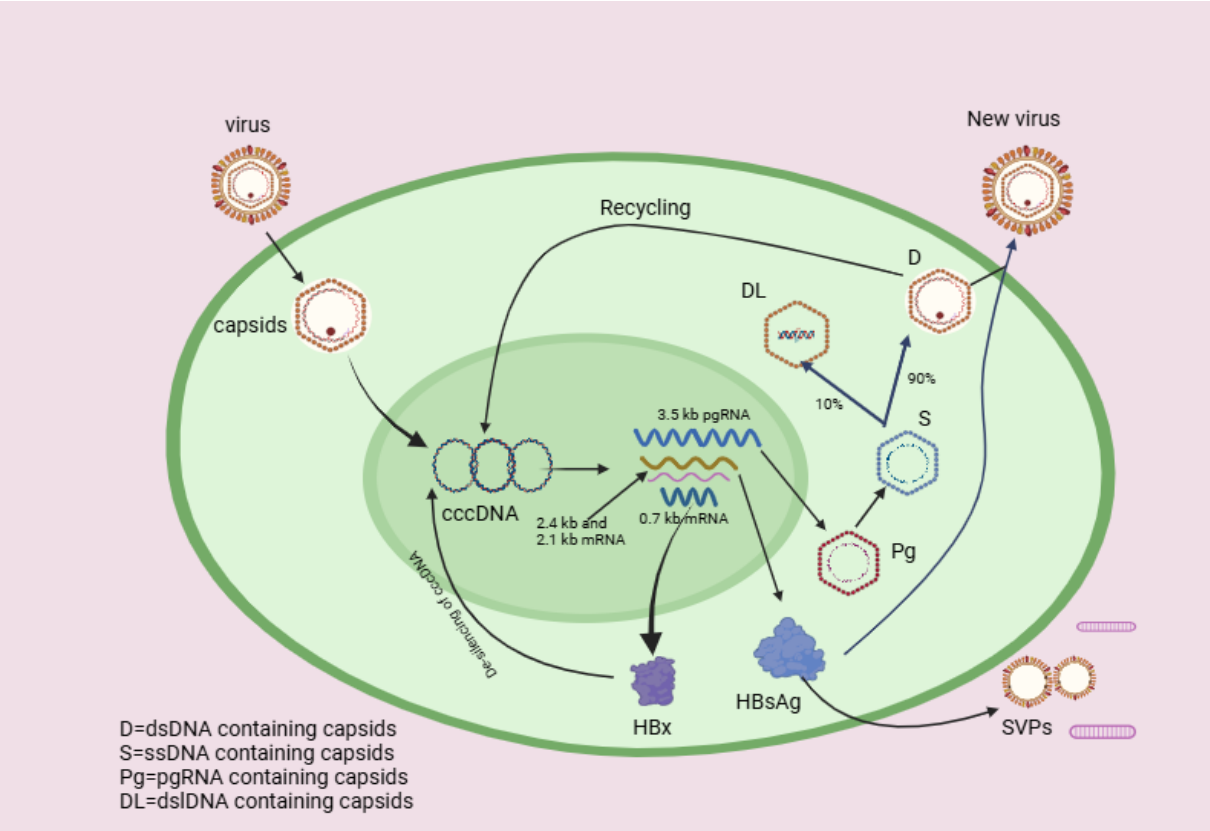

Figure 1.1: Life cycle of the hepatitis B virus.

viral load, significant liver disease, or with a history of resistance to a particular monotherapy, CT is often recommended. In this context, Paul and Han [16] analyzed the current roles of CT in chronic hepatitis B (CHB) infection and mentioned several CTs in various settings. Hui et al. [17] conducted a study comparing the combination of adefovir and emtricitabine to adefovir alone in a cohort of 30 patients over 96 weeks. In that study, Hui et al. [17] observed that while the combination group exhibiting significantly higher levels of HBV DNA suppression and the ALT normalization, the rate of HBeAg seroconversion remained similar in both the groups. The utilization of multi-target therapies for treating complex diseases can increasingly benefit patients [18]. It is noticed that patients with CHB who were treated with a combination of telbivudine and tenofovir showed significant improvements at both the virus levels and in biochemical markers over a one-year period of time [19]. Recently, Ntaganda [20] investigated the impacts of combination therapies on CHB patients using Pontryagin's maximum principle and concluded that employing a combination of two drugs can effectively control the HBV infection, promoting a healthy life. In many cases, the decay of viral load in HBV patients undergoing therapy exhibits a biphasic pattern [21], characterized by a rapid decline in the first few weeks, followed by a slower decline. In other cases, the decay can be triphasic or stepwise. There are some instances where primary

treatment fails within the first six months, or secondary treatment fails after an initial response to primary treatment [21].

1.1.3 Background and motivation

In the literature, several viral dynamics models have been proposed over the last two decades. Some of these are associated with HBV infection. These models are valuable for understanding the pathogenesis of disease as well as for devising better treatment protocols. In the year 1996, Nowak et al. [22] analyzed a HBV infection dynamics model composed of three compartments: uninfected hepatocytes, infected hepatocytes, and virions. This model is referred as the 'basic model' in the literature. Wodraz et al. [23] improved the basic model by including the effects of cytotoxic T cells and antibodies. By putting a standard incidence function in the place of mass action term of the uninfected hepatocytes and viruses, Min et al. [24] further modified the basic viral infection model proposed in the article [22]. According to Min et al. [24], the mass action term is not rational for HBV infection because it implies that someone with a smaller liver is unlikely to be infected. In addition to the standard incidence function, the time delay during the production of the virus was also taken into account by Gourley et al. [25]. Rather than using constant growth terms, Hews et al. [26] introduced a modified model that considers the logistic growth of uninfected hepatocytes. Eikenberry et al. [27] presented a delay model for HBV infection in which uninfected hepatocytes proliferate following a logistic growth. Huang et al. [28] proposed another HBV dynamics model using a different incidence function, known as Beddington-DeAngelis type incidence function and Wang et al. [29] studied the global stability of this type of models. Through a comprehensive investigation, Yu Ji et al. [30] showed for the first time that the effects of immune response are not constant, and instead follow a periodic function. The immune-mediated cure of infected hepatocytes is an important factor in combating viral infections. Incorporating cure rate of infected hepatocytes, Wang et al. [31] extended the model proposed by Min et al. [24]. Fatehi et al. [32] determined that in HBV infection, NK cells takes a significant role in apoptosis as these kill the infected cells by producing the perforin and granzymes. Murray et al. [33] proposed an intracellular HBV dynamics model with three compartments and measured the half-life of HBV to be approximately four hours. Manna and Chakrabarty [34] modified the model proposed by Murray et al. [33] by considering the uninfected hepatocytes and subsequently studied the effects of delay in intracellular process. Considering the impacts of antibodies and cytotoxic T lymphocytes (CTLs), Danane et al. [35] extended the model proposed by Manna and Chakrabarty [34] and examined the roles of optimal therapy in controlling viral replication. Using an average incidence rate, Guo et al. [36] established the global stability of a delayed-diffusive HBV infection model. Fatehi et al. [11] built up an intracellular model of HBV infection and compared various kinds of therapeutic strategies that can be applied in the future. The age of infected cells serves as a key biological indicator, providing valuable insights into the

dynamics of virus infection. Recently, Liu et al. [37] proposed an age-structured model that treats HBV capsids as a separate cellular compartment. Song et al. [38] reported that effective treatments could rapidly activate CTLs responses, mitigating the impacts of immune delay and significantly impeding virus production. Besides the studies mentioned above, a broad range of literature exists, examining various aspects of HBV infection.

Cellular proliferation or mitosis stands as one of the pivotal biological processes influenced by this viral infection as HBV promotes cell proliferation through HBx-induced microRNA-21 in HCC [39]. In some mouse models, HBx protein has been found to significantly impair liver regeneration [40, 41]. In the literature, a limited number of studies have investigated the impacts of cellular proliferation of uninfected as well as infected hepatocyte during this viral infection. For example, in the year 2010, Hews et al. [26] introduced an HBV infection dynamics model considering the logistic growth of uninfected hepatocytes with standard incidence function, and found that the proliferation itself can affect virus replication and expression. However, it is worth noting that their model incorporated numerous assumptions. Taking into account the assumption that infected hepatocytes also undergo proliferation at a rate similar to or lower than that of healthy hepatocytes during the infection, Hews et al. [42] modified their previously proposed model given in [26]. Hews et al. [42] obtained some new findings, such as healthy hepatocytes can be found in chronic HBV infection only when the proliferation of infected hepatocytes is significantly impaired. Dahari et al. [21] suggested that variations in proliferation rates between uninfected and infected hepatocytes could offer a rich explanation for the diverse patterns that are observed in the time of decline of viral load. Some studies have also done considering the proliferation of infected hepatocytes (POIH) under the assumption that POIH can only produce infected hepatocytes [43, 44]. The fate of viral DNA following mitosis is a matter of controversy. The roles of proliferation in the clearance of both acute and chronic HBV infections continue to be subjects of ongoing debate [45–47]. During mitosis, when the nuclear membrane is reformed, there is a possibility of cccDNA loss if the cccDNAs fail to reintegrate into the nucleus. Also, if the count of cccDNAs within the infected hepatocytes is extremely low, the progeny may be devoid of cccDNAs, leading to the resolution of acute HBV infection [48]. Recently, Tu et al. [49] corroborated with the fact that the mitosis of HBV-infected hepatocytes can lead to the production of two uninfected daughter cells. This research team also suggested that mitosis of infected hepatocytes could offer a potent avenue for addressing HBV persistence. Murray and Goyal [50] also emphasized the significance of cccDNA loss during cellular proliferation for the non-destructive clearance of HBV infection. Using experimental data from six HBV-infected patients, Goyal et al. [48] further affirmed that the resolution of acute HBV infection is strongly associated upon the proliferation of infected hepatocytes, leading to the generation of two uninfected daughter cells.

Over the past two decades, many researchers have been diligently researching on HBV infections from different perspectives [24, 32, 50–52]. The primary reasons for the persistence of this infection include the high stability of cccDNAs, the intricate life cycle of the virus, and

the crucial functions played by certain viral components, such as HBx proteins, surface proteins (L/M/SHBs), sub-viral particles (SVPs). SVPs which are produced by HBV-infected hepatocytes during infection period are non-infectious in nature. These particles are predominantly composed of viral surface antigen (HBsAg) proteins that are the main components of the lipid bilayer envelope [13]. SVPs don't contain nucleocapsid proteins and viral nucleic acids, *i.e.*, lack the rcDNA-containing capsids or the viral genome. The production of SVPs is a natural biological process. While the viruses replicate within the hepatocytes, both complete viral particles and SVPs are produced simultaneously and are released into the bloodstream. Generally, SVPs are found in the blood of the infected individuals in two main forms: (i) spherical particles measuring approximately 25 nm in diameter and (ii) filaments with a diameter of 22 nm that vary in length [53, 54]. In the literature, many authors have reported that the ratio of Dane particles to SVPs ranges from 1:10,000 to 1:100,000 [54–56], *i.e.*, a large quantity of HBsAg derived from viral particles has no effect on the reservoir of viral replication. However, the actual reasons behind their overproduction and their exact roles in HBV pathogenesis are still under investigation [57]. The assembly and secretion pathways for SVPs are typically distinct from those used by the virus. Researchers are dedicated to unravel the primary causes underlying their excessive production and understand their critical roles in the development of HBV-related illnesses. In individuals with chronic HBV infection, the number of SVPs in the bloodstream far exceeds that of infectious virions. To the best of our knowledge, despite the significant overproduction of SVPs, the functions of these particles have been widely overlooked so far [3, 11, 22, 26, 27, 36, 50, 52, 58–62], leaving a gap in understanding of biological importance of SVPs. Recently, Cao et al. [63] demonstrated the distribution of Dane particles, spherical particles, and filamentous particles using micrographs and suggested that there is a universal folding shape of HBsAg on SVPs. According to Rydell et al. [63, 64], SVPs are believed to potentially facilitate cell-to-cell spread, particularly in neutralizing antibodies. SVPs function as a disguise for the virus. Due to this characteristic of SVPs, a substantial portion of HBV-specific antibodies produced by the host's immune system is directed at neutralizing SVPs, thereby helping the virus evade the immune response [64]. However, to our knowledge, these effects have not yet been demonstrated experimentally or in animal models so far. Additionally, SVPs are less efficient in blocking the entry of virions particles by binding to target cells [65]. High levels of SVPs can stimulate the immune system, leading to the production of antibodies against HBsAg. For this virus, Bruns et al. [66], and Klingmüller and Schaller [67] reported that SVP has capability to both enhance and inhibit viral attachment to the cells. The collective evidence suggests that SVPs have some notable impacts on the advancement and perpetuation of the infection. Based on these findings, it is clear that more detailed studies are needed to improve the understanding of SVPs.

The propagation of viral particles both between and within the hosts is inherently a spatial process. Diffusion plays a pivotal role in viral infection by facilitating the spread of viral particles both locally within the liver and systemically throughout the body. This

diffusion also affects the immune system because SVPs diffuse widely, potentially diverting immune attention away from infectious virions and thereby contributing to immune evasion. Some researchers have already addressed how spatial heterogeneity influences the dynamics of infection of certain viruses, such as HIV [68], Covid-19 [69]. In the case of HBV infection, a number of studies available in the literature, such as [70–72] have documented the effects of diffusion of virus particles in the literature. However, none of these above-mentioned studies have taken into account all the following together: the effects of capsid recycling, the roles of SVPs, and the functions of antibodies.

Most of the previous studies on this viral infection have mainly focused on the cell population. By analyzing the cell population, one can get a general overview of the clinical signs and progression of the viral infection. In a cell population, there are various types of cells that may differ in identity, state, functions, and other characteristics. Naturally, cells are heterogeneous. The variation in DNA sequence is one of the reasons for this heterogeneity [73]. In the literature, it is observed that when cell populations are considered to study any kind of viral infection, the total number of cells is typically divided into two classes: uninfected and infected cells. Due to this classification, some salient features of the cells, the roles of some specific phenotypes, the impacts of some intracellular components of viruses and the effects of several parameters involved in the infection are often overlooked [74, 75]. Therefore, it is important to explore intrinsic processes at the level of single cells. In 1940, Delbrück [76] considered the phage-infected E.coli cells to study the heterogeneity in virus infected cells. In that experiment, it was observed that the amount of progeny viruses released from each cell differed significantly, revealing a surprisingly broad distribution of virus growth throughout the infection.

Nowadays, single-cell analyses have become a significant milestone in many fields, including immunology, oncology, stem cell research, virology, etc. [77–79]. The following are some key advantages of single-cell analysis in virology:

1. The dynamics of infection in each infected cell can be studied at the micro level.

2. The intracellular components of the virus that have a significant influence on infection can be identified.

3. One can determine the most sensitive parameter for infection.

4. A large cell population analysis may overlook individual cell responses to the viruses during viral infection.

5. Single-cell analysis helps in designing the new antiviral therapies.

1.2 Preliminaries

This section provides the fundamental basis for the research presented in this thesis by introducing essential background information, definitions, and theoretical concepts relevant to the study. It aims to ensure the reader with a thorough understanding of the fundamental principles and frameworks that underpin the research discussed in subsequent chapters. These preliminaries will be referred and utilized throughout the thesis.

1.2.1 Basic reproduction number

The basic reproduction number, often denoted as R_0, is defined as the average number of newly infected cases generated by a single infectious individual during its entire infectious period in a completely susceptible population [80]. In the context of viral dynamics, R_0 refers to the expected number of secondary infected cells produced by a single infected cell throughout its infectious lifespan. Generally, R_0 serves as a threshold parameter that indicates the possibility of infection transmission. Various techniques are employed to determine R_0 in viral dynamics models. Among these, the next generation method is the most commonly used. In this approach, R_0 is defined as the spectral radius (dominant eigenvalue) of the next generation matrix [80].

1.2.2 Stability theory

Stability theory addresses the stability of solutions of differential equations under small perturbations of initial conditions. In order to study the stability analysis, at first, the equilibrium points of the system have to be determined. For local stability, linearization techniques are used to discuss the behavior of the solutions around the equilibrium points. To this purpose, *Routh-Hurwitz* Criteria are generally used to examine the local stability of the equilibrium points, whereas, Lyapunov theory are applied to investigate global stability. If the equilibrium is not stable, there may exist some bifurcation. Let us consider a nonlinear continuous autonomous system of differential equations

$$\frac{dx}{dt} = f(x), \ x(t_0) = x_0 \geq 0, \tag{1.2.1}$$

on $t \geq t_0$, where $x = (x_1, x_2, \ldots, x_n)^T \in \mathbb{R}^n$, $f : \mathbb{D} \to \mathbb{R}^n$, $\mathbb{D} \subseteq \mathbb{R}^n$, and $f(x)$ does not depend explicitly on time t.

1.2.2.1 Local stability analysis

An equilibrium point or steady-state solution of the system (1.2.1) is a solution of $f(x) = 0$. We define $\bar{x}$ to be an equilibrium point of (1.2.1).

Definition 1.2.1. *[81] An equilibrium point $\bar{x}$ of the system (1.2.1) is said to be* ***locally stable*** *if for every $\epsilon > 0$, there exists a $\delta > 0$ such that every solution $x(t)$ of the system (1.2.1) satisfies*

$$\|x(t) - \bar{x}\| < \epsilon, \quad \text{whenever } \|x_0 - \bar{x}\| < \delta, \quad \forall t \geq t_0.$$

If an equilibrium point does not satisfy the condition of local stability, then it is said to be an unstable equilibrium point.

Definition 1.2.2. *[81] An equilibrium point $\bar{x}$ of the system (1.2.1) is said to be* ***locally asymptotically stable*** *if it is locally stable and moreover, if there exists some $r > 0$ such that*

$$\lim_{t\to\infty} \|x(t) - \bar{x}\| = 0, \quad \text{whenever } \|x_0 - \bar{x}\| < r.$$

1.2.2.2 Global stability analysis

Global stability means that the solution of a dynamical system converges to the attractor of the system regardless of the initial conditions. Global stability represents a strong property of the system. Moreover, if an equilibrium point is globally stable, it necessarily implies that the equilibrium is also locally stable.

Definition 1.2.3. *[82] An equilibrium point $\bar{x}$ of equation (1.2.1) is said to be globally stable if there exists some $\epsilon > 0$ such that*

$$\|x(t) - \bar{x}\| < \epsilon, \quad \forall t > t_0.$$

Definition 1.2.4. *[82] An equilibrium point $\bar{x}$ of the system (1.2.1) is said to be globally asymptotically stable if it is globally stable and moreover,*

$$\lim_{t\to\infty} \|x(t) - \bar{x}\| = 0.$$

1.2.3 Sensitivity analysis

The goal of sensitivity analysis (SA) is to examine how the model output is affected by the variations in its input variables, such as initial conditions, boundary conditions, model parameters. SA plays an important role in the modeling, uncertainty quantification and risk management of complex systems. It has wide usage in the field of medical science as small changes can result a big loss. There are mainly two types of SA, (i) local sensitivity analysis (LSA), (ii) global sensitivity analysis (GSA).

1.2.3.1 Local sensitivity analysis

The LSA is applied to study the influence of a single input parameter on the model output keeping fixed the remaining input parameters. Such sensitivity is often evaluated through

gradients or partial derivatives of the output functions with respect to input variables. The local sensitivity of quantity $\mathcal{Q}$ with respect to the parameter p is given by

$$\mathcal{S}_p^{\mathcal{Q}} = \frac{\partial \mathcal{Q}}{\partial p}.$$

1.2.3.2 Global sensitivity analysis

Global sensitivity analysis is the process of apportioning the uncertainty in outputs to the uncertainty in each input factor over their entire range of interest. A sensitivity analysis is considered to be global when all the input factors are varied simultaneously and the sensitivity is evaluated over the entire range of each input factor.

Compared to LSA, GSA provides more detailed information, as GSA considers the entire range of parameters rather than focusing on specific points or individual parameters. In the literature, different types of methods are available to examine the global sensitivity of model parameters, as follows:

1. Sobol method [83, 84].
2. Latin hypercube sampling-Partial rank correlation coefficient (LHS-PRCC) [85].
3. Fourier amplitude sensitivity test (FAST) [86].

1.2.4 Identifiability analysis

Identifiability analysis stands as the first step in determining the unknown model parameters. A dynamical system is said to be identifiable if Θ (the set of model parameters) can be uniquely determined from the measurable or observable system output $y(t)$ and the provided system input $u(t)$. Otherwise, the system is considered to be as unidentifiable. Specifically, we need to know whether the dynamical system is properly structured to uncover its parameters from observable data. This identifiability analysis is referred to as structural identifiability [87]. Examination of structural identifiability of ODE models through differential algebra methods can be applied using various platforms and open-source software as follows:

1. The **D**ifferential **A**lgebra for **I**dentifiability of **Sy**stem (DAISY) [88].
2. The Identifiable **Comb**inations web application (COMBOS) [89].
3. The Structural**I**dentifiability.jl in JULIA [90].

These three methods share many similarities, including their underlying principles, computational techniques, and applications in analyzing complex systems. These methods employ a differential elimination technique to derive input-output equations (differential polynomial equation involving only observed state variables and model parameters) for the considered

system and test the one-to-one correspondence between the coefficients of these input-output equations and the model parameters.

1.2.5 Fractional-order derivative

1.2.5.1 Definition

Definition 1.2.5. *[91, 92]* Let the function $f : \mathbb{R} \to \mathbb{R}$ be differentiable. Consider $\alpha \in \mathbb{C}$ such that $Re(\alpha) > 0$. Then the Riemann-Liouville integral operator of order α of the function $f(t)$ is defined as

$$ {}^{RL}_{0}D_{t}^{-\alpha} f(t) = \int_0^t \frac{(t-\tau)^{\alpha-1}}{\Gamma(\alpha)} f(\tau) d\tau, \ t > 0, \tag{1.2.2} $$

where, $\Gamma(\alpha) = \int_0^\infty e^{-t} t^{\alpha-1} dt$ is the Gamma function.

Definition 1.2.6. *[91]* Let $\alpha \in \mathbb{C}$ such that $Re(\alpha) > 0$ and $f : \mathbb{R} \to \mathbb{R}$ be a differential function. The Caputo fractional derivative of the function $f(t)$ of order α is defined as

$$ {}^{C}_{0}D_{t}^{\alpha} f(t) = \begin{cases} \dfrac{1}{\Gamma(n-\alpha)} \int_{t_0}^t (t-\tau)^{n-\alpha-1} f^{(n)}(\tau) d\tau \ , \text{if } \alpha \notin \mathbb{N}, n = [\alpha] + 1 \\ f^{(n)}(t), \ \text{if } \alpha = n \in \mathbb{N}. \end{cases} $$

It is also called Gerasimov–Caputo fractional derivative [93].

Definition 1.2.7. *[91, 92] The Mittag-Leffler function of two parameters is defined as*

$$ E_{\alpha,\beta}(z) = \sum_{n=0}^{\infty} \frac{z^n}{\Gamma(n\alpha + \beta)}, \ Re(\alpha), \ Re(\beta) > 0. \tag{1.2.3} $$

The Laplace transform of two-parameter Mittag-Leffler function is given by

$$ \mathcal{L}\left[t^{\beta-1} E_{\alpha,\beta}(\widehat{a} t^{\alpha})\right] = \frac{S^{\alpha-\beta}}{S^{\alpha} - \widehat{a}}, \tag{1.2.4} $$

and

$$ \mathcal{L}^{-1}\left\{ \frac{S^{\alpha-\beta}}{S^{\alpha} - \widehat{a}} \right\} = t^{\beta-1} E_{\alpha,\beta}(\widehat{a} t^{\alpha}). \tag{1.2.5} $$

An important characteristic of Mittag-Leffler function is $0 < E_{\alpha}(-\rho t^{\alpha}) \leq 1$, *where* $\rho > 0$.

1.2.5.2 Laplace transform of Caputo fractional derivative

The Laplace transform of Caputo fractional derivative [91] of order α is given as follows:

$$\mathcal{L}\left[{}_0^C D_t^\alpha f(t); s\right] = \int_0^\infty e^{-st}\, {}_0^C D_t^\alpha f(t) dt = s^\alpha F(s) - \sum_{k=0}^{n-1} s^{\alpha-k-1} f^{(k)}(0), \quad n-1 < \alpha \leq n, \tag{1.2.6}$$

where $\mathcal{L}\{\cdot\}$ represents the Laplace transform, $F(s)$ is the Laplace transform of the function $f(t)$, and t and s represent the time domain and the Laplace domain variables, respectively.

1.2.5.3 Existence and uniqueness of the solution

Lemma 1.2.8. *[94] Suppose the function $f(t, x(t)) : \mathbb{R}^+ \times \mathbb{R}^4 \to \mathbb{R}^4$ meets the following conditions:*

1. *the function $f(t, x(t))$ is Lebesgue measurable with respect to $t \in \mathbb{R}^+$,*
2. *the function $f(t, x(t))$ is continuous with respect to $x(t)$ on $\mathbb{R}^4$,*
3. *$\dfrac{\partial f(t, x(t))}{\partial x}$ is continuous with respect to $x(t)$ on $\mathbb{R}^4$,*
4. *$||f(t, x(t))|| \leq \lambda ||x(t)|| + \omega,\ \forall\ t \in \mathbb{R}^+,\ x(t) \in \mathbb{R}^4$ where ω, λ are two positive constants.*

Then, the following initial value problems (IVP)

$${}_0^C D_t^\alpha x(t) = f(t, x(t)), \alpha \in (0, 1], x(0) = x_0, \tag{1.2.7}$$

has unique solution.

1.2.5.4 Monotonicity of the solution

Lemma 1.2.9. *[95] Let $f(t)$ and ${}_0^C D_t^\alpha f(t)$ be continuous functions on $[a, b]$, and $\alpha \in (0, 1]$, then*

1. *$f(t)$ is a non-decreasing function on $[a, b]$, if ${}_0^C D_t^\alpha f(t) \geq 0$, for all $t \in (a, b)$.*
2. *$f(t)$ is a non-increasing function on $[a, b]$, if ${}_0^C D_t^\alpha f(t) \leq 0$, for all $t \in (a, b)$.*

1.2.5.5 Local stability of equilibrium solution

Lemma 1.2.10. *[96] Consider the autonomous incommensurate order fractional system:*

$$ {}_0^C D_t^{\widehat{\alpha}} y(t) = f(y(t)),\ y(0) = y_0, \tag{1.2.8} $$

where ${}_0^C D_t^{\widehat{\alpha}} y(t) = \left({}_0^C D_t^{\alpha_1} y_1(t),\ {}_0^C D_t^{\alpha_2} y_2(t), \cdots, {}_0^C D_t^{\alpha_n} y_n(t)\right)^T$, $\alpha_i \in (0,1] \cap \mathbb{Q}$ *for* $i = 1, 2, ..., n$. *Let,* $y_{eq} = (y_1^\star, y_2^\star, ..., y_n^\star)$ *be an equilibrium point of* (1.2.8) *and* $J(y_{eq})$ *denotes the Jacobian matrix evaluated at* y_{eq}. *Consider the characteristic equation*

$$ \det\left(diag\left(x^{M\alpha_1}, x^{M\alpha_2}, ..., x^{M\alpha_n}\right) - J(y_{eq})\right) = 0, \tag{1.2.9} $$

where M *is the l.c.m of denominators of* $\alpha_1, \alpha_2, ..., \alpha_n$. *Then, the equilibrium point* y_{eq} *is asymptotically stable if all roots of the equation* (1.2.9) *satisfy the inequality*

$$ |\arg(roots)| > \frac{\pi}{2M}. \tag{1.2.10} $$

This condition is known as instability measure for equilibrium points in fractional order system. As a convenience, $\left(\min|arg(\lambda_i)| - \frac{\pi}{2M}\right)$ *is denoted by IMFOS.*

1.3 Structure of the thesis

The thesis consists of seven chapters that explore the dynamics of HBV infection, addressing both the intercellular and intracellular dynamics. The structure of the thesis is outlined as follows:

In **Chapter 2**, we explore the roles of cytoplasmic recycling of rcDNA-containing capsids in HBV infection. To this purpose, considering the recycling of capsids, a novel mathematical model is proposed in order to understand the dynamics of this viral infection in a better way. Through a rigorous comparison with the experimental data obtained from two chimpanzees, the proposed model exhibits an excellent agreement with the dynamics of infection. The effects of three parameters (recycling rate, virus production rate, and volume fraction of newly produced capsids) are examined. A comprehensive global sensitivity analysis is also conducted to identify the most positively as well as most negatively sensitive parameters for each model compartment.

In **Chapter 3**, we consider two nonlinear fractional-order HBV infection models with recycling effects of capsids via the Caputo derivative. Each model contains four compartments, namely, susceptible hepatocytes, infected hepatocytes, HBV capsids, and viruses. In the first model, the order of fractional derivatives is same for each compartment, whereas, in the second model, the order is incommensurate. The existence and uniqueness of solutions for both the models are discussed separately. The parameters are estimated in order to validate

the proposed model with experimental data obtained from a chimpanzee. Stability analyses are carried out for both the models theoretically. The models are solved numerically using the predictor–corrector Adams–Bashforthm–Moulton method (for commensurate order) and implicit product integration of trapezoidal type method (for incommensurate order) with various choices of fractional orders and initial conditions.

In **Chapter 4**, the temporal dynamics of this viral infection are investigated through two intercellular mathematical models considering proliferation of both types of hepatocytes (uninfected and infected) and recycling effects of capsids. Both the models are formulated on the basis of a key finding in the existing literature: mitosis of an infected hepatocytes yields in two uninfected progenies. In the first model (defined by P-model), we examine the regular proliferation (which occurs continuously), while the second model (defined by M-model) deals with the discontinuous proliferation (happen when the total number of liver cells decreases to less than 70% of its initial volume). The proposed models are calibrated with the experimental data obtained from an adult chimpanzee.

In **Chapter 5**, another mathematical model is proposed for the first time by incorporating the roles of SVPs and including the effects of capsids recycling. The impacts of spatial mobility of capsids, viruses, SVPs and antibodies are also taken into account in this model. Overall, this model carries unique characteristics in the context of this viral infection. This study investigates the changes in the dynamics of infection considering both single-point as well as multi-point infection initial conditions.

In **Chapter 6**, an intracellular hepatitis B virus (HBV) infection model is proposed by considering the intracellular steps that are seen in the viral life cycle. The well-known fourth order Runge-Kutta method is employed to solve the proposed model numerically. In order to identify the most influencing parameters, the global sensitivity analysis of the parameters is also performed using partial rank correlation coefficients based on Latin hypercube sampling method. Effects of initial HBx proteins, surface proteins, dslDNA-containing capsids and concentration of cccDNAs are explained very well in this model.

Finally, in **Chapter 7**, we conclude this thesis work with a note and outline some proposed future works in this direction. All numerical simulations included in this thesis are performed using the sophisticated computational software tool MATLAB.

CHAPTER 2

The Roles of Cytoplasmic Recycling of rcDNA-containing Capsids on HBV Infection

In this chapter, we study the roles of cytoplasmic recycling of rcDNA-containing capsids in the persistence of HBV infection. To this purpose, including cytoplasmic recycling of rcDNA-containing capsids, a novel mathematical model is proposed to better understand the dynamics of this viral infection. The proposed model shows excellent agreement with experimental data from two chimpanzees. The effects of three parameters (recycling rate, virus production rate, and volume fraction of newly produced capsids) are investigated. Furthermore, a comprehensive global sensitivity analysis is performed to identify the most positively as well as most negatively sensitive parameter for each model compartment.

2.1 Introduction

Hepatitis B virus causes a deadly liver disease hepatitis B. The life cycle of this virus is unique and quite complex. In the literature, several viral dynamic models have been proposed over the last two decades. These models are useful in understanding the pathogenesis of infection as well as devising better treatment protocols. In the year 1996, Nowak et al. [22] analyzed a basic HBV infection model comprised of three compartments: uninfected hepatocytes, infected hepatocytes, and virions for the first time in the literature. By putting a standard incidence function in the place of mass action term of the uninfected hepatocytes and viruses, Min et al. [24] modified the basic viral infection model [22]. According to them (Min et al. [24]) the mass action term is not rational for the HBV infection since it implies that someone with a smaller liver is unlikely to be infected. Murray et al. [33] proposed another intracellular HBV dynamics model and measured the half-life of HBV as approximately four hours. Manna and Chakrabarty [34] modified this model (proposed by Murray et al. [33]) by considering the uninfected hepatocytes and subsequently studied the effects of delay in intracellular process. Considering the impacts of antibodies and CTLs, Danane et al. [35] extended the model proposed by Manna and Chakrabarty [34] and examined the roles of optimal therapy in controlling viral replication. Using an average incidence rate, Guo et al. [36] established the global stability of a delayed-diffusive HBV infection model. Fatehi et al. [11] built up an intracellular model of HBV infection and compared various kinds of therapeutic strategies that can be applied in the future. Beyond the studies mentioned above, a broad range of literature exists, examining various aspects of HBV infection. Although, to the best of our knowledge, none of the aforementioned studies addressed the roles of capsid recycling in the infection.

In some recent biological studies [12, 13, 97], it is observed that the severity of HBV infection is greatly affected by the recycling of rcDNA-containing capsids. Recently, Thio et al. [98] established the fact that HBV maintains a consistent reservoir of cccDNA through the intracellular recycling of HBV genomes. Nonetheless, the clear concept about how this recycling of HBV capsids contributes to the virus replication is lacking and poorly understood. In order to control HBV transmission in host, having clear knowledge on recycling of capsids is extremely important and exceedingly necessary. Although some mathematical

♣ *The contents of this chapter are published in the form of an article titled "**Cytoplasmic recycling of rcDNA-containing capsids enhances HBV infection**", Nonlinear Dynamics, 112 (14) (2024) 1264112666.*

studies have been conducted on HBV transmission in a host, only a few of them considered the rcDNA-containing capsids as a separate compartment. However, these models failed to capture the actual dynamics of HBV infection. The main reason for this failure could be ignoring the recycling effects of capsids. In this study, an improved mathematical model incorporating the recycling effects of HBV capsids is proposed for the first time. This model is expected to reveal the HBV intracellular dynamics more realistically compared to already available models. In a nutshell, we have mainly concentrated on the following things:

1. The effects of volume fraction of capsids on the disease dynamics.

2. The effects of recycling of capsids in the HBV infection.

3. The effects of virus production rate on infection.

4. Global sensitivity analysis (GSA) of model parameters.

    - Long-term temporal behavior of parameter.

2.2 Model formulation

The persistence of HBV infection for a long period of time depends on the stability and maintenance of cccDNAs in the infected hepatocytes. cccDNAs play a central role in disease progression. There are two main sources of cccDNAs: (i) rcDNA-containing capsids produced directly from the incoming viruses from extracellular space, and (ii) rcDNA-containing capsids produced within the infected hepatocytes due to capsid recycling [11, 12, 97]. The recycling of capsids is not a continuous intracellular process. Depending on the availability of viral surface proteins (L, M, S), a portion of newly produced rcDNA-containing capsids returns to the nucleus and amplifies the pool of cccDNAs [99]. So, the volume fraction of capsids (η) responsible for virus production is generally a function of the surface protein (L, M, S), *i.e.*, $\eta = \eta(\text{surface proteins})$. However, a fixed estimated value of η is used throughout this chapter for simulation purposes. Incorporating recycling of capsids, HBV infection dynamics can be described by the following system of ordinary differential equations (2.2.1). The temporal change of each compartment is calculated based on the mass-action principle.

$$\left.\begin{aligned}
&\text{Susceptible hepatocytes :} && \frac{dX(t)}{dt} = \lambda - \mu X(t) - kV(t)X(t),\\
&\text{Infected hepatocytes:} && \frac{dY(t)}{dt} = kV(t)X(t) - \delta Y(t),\\
&\text{rcDNA-containing capsids:} && \frac{dU(t)}{dt} = aY(t) + \gamma(1-\eta)U(t) - \eta\beta U(t) - \delta U(t),\\
&\text{Free viruses:} && \frac{dV(t)}{dt} = \eta\beta U(t) - \delta_v V(t).
\end{aligned}\right\} \quad (2.2.1)$$

Here, $X(t), Y(t), U(t)$ and $V(t)$ denote the numbers of susceptible hepatocytes, infected hepatocytes, rcDNA-containing capsids, and free viruses, respectively. All the parameters $\lambda, \mu, k, a, \delta, \eta, \beta, \gamma$ and δ_v are non-negative real numbers. In this model, λ is assumed to be a constant growth rate of the susceptible hepatocytes, and μ is considered as their natural death rate. The usual death rate of infected hepatocytes as well as capsids is assumed to be same (say, δ) since capsids are within infected hepatocytes, so they will be cleared out at the same rate with the infected hepatocytes. Let, the parameter k describes the rate at which the susceptible hepatocytes are infected by the viruses. It is considered that HBV capsids are produced at a rate a from the infected hepatocytes, and β denotes the production rate of new viruses. Here, δ_v is the virus clearance rate. We denote the recycling rate of newly produced rcDNA-containing capsids as the parameter γ. Recycling of capsids happens within the infected host cells. In Figure 2.1, the diagrammatic representation of the system of equations (2.2.1) is shown.

2.3 Properties of the solution

Here, the existence and uniqueness of the solution for the system (2.2.1) are discussed. In order to ensure the feasibility of the proposed model from biological point of view, it is crucial to show that all solutions remain non-negative and bounded across all non-negative initial conditions. The rationale behind this is that the number of cells or viruses must not drop below zero or exhibit limitless growth during infection. The subsequent discussion confirms non-negativity and boundedness of the solutions.

2.3.1 Existence and uniqueness of solution

Each function on the right-hand side of the system (2.2.1) is a polynomial function of four variables $X(t)$, $Y(t)$, $U(t)$, $V(t)$. So, each function is continuous and satisfies Lipschitz's

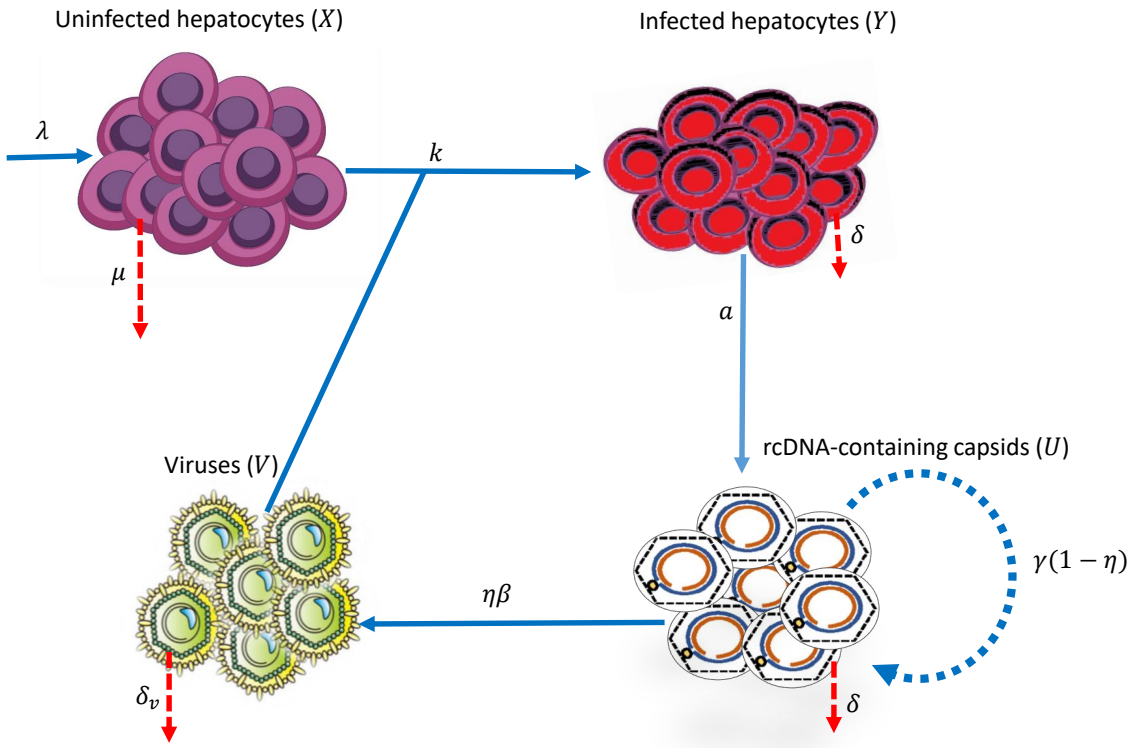

Figure 2.1: The diagrammatic representation of the system (2.2.1).

condition on any closed interval $[0, \eta]$, $\eta \in \mathbb{R}^+$, the set of all positive real numbers. Therefore, solution of the system (2.2.1) exists and is unique.

2.3.2 Non-negativity of solution

Theorem 2.3.1. *Under non-negative initial conditions* $(X(0) \geq 0,\ Y(0) \geq 0,\ U(0) \geq 0,\ V(0) \geq 0)$*, solutions of the system* (2.2.1) *remain non-negative.*

Proof. It is clear that $\left[\frac{dX(t)}{dt}\right]_{X(t)=0} = \lambda$, $\left[\frac{dY(t)}{dt}\right]_{Y(t)=0} = kV(t)X(t)$, $\left[\frac{dU(t)}{dt}\right]_{U(t)=0} = aY(t)$, and $\left[\frac{dV(t)}{dt}\right]_{V(t)=0} = \alpha\beta U(t)$. Since $\left[\frac{dX(t)}{dt}\right]_{X(t)=0} > 0$, so $X(t)$ is always non-negative $\forall\ t > 0$.

In order to prove the non-negativity of $Y(t)$, it is essential to show first the non-negativity of $V(t)$. With that aim, it is assumed that $V(t)$ does not satisfy the non-negativity condition,

i.e., $\exists$ a time t_V such that,

$$t_V = \inf\left\{t:\ t>0,\ V(t)=0, \frac{dV(t)}{dt} \leq 0\right\}.$$

This implies that $\left[\frac{dV(t)}{dt}\right]_{V(t_V)=0} = \alpha\beta U(t_V) \leq 0$, *i.e.*, $\exists$ a time t_U such that

$$t_U = \inf\left\{t:\ t>0,\ U(t)=0, \frac{dU(t)}{dt} \leq 0\right\},$$

which gives $\left[\frac{dU(t)}{dt}\right]_{U(t_U)=0} = aY(t_U) \leq 0$. One may also find a time t_Y such that

$$t_Y = \inf\left\{t:\ t>0,\ Y(t)=0, \frac{dY(t)}{dt} \leq 0\right\}.$$

Clearly, $t_V > t_U > t_Y$ and $\left[\frac{dY(t)}{dt}\right]_{Y(t_Y)=0} = kV(t_Y)X(t_Y) \leq 0 \implies V(t_Y) \leq 0$. Since $V(t_Y) > 0$, this leads to a contradiction with the definition of t_V. So, $V(t) \geq 0,\ \forall\ t > 0$. Consequently, $U(t) \geq 0$ and $Y(t) \geq 0,\ \forall\ t > 0$. □

2.3.3 Boundedness of solution

Theorem 2.3.2. *For non-negative initial condition* $(X(0) \geq 0,\ Y(0) \geq 0,\ U(0) \geq 0,\ V(0) \geq 0)$*, solutions of the system* (2.2.1) *are bounded for all* $t > 0$*, provided* $R_s := \eta\beta - (1-\eta)\gamma + \delta > 0$.

Proof. In order to show the boundedness of solutions, a new variable $F(t)$ is introduced as,

$$F(t) = X(t) + Y(t).$$

Then, $\frac{dF(t)}{dt} = \lambda - \mu X(t) - \delta Y(t)$. Define $\rho^* = \min\{\mu, \delta\}$. Then we have,

$$\frac{dF(t)}{dt} \leq \lambda - \rho^*(X(t) + Y(t)) \implies \frac{dF(t)}{dt} \leq \lambda - \rho^* F(t),$$

which implies that $\limsup_{t\to\infty} F(t) \leq \frac{\lambda}{\rho^*}$. This shows that $\limsup_{t\to\infty} X(t) \leq \frac{\lambda}{\rho^*}$ and $\limsup_{t\to\infty} Y(t) \leq \frac{\lambda}{\rho^*}$. So, $X(t)$ and $Y(t)$ are bounded for all $t > 0$. Now, from the third

equation of the system (2.2.1), one can get

$$\frac{dU(t)}{dt} \leq \frac{a\lambda}{\rho^*} + (\gamma(1-\eta) - \eta\beta - \delta)U(t) \implies \limsup_{t\to\infty} U(t) \leq \frac{a\lambda}{\rho^* R_s}.$$

Therefore, $U(t)$ is bounded for all $t > 0$. Using the boundedness of $U(t)$, from the last equation of the system (2.2.1) it can be obtained as,

$$\frac{dV(t)}{dt} \leq \frac{a\lambda\eta\beta}{\rho^*(\eta\beta + \delta - \gamma(1-\eta))} - \delta_v V(t),$$
$$\implies \limsup_{t\to\infty} V(t) \leq \frac{a\lambda\eta\beta}{\rho^*\delta_v R_s}.$$

Hence, $V(t)$ is bounded for all $t > 0$. Therefore, the populations $X(t), Y(t), U(t)$ & $V(t)$ are bounded. Consequently, a closed, bounded, and positively invariant set is defined as follows:

$$\mathcal{D} = \left\{ \Big(X(t), Y(t), U(t), V(t)\Big) \in \mathbb{R}^4_+ : 0 \leq X(t) + Y(t) \leq \frac{\lambda}{\rho^*}, 0 \leq U(t) \leq \frac{a\lambda}{\rho^* R_s}, \right.$$
$$\left. 0 \leq V(t) \leq \frac{a\lambda\eta\beta}{\rho^*\delta_v R_s} \right\}.$$

□

Remark 2.3.3. *The condition* $R_s > 0 \implies \eta\beta - (1-\eta)\gamma + \delta > 0 \implies \gamma < \dfrac{\eta\beta + \delta}{1-\eta}$. *If* γ *meets this condition, then* $U(t)$ *remains bounded for all* t. *Otherwise,* $U(t)$ *diverges to positive infinity, i.e., the severity of infection increases significantly and situation of the patient becomes worse with time. This relationship amongst these four parameters is very important while treating HBV patients.*

2.4 Parameter estimation and model calibration

In order to enhance the realism of viral dynamics and to improve the reliability of our robust predictions, the proposed model (2.2.1) is calibrated with the experimental data collected from the article of Asabe et al. [100]. In their study, Asabe et al. [100] examined the effects of varying viral inoculum sizes on the kinetics of viral spread and immune system in a cohort of nine young, healthy, HBV-seronegative chimpanzees. It was observed that the viral load of six out of nine chimpanzees reached a peak level of 2×10^{10} within three weeks from the time of inoculation. Later, the virion load decreased within 15 weeks and reached below the detection level. On the other hand, the experiment also documented that the remaining three

chimpanzees developed chronic infection. Out of these nine chimpanzees, the concentration profiles of HBV DNA of two chimpanzees which were labeled as Ch1603 and Ch1616, are considered to estimate the model parameters and to validate this model (2.2.1). In each case, the model parameters are estimated by minimizing the sum-of-squares error (SSE) which is given by

$$\text{SSE} = \sum_{i=1}^{n} (P_i - p(i))^2, \tag{2.4.1}$$

where P_i and $p(i)$ denote the experimental data and model solution, respectively and n denotes the total number of the experimental data points. However, before attempting to estimate model parameters using the experimental data, it is essential to verify if the system of equations (2.2.1) is identifiable or not with this experimental data.

2.4.1 Identifiability analysis

Identifiability analysis stands as the first step in determining the unknown model parameters. A dynamical system is said to be identifiable if the set of model parameters can be uniquely determined from the measurable or observable system output $y(t)$ and the provided system input $u(t)$. Otherwise, the system is considered to be as unidentifiable. Specifically, it is needed to know whether the proposed HBV infection dynamics model is properly structured to uncover its parameters from observable data. We tackle this problem in an ideal setting. This analysis is referred to as structural identifiability [87]. The concept of structural identifiability was first introduced by Bellman and Åström in the year 1970 [101].
The observed data extracted from the work of Asabe et al. [100] is modeled in the system of equations (2.2.1) by the variable $U(t)$. This observed variable is denoted as

$$y(t) = U(t).$$

In terms of observed variable $y(t)$, structural identifiability means the following: Let θ_1 and θ_2 be two distinct vectors of model parameters. Then, we say that the proposed model is structurally identifiable if and only if

$$y(t, \theta_1) = y(t, \theta_2) \implies \theta_1 = \theta_2,$$

i.e., two identical observations yield the same set of parameters. In order to show the structural identifiability of a non-linear compartmental model, few methods are available,

such as similarity transformation method [102], direct test method [103], the method based on implicit function theorem [104], differential algebra method (DAM). The DAM is well summarized in the article of Miao et al. [87]. In this study, the DAM is used to establish the structural identifiability of the proposed model. The first step of this method is to obtain the input-output equation (a differential polynomial equation involving only observed state variables and model parameters) of the proposed model. To this purpose, we need to eliminate the unobserved state variables $(X(t), Y(t), V(t))$ from the system of equations (2.2.1). Since this procedure involves intricate complexities, we opt to utilize DAISY [88], a sophisticated computational software tool, and obtain an input-output equation of the proposed model. The standard ranking (input $<$ output $<$ state variables) of the output and the state variables is assigned as follows:

$$y < \dot{y} < \ddot{y} < \cdots < X(t) < Y(t) < U(t) < V(t) < \dot{X}(t) < \dot{Y}(t) < \dot{U}(t) < \dot{V}(t) \cdots$$

It is important to note that solving input-output equation is equivalent to solving the system of equations (2.2.1) for the state variable $U(t)$. The simulation starts with the parameter set $\Theta = \{\lambda, \mu, k, \delta, a, \gamma, \eta, \beta, \delta_v\}$ and a set of initial values of model variables $I_c = \{X_0, Y_0, U_0, V_0\}$. As a result, we get that the model is algebraically observable but non-identifiable from input-output data. Therefore, it is necessary to reduce the number of model parameters. Based on the output of DAISY, it is observed that the proposed model can be made identifiable once the value of η is provided. According to the study of Murray et al. [50], one possible value of η can be chosen as 0.8 [105]. Now, with this new set of parameters $\Theta = \{\lambda, \mu, k, \delta, a, \gamma, \beta, \delta_v\}$ (deleting η), the model is re-simulated using DAISY, and it is seen that the model is globally identifiable.

2.4.2 Methodology and estimation

Now, we are at a position to estimate the model parameters with the experimental data. It is expected that parameters associated with the infection may change their values during the course of the infection. Infection is a dynamic process involving interactions between pathogens, the host's immune response, environmental factors, and sometimes medical interventions like treatments or vaccinations. As a result, various parameters can fluctuate over time, influencing the progression and outcomes of the infection. In order to compare the model solution with the experimental data, we follow the technique outlined in the article of Chen et al. [106]. Chen et al. [106] divided the whole time interval (0-59 weeks) into six sub-intervals (0-15, 15-28, 28-38, 38-40, 40-41, 41-59 weeks). They considered different values

of immune system related parameters like production rate of CTLs, death rate of infected cells by immune response, and death rate of CTLs on each sub-interval. In this context, Sontag [107] reported that for any ODE model with p unknown parameters, $2p+1$ experimental observations are enough to identify p parameters if the measurements are absolutely accurate. The number of unknown parameters in our model stands at 8. Consequently, the value of $2p+1$ equals to 17.

Based on the "$2p+1$ rule" [107] and the approach mentioned by Chen et al. [106], the model parameters are estimated. The standard Matlab function 'fminsearchbnd' is applied to minimize the SSE. The built-in MATLAB function `fminsearch` is designed for nonlinear optimization in unconstrained problems. By extending `fminsearch`, the function `fminsearchbnd` is developed to handle constrained optimization. This function transforms the search space to ensure that solutions stay within predefined upper and lower bounds.

Matlab syntax

$$\begin{aligned} \text{options} &= \text{optimset}('\text{TolX}', 1e-6, '\text{MaxIter}', 500, '\text{Display}', '\text{iter}'); \\ [x_{\text{opt}}, f_{\text{val}}] &= \text{fminsearchbnd}(\text{fun}, x_0, LB, UB, \text{options}); \end{aligned}$$

Inputs:

- `fun` → Objective function to minimize
- `x0` → Initial guess for variables
- `LB` → Lower bounds (set $-\infty$ for unbounded variables)
- `UB` → Upper bounds (set $+\infty$ for unbounded variables)
- `options` → Options structure for `fminsearch` (optional)

Outputs:

- `x_opt` → Optimized variable values
- `fval` → Function value at the optimal solution

2.4.2.1 Chimpanzee: Ch1603

According to the experimental data structure of the chimpanzee Ch1603, the entire time span of the experiment is split into two sub-intervals: (i) 28-189 days (23 data points), (ii) 189-413 days (17 data points). On both sub-intervals, the parameters are estimated, and the estimated values are shown in Table 5.1. The corresponding results are depicted in the Figure 2.2A.

2.4.2.2 Chimpanzee: Ch1616

As Ch1603, the division is also done for Ch1616 as follows: (i) 28-182 days (23 data points) (ii) 182-385 days (24 data points). The corresponding values of parameters are enlisted in Table 2.1. We compare the model solutions with the experimental data estimating the parameters on each sub-interval and display the associated outcomes in Figure 2.2(B).

In Figure 2.2, the experimental data and solutions of the proposed model are compared for both chimpanzees. It is observed that model solutions agree well with the experimental data, *i.e.*, infection dynamics are captured well by this proposed model. The estimated values of all parameters for the chimpanzees Ch1603 and Ch1616 are enlisted in Table 2.1.

Based on the existing literature, a huge number (300 million) of people are living with a chronic HBV infection. Approximately, more than 90% of infected infants with this virus infection develop chronic infection [108]. Moreover, chronic HBV infection is frequently a lifelong and incurable condition, leading to various personal consequences, including anxiety regarding disease progression, stigma, discrimination, and long-term healthcare costs [109]. Due to this, our interest lies in exploring the dynamics of infection in case of chronic situations. The average estimated values of parameters of Ch1616 are used to facilitate further analysis and numerical simulations, such as the effects of some model parameters, sensitivity analysis in this chapter.

2.5 Existence and stability of equilibria

Before proceeding to the detailed study, it is mentioned that the condition $R_s > 0$ will be considered throughout now on.

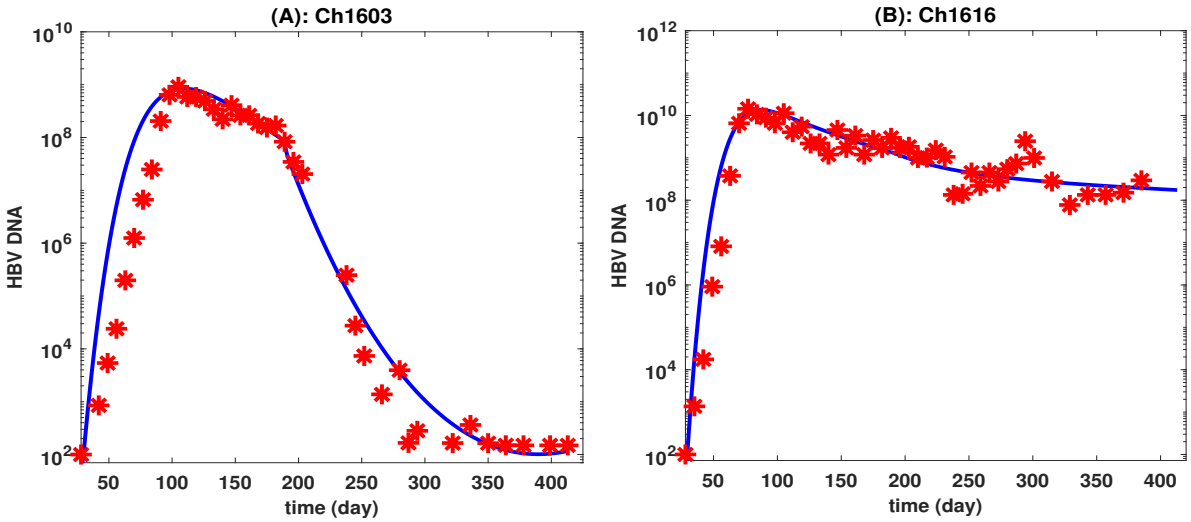

Figure 2.2: Experimental validation of the model (2.2.1). The experimental data is represented by red circles, while the solid blue line corresponds to the numerical solution of the system (2.2.1).

2.5.1 Existence of equilibria

In order to evaluate the equilibrium points of the system (2.2.1), one need to consider the zero growth isoclines and their points of intersection. Thus, the equilibrium points of the system (2.2.1) are found by solving the system of equations

$$\lambda - \mu X(t) - kV(t)X(t) = 0, \tag{2.5.1}$$

$$kV(t)X(t) - \delta Y(t) = 0, \tag{2.5.2}$$

$$aY(t) + \gamma(1-\eta)U(t) - \eta\beta U(t) - \delta U(t) = 0, \tag{2.5.3}$$

$$\eta\beta U(t) - \delta_v V(t) = 0. \tag{2.5.4}$$

It can be shown that the system (2.2.1) possesses two sets of equilibrium points.

1. **The uninfected steady-state or disease-free equilibrium point (E_u):** The uninfected steady-state or disease-free equilibrium point always exists, and it is denoted by $E_u = (X_0, Y_0, U_0, V_0) = \left(\frac{\lambda}{\mu}, 0, 0, 0\right)$.

   In case of viral infection, the basic reproduction number is the number of secondary infective cells produced by a single infective cell which is introduced into a fully susceptible population [110]. The first equation of the system (2.2.1) is associated with the uninfected class and the last three equations are meant for the infected class. The

Table 2.1: Estimation of parameters.

Para	Descriptions	Estimated Parameters Values				Units
		Ch1603		Ch1616		
		Days (28-189)	Days (189-415)	Days (28-182)	Days (182-385)	
λ	Constant growth rate of uninfected hepatocytes	2.51×10^7	2.52×10^7	2.53×10^7	2.58×10^7	cell day^{-1}
μ	Natural death rate of uninfected hepatocytes	0.045	0.020	0.066	0.019	day^{-1}
k	Virus-to-cell infection rate	2.02×10^{-12}	1.36×10^{-12}	3.18×10^{-12}	1.01×10^{-12}	virion^{-1}day^{-1}
a	Production rate of capsids from infected hepatocytes	195	190	172	110	day^{-1}
β	Production rate of viruses from capsids	0.86	1.55	2.92	2.00	day^{-1}
δ	Death rate of infected hepatocytes and capsids	0.105	0.200	0.070	0.038	day^{-1}
δ_v	Death rate of viruses	3.93	5.82	3.80	4.48	day^{-1}
γ	Capsids to capsids production rate or recycling rate of capsids	0.21	0.45	0.21	0.49	day^{-1}
η	Volume fraction of capsids in favor of virus production	0.8	0.8	0.8	0.8	Unitless

next-generation approach [111] is applied to determine the basic reproduction number. The basic reproduction number of the system of equations (2.2.1) is denoted by R_0, and it is given by $R_0 = \dfrac{ak\lambda\eta\beta}{(\delta_v\eta\beta\delta - \delta_v\gamma\delta + \delta_v\eta\gamma\delta + \delta_v\delta^2)\,\mu}$. R_0 remains positive if $R_s > 0$.

2. **The infected steady-state or endemic equilibrium point (E_i):** Mathematically, infected steady-state or endemic equilibrium point should exist always. But biologically, the existence of this steady-state depends on the basic reproduction number (R_0) and R_s (which is defined earlier). When $R_0 > 1$, and $R_s > 0$, the endemic equilibrium point (E_i) occurs and is given by $E_i = (X_1, Y_1, U_1, V_1)$, where

$$X_1 = \frac{\delta_v\delta R_s}{a\eta\beta k},\ Y_1 = \frac{a\eta\beta k\lambda - \delta_v\delta\mu R_s}{a\eta\beta\delta k},\ U_1 = \frac{a\eta\beta k\lambda - \delta_v\delta\mu R_s}{\eta\beta\delta k R_s},\quad V_1 = \frac{a\eta\beta k\lambda - \delta_v\delta\mu R_s}{\delta_v\delta k R_s}.$$

2.5.2 Global stability analysis of equilibria

In order to prove the global stability of equilibria, Theorem 7.1 of the book [112] is used. For this purpose, two suitable Lyapunov functions are defined as follows:

$$\mathcal{L}_1(t) = X_0\left\{\frac{X(t)}{X_0} - 1 - \ln\left(\frac{X(t)}{X_0}\right)\right\} + Y(t) + \frac{\delta}{a}U(t) + \frac{\delta R_s}{a\eta\beta}V(t).$$

$$\mathcal{L}_2(t) = X_1\left\{\frac{X(t)}{X_1} - 1 - \ln\left(\frac{X(t)}{X_1}\right)\right\} + Y_1\left\{\frac{Y(t)}{Y_1} - 1 - \ln\left(\frac{Y(t)}{Y_1}\right)\right\}$$
$$+ \frac{\delta U_1}{a}\left\{\frac{U(t)}{U_1} - 1 - \ln\left(\frac{U(t)}{U_1}\right)\right\} + \frac{\delta R_s V_1}{a\eta\beta}\left\{\frac{V(t)}{V_1} - 1 - \ln\left(\frac{V(t)}{V_1}\right)\right\}.$$

Both functions are radially unbounded and globally positive definite. Therefore, the choices of Lyapunov functions are appropriate.

Theorem 2.5.1. *The disease-free equilibrium point E_u is globally asymptotically stable if $R_0 < 1$.*

Proof. In order to prove the asymptotic global stability of disease-free equilibrium point, the first Lyapunov function $\mathcal{L}_1(t)$ is considered.

$$\mathcal{L}_1(t) = X_0\left\{\frac{X(t)}{X_0} - 1 - \ln\left(\frac{X(t)}{X_0}\right)\right\} + Y(t) + \frac{\delta}{a}U(t) + \frac{\delta R_s}{a\eta\beta}V(t).$$

Now,

$$\begin{aligned}
\frac{d\mathcal{L}_1(t)}{dt} &= X_0\left(\frac{X'(t)}{X_0} - \frac{X'(t)}{X(t)}\right) + Y'(t) + \frac{\delta}{a}U'(t) + \frac{\delta R_s}{a\eta\beta}V'(t) \\
&= \left(1 - \frac{X_0}{X(t)}\right)X'(t) + Y'(t) + \frac{\delta}{a}U'(t) + \frac{\delta R_s}{a\eta\beta}V'(t) \\
&= \left(1 - \frac{X_0}{X(t)}\right)(\lambda - \mu X(t) - kV(t)X(t)) + kV(t)X(t) - \delta Y(t) \\
&+ \frac{\delta}{a}\Big(aY(t) + (\gamma(1-\eta) - \eta\beta - \delta)U(t)\Big) + \frac{\delta R_s}{a\eta\beta}\Big(\eta\beta U(t) - \delta_v V(t)\Big) \\
&= \lambda\left(2 - \frac{X(t)}{X_0} - \frac{X_0}{X(t)}\right) + \frac{a\eta\beta k\lambda - \delta_v\delta\mu R_s}{a\eta\beta\mu}V(t).
\end{aligned}$$

From the article of Kajiwara et al. [113], it follows that $\left(2 - \frac{X(t)}{X_0} - \frac{X_0}{X(t)}\right) \leq 0$ and since $R_0 \leq 1$, we have $a\eta\beta k\lambda - c\delta\mu R_s \leq 0$. Therefore, $\frac{d\mathcal{L}_1(t)}{dt} \leq 0$. We consider the largest invariant set $\mathcal{M}_1 = \left\{(X(t), Y(t), U(t), V(t)) \in \mathbb{R}^4 : \frac{d\mathcal{L}_1(t)}{dt} = 0\right\}$. The solution of the equa-

tion $\frac{d\mathcal{L}_1(t)}{dt} = 0$ is only $\left(\frac{\lambda}{\mu}, 0, 0, 0\right)$ which is the equilibrium point E_u. So, based on the Lyapunov-LaSalle invariance principle [112], the disease-free equilibrium point (E_u) is globally asymptotically stable whenever $R_0 \leq 1$. In terms of biology, the global asymptotic stability of E_u implies that the infection will not persist within the host if the parameters meet the following condition:

$$\frac{ak\lambda\eta\beta}{\left(\delta_v\eta\beta\delta - \delta_v\gamma\delta + \delta_v\eta\gamma\delta + \delta_v\delta^2\right)\mu} \leq 1.$$

□

Theorem 2.5.2. *The endemic equilibrium E_i is globally asymptotically stable if $R_0 > 1$.*

Proof. We approach the problem by taking into account the second Lyapunov function $\mathcal{L}_2(t)$.

$$\begin{aligned}\mathcal{L}_2(t) = {} & X_1\left\{\frac{X(t)}{X_1} - 1 - \ln\left(\frac{X(t)}{X_1}\right)\right\} + Y_1\left\{\frac{Y(t)}{Y_1} - 1 - \ln\left(\frac{Y(t)}{Y_1}\right)\right\} \\ & + \frac{\delta U_1}{a}\left\{\frac{U(t)}{U_1} - 1 - \ln\left(\frac{U(t)}{U_1}\right)\right\} + \frac{\delta R_s V_1}{a\eta\beta}\left\{\frac{V(t)}{V_1} - 1 - \ln\left(\frac{V(t)}{V_1}\right)\right\}. \end{aligned} \tag{2.5.5}$$

Differentiating $\mathcal{L}_2(t)$ with respect to t, we have

$$\begin{aligned}\frac{d\mathcal{L}_2(t)}{dt} &= X_1\left(\frac{X'(t)}{X_1} - \frac{X'(t)}{X(t)}\right) + Y_1\left(\frac{Y'(t)}{Y_1} - \frac{Y'(t)}{Y(t)}\right) \\ &\quad + \frac{\delta U_1}{a}\left(\frac{U'(t)}{U_1} - \frac{U'(t)}{U(t)}\right) + \frac{\delta R_s V_1}{a\eta\beta}\left(\frac{V'(t)}{V_1} - \frac{V'(t)}{V(t)}\right) \\ &= \left(1 - \frac{X_1}{X(t)}\right)X'(t) + \left(1 - \frac{Y_1}{Y(t)}\right)Y'(t) + \frac{\delta U_1}{a}\left(1 - \frac{U_1}{U(t)}\right)U'(t) \\ &\quad + \frac{\delta R_s V_1}{a\eta\beta}\left(1 - \frac{V_1}{V(t)}\right)V'(t) \\ &= -\mu X(t)\left(1 - \frac{X_1}{X(t)}\right)^2 + \delta Y_1\left(4 - \frac{Y(t)U_1}{U(t)Y_1} - \frac{U(t)V_1}{U_1V(t)} - \frac{X(t)Y_1V(t)}{X_1Y(t)V_1} - \frac{X_1}{X(t)}\right). \end{aligned}$$

$$\left[\text{Using } U_1 = \frac{a}{R_s}Y_1 \text{ and } V_1 = \frac{a\eta\beta}{R_s\delta_v}Y_1\right]$$

Clearly, the first term of the above equation is negative unless $X(t) = X_1$. To prove the negativity of the second term, define

$$x_1 = \frac{Y(t)U_1}{U(t)Y_1},\ x_2 = \frac{U(t)V_1}{U_1V(t)},\ x_3 = \frac{X(t)Y_1V(t)}{X_1Y(t)V_1},\ x_4 = \frac{X_1}{X(t)}.$$

It is clear that $x_i \geq 0$ for $i = 1, 2, 3, 4$ and $x_1x_2x_3x_4 = 1$. Applying $A.M \geq G.M$,

$$\frac{x_1 + x_2 + x_3 + x_4}{4} \geq (x_1x_2x_3x_4)^{\frac{1}{4}},$$
$$\implies \frac{Y(t)U_1}{U(t)Y_1} + \frac{U(t)V_1}{U_1V(t)} + \frac{X(t)Y_1V(t)}{X_1Y(t)V_1} + \frac{X_1}{X(t)} \geq 4.$$

Hence, it is clear that $\frac{d\mathcal{L}_2(t)}{dt} \leq 0$ when $R_0 > 1$. Let the largest invariant set $\mathcal{M}_2 = \left\{(X(t), Y(t), U(t), V(t)) \in \mathbb{R}^4 : \frac{d\mathcal{L}_2(t)}{dt} = 0\right\}$. It is noticed that the solution of the equation $\frac{d\mathcal{L}_2(t)}{dt} = 0$ is only (X_1, Y_1, U_1, V_1) which is the equilibrium point E_i. So, based on the Lyapunov-LaSalle invariance principle, the endemic equilibrium point is globally asymptotically stable whenever $R_0 > 1$, *i.e.*, the situation of the patient will be stable after a certain period of time. In viral infection, endemic steady-state also denotes a stable and persistent viral prevalence within a host, reflecting a dynamical balance among viral transmission, host immunity, and other influencing factors, such as host susceptibility, treatments, vaccination. □

2.6 Bifurcation analysis

In this section, the bifurcation analysis of the model (2.2.1) is performed. Stability criteria of E_u indicates that E_u will be stable if $\mu > \frac{ak\eta\beta\lambda}{R_sc\delta}(= \mu^*)$, otherwise it will be unstable, *i.e.*, the stability of E_u changes as μ crosses the threshold value $\mu = \mu^*$. In Figure 2.3, stable E_u, unstable E_u, stable E_i, unstable E_i, and biologically non-existent equilibrium points are visually represented. On the other hand, the endemic equilibrium E_i (although E_i is not feasible in the context of biology) becomes unstable if $\mu > \mu^*$. Thus, the equilibrium points coincide when $\mu = \mu^*$ and exchange their stabilities. This leads to the transcritical bifurcation of the system (2.2.1) around the point E_u at $\mu = \mu^*$ with parameter μ as the bifurcation parameter. The Jacobian matrix calculated at E_u is given by

$$\begin{bmatrix} -\mu & 0 & 0 & -\frac{k\lambda}{\mu} \\ 0 & -\delta & 0 & \frac{k\lambda}{\mu} \\ 0 & a & \gamma(1-\eta) - \eta\beta - \delta & 0 \\ 0 & 0 & \eta\beta & -\delta_v \end{bmatrix}. \tag{2.6.1}$$

The matrix (2.6.1) has one zero eigenvalue when $\mu = \mu^*$. In order to verify the existence of transcritical bifurcation analytically, Sotomayor's theorem [82] is applied on the system (2.2.1) around the disease-free equilibrium point E_u when $\mu = \mu^*$. The R.H.S of system (2.2.1) can be represented in vector form as

$$f(X(t), Y(t), U(t), V(t)) = \begin{pmatrix} \lambda - \mu X(t) - kV(t)X(t) \\ kV(t)X(t) - \delta Y(t) \\ aY + \gamma(1-\eta)U(t) - \eta\beta U(t) - \delta U(t) \\ \eta\beta U(t) - \delta_v V(t) \end{pmatrix}. \tag{2.6.2}$$

Differentiating the function $f(X(t), Y(t), U(t), V(t))$ partially with respect to μ, it is obtained that $f_\mu(X(t), Y(t), U(t), V(t)) = (-X(t) \quad 0 \quad 0 \quad 0)^T$. The Jacobian matrix (2.6.1) and its transpose matrix have an eigenvalue $\xi = 0$ with eigenvectors

$$v = \begin{pmatrix} \frac{k\lambda}{\mu^2} & \frac{a\lambda}{\mu\delta} & \frac{ak\lambda}{R_s\mu\delta} & 1 \end{pmatrix}^T \text{ and } w = \begin{pmatrix} 0 & \frac{a\eta\beta}{\delta R_s} & \frac{\eta\beta}{R_s} & 1 \end{pmatrix}^T.$$

Now, we have verified the following transvesality conditions at E_u:

1. $w^T f_\mu(E_u, \mu^*) = \begin{pmatrix} 0 & \frac{a\eta\beta}{\delta R_s} & \frac{\eta\beta}{R_s} & 1 \end{pmatrix} \begin{pmatrix} -\frac{\lambda}{\mu^*} & 0 & 0 & 0 \end{pmatrix}^T = 0,$
2. $w^T[Df_\mu(E_u, \mu^*)v] = -\frac{k\lambda}{\mu^{*2}} \neq 0,$
3. $w^T[D^2 f(E_u, \mu^*)(v, v)] = -\frac{2\eta\beta k^2\lambda}{R_s\delta\mu^{*2}} \neq 0.$

All the notations used here are same as in the book of Lawrence Perko [82]. Therefore, all three conditions of Sotomayor's theorem hold and the system (2.2.1) undergoes transcritical bifurcation at E_u as the natural death rate of uninfected hepatocytes μ, crosses the threshold value μ^*.

In addition, considering three different initial conditions, system (2.2.1) is solved numerically for both cases: (i) $\mu > \mu^* (\implies R_0 < 1)$, and (ii) $\mu < \mu^* (\implies R_0 > 1)$. The obtained results are visually displayed in Figure 2.4. Consequently, it is observed that the stabilities of the equilibrium points changes depending on the value of the bifurcation parameter (μ^*). When

1. $\mu > \mu^*$, solutions of the system (2.2.1) converges to disease-free steady-state.

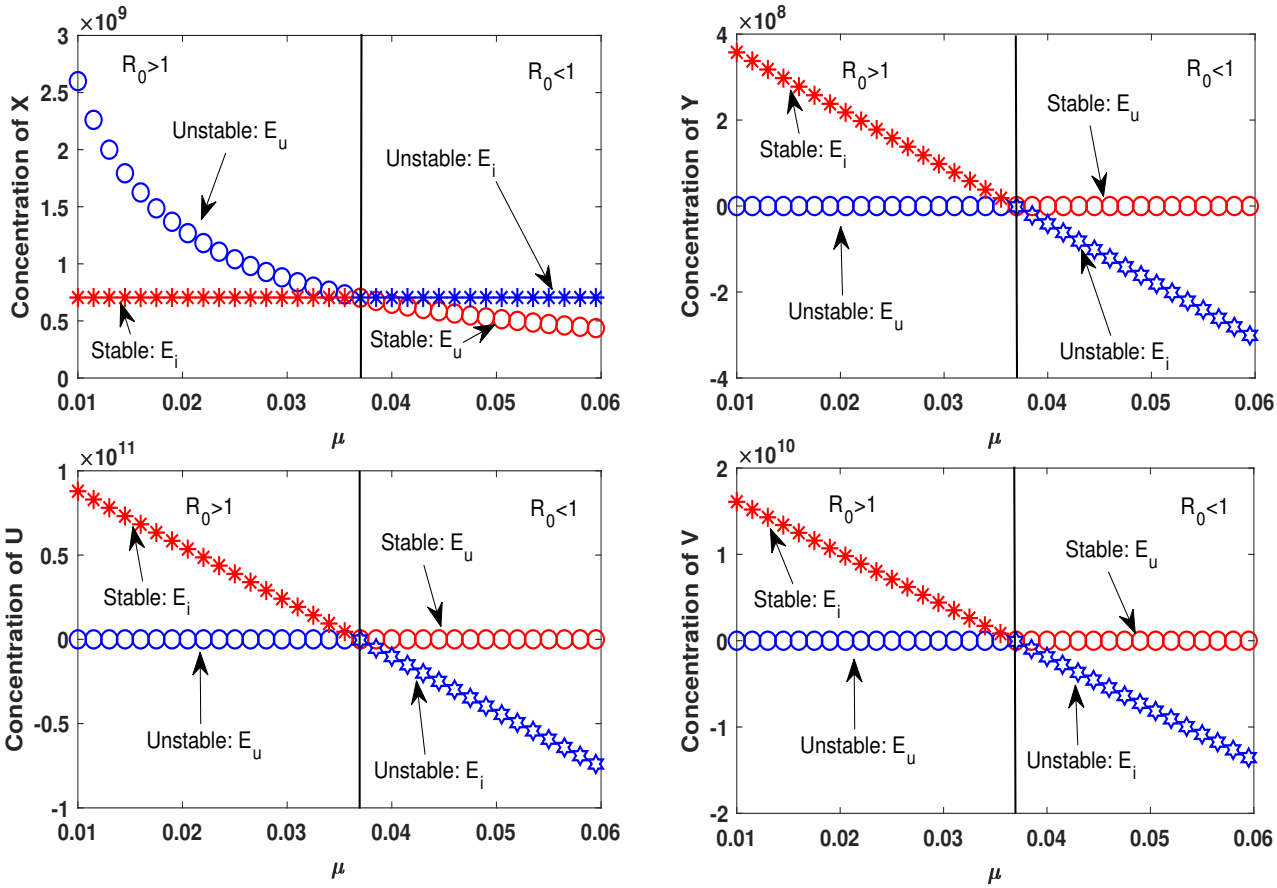

Figure 2.3: The bifurcation diagram for model (2.2.1). Here, blue circles represent unstable disease-free equilibrium points, red circles denote stable disease-free equilibrium points, red stars indicate stable endemic equilibrium points, blue stars mean unstable endemic equilibrium points, blue hexagons represent unstable endemic equilibrium points but due to negative values, these equilibrium points do not exist in the context of biology.

2. $\mu < \mu^*$, solutions of the system (2.2.1) attain endemic steady-state.

Hence, system (2.2.1) exhibits transcritical bifurcation.

2.7 Numerical simulation

Two new parameters are introduced in our model: (i) the volume fraction of capsids in favor of virus production (η), and (ii) the recycling rate (γ) of newly produced capsids. In this section, the changes in infection dynamics with the changes of these two parameters and virus production rate (β) are depicted through numerical simulation. It is also illustrated how the recycling of capsids reverses the impact of volume fraction and virus production rate on the

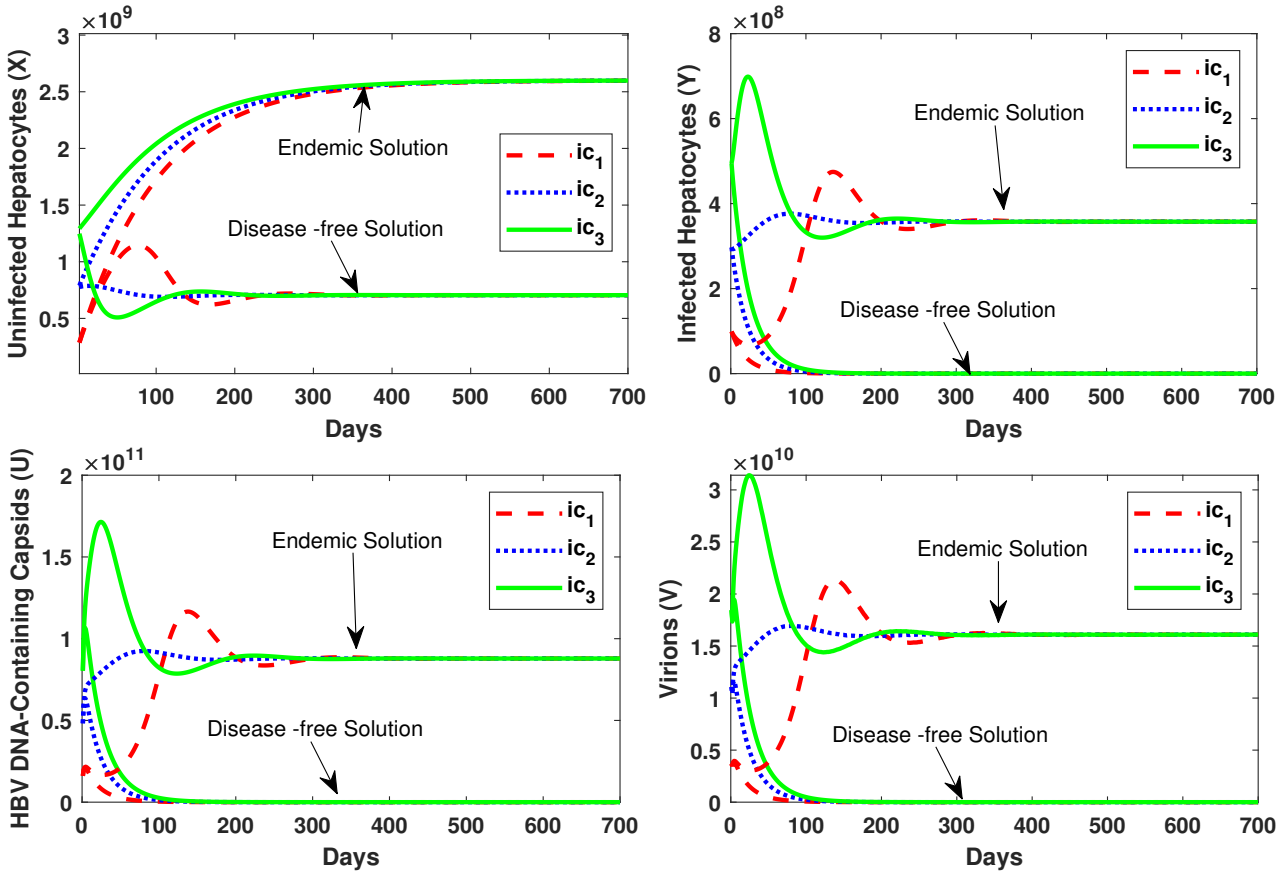

Figure 2.4: Two types of solutions for three different initial conditions. When $\mu > \mu^*$, we get disease-free solutions, and when $\mu < \mu^*$, we get endemic solutions. Here, $ic_1 = (2.56 \times 10^8, 0.99 \times 10^8, 1.60 \times 10^{10}, 0.369 \times 10^{10})$, $ic_2 = (7.68 \times 10^8, 2.97 \times 10^8, 4.82 \times 10^{10}, 1.10 \times 10^{10})$ and $ic_3 = (12.79 \times 10^8, 4.95 \times 10^8, 8.04 \times 10^{10}, 1.85 \times 10^{10})$.

infection. The system (2.2.1) is solved with the help of well-known fourth-order *Runge–Kutta* method and the results are plotted graphically. The entire numerical experiment is carried out in case of chronic infection. The average value of parameters are taken from Table 2.1 for the chimpanzee Ch1616.

2.7.1 Experiment-1: Effects of volume fraction (η) of rcDNA-containing capsids on infection dynamics

The effects of volume fraction of capsids (η) on the system (2.2.1) are examined for two distinct cases. In the first case, impacts of recycling of capsids on the system (2.2.1) are ignored, whereas in the second case, it is considered. In Figure 2.5, effects of η in the absence of recycling of capsids are shown. The numerical simulation is performed for six

values of η, namely, $\eta = 0.5, 0.6, 0.7, 0.8, 0.9$ & 1.0, keeping the other parameters fixed. Both the condition $R_s > 0$ and $R_0 > 1$ are satisfied for every value of η, *i.e.*, solutions of the system converge to endemic equilibrium point. Figure 2.5 shows that the stability level of uninfected hepatocytes and HBV capsids decline, but the stability levels of infected hepatocytes and viruses progressively increase while η increases.

Upon incorporating the recycling effects of capsids into the model, opposite patterns are observed for uninfected hepatocytes, infected hepatocytes, and viruses in Figure 2.6. There is no change observed in the trend of capsids compartment, but the stability level significantly increases for the same value of volume fraction. Consequently, when $\eta = 1.0$, it is clear that the concentration level of uninfected hepatocytes is at the highest level while that of infected hepatocytes, HBV capsids, and viruses get stabilized at the lowest level. Thus, the results for these two cases are different. The low value of volume fraction of capsids implies that a less number of capsids can produce new viruses, and a large number of capsids get accumulated inside the hepatocytes. Therefore, the accumulation of core particles (capsids) within the infected hepatocytes can lead to severe infection, rather than the rapid release of infectious virus particles.

2.7.2 Experiment-2: Effects of recycling rate (γ)

In Figure 2.7, the impacts of recycling rate (γ) on all four compartments of system (2.2.1) are presented. Six different values of $\gamma(= 0.5, 1.0, 1.5, 2.0, 2.5, 3.0)$ are chosen for simulation in such a way that the criteria for boundedness of solution $R_s > 0$ is satisfied. For these values of the parameter, the corresponding values of R_0 exceed unity indicating chronic infection. The main observation of this experiment is that when recycling of capsids is not considered, system asymptotically achieves its stability with maximum concentration of uninfected hepatocytes. Concentration level of uninfected hepatocytes drops when γ rises. On the other side, the concentration level of infected hepatocytes increases with the increase in γ and attains its minimum value when $\gamma = 0$. A similar scenario is observed for capsids and virions. It is also observed that the peak level of infected, capsid and virus compartment becomes smaller as γ decreases, *i.e.*, the critical phase of the patient diminishes and disappears more rapidly. From biological point of view, it is seen that for higher value of γ, the situation becomes more critical for the sufferers/patients, and it is difficult to be cured. For some values of γ, the concentration level of uninfected hepatocytes falls below the biologically plausible threshold (20% of the original hepatocytes) mentioned in the article [48]. Therefore, this experiment also underscores the importance of incorporation of HBV capsid recycling into the model for a more realistic understanding about HBV

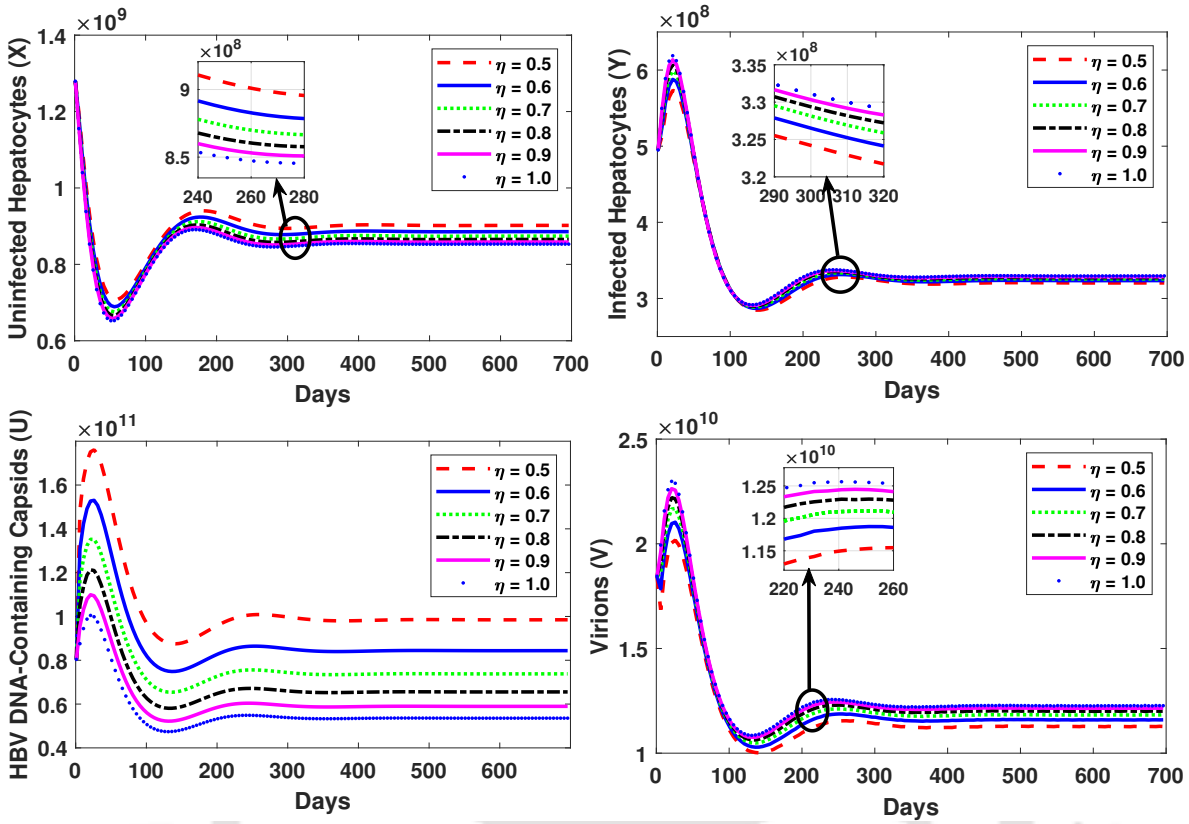

Figure 2.5: The effects of volume fraction of capsids (η) on the dynamical system (2.2.1) in the absence of recycling of capsids ($\gamma = 0$).

infection dynamics.

2.7.3 Experiment-3: Effects of capsids to virus production rate (β)

For different values of capsids to virus production rates, the variations in the dynamics of uninfected hepatocytes, infected hepatocytes, capsids, and viruses are shown in Figure 2.8 (without recycling) and Figure 2.9 (with recycling). Six values of β(=0.6, 0.7, 0.8, 0.9, 1.0, 1.1) are considered keeping other parameters fixed. For each value of β, the conditions $R_s > 0$ and $R_0 > 0$ hold. Similarly, as Experiment-1, in this case we also consider two cases: without and with capsid recycling. In both cases, the effects of β on infection dynamics closely resemble to the impacts of η observed in Experiment-1. Figure 2.9 demonstrates that lower value of β makes things worse for the sufferer, thus making it difficult to cure. Small virion release rate (β) in the HBV replication process may be an additional risk factor for chronic hepatitis exacerbation over time. Therefore, this discussion underlines

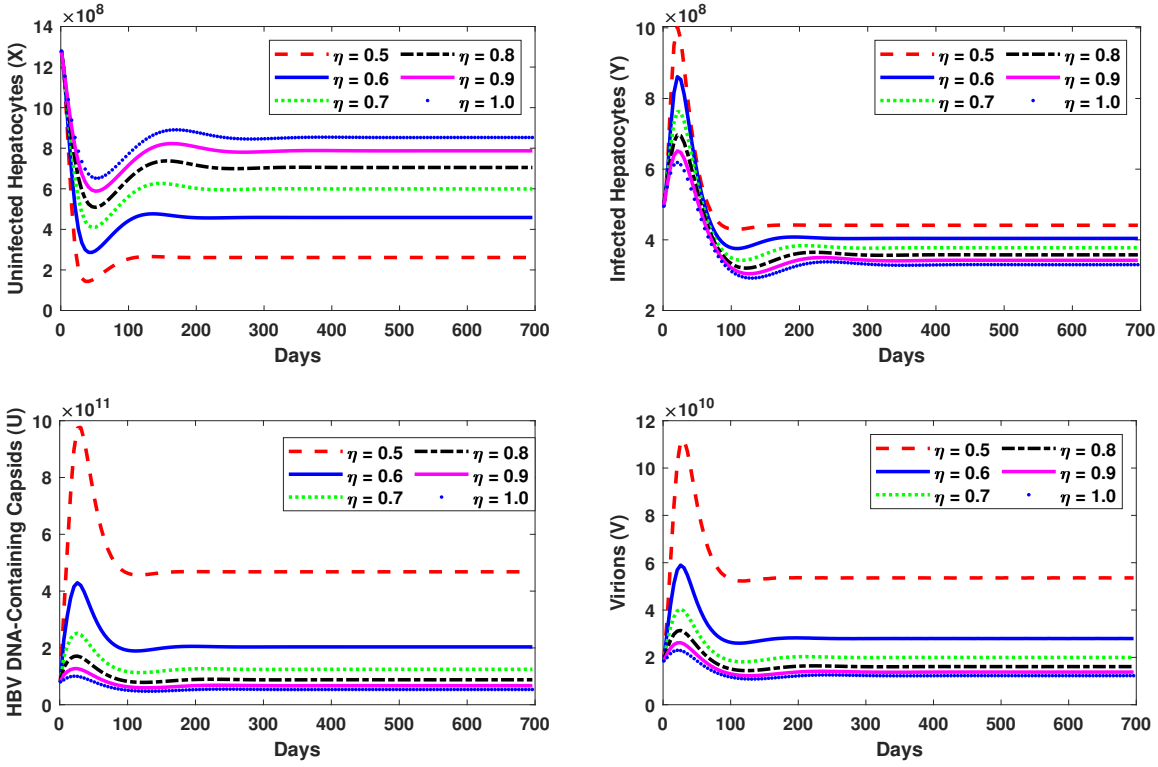

Figure 2.6: The effects of volume fraction of capsids (η) on the dynamical system (2.2.1) when the effects of recycling of capsids is considered ($\gamma > 0$).

the importance of virions production rate and the impacts of recycling of capsids on virions production in cases of HBV infection.

Observation:

Based on the results obtained from these three experiments, it is observed that the recycling of capsids is appeared to be an influential factor in progression of the infection. Recycling of capsids enhances the number of viruses amplifying the pool of cccDNA. As a result, infection becomes severer. In a nutshell, recycling of capsids acts as a positive feedback loop in case of HBV infection. Through the study of intracellular HBV dynamics, Nakabayashi [114] concluded that recycling of capsids can contribute to the accumulation of core particles, indicating a risk factor for the exacerbation of the disease. Recently, Sakaguchi [115] noted that HBV infection can be reduced substantially by disrupting the capsid recycling which implies that the prompt import of newly produced capsids creates a more robust infection. Ko et al. [105] established that the stability of the cccDNA pool in HBV infection is main-

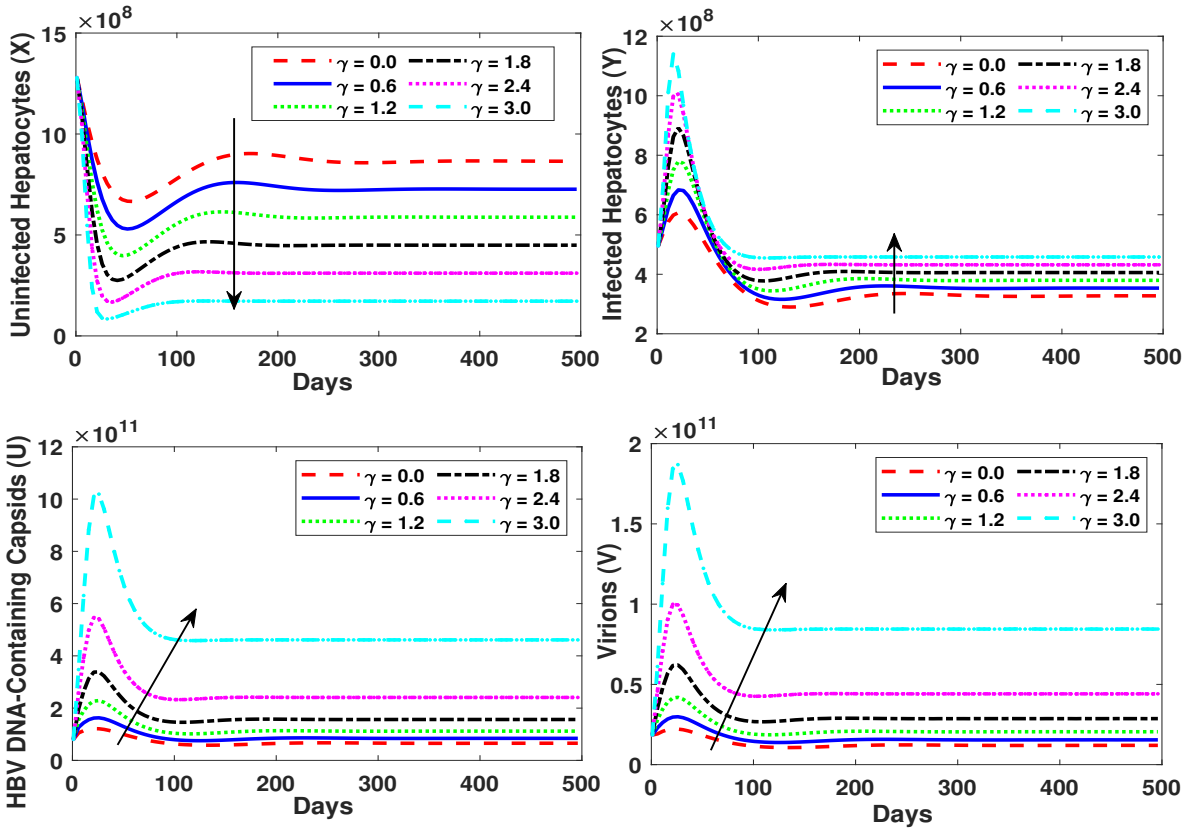

Figure 2.7: The effects of recycling rate of capsids (γ) on the dynamical system (2.2.1). The arrows indicate the direction of growth of the parameter γ.

tained through the internal recycling of HBV genomes, *i.e.*, recycling emerges as a pivotal factor in the persistence of HBV infection.

In the absence of capsid recycling, uninfected hepatocytes reach a steady state with its highest value for low value of volume fraction or of virus production rate (refer to Figure 2.5 and Figure 2.8). However, this observation does not accurately reflect the actual dynamics of the infection. Consequently, Figure 2.5 and Figure 2.8 fail to display the true roles of η and β in the infection dynamics. On the other hand, when recycling of capsids is considered, a low value of volume fraction or of virus production rate results in a substantial increase in the number of capsids through recycling loop, thereby amplifying the production of new viruses. In this case, Figure 2.6 and Figure 2.9 provide a more accurate representation of the underlying biological dynamics. The obtained results due to the inclusion of capsid recycling also corroborate with the conclusions shown in previous biological studies [105, 114, 115]. Incorporation of capsid recycling enriches the virus dynamics and enhance the infection. The nature of HBV infection found in the existing dynamics models [34, 35, 37, 62], which did not consider the capsid recycling, is not similar to the nature of HBV infection observed

in the biological studies [105, 114, 115]. In contrast, this study offers a more comprehensive depiction of HBV infection dynamics and close align with the actual dynamics of infection. This is the novelty of this study. Therefore, it is very important to consider the effects of recycling of capsids while treating the infection and proposing any new antiviral therapy.

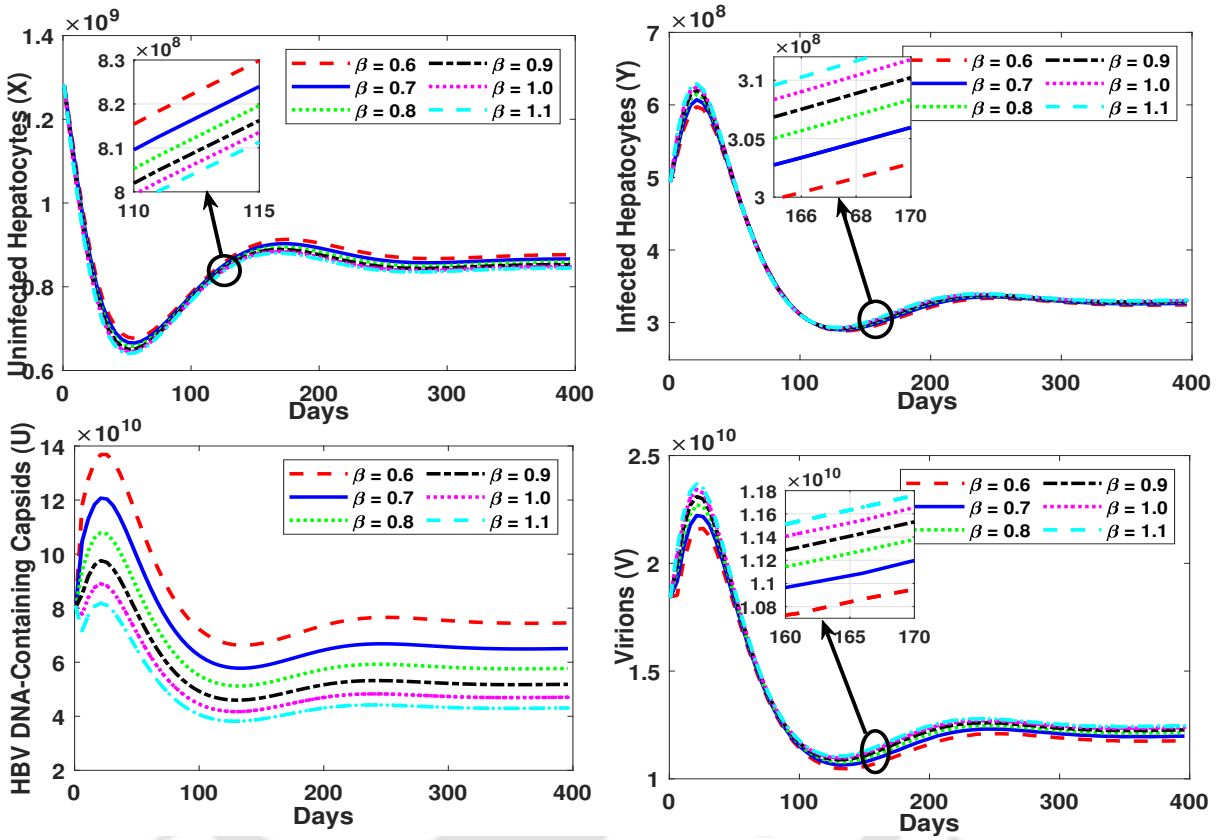

Figure 2.8: The effects of virus production rate (β) in the absence of recycling of capsids ($\gamma = 0$) on the dynamical system (2.2.1).

2.8 Global sensitivity analysis of the parameters

The accuracy of the results of a mathematical model related to some biological phenomena often becomes poor because of uncertainties in experimental data which are utilized in the estimation of model parameters. Recently, many authors have studied the effects of single parameter keeping all others parameters fixed at their estimated values. This type of sensitivity analysis is called local sensitivity analysis. But local sensitivity analysis doesn't provide proper information of uncertainty and sensitivity of the parameters. In order to find out the contributions of each model parameters globally in HBV infection dynamics, the global sen-

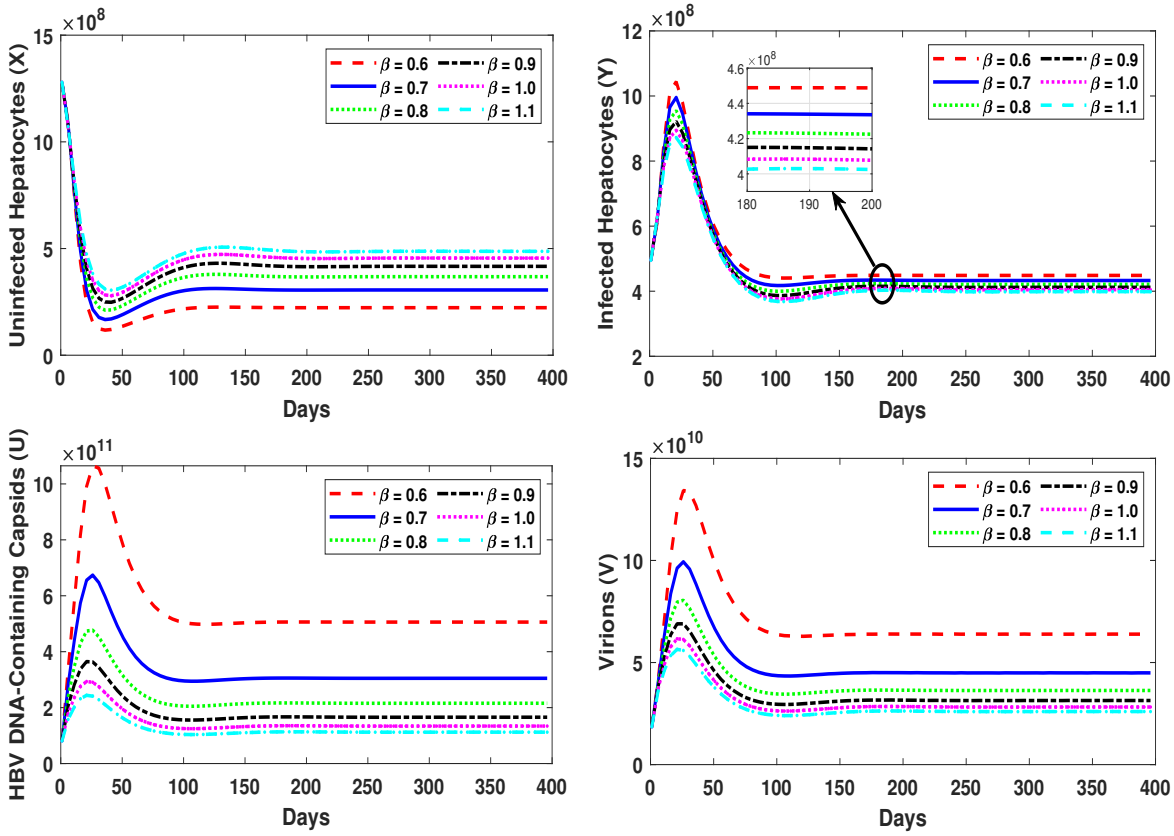

Figure 2.9: The effects of virus production rate (β) on the dynamical system (2.2.1) when effects of recycling of capsids are considered ($\gamma > 0$).

sitivity analysis is performed using the technique "Latin Hypercube Sampling-Partial Rank Correlation Coefficient" (LHS-PRCC) described by Marino et al. [116].

2.8.1 Latin Hypercube Sampling (LHS)-Partial Rank Correlation Coefficient (PRCC)

Latin hypercube sampling is one kind of Monte Carlo class of sampling methods. In the year 1979, McKay et al. [117] first introduced this sampling method. With the help of LHS, sample inputs of the model are arranged within a "hypercube of dimensions p", where p represents the number of model parameters. For our proposed model (2.2.1), the number of model parameters (p) is equal to 9. A probability density function (pdf) is employed for sampling the values of each parameter. In this study, the uniform distribution is chosen for all parameters depending on a priori information and existing data. The model is then simulated iteratively over all p-tuples parameter pairs. It is recommended that the sample size (N) will be at least $(p + 1)$, but it is better to take a larger sample size to ensure the

desired accuracy of the results. Here, the sample size is set to 1000.

The correlation coefficient (CC) measures the strength of a linear relationship between the inputs and the outputs. The CC is calculated between the input variable (P) and output variable (Q) as follows:

$$r^* = \frac{\sum(P(t) - \bar{P})(Q(t) - \bar{Q})}{\sqrt{\sum(P(t) - \bar{P})^2 \sum(Q(t) - \bar{Q})^2}},$$

where $\bar{P}$ and $\bar{Q}$ represent the sample means of $P(t)$ and $Q(t)$ respectively and $r \in [-1, 1]$. In case of raw data of P and Q, the coefficient r^* is known as sample or Pearson correlation coefficient. The CC (r^*) is called Spearman or rank correlation coefficient if the data are rank-transformed. In this study, the model parameters $(\lambda, k, \mu, \delta, a, \gamma, \eta, \beta, \delta_v)$ and model variables $(X(t), Y(t), U(t), V(t))$ are considered as input and output data, respectively. By using LHS-PRCC, one can derive insightful conclusions about how the model parameters influence the outputs of a system.

2.8.2 Scatter plots: The monotonic relationship between input and output variables

Besides the improvement and generalization of a dynamical system, it has attracted the attention of many researchers to know how the outputs are affected if the parameters' values vary in a reasonable range. In the practical field of application especially in virus dynamics model, it is very important and essential to study the sensitivity of parameters. In such cases, PRCC values can provide useful information. Based on the PRCC values, one can identify which set of parameters is the most significant for achieving some specific goals such as control or regulatory mechanisms, reduce viral load, increase immune response, proposing any new therapy and optimization of drug usage, etc. In order to analyze the sensitivity of parameters, the baseline values are taken from Table 2.1 (average values of chimpanzee Ch1616). To this purpose, we systematically vary all parameters within the range from 80% to 120% of their base values. The algorithm of global sensitivity analysis using LHS-PRCC method is displayed in Figure 2.10 in the form of a flow chart. Simulation results of the proposed model (2.2.1) are visualized by scatter plots on Figure 2.11 - Figure 2.14. The PRCC values of all parameters are calculated at 1200^{th} day with respect to the dependent variables. The positive correlation of a compartment to a model parameter (PRCC value positive) ensures that if the value of the parameter increases individually or simultaneously, the concentration of the compartment increases accordingly. On the other hand, negative correlation (PRCC value negative) tells us the opposite aspects. Based on the PRCC values,

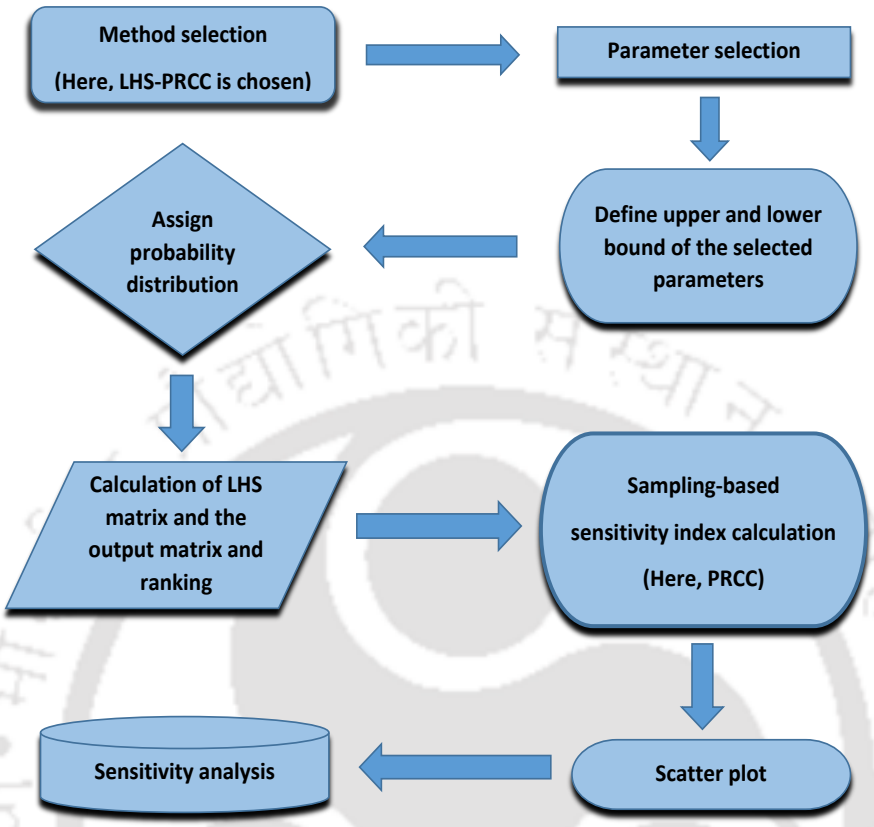

Figure 2.10: Working steps of global sensitivity analysis are shown concisely in this diagram.

the model parameters are arranged in descending order for the uninfected, infected, capsids, and virus classes as follows:

- **Uninfected hepatocytes**: $\eta,\ \delta,\ \delta_v,\ \beta,\ \lambda,\ \mu,\ a,\ k,\ \gamma$.
- **Infected hepatocytes**: $\lambda,\ a,\ k,\ \ \gamma,\ \beta,\ \delta_v,\ \eta,\ \mu,\ \delta$.
- **Capsids**: $\lambda,\ \mu,\ k,\ a,\ \beta,\ \delta,\ \delta_v,\ \gamma,\ \eta$.
- **Viruses**: $\gamma,\ a,\ \lambda,\ k,\ \mu,\ \delta_v,\ \beta,\ \delta,\ \eta$.

In Figure 2.15, the PRCC values of each parameter against the model variables $(X(t),\ Y(t),\ U(t),\ V(t))$ are demonstrated where bars show the PRCC value of each mentioned parameters at time $t = 1200^{th}$ day.

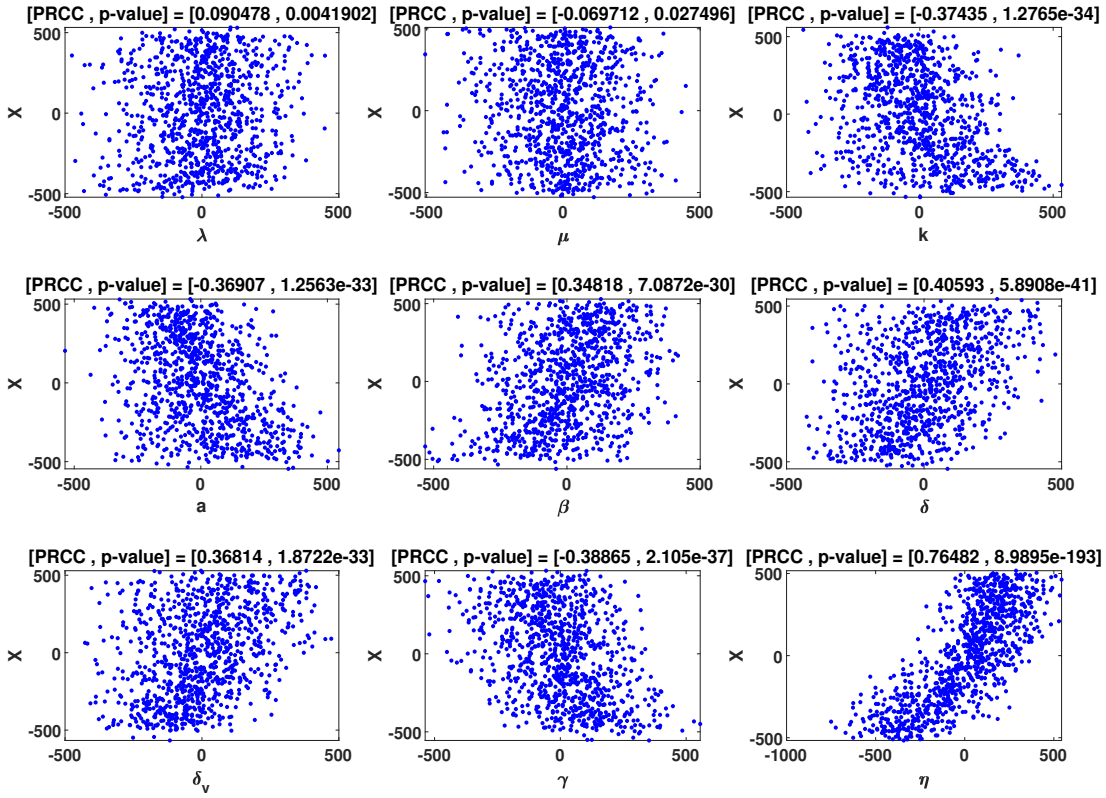

Figure 2.11: Scatter plots for uninfected hepatocytes ($X(t)$). PRCC values of parameters at $t = 1200^{th}$ day.

2.8.3 Long-term behavior of the sequence of PRCC values

Initially, we study the GSA for the outputs at $t = 1200^{th}$ day. However, focusing on GSA at a single time point doesn't provide a comprehensive understanding of a parameter's behavior over the entire infection period. In order to gain a holistic understanding about the behavior of a parameter throughout the whole time span, we perform GSA for each parameter for entire time span. Figure 2.16 illustrates how the PRCC value of each parameter is changed across all compartments over time. The changing tendency of a specific parameter on different compartments reveals significant variations. Figure 2.16 also indicates that the sequence of PRCC values of each parameter across all four compartments, *i.e.*, sensitiveness of each parameter is convergent, ensuring the robustness and stability of the sensitivity analysis. Based on the long-term tendency of PRCC value, we note that at the onset of the experiment, certain parameters (e.g., λ and μ for uninfected hepatocytes) exhibit heightened

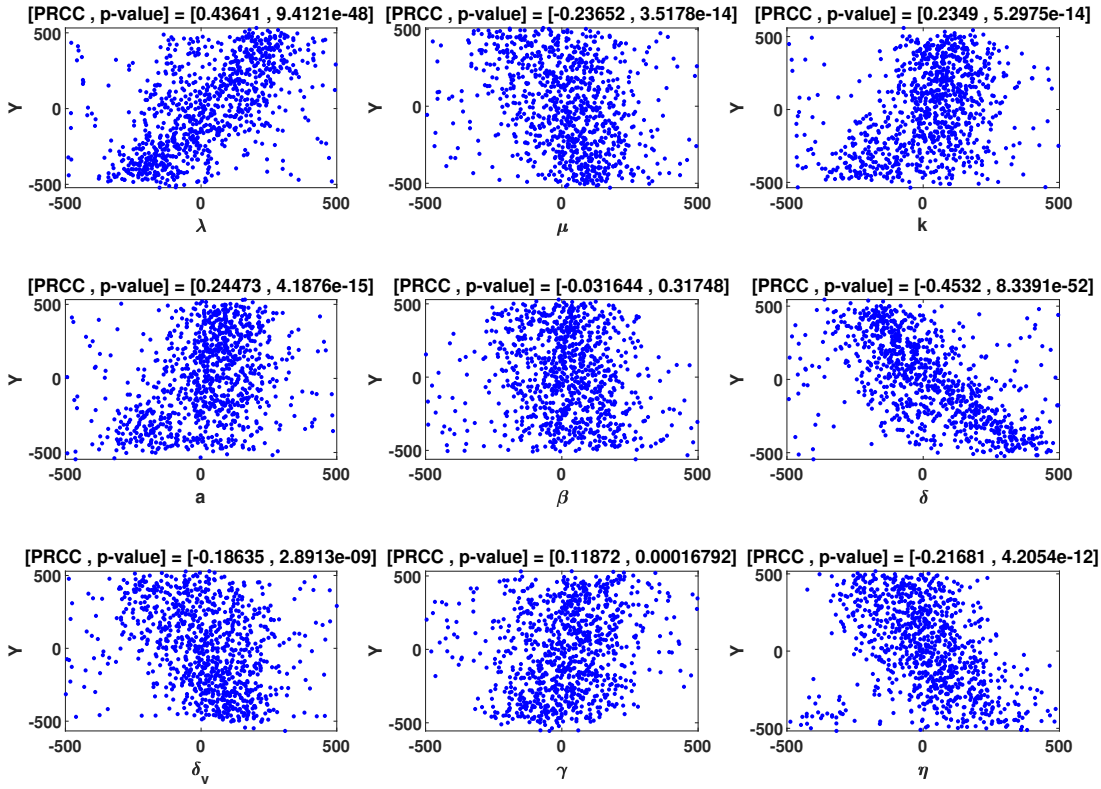

Figure 2.12: Scatter plots for infected hepatocytes ($Y(t)$). PRCC values of parameters at $t = 1200^{th}$ day.

sensitivity, but over time, their significance diminishes. Similarly, some other parameters (e.g., η, k for uninfected hepatocytes) initially appear insignificant but become sensitive after a certain time.

Global sensitivity analysis discloses numerous new and remarkable findings which are outlined as follows:

1. The parameters η, λ, γ are identified as the most positively sensitive parameters for uninfected hepatocytes, infected hepatocytes, and viruses compartments, respectively. On the other hand, the parameters γ, δ, η are found to be the most negatively sensitive parameters for the same.

2. In chronic infection, it is observed that the virus production rate (β) has a relatively less influence on the overall infection dynamics.

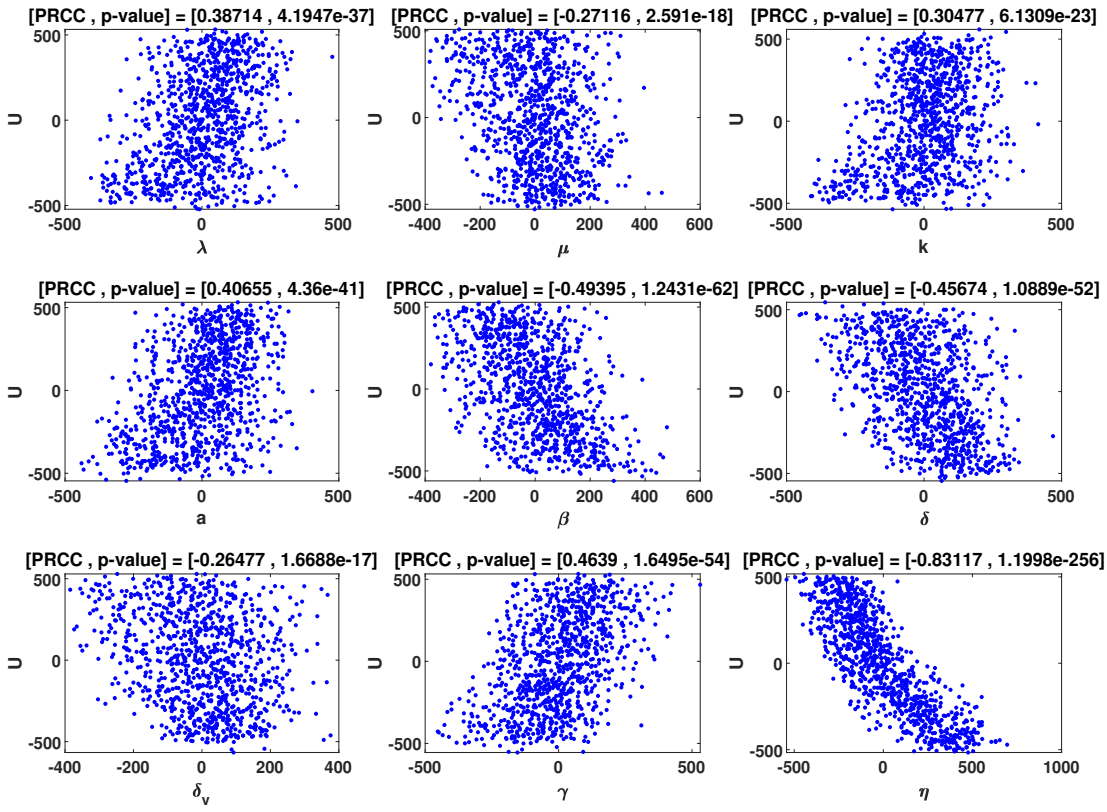

Figure 2.13: Scatter plots for rcDNA-containing capsids ($U(t)$). PRCC values of parameters at $t = 1200^{th}$ day.

3. The recycling rate of capsids (γ) is seen to be the most negatively sensitive parameter for uninfected hepatocytes and most positively sensitive parameter for virions compartment. This implies that if the value of γ increases, the number of viruses increases whereas the number of uninfected hepatocytes decreases simultaneously. Therefore, GSA also proves that the recycling of capsids acts as a positive feedback loop in this viral infection.

4. The volume fraction of capsids is identified as the most positively sensitive parameter for the uninfected compartment. That means if less number of capsids involved in producing new virions and a larger number of capsids undergoes in recycling pathway, then, as a result, this would make the infection more severe.

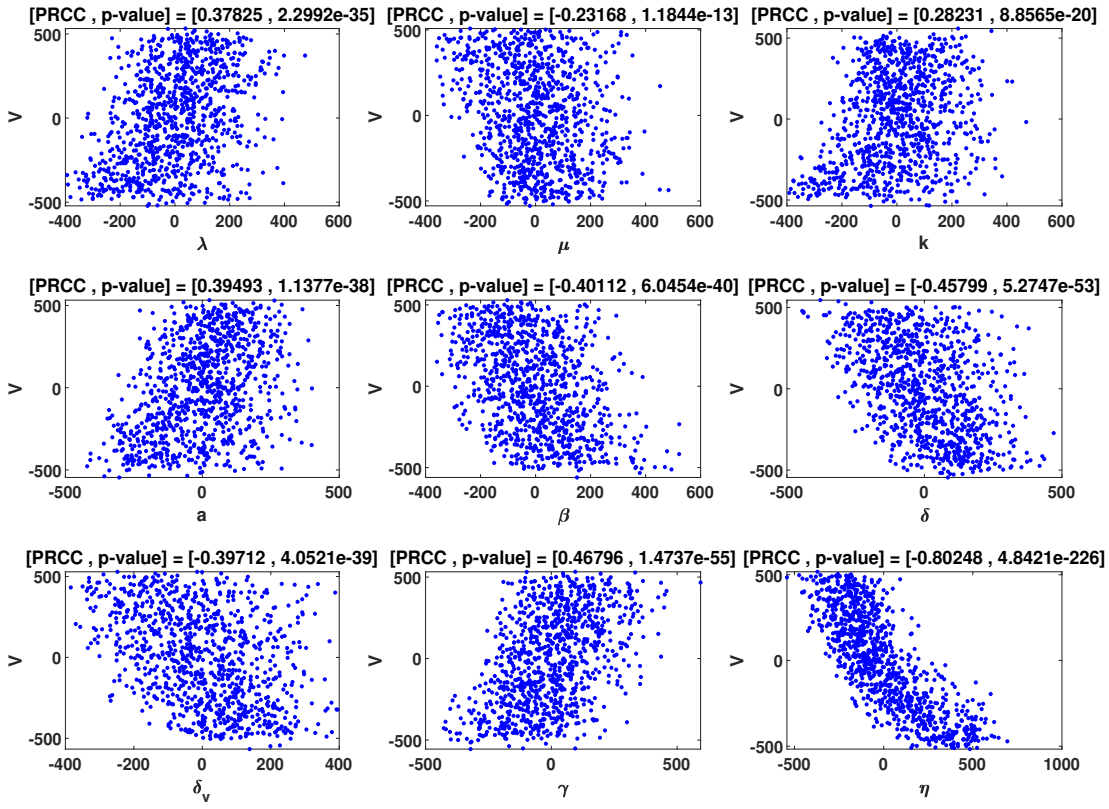

Figure 2.14: Scatter plots for viruses ($V(t)$). PRCC values of parameters at $t = 1200^{th}$ day.

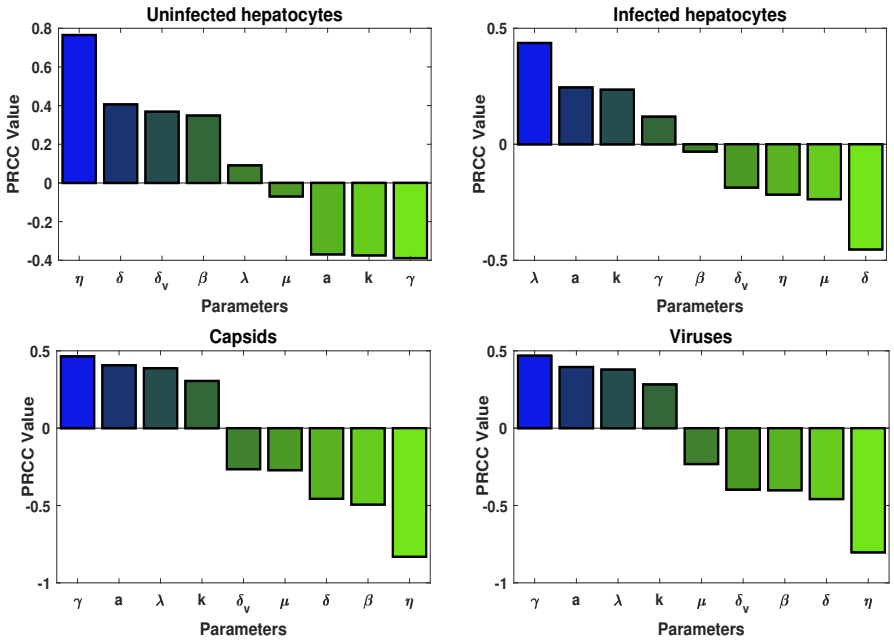

Figure 2.15: PRCC values of parameters corresponding to uninfected hepatocytes, infected hepatocytes, capsids and viruses classes at time $t = 1200^{th}$ day are plotted.

Table 2.2: PRCC values and p-values of the model parameters.

PRCC value and P-value of each parameter in $X(t)$

$X(t)$	Parameters	η	δ	δ_v	β	λ	μ	a	k	γ
	PRCC value	0.7648	0.4059	0.3681	0.3482	0.0905	-0.0697	-0.3691	-0.3744	-0.3886
	P-value	0	0	0	0	0.00419	0.027496	0	0	0

PRCC value and P-value of each parameter in $Y(t)$

$Y(t)$	Parameters	λ	a	k	γ	β	δ_v	η	μ	δ
	PRCC value	0.4364	0.2447	0.2349	0.1187	-0.0316	-0.1864	-0.2168	-0.2365	-0.4532
	P-value	0	0	0	0.000168	0.317476	2.90E-09	0	0	0

PRCC value and P-value of each parameter in $U(t)$

$U(t)$	Parameters	λ	μ	k	a	β	δ	δ_v	γ	η
	PRCC value	0.3871	-0.2712	0.3048	0.4065	-0.4939	-0.4567	-0.2648	0.4639	-0.8312
	P-value	0	0	0	0	0	0	0	0	0

PRCC value and P-value of each parameter in $V(t)$

$V(t)$	Parameters	γ	a	λ	k	μ	δ_v	β	δ	η
	PRCC value	0.468	0.3949	0.3782	0.2823	-0.2317	-0.3971	-0.4011	-0.458	-0.8025
	P-value	0	0	0	0	0	0	0	0	0

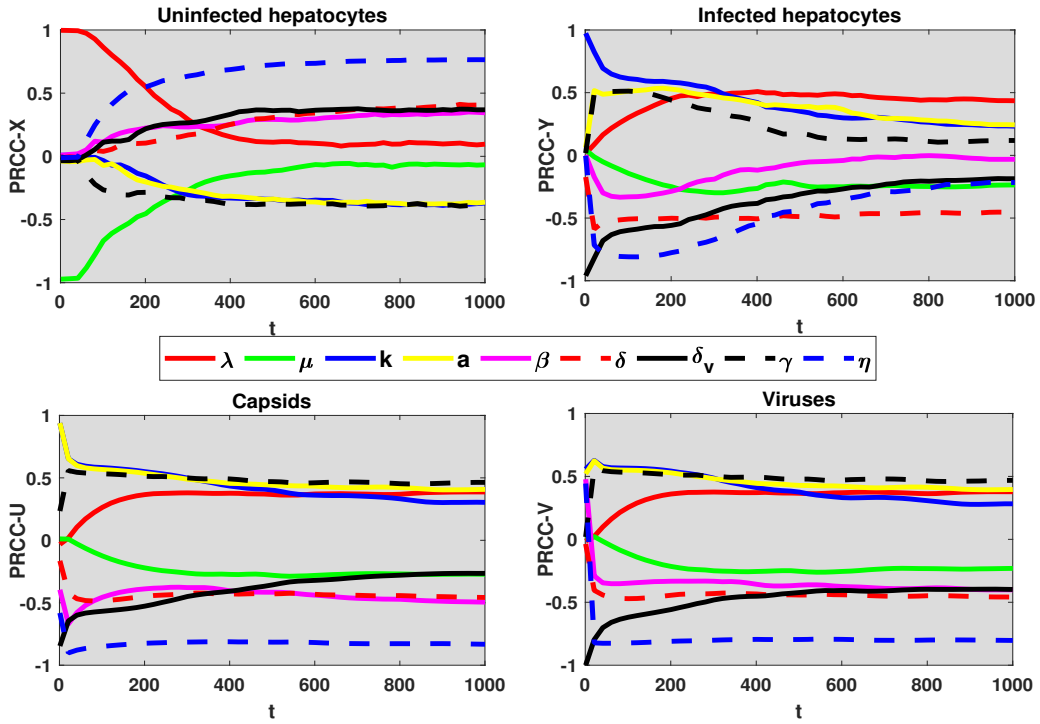

Figure 2.16: PRCC value of each parameter over the entire time period of the infection for all compartments.

2.9 Conclusions

In this study, HBV infection dynamics is modeled based on the biological findings. In order to describe this viral infection in a more realistic way, the recycling effects of capsids are incorporated into this proposed model. The inclusion of recycling effects leads to a notable paradigm shift in the outcomes of the model. The non-negativity and boundedness of the solutions for any non-negative initial condition establish the feasibility of the system. The stability analysis of the system indicates that both the equilibrium points are globally asymptotically stable under some conditions (disease-free: $R_0 < 1$, endemic: $R_0 > 1$), *i.e.*, the patient will either achieve a full recovery, or the viral infection will persist at a stable level for the rest of the life. Upon comparing the model solution with the experimental data collected from two chimpanzees [100], it is seen that the model solution agrees well with the experimental data. Hence, the proposed model effectively can capture and represent the intricate dynamics of HBV infection, making it a more realistic and reliable tool for studying this disease. In addition, it is further observed that due to recycling, the viral load

increases considerably. The long-term behavior of parameters are also discussed through global sensitivity analysis by applying the LHS-PRCC method.

From the simulated results, the following findings are observed.

1. Most of the mathematical models on HBV infection developed so far, underestimate the production of virions and suppress the production of capsids as the recycling effects of capsids were ignored. Consequently, these models fail to capture the actual dynamics of HBV infection, whereas, the proposed model shows a more realistic production of virions and the actual dynamics of the infection.

2. Recycling rate of capsids (γ) is one of the deciding parameters to determine the severity of infection. So, it is very important to pay attention to this kind of parameter while proposing any new strategy to control this disease.

3. This study analyses the effects of volume fraction of capsids (η) on disease dynamics probably for the first time. It is found that the inclusion of recycling of capsids reverses the effects of volume fraction on the infection. This is a striking outcome of the present study that changes the usual understandings of viral dynamics. So, volume fraction of capsids emerges as a viable member in the set of disease-controlling parameters.

4. It is also observed that the number of released viruses increases in spite of low virus production rate due to recycling of capsids. Though this result appears to be contradictory to the known fact, but our study has clearly explained this new findings. In order to gain deeper insights about this infection, the emergence of this unusual behavior becomes very important. On the other words, the recycling of capsids acts as a positive feedback loop in this viral infection.

5. Based on the value of partial rank correlation coefficient, the global sensitivity analysis unequivocally identifies that the disease progression is highly influenced by the volume fraction of capsids as well as its recycling rate. These findings highlight the pivotal role of these two factors in shaping the dynamics of the disease and warrant further attention in future studies.

6. The strong concurrence between the model solution and the experimental data substantiates that the proposed model is biologically reliable.

CHAPTER 3

The Effects of Fractional-order Derivative on Hepatitis B Virus Infection

In this chapter, incorporating Caputo fractional derivative into model (2.2.1) proposed in chapter 2, we obtain two nonlinear fractional-order model on HBV infection dynamics. Each model comprises four compartments: susceptible hepatocytes, infected hepatocytes, HBV capsids, and viruses. In the first model, the order of fractional derivative is same for all compartments, while in the second model, the orders are incommensurate. We discuss the existence and uniqueness of the solutions for both models separately. Stability analyses are carried out theoretically for both models. Numerical solutions are obtained using the predictor-corrector Adams-Bashforth-Moulton method for commensurate-order model and the implicit product integration of the trapezoidal type method for incommensurate-order model considering various choices of fractional orders and initial conditions. The aim of this chapter is to find how the dynamics of infection is influenced by the order of fractional order derivatives.

3.1 Introduction

For many real-life problems, fractional derivatives play an important role in model development. There are several reasons behind these. The most notable fact is that the fractional derivative is a non-local property of the functions as the calculation of the fractional derivative with respect to time at a point also depends on the previous times. In biology, fractional derivatives are crucial because the gene-based properties, such as growth rates, immune cell activities, and hereditary characteristics are highly individual [118]. Furthermore, the characteristics of cells and viruses are totally different. Viruses are capable of mutating themselves to escape from antiviral treatments [119]. Only fractional derivatives can capture all these intricate features. One can provide more realistic results and accurate predictions of virus dynamics using fractional derivatives. Besides mathematics, fractional derivatives have several applications in a variety of domains, including physics, finance, biology [120], medicine, ecology [121], and so on. There are several ways to define the fractional derivatives of a function, including the Riemann-Liouville definition, the Atangana-Baleanu derivative, the Caputo fractional derivative, etc. In the case of fractional differential equations (FDEs) with Caputo derivatives, one of its key advantages is that the initial conditions are the same as those for ordinary differential equations and have a physical interpretation relating to the real phenomena. Moreover, in this case, the fractional derivative of a constant is zero [91].

Inspired by the above discussion, two mathematical models of HBV infection are developed in this study. For the first model, the order of fractional derivative for each compartment is equal (commensurate order model), whereas in the second model, the orders are different (incommensurate model). The present models also include the recycling effects of newly produced HBV capsids. Standard incidence function which is more realistic for human diseases is used to formulate the models. We have demonstrated how the infection is influenced by the patient's initial conditions and the order of fractional derivative. The effects of the incommensurate order derivative on infection are well examined in this chapter. It is expected that this model provides a clear explanation of how memory, history, experiences, hereditary characteristics, and knowledge play a role in viral disease dynamics.

♣ *The contents of this chapter are published as an article titled "**Fractional-order models of hepatitis B virus infection with recycling effects of capsids**", Mathematical Methods in the Applied Sciences, 46 (14) (2023) 15599-15625.*

3.2 Model formulation

In recent years, the fractional-order derivatives have been widely used in modeling virus dynamics. One of the most common reasons is that fractional calculus, and more specifically, fractional derivatives have a direct connection to the memory of the systems. When we are first exposed to some viruses, our immune cells may not recognize or effectively combat them; however, cells learn from their experiences fighting against any pathogen. In most of the cases, the memory effects of cells are ignored in infection dynamics models while ordinary derivatives are considered. Another important thing is that the ordinary derivatives are local properties of the functions, whereas the fractional derivatives are non-local. As a result, prior memory is required to compute the fractional derivatives with respect to time. Furthermore, by using fractional derivatives into the model, the errors caused by ignoring the memory effects of variables can be reduced. In explaining the dynamics of HBV infection, fractional-order derivatives are more precise than ordinary derivatives. Due to these advantages, incorporating the Caputo fractional derivative into model (2.2.1), two fractional-order models are considered. The recycling effects of HBV DNA-containing capsids are also taken into account. The commensurate fractional order model is developed as follows: In order to ensure the consistency of fractional-order model in context of dimension, it is very important to make equal dimension of each model compartment. The unit of $\frac{d}{dt}$ is time^{-1}, whereas the unit of $\frac{d^\alpha}{dt^\alpha}$ is time$^{-\alpha}$, $0 < \alpha \leq 1$. To avoid this inconsistency in dimension, the techniques given in the articles [122, 123] are adopted. A new parameter Ω (called characteristic time) is introduced in the following general form:

$$\frac{d}{dt} \to \frac{1}{\Omega^{1-\alpha}} \frac{d^\alpha}{dt^\alpha}$$

The dimension of $\Omega^{1-\alpha}$ is time$^{1-\alpha}$. It is called a fractional time parameter that represents the fractional time components in the system. Therefore, incorporating Caputo fractional order derivative into the system (2.2.1), we get the following fractional-order model given by

$$\left.\begin{aligned}
\frac{1}{\Omega^{1-\alpha}} {}_0^C D_t^\alpha X(t) &= \bar{\lambda} - \bar{\mu} X(t) - \bar{k} V(t) X(t), \\
\frac{1}{\Omega^{1-\alpha}} {}_0^C D_t^\alpha Y(t) &= \bar{k} V(t) X(t) - \bar{\delta} Y(t), \\
\frac{1}{\Omega^{1-\alpha}} {}_0^C D_t^\alpha U(t) &= \bar{a} Y(t) + \bar{\gamma}(1-\eta) U(t) - \eta \bar{\beta} U(t) - \bar{\delta} U(t), \\
\frac{1}{\Omega^{1-\alpha}} {}_0^C D_t^\alpha V(t) &= \eta \bar{\beta} U(t) - \bar{\delta}_v V(t),
\end{aligned}\right\} \tag{3.2.1}$$

where ${}_0^C D_t^\alpha$ represents Caputo derivative of order α, $0 < \alpha \leq 1$. Considering $\lambda = \Omega^{1-\alpha}\bar{\lambda}$, $\mu = \Omega^{1-\alpha}\bar{\mu}$, $k = \Omega^{1-\alpha}\bar{k}$, $\delta = \Omega^{1-\alpha}\bar{\delta}$, $a = \Omega^{1-\alpha}\bar{a}$, $\gamma = \Omega^{1-\alpha}\bar{\gamma}$, $\beta = \Omega^{1-\alpha}\bar{\beta}$ and $\delta_v = \Omega^{1-\alpha}\bar{\delta}_v$, the system (3.2.1) can be written as

$$\left.\begin{aligned} {}_0^C D_t^\alpha X(t) &= \lambda - \mu X(t) - kX(t)V(t), \\ {}_0^C D_t^\alpha Y(t) &= kV(t)X(t) - \delta Y(t), \\ {}_0^C D_t^\alpha U(t) &= aY(t) + \gamma(1-\eta)U(t) - \eta\beta U(t) - \delta U(t), \\ {}_0^C D_t^\alpha V(t) &= \eta\beta U(t) - \delta_v V(t), \end{aligned}\right\} \tag{3.2.2}$$

where, $X(0) = X_0 \geq 0$, $Y(0) = Y_0 \geq 0$, $U(0) = U_0 \geq 0$ and $V(0) = V_0 \geq 0$ are supposed to be non-negative initial conditions. There are four dependent variables in the system (3.2.2). Generally, it is considered that $\Omega = 1$ in the fractional-order system (more details are available in the article of Pan et al. [124]). The descriptions of all model parameters are given in Table 2.1 (chapter 2).

3.3 Existence, uniqueness, non-negativity, and boundedness of solution

The existence of the solution of the system (3.2.2) follows from the article of Lin Wei [94]. In order to establish the uniqueness of the solution, it is necessary to show the boundedness of the solution first.

3.3.1 Boundedness of solution

Theorem 3.3.1. *For any non-negative initial condition, the solutions of the system (3.2.2) are bounded provided* $R_s := \eta\beta - (1-\eta)\gamma + \delta > 0$.

Proof. We recall the variable $F(t)$, and parameter ρ^*. Both are defined in chapter 2 where $F(t) = X(t) + Y(t)$ and $\rho^* = \min\{\mu, \delta\}$. Then, from system of FDEs (3.2.2), we have

$${}_0^C D_t^\alpha F(t) = {}_0^C D_t^\alpha X(t) + {}_0^C D_t^\alpha Y(t) = \lambda - \mu X(t) - \delta Y(t) \leq \lambda - \mu F(t).$$

Consider the equation

$$Z^*(t) = {}_0^C D_t^\alpha F(t) - \lambda + \mu F(t). \tag{3.3.1}$$

Clearly, $Z^*(t) \leq 0$ for $t \geq 0$. Applying Laplace transform both sides of (3.3.1), we have

$$F_L(s) = \frac{Z_L^*(s)}{s^\alpha + \mu} + \frac{s^{\alpha-1}}{s^\alpha + \mu}F(0) + \frac{\lambda}{s(s^\alpha + \mu)}, \tag{3.3.2}$$

where $Z_L^*(s) = \mathcal{L}\{Z^*(t)\}$, $F_L(s) = \mathcal{L}\{F(t)\}$. Taking inverse Laplace transform, we have

$$\begin{aligned} F(t) &= \mathcal{L}^{-1}\left\{Z_L^*(s)\frac{1}{s^\alpha + \mu}\right\} + \mathcal{L}^{-1}\left\{\frac{s^{\alpha-1}}{s^\alpha + \mu}\right\}F(0) + \mathcal{L}^{-1}\left\{\frac{\lambda}{s(s^\alpha + \mu)}\right\}, \\ &= \mathcal{L}^{-1}\left\{Z_L^*(s)\frac{1}{s^\alpha + \mu}\right\} + E_\alpha(-\mu t^\alpha)F(0) + \frac{\lambda}{\mu}\left\{1 - E_\alpha(-\mu t^\alpha)\right\}. \end{aligned} \tag{3.3.3}$$

In order to calculate $\mathcal{L}^{-1}\left\{Z_L^*(s)\frac{1}{s^\alpha + \mu}\right\}$, the well-known convolution theorem of Laplace transform is used here. $\mathcal{L}^{-1}\left\{Z_L^*(s)\right\} = Z^*(t)$ and $\mathcal{L}^{-1}\left\{\frac{1}{s^\alpha + \mu}\right\} = t^{\alpha-1}E_\alpha(-\mu t^\alpha)$. Therefore,

$$\mathcal{L}^{-1}\left\{Z_L^*(s)\frac{1}{s^\alpha + \mu}\right\} = \int_0^t (t-\tau)^{\alpha-1}E_\alpha\left(-\mu(t-\tau)^\alpha\right)Z^*(\tau)d\tau \leq 0, \tag{3.3.4}$$

because $(t-\tau) \geq 0$, $E_\alpha\left(-\mu(t-\tau)^\alpha\right) > 0$ and $Z^*(t) \leq 0$. From equation (3.3.3) and (3.3.4), it is obtained

$$\begin{aligned} F(t) &= \int_0^t (t-\tau)^{\alpha-1}E_\alpha\left(-\mu(t-\tau)^\alpha\right)F(\tau)d\tau + E_\alpha(-\mu t^\alpha)F(0) + \frac{\lambda}{\mu}\left\{1 - E_\alpha(-\mu t^\alpha)\right\}, \\ \implies F(t) &\leq E_\alpha(-\mu t^\alpha)F(0) + \frac{\lambda}{\mu}\left\{1 - E_\alpha(-\mu t^\alpha)\right\}. \end{aligned} \tag{3.3.5}$$

By definition (1.2.7), $0 < E_\alpha(-\mu t^\alpha) \leq 1$ and $(1 - E_\alpha(-\mu t^\alpha)) \leq 1$. So, $F(t) \leq F(0) + \frac{\lambda}{\mu}$. Therefore, $F(t)$ is bounded and this implies that $X(t)$ and $Y(t)$ both are bounded functions. One can easily prove the boundedness of $U(t)$ by using the boundedness of $Y(t)$. Similarly, by using the boundedness of $U(t)$, the boundedness of $V(t)$ can be also shown. □

3.3.2 Uniqueness of solution

The system of equations (3.2.2) can be written as ${}_0^C D_t^\alpha W(t) = f(W(t))$ where,

$$W(t) = \begin{pmatrix} X(t) \\ Y(t) \\ U(t) \\ V(t) \end{pmatrix}, \text{and } f(W(t)) = \begin{pmatrix} \lambda - \mu X(t) - kX(t)V(t) \\ kV(t)X(t) - \delta Y(t) \\ aY(t) + \gamma(1-\eta)U(t) - \eta\beta U(t) - \delta U(t) \\ \eta\beta U(t) - \delta_v V(t) \end{pmatrix}.$$

Let us consider

$$A_1 = \begin{pmatrix} \lambda \\ 0 \\ 0 \\ 0 \end{pmatrix}, \; A_2 = \begin{pmatrix} \mu & 0 & 0 & 0 \\ 0 & \delta & 0 & 0 \\ 0 & a & \gamma(1-\eta) - \eta\beta - \delta & 0 \\ 0 & 0 & \eta\beta & -\delta_v \end{pmatrix}, \; A_3 = \begin{pmatrix} -k & 0 & 0 & 0 \\ -k & 0 & 0 & 0 \\ 0 & 0 & 0 & 0 \\ 0 & 0 & 0 & 0 \end{pmatrix}.$$

Then, $f(W(t)) = A_1 + A_2W(t) + V(t)A_3W(t)$. Now,

$$\begin{aligned} ||f(W(t))|| &= ||A_1 + A_2W(t) + V(t)A_3W(t)|| \\ &\leq ||A_1|| + ||A_2||||W(t)|| + ||V(t)||||A_3||||W(t)|| \\ &\leq ||A_1|| + \left(||A_2|| + \frac{a\lambda\eta\beta}{\mu\delta_v(\eta\beta + \delta - \gamma(1-\eta))} ||A_3|| \right) ||W(t)||. \end{aligned}$$

[using boundedness of $V(t)$]

Taking $c_1 = ||A_1||$ and $c_2 = \left(||A_2|| + \frac{a\lambda\eta\beta}{\mu\delta_v(\eta\beta + \delta - \gamma(1-\eta))} ||A_3|| \right)$, the function $f(W(t))$ satisfies all the conditions of lemma (1.2.8). So, the solution of the system (3.2.2) is unique.

3.3.3 Non-negativity of solution

Since we deal with a biological phenomenon, it makes no sense if the system (3.2.2) has negative solution for some value of $t > 0$. The following theorem establishes the non-negativity of all state variables $X(t), Y(t), U(t),$ and $V(t)$.

Theorem 3.3.2. *For any non-negative initial condition, the solutions of the system (3.2.2) remain non-negative.*

Proof. From system (3.2.2), it can be easily obtained that

$$
\begin{aligned}
{}_0^C D_t^\alpha|_{X(t)=0} &= \lambda \geq 0,\\
{}_0^C D_t^\alpha|_{Y(t)=0} &= kV(t)X(t) \geq 0,\\
{}_0^C D_t^\alpha|_{U(t)=0} &= aY(t) \geq 0,\\
{}_0^C D_t^\alpha|_{V(t)=0} &= \eta\beta U(t) \geq 0.
\end{aligned}
$$

So, the solutions starting from non-negative initial conditions are non-negative by Lemma (1.2.9). □

3.4 Validation of the model with experimental data

Validation of a model is necessary to determine whether the model accurately represents the behavior of a system. According to the study of Wieland [125], seven chimpanzees were inoculated with 1 to 10^{10} genome equivalents (GE) of HBV DNA to determine the effects of viral inoculum dose on the outcome of the infection. Throughout the experiment, the chimpanzees were handled for humane use. It was observed that the concentration level of HBV DNA in five chimpanzees increased gradually and reached a pick level, then decreased and fell below the detectable levels at or before 39 weeks. Another two chimpanzees (labeled Ch1603 and Ch1616) which were initially inoculated with 10 GE of HBV DNA became infected for an extended period of time, or developed persistent infections. Our numerical solutions of the system (3.2.2) are compared with the experimental data obtained from the chimpanzee Ch1616 [125]. By minimizing the sum-of-squares error (SSE) between the model solution and experimental data, all parameters are estimated. The estimated values of each parameter lie within a realistic range. In Table 3.1, the estimated values of parameters are mentioned. The experimental data and numerical solutions are plotted in Figure 3.1. It is observed that the numerical solutions of the system agree well with the experimental data. Therefore, the proposed model is biologically sound and reliable.

3.5 Equilibrium points and basic reproduction number

Caputo fractional derivative of a constant is zero. Therefore, the equilibrium points of the system (3.2.2) can be obtained by solving the equations ${}_0^C D_t^\alpha X(t) = 0$, ${}_0^C D_t^\alpha Y(t) = 0$, ${}_0^C D_t^\alpha U(t) = 0$ and ${}_0^C D_t^\alpha V(t) = 0$. The system (3.2.2) has two equilibrium points or steady-states (E_0 and E_i) which are exactly same as the equilibrium points of the ODE

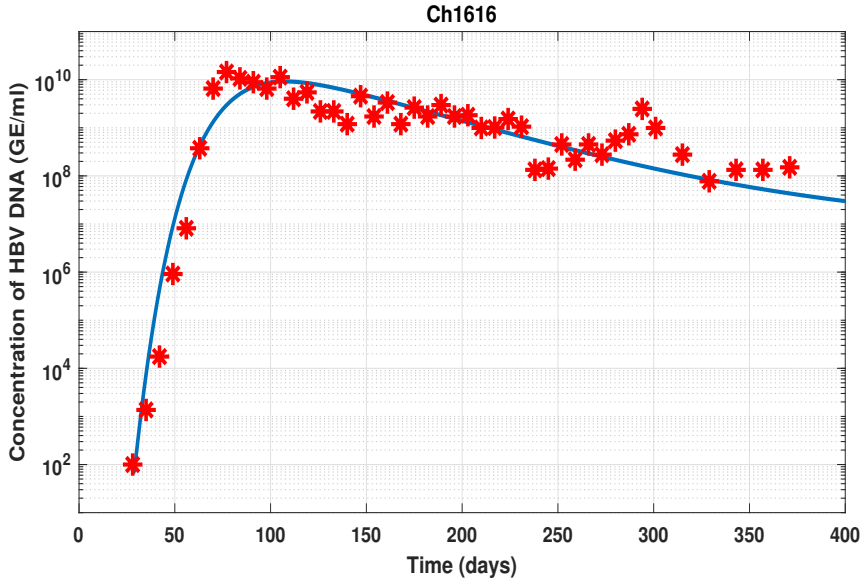

Figure 3.1: Outcomes of the infection of chimpanzee Ch1616. Here, the red circles denote the experimental data; the solid blue line represents the numerical solution of the system (3.2.2).

system (2.2.1). Moreover, the expression of basic reproduction number is also same for both model (2.2.1) and (3.2.2).

3.6 Stability of the equilibria

The local stability of these equilibrium points of the system (3.2.2) is established using the Routh-Hurwitz criteria [112]. All the eigenvalues of the Jacobian matrix for each equilibrium point are either negative or have the negative real part. So, $\min|\arg(\text{eigenvalues})| > \alpha\frac{\pi}{2}$ for $\alpha \in (0, 1]$, where the function $\arg(z)$ denotes the argument of the complex number z. The global stability of the equilibria can be shown by using the same Lyapunov functionals $\mathcal{L}_1(t)$ and $\mathcal{L}_2(t)$ which are defined in chapter 2 under the conditions: (i) $R_0 \leq 1$ for disease-free steady-state, and (ii) $R_0 > 1$ for endemic steady-state.

3.7 Numerical simulation

In general, the mathematical models related to biological phenomena are nonlinear and complicated in nature. So, it is not always easy to solve the models analytically. Researchers often use numerical methods to find the solutions. In this section, the predictor-corrector

Table 3.1: Estimated values of model parameters.

Parameters	Values (units)
λ	2.6×10^7 (cells ml^{-1}day^{-1})
k	5.28×10^{-12} (ml virion^{-1}day^{-1})
a	140 (capsids cell^{-1}day^{-1})
γ	0.446 (day^{-1})
β	1.52 (day^{-1})
η	$0 \leq \eta \leq 1$ (0.9) (unitless)
μ	0.06 (day^{-1})
δ	0.09 (day^{-1})
δ_v	4.99 (day^{-1})

Adams–Bashforthm–Moulton (ABM) method [126] is used to solve the commensurate order model (3.2.2) because ABM method has higher order accuracy and is easy to implement. This method also takes less time in simulation. One more important advantage of this method is that it can handle the stiff differential equations and can be applied for multi-term FDEs. Various types of possible outcomes related to the HBV infection dynamics are discussed here.

3.7.1 Disease-free

The disease-free equilibrium point always exists, and it is stable when $R_0 < 1$. Figure 3.2 presents the outcomes of uninfected cells, infected cells, capsids, and viruses for five different values of fractional order α. The values of the parameters used in the simulation are shown in Table 3.1, and the corresponding value of R_0 is $0.3688 < 1$, which implies that the infection will eventually die out regardless of any medical intervention. Five values of $\alpha(= 1, 0.95, 0.90, 0.85, 0.80)$ are considered here. Based on the results shown in Figure 3.2, it is observed that fractional-order has significant effects on dynamics of all compartments. In each case, solutions of the system converge to the disease-free equilibrium point $(4.33 \times 10^8, 0, 0, 0)$. The numerical studies on α reveal that the solution of the system converges more quickly to the equilibrium point for higher value of α, *i.e.*, the convergence rate increases while α increases. It is also seen that smaller values of α result in a longer period of infection, which indicates that a long time is required to cure the disease. On the other hand, Figure 3.3 illustrates the results corresponding to three different initial states. In this case, the order of the fractional derivative is kept fixed ($\alpha = 0.8$). It is observed that initial conditions

have no effect on the stability of the disease-free equilibrium point.

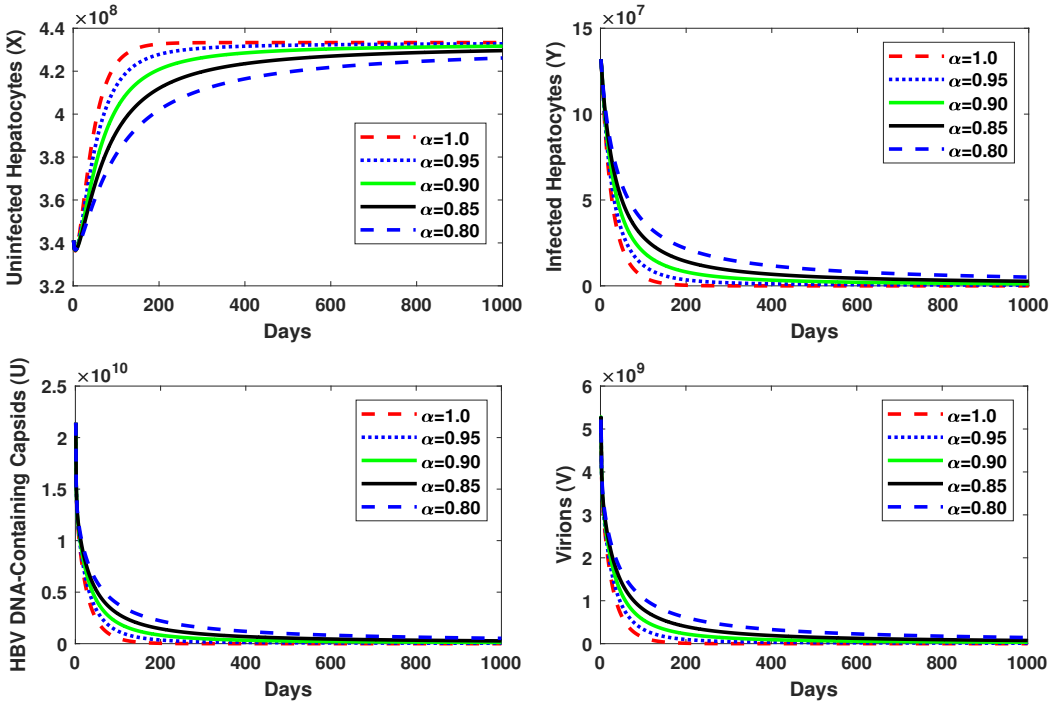

Figure 3.2: Time series of the system (3.2.2) for different order of fractional derivative (α) when $R_0 < 1$.

3.7.2 Endemic

In Figure 3.4 and Figure 3.5, the numerical solutions are plotted when $R_0 > 1$. Figure 3.4 shows the dynamics of infection for different orders of fractional derivatives. Figure 3.5 displays the results for three different initial conditions. In Figure 3.4, the simulations are performed for five different values of fractional derivative ($\alpha = 1.0, 0.95, 0.90, 0.85, 0.80$). The trajectories of all populations oscillate in each case for a period of time before approaching the endemic equilibrium point $(1.45 \times 10^8, 1.91 \times 10^8, 1.90 \times 10^{10}, 5.20 \times 10^9)$ as shown in Figure 3.4. The initial conditions are the same as in disease-free case. It is also observed from Figure 3.4 that with the increase in α, the infection rate increases sharply, and the peaks of the solutions occur early. However, with time the condition of the patient becomes stable irrespective of values of α. The solutions converge quickly to the steady state for higher value of α, which means that the long-term memory behavior of cells increases the instability of the disease. It is also noticed from Figure 3.5 that for each initial condition,

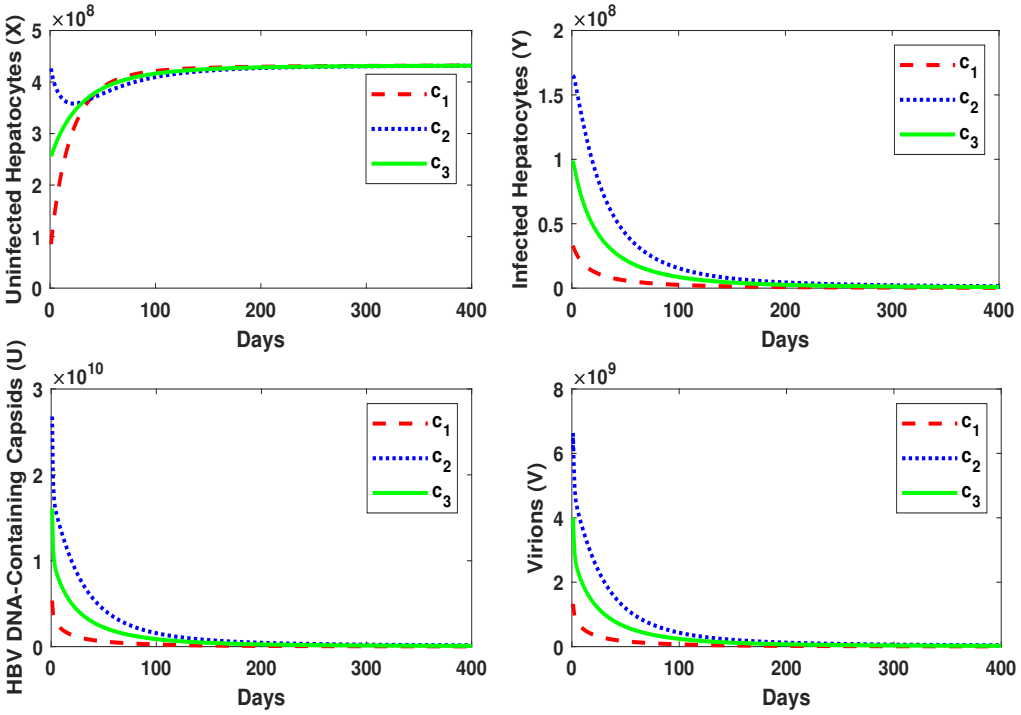

Figure 3.3: The time series of the system (3.2.2) for three different initial conditions ic_1, ic_2, ic_3 where $ic_1 = (8.53 \times 10^7; 3.3 \times 10^7; 5.36 \times 10^9; 1.23 \times 10^9)$, $ic_2 = (4.0 \times 10^8; 1.0 \times 10^8; 2.68 \times 10^{10}; 6.15 \times 10^9)$, $ic_3 = (2.5 \times 10^8; 9.9 \times 10^8; 1.6 \times 10^{10}; 3.6 \times 10^9)$ and the parameter's value are taken from Table 3.1.

the endemic equilibrium point exists and is globally asymptotically stable. So, the numerical results support the theoretical findings. As a consequence, fractional derivatives, *i.e.*, the memories of the system highly influence the dynamics of infection.

3.8 Modified model with incommensurate order of fractional derivatives

In literature, most of the mathematical models [123, 127, 128] have described the viral dynamics using fractional differential equations with commensurate order. The authors of these articles overlooked the fact that cells and viruses have different capacities to store memories and experiences. It is well-known fact that the characteristics of cells and viruses are different. The viral strain can change through countless mechanisms in order to escape from its host's immune system [119]. In accordance with these, their memory effects differ significantly for future actions. In order to capture all of these phenomena in a mathematical

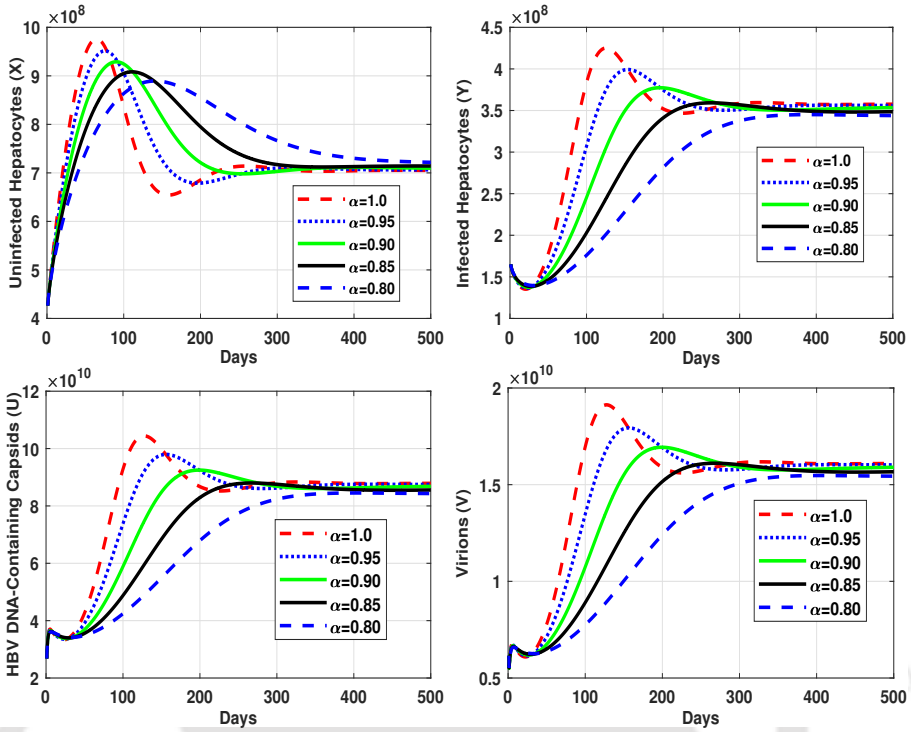

Figure 3.4: The time series of the system (3.2.2) for different order of fractional derivative (α) when $R_0 > 1$.

model, the system (3.2.2) is modified by considering different order fractional derivatives for susceptible cells, infected cells, capsids, and viruses. As a result, the following modified FDE model with incommensurate orders is obtained as follows:

$$\left.\begin{aligned} {}_0^C D_t^{\alpha_1} X(t) &= \lambda - \mu X(t) - kX(t)V(t), \\ {}_0^C D_t^{\alpha_2} Y(t) &= kV(t)X(t) - \delta Y(t), \\ {}_0^C D_t^{\alpha_3} U(t) &= aY(t) + \gamma(1-\eta)U(t) - \eta\beta U(t) - \delta U(t), \\ {}_0^C D_t^{\alpha_4} V(t) &= \eta\beta U(t) - \delta_v V(t), \end{aligned}\right\} \tag{3.8.1}$$

where $\alpha_1, \alpha_2, \alpha_3, \alpha_4$ are the orders of fractional derivatives for susceptible cells, infected cells, capsids, and viruses, respectively. The system (3.8.1) can be written as

$$ {}_0^C D_t^{\alpha} W(t) = f(t, W(t)),\ t \in [0, \infty), \tag{3.8.2}$$

where, $W(t) = (X(t), Y(t), U(t), V(t))'$, and $W(t) : [0, \infty) \to \mathbb{R}_+^4$ is a vector-valued function. $\alpha = (\alpha_1, \alpha_2, \alpha_3, \alpha_4) \in (0, 1]^4$, $f = (f_1, f_2, f_3, f_4)'$ and $f : [0, \infty) \times \mathbb{R}_+^4 \to \mathbb{R}^4$ is a continuous function. Each component function f_i satisfies the Lipchitz condition with respect to the

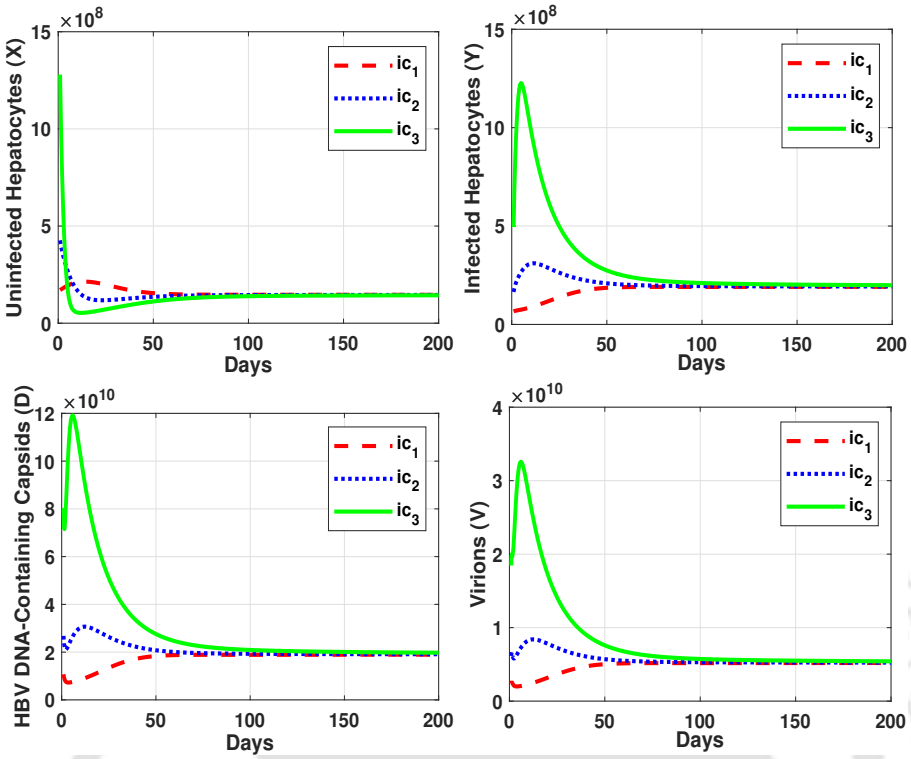

Figure 3.5: The time series of the system (3.2.2) for three different initial condition ic_1, ic_2, ic_3 where ic_1, ic_2, ic_3 are given in Figure 3.3.

variable $W(t)$. Corollary 2.4 of the work of Diethelm et al. [129] guarantees the existence and uniqueness of solutions of the system (3.8.1).

The solutions of the modified system (3.8.1) remains non-negative and bounded under non-negative initial conditions. In order to find out the changes of dynamics of the system (3.8.1), numerical simulations are conducted for both commensurate and incommensurate order models. In this case, to solve the systems of FDEs (3.8.1) numerically, the Implicit Product-Integration of trapezoidal type method is used [130] for the incommensurate order model, although there are some other numerical schemes available to solve multi-order system of fractional differential equation, such as Explicit Product-Integration of rectangular type, Implicit Product-Integration of rectangular type, Product-Integration with predictor-corrector [130]. It is verified that each scheme produces almost similar solution of the system (3.8.1). Consider the case of $R_0 < 1$ and pick the value of the parameters from Table 3.1. Four different orders of fractional derivative, namely, $\alpha_1 = 0.95, \alpha_2 = 0.85, \alpha_3 = 0.75$ and $\alpha_4 = 0.65$ are considered for the incommensurate order model. For the commensurate order model, $\alpha = 0.8$ is used. Initial condition ic_1 is taken into account to start the simulation. A significant change is observed in the solutions of the incommensurate order model. Both solutions approach

the steady-states, but their convergence rates are different. In Figure 3.6, the numerical solutions of both systems are plotted.

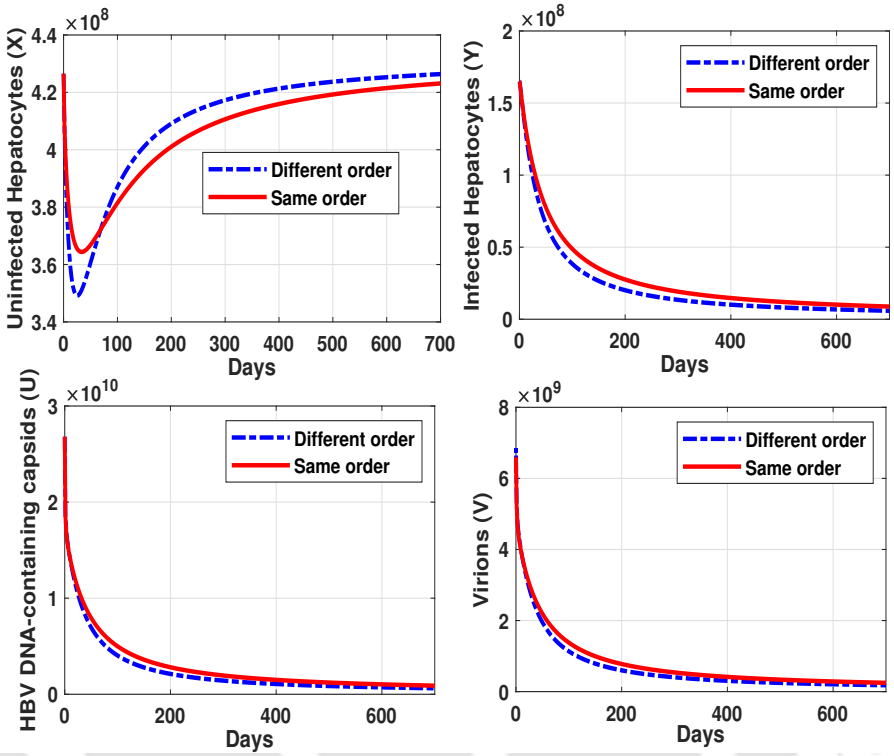

Figure 3.6: Numerical solutions of systems (3.2.2) and (3.8.1) are presented here. For incommensurate order model, the derivative orders are considered as follows: $\alpha_1 = 0.95, \alpha_2 = 0.85, \alpha_3 = 0.75$ and $\alpha_4 = 0.65$. For commensurate order model, we take $\alpha = 0.8$. Blue dotted curves represent the solutions for incommensurate order and continuous red curves represent the solutions of commensurate order model.

3.9 Stability analysis of incommensurate order model

The equilibrium solutions of the system (3.8.1) can be found by solving the equations ${}_0^C D_t^{\alpha_1} X(t) = 0$, ${}_0^C D_t^{\alpha_2} Y(t) = 0$, ${}_0^C D_t^{\alpha_3} U(t) = 0$, and ${}_0^C D_t^{\alpha_4} V(t) = 0$. In this case, the equilibrium points are $E_u = (X_0, Y_0, U_0, V_0)$ and $E_i = (X_1, Y_1, U_1, V_1)$ as mentioned in chapter 2. In order to determine the stability of these equilibrium points, the Jacobian matrix of the system (3.8.1) is calculated as:

$$J = \begin{bmatrix} -\mu - kV(t) & 0 & 0 & -kX(t) \\ kV(t) & -\delta & 0 & kX(t) \\ 0 & a & \gamma(1-\eta) - \eta\beta - \delta & 0 \\ 0 & 0 & \eta\beta & -\delta_v \end{bmatrix}. \tag{3.9.1}$$

3.9.1 Stability of disease-free equilibrium (E_u) for incommensurate model (3.8.1)

In order to show the local stability of E_u, the similar criteria for asymptotic stability of autonomous fractional systems discussed by Lenka and Banerjee [96] are used here. The Jacobian matrix evaluated at $E_u = \left(\frac{\lambda}{\mu}, 0, 0, 0\right)$ is

$$J\big|_{E_u} = \begin{bmatrix} -\mu & 0 & 0 & -k\lambda/\mu \\ 0 & -\delta & 0 & k\lambda/\mu \\ 0 & a & \gamma(1-\eta) - \eta\beta - \delta & 0 \\ 0 & 0 & \eta\beta & -\delta_v \end{bmatrix}. \tag{3.9.2}$$

In order to apply lemma (1.2.10) to the system (3.8.1), values of order of fractional derivative $\alpha_1, \alpha_2, \alpha_3$, and α_4 are chosen as rational number, and $\alpha_i \in (0, 1], i = 1, 2, 3, 4$. It is assumed that M is the least common multiple of the denominators q_i's of α_i's, where $\alpha_i = \frac{p_i}{q_i}$ such that $\gcd(p_i, q_i) = 1$ with $p_i, q_i \in \mathbb{N}, i = 1, 2, 3, 4$. Consider the characteristic equation of the Jacobian matrix (3.9.2) as

$$\det \begin{bmatrix} -\mu - x^{M\alpha_1} & 0 & 0 & -k\lambda/\mu \\ 0 & -\delta - x^{M\alpha_2} & 0 & k\lambda/\mu \\ 0 & a & \gamma(1-\eta) - \eta\beta - \delta - x^{M\alpha_3} & 0 \\ 0 & 0 & \eta\beta & -\delta_v - x^{M\alpha_4} \end{bmatrix} = 0. \tag{3.9.3}$$

Clearly, some of the roots of equation (3.9.3) can be found by solving the equation

$$x^{M\alpha_1} = -\mu. \tag{3.9.4}$$

Now, by using De-Moivre's formula, the roots of the equation (3.9.4) are obtained as

$$x_n = (-\mu)^{\frac{1}{M\alpha_1}} \left\{ \cos\left(\frac{(2n+1)\pi}{M\alpha_1}\right) + i \sin\left(\frac{(2n+1)\pi}{M\alpha_1}\right) \right\}, \tag{3.9.5}$$

where $n = 0, 1, 2, ..., (M\alpha_1 - 1)$. It is observed that $|\arg(x_n)| = \frac{\pi}{M\alpha_1}, \frac{3\pi}{M\alpha_1}, ..., \frac{(2M\alpha_1 - 1)\pi}{M\alpha_1}$. By the definition of α_1, $|\arg(x_n)| > \frac{\pi}{2M}$ for $n = 0, 1, 2, ..., (M\alpha_1 - 1)$. So, the stability conditions are satisfied by these eigenvalues. The remaining roots of (3.9.3) can be obtained by solving the equation

$$\det \begin{bmatrix} -\delta - x^{M\alpha_2} & 0 & k\lambda/\mu \\ a & \gamma(1-\eta) - \eta\beta - \delta - x^{M\alpha_3} & 0 \\ 0 & \eta\beta & -\delta_v - x^{M\alpha_4} \end{bmatrix} = 0. \tag{3.9.6}$$

Simplification of (3.9.6) gives

$$\begin{aligned} x^{M(\alpha_2+\alpha_3+\alpha_4)} + \delta_v x^{M(\alpha_2+\alpha_3)} + (-\gamma + \delta + \beta\eta + \gamma\eta) x^{M(\alpha_2+\alpha_4)} + \delta x^{M(\alpha_3+\alpha_4)} \\ + \delta_v(-\gamma + \delta + \beta\eta + \gamma\eta) x^{M\alpha_2} + \delta_v \delta x^{M\alpha_3} + \delta(-\gamma + \delta + \beta\eta + \gamma\eta) x^{M\alpha_4} \\ + \beta\delta_v\delta\eta + \delta_v\gamma\delta\eta - \delta_v\gamma\delta + \delta_v\delta^2 - \frac{a\beta\eta k\lambda}{\mu} = 0. \end{aligned} \tag{3.9.7}$$

All the coefficients of the polynomial equation (3.9.7) are positive. Therefore, according to Descartes' rule of sign, equation (3.9.7) has no positive root. So, the eigenvalues are either negative real numbers or complex conjugate. In order to show the stability of E_0, two cases are considered which are described below:

(i) Commensurate order: Let $\alpha_2 = \alpha_3 = \alpha_4 = \alpha < 1$. In this case, the incommensurate order model (3.8.1) is converted to commensurate order model (3.2.2). Hence, the stability is established in Section 3.6.

(ii) Incommensurate order: Let $\alpha_2 \neq \alpha_3 \neq \alpha_4$ and $0 < \alpha_i \leq 1$ for $i = 2, 3, 4$. If the eigenvalues of equation (3.9.6) satisfies the condition

$$|\arg(x_n)| > \frac{\pi}{2M} \text{ for } n = 1, 2, ..., M(\alpha_2 + \alpha_3 + \alpha_4), \tag{3.9.8}$$

then E_0 becomes asymptotically stable. To support this result, an example is presented. The parameters' values are taken from Table 3.1 and $\eta = 0.8$. The corresponding value

of R_0 is $0.3163 < 1$. The values of $\alpha_1 = 0.95, \alpha_2 = 0.90, \alpha_3 = 0.85$ and $\alpha_4 = 0.80$ are considered. For these values of fractional orders, equation (3.9.3) becomes

$$\begin{aligned} &x^{70} + 3.8x^{54} + 0.610371x^{53} + 0.053x^{52} + 0.01x^{51} + 2.31941x^{37} + 0.2014x^{36} \\ &+ 0.0703496x^{35} + 0.00610371x^{34} + 0.00053x^{33} + 0.0775982x^{19} + 0.0231941x^{18} \\ &+ 0.002014x^{17} + 0.000323496x^{16} + 0.000775982 = 0. \end{aligned} \tag{3.9.9}$$

Consequently, one gets $\min_i |\arg(\lambda_i)| \approx 0.16534$, where λ_i's are the roots of the equation (3.9.9) and $\frac{\pi}{2M} = \frac{\pi}{40} \approx 0.07853$. Thus, $\min_i |\arg(\lambda_i)| > \frac{\pi}{2M}$. Hence, by lemma (1.2.10), it follows that the equilibrium point E_u becomes locally asymptotically stable. A visual representation of the region of stability is shown in Figure 3.7.

3.9.2 Stability of the endemic equilibrium (E_i) for incommensurate model (3.8.1)

In endemic case, the value of R_0 should be greater than one. In order to have this, the virus-to-cell infection rate (k) is considered to be 1.67×10^{-12} as mentioned in the article of Ciupe et al. [131]. Rest of the parameters are kept fixed as shown in Table 3.1 and $\eta = 0.8$. In this case, $R_0 = 3.164$ (> 1).
The Jacobian matrix of the system (3.8.1) at E_i is given by

$$J\Big|_{E_i} = \begin{bmatrix} -\mu - kV_1 & 0 & 0 & -kX_1 \\ kV_1 & -\delta & 0 & kX_1 \\ 0 & a & \gamma(1-\eta) - \eta\beta - \delta & 0 \\ 0 & 0 & \eta\beta & -\delta_v \end{bmatrix} \tag{3.9.10}$$

The characteristic equation becomes

$$\det \begin{bmatrix} -\mu - kV_1 - x^{M\alpha_1} & 0 & 0 & -kX_1 \\ kV_1 & -\delta - x^{M\alpha_2} & 0 & kX_1 \\ 0 & a & \gamma(1-\eta) - \eta\beta - \delta - x^{M\alpha_3} & 0 \\ 0 & 0 & \eta\beta & -\delta_v - x^{M\alpha_4} \end{bmatrix} = 0, \tag{3.9.11}$$

where the values of $\alpha_1, \alpha_2, \alpha_3,\ \alpha_4$ and M are taken the same as considered in Section 3.9.1. It is noticed that $\min|\arg(\lambda_i)| \approx 0.160527$, and $\frac{\pi}{2M} = \frac{\pi}{40} \approx 0.07853$. This implies that $\min|\arg(\lambda_i)| > \frac{\pi}{2M}$. Therefore, the equilibrium point is locally asymptotically stable based on the lemma (1.2.10). Figure 3.7 displays the stable and unstable regions.
Based on the qualitative analysis of the incommensurate order model (3.8.1), the following results are found:

- The disease-free equilibrium point exists for all values of R_0, and it will be asymptotically stable if $R_0 < 1$ and all eigenvalues of the equation (3.9.6) hold the inequality (1.2.10).
- The endemic equilibrium point exists only if $R_0 > 1, R_s > 0$ and is asymptotically stable if all eigenvalues of the equation (3.9.11) satisfy the condition (1.2.10).

Remark 3.9.1. In the above discussion, it is shown that both equilibrium points E_u and E_i are locally asymptotically stable for a set of fractional order $(\alpha_1, \alpha_2, \alpha_3, \alpha_4)$. In addition, for some other values of $\alpha_i \in (0, 1] \cap \mathbb{Q},\ i = 1, 2, 3, 4$, the stability of the system is verified numerically. In each of the case, $\min|\arg(\lambda_i)| > \frac{\pi}{2M}$ for both of the equilibrium points.

3.10 The effects of incommensurate orders on the system

In section 3.7, it is seen that α has notable impacts on the infection dynamics. Additionally, it is also relevant to identify that component of α which has a relatively greater impact on infection. For this purpose, we concentrate on each component of α and explain their roles in disease dynamics with proper justifications. Disease-free and endemic both the cases are considered here.

3.10.1 Effects of α_1 on all compartments of the model

In Figure 3.8, the effects of α_1 are demonstrated. We set $\alpha_1 = 0.3 : 0.1 : 1$, and $\alpha_2 = \alpha_3 = \alpha_4 = 0.9$ for simulation purpose.

- **Disease-free case:** As α_1 increases, there is a rapid increase in the number of uninfected hepatocytes. No significant change is observed in infected hepatocytes, capsids, and viruses compartments, but in each case, biphasic clearance of HBV infection is found.

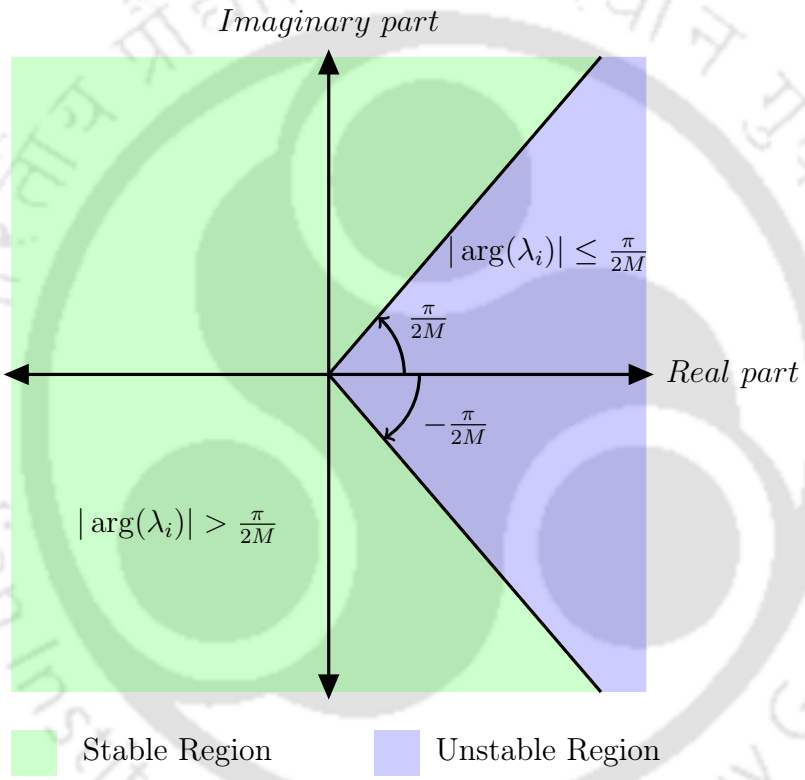

Figure 3.7: The stable and unstable regions for system (3.8.1). It turns out that the fractional-order model has a larger stability region than the integer-order model.

- **Endemic case:** On all compartments, α_1 has significant impacts. When α_1 decreases, a larger peak occurs in the infected hepatocytes, capsids, and virus compartments. Biologically, it indicates that number of infected hepatocytes as well as the severity of the infection increases. Nevertheless, for all values of α_1, the solution converges to the endemic steady-state, *i.e.*, the situation of the sufferer will be stable after a period of time . On the contrary, initially the number of uninfected hepatocytes decreases rapidly and converges in a biphasic manner for low values of α_1 and in a triphasic manner for higher values of α_1.

3.10.2 Effects of α_2 on all compartments of the model

In order to determine the effects of α_2 on all compartments, the values of $\alpha_1, \alpha_3,$ and α_4 are kept fixed at 0.9, and α_2 is varied between 0.3 and 1. In Figure 3.9, the outcomes of all compartments for different values of α_2 are shown for both the cases: disease-free and endemic.

- **Disease-free case:** In this case, for a small change in α_2, a substantial change is observed in the solutions of all compartments. For a higher value of α_2, the trajectories converge faster to the equilibrium point, *i.e.*, long-term memory increases the instability of the disease, and it makes the patient suffer for a longer period.

- **Endemic case:** From Figure 3.9, it is found that for a low value of α_2, the trajectories converge to the steady state. So, its biological implication is that there will be a smooth transition from infection to recovery at a stable position for the patient. For $\alpha_2 \geq 0.7$, the number of the infected hepatocytes, capsids, and viruses increase with time to a maximum value and subsequently drop to the endemic equilibrium state. Therefore, the patients experience a critical phase of infection and then the health condition slowly comes to a stable state.

3.10.3 Effects of α_3 on all compartments of the model

The effects of α_3 on the system (3.8.1) are examined and shown in Figure 3.10. In disease-free case, no significant change is found for uninfected and infected compartments for different values of α_3, whereas there is a small change in capsid and virus compartments.

On the other hand, there is a high prevalence in endemic situations. In this case, the effects of α_3 on the disease outcomes are similar to that of α_2.

3.10.4 Effects of α_4 on all compartments of the model

In Figure 3.11, it is seen that the solutions do not change considerably for the change in $\alpha_4 \in (0, 1]$. So, there are no significant effects of α_4 on the system (3.8.1) for disease-free and endemic cases.

Remark 3.10.1. *Based on the study of different orders of fractional derivatives, α_2 has the significant effects on the system (3.8.1). In terms of effectiveness, the fractional-order can be arranged in the following order: $\alpha_2 > \alpha_1 > \alpha_3 > \alpha_4$.*

Remark 3.10.2. *Besides, the model parameters, $\alpha_1, \alpha_2, \alpha_3$, and α_4 can be considered as disease controlling parameters. But for this, further investigation is necessary.*

3.11 Bifurcation analysis of modified model

From stability analysis, it is seen that if the eigenvalues of matrix (3.9.6) satisfy the condition (1.2.10) with $R_0 < 1$, then disease-free equilibrium will be stable. On the other hand, if the eigenvalues of Jacobian matrix (3.9.10) meet the condition (1.2.10), then endemic equilibrium point will be stable while $R_0 > 1$. From the inequality (1.2.10), it is clear that the stability of the equilibrium points depends not only on parameters but also on fractional derivative orders $(\alpha_1, \alpha_2, \alpha_3, \alpha_4)$. It is therefore possible that the system may be bifurcated from both the parameter's side and the fractional order's side. In order to investigate the bifurcation of the modified system (3.8.1), we concentrate on both the parameters and order of fractional derivatives.

3.11.1 Bifurcations with the variation of the system parameters

Here, five different set of four triplet $(\alpha_1, \alpha_2, \alpha_3, \alpha_4)$ are considered to demonstrate a few cases. When $\beta < \dfrac{R_s\mu}{a\lambda\eta k}(= \beta^*)$, disease-free equilibrium will be stable if $\left(\min|\arg(\lambda_i)| - \frac{\pi}{2M}\right) > 0$, where λ_i's denote the eigenvalues of corresponding Jacobian matrix (3.9.2). Similarly, endemic equilibrium will be stable if $\beta > \dfrac{R_s\mu}{a\lambda\eta k}(= \beta^*)$ and $\left(\min|\arg(\lambda_i)| - \frac{\pi}{2M}\right) > 0$. Only, the value of the parameter β is varied here. In this case, it is seen that for all value of β, the value of R_0 is greater than unity. The instability measure for equilibrium points in fractional order system (IMFOS) is defined by $\left(\alpha\frac{\pi}{2} - \min|\arg(\lambda_i)|\right)$. From Figure 3.13, it is clear that IMFOS is positive whenever $\beta \in (0, 0.91)$ and negative whenever $\beta \in (0.91, 3]$. Therefore, the endemic equilibrium point is asymptotically stable whenever $\beta \in (0, 0.91)$. Opposite scenario is observed for E_0. Figure 3.12 displays that E_0 becomes asymptotically

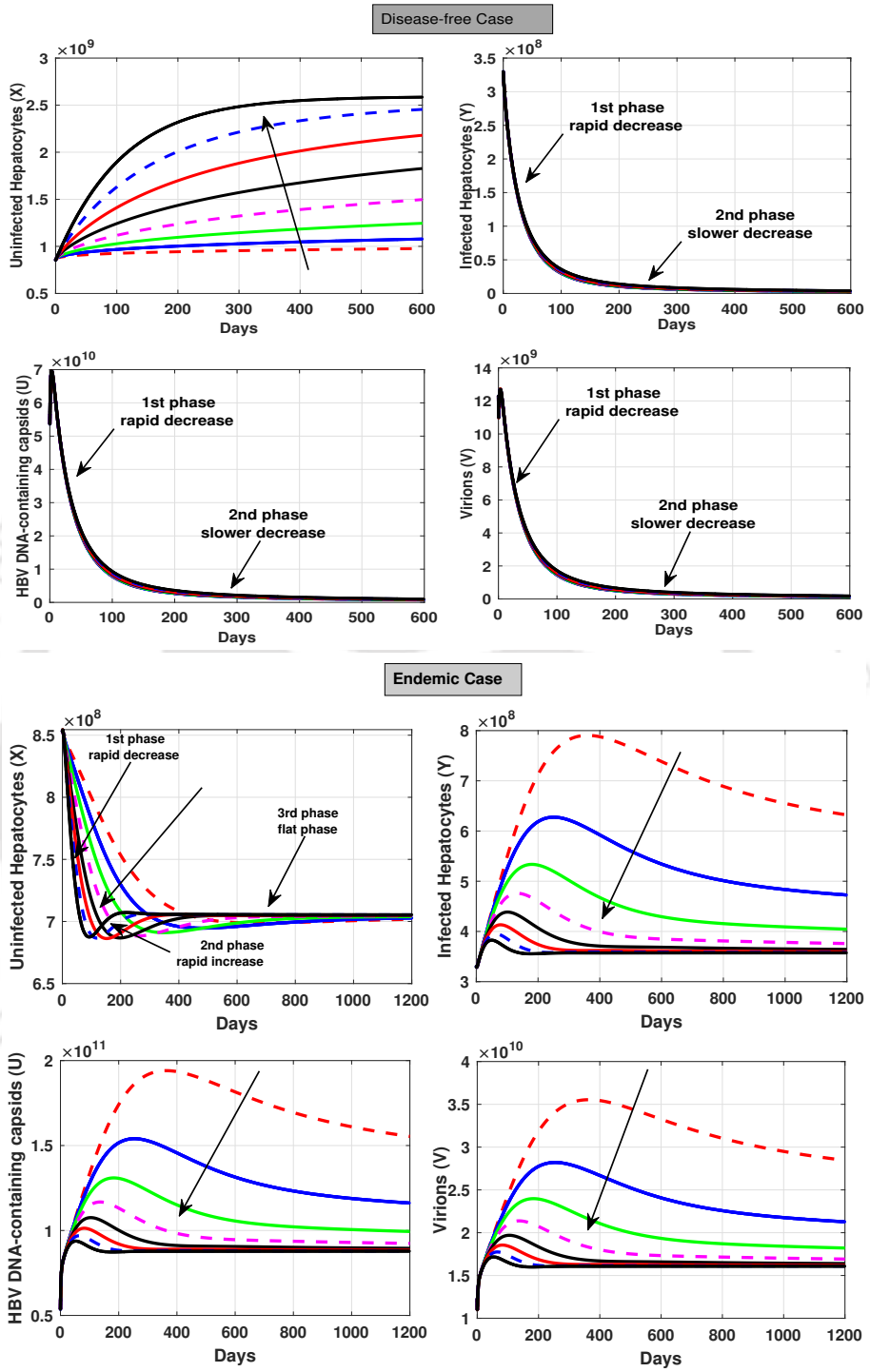

Figure 3.8: Effects of α_1 on $X(t), Y(t), U(t)$, and $V(t)$. The values of parameters are taken from Table 3.1. $\alpha_1 = 0.3 : 0.1 : 1, \alpha_2 = 0.9, \alpha_3 = 0.9, \alpha_4 = 0.9$. The arrows indicate the direction of growth of the parameter α_1.

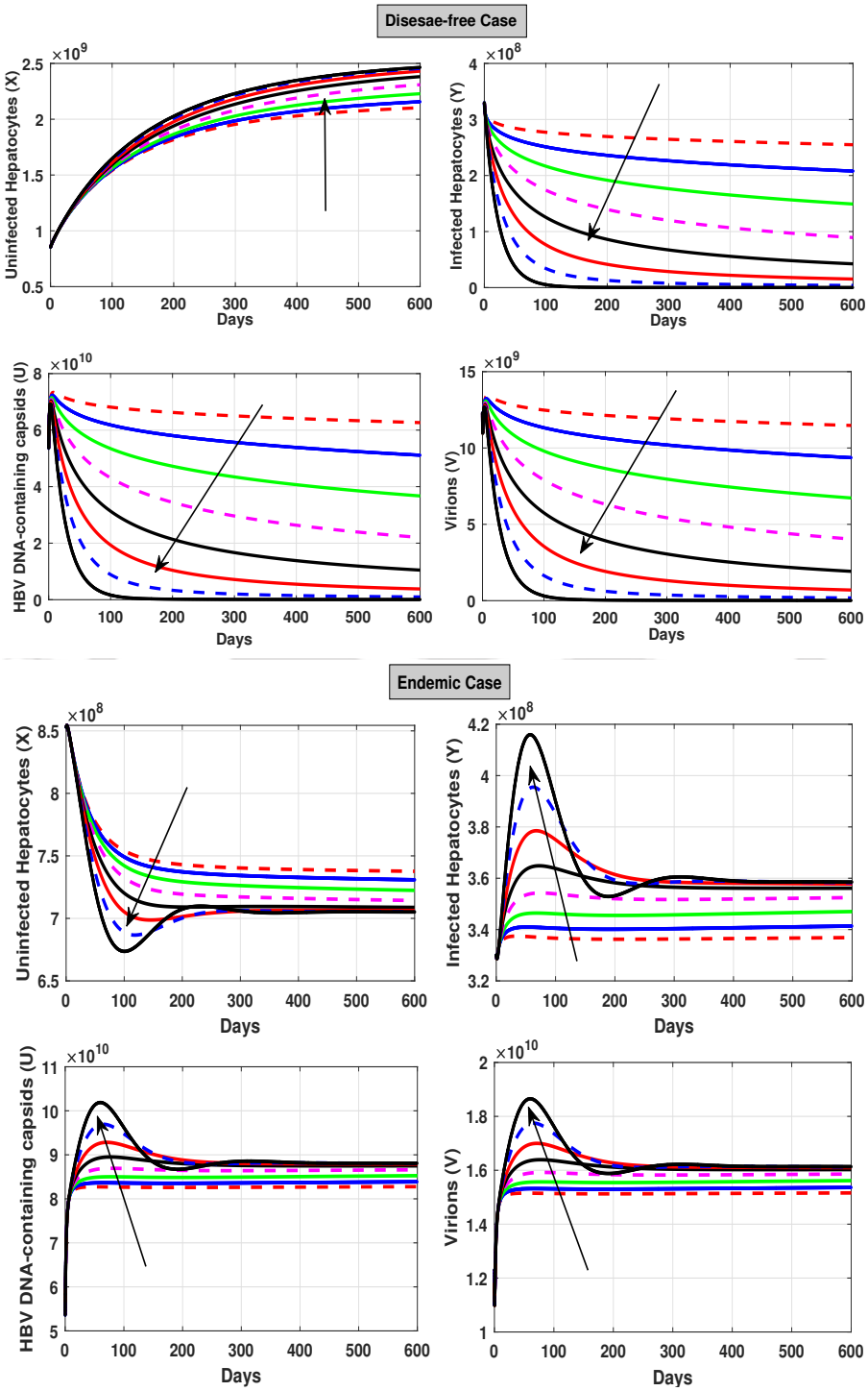

Figure 3.9: Effects of α_2 on $X(t), Y(t), U(t)$, and $V(t)$. The values of parameters are taken from Table 3.1. $\alpha_1 = 0.9, \alpha_2 = 0.3 : 0.1 : 1, \alpha_3 = 0.9, \alpha_4 = 0.9$. The arrows indicate the direction of growth of the parameter α_2.

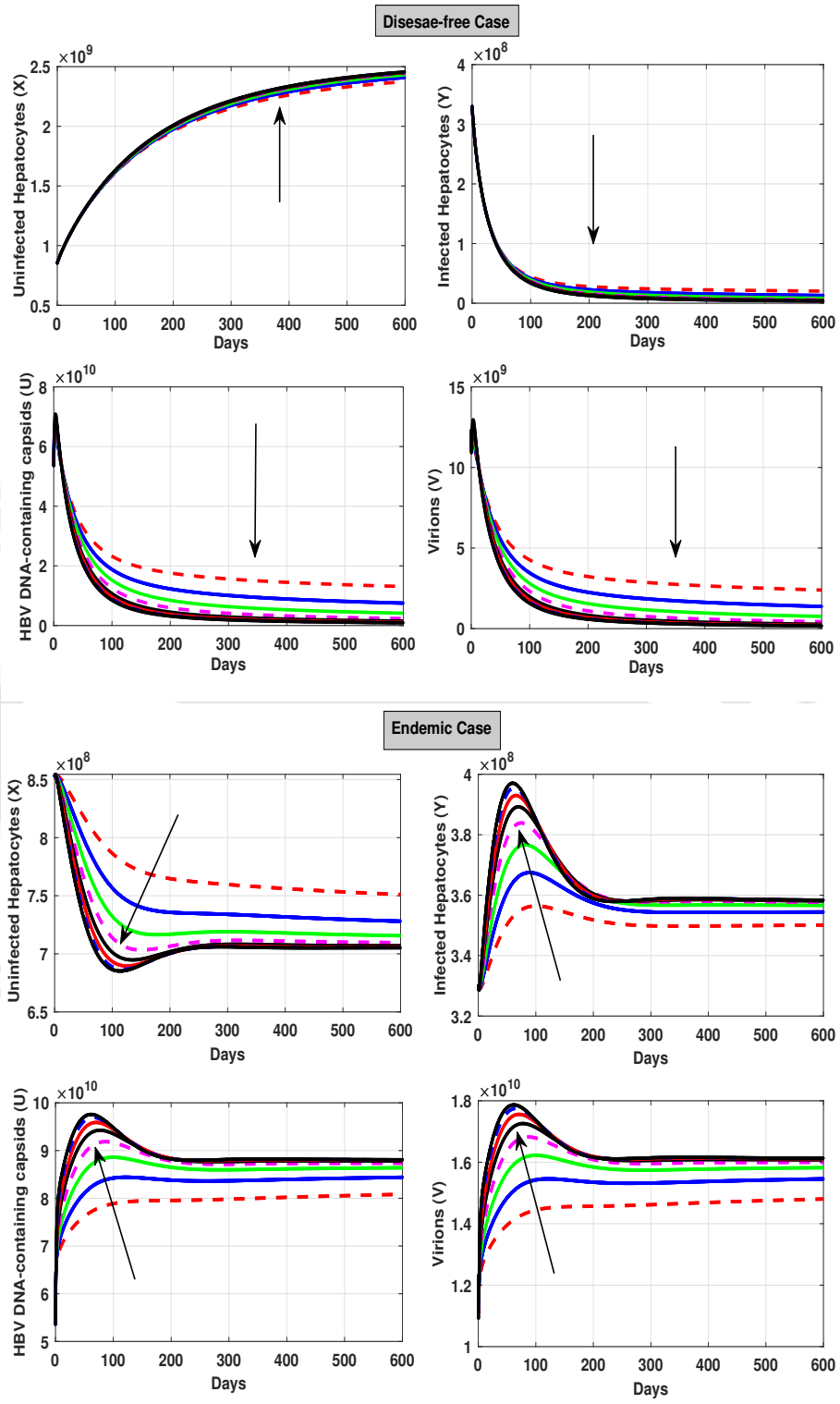

Figure 3.10: Effects of α_3 on $X(t), Y(t), U(t)$, and $V(t)$. The values of parameters are taken from Table 3.1. $\alpha_1 = 0.9, \alpha_2 = 0.9, \alpha_3 = 0.3 : 0.1 : 1, \alpha_4 = 0.9$. The arrows indicate the direction of growth of the parameter α_3.

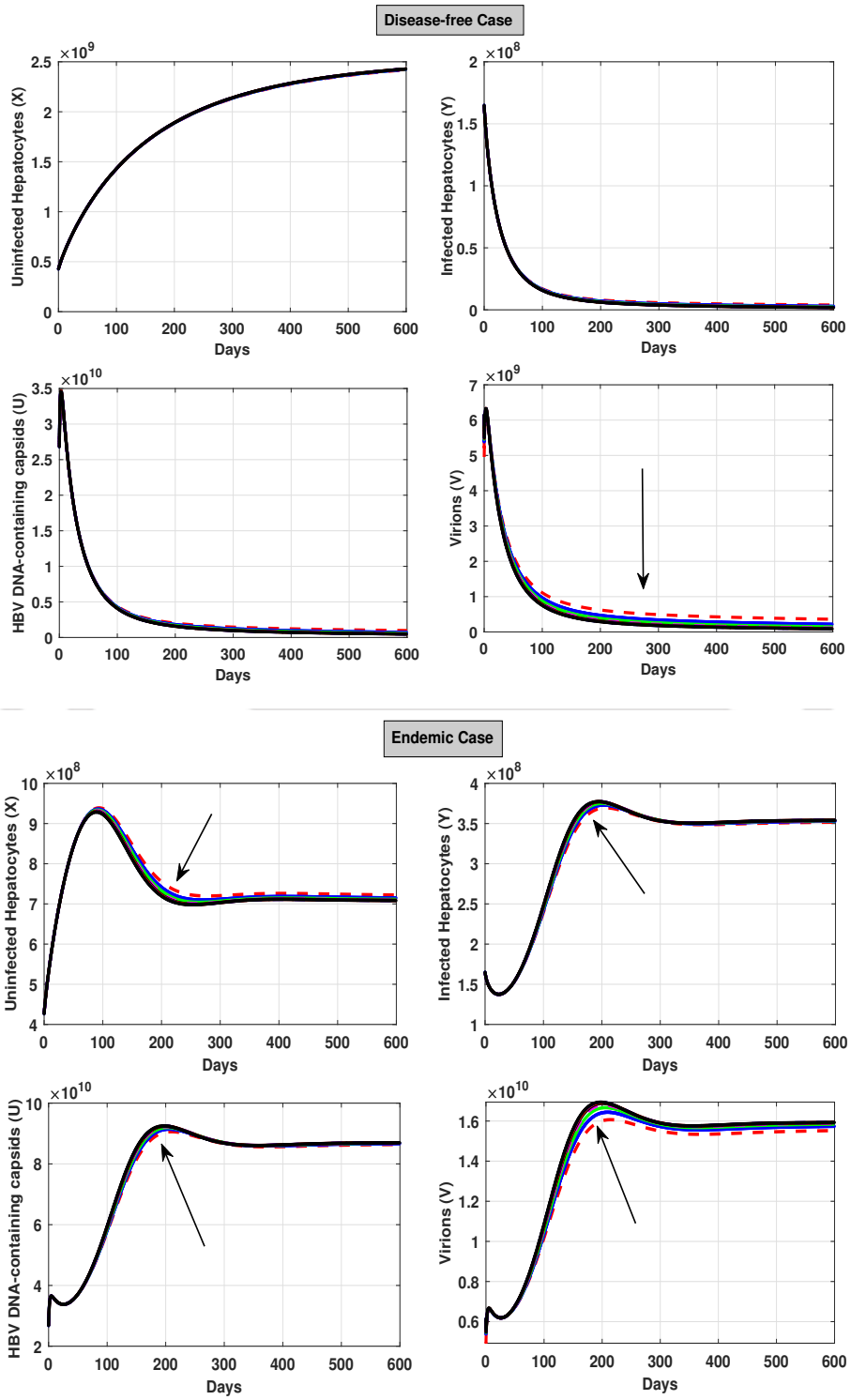

Figure 3.11: Effects of α_4 on $X(t), Y(t), U(t)$, and $V(t)$. The values of parameters are taken from Table 3.1. $\alpha_1 = 0.9, \alpha_2 = 0.9, \alpha_3 = 0.9, \alpha_4 = 0.3 : 0.1 : 1$. The arrows indicate the direction of growth of the parameter α_4.

stable when $\beta \in (0.91, 3]$. The stability of endemic equilibrium changes as β crosses the threshold value $\beta = \beta^* = 0.91$. Thus, the equilibrium points exchange their stability at the points of bifurcation $\beta = \beta^* = 0.91$.

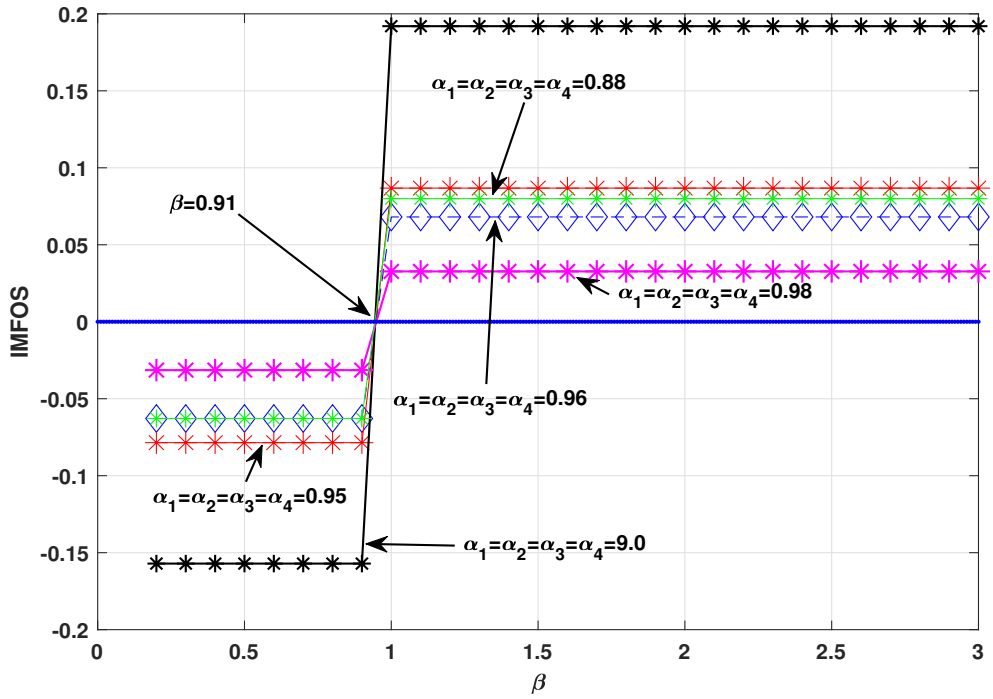

Figure 3.12: Instability measure of the disease-free equilibrium point.

3.11.2 Bifurcations with the variation of the fractional orders $(\alpha_1, \alpha_2, \alpha_3, \alpha_4)$

In this case, all model parameters are kept fixed, and their values are taken from the Table 3.1. In the modified system (3.8.1), the orders of fractional derivative (α_1, α_2, α_3, α_4) form a four dimensional space $(0, 1]^4$. Here, we study the stability of the system (3.8.1) by considering the following cases.

Case-I: ($\alpha_2 = 1$, $\alpha_3 = 1$, $\alpha_4 = 1$ **and** α_1 **is varied**)

For all values of α_1, IMFOS for endemic equilibrium point, $\left(\min|\arg(\lambda_i)| - \frac{\pi}{2M}\right) > 0$ as shown in Figure 3.14, where α_1 is varied from 0.1 to 1 with a fixed step length 0.02. Figure 3.14 indicates asymptotically stability of endemic equilibrium point.

Case-II: ($\alpha_1 = 1$, $\alpha_3 = 1$, $\alpha_4 = 1$ **and** α_2 **is varied**)

Similarly, Figure 3.15 demonstrates that for the value of α_2=0.1:0.02:1, IMFOS for endemic

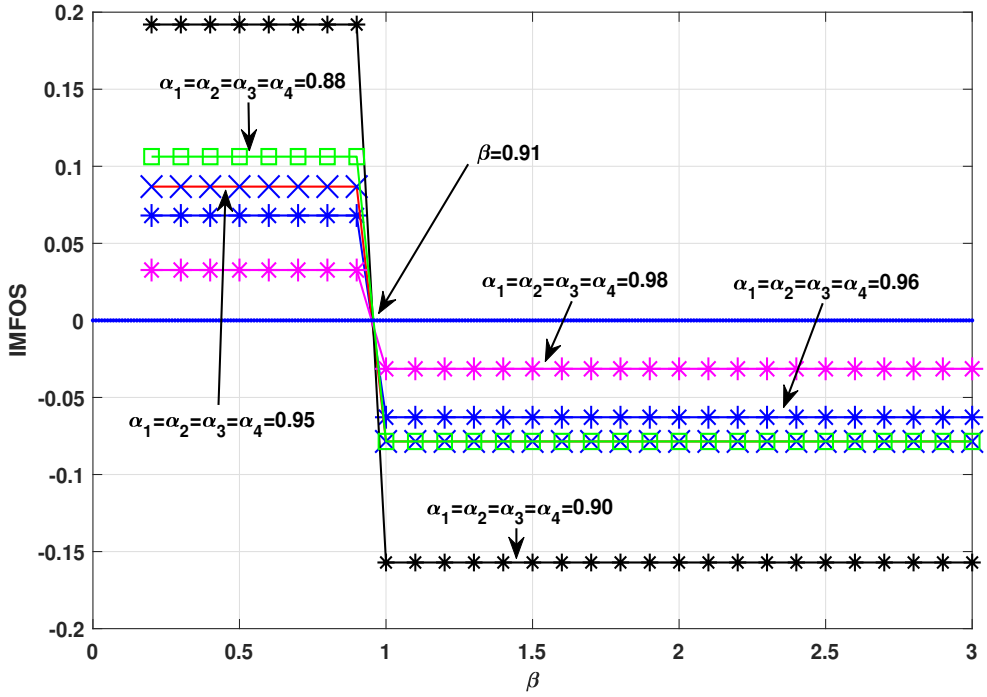

Figure 3.13: Instability measure of the endemic equilibrium point.

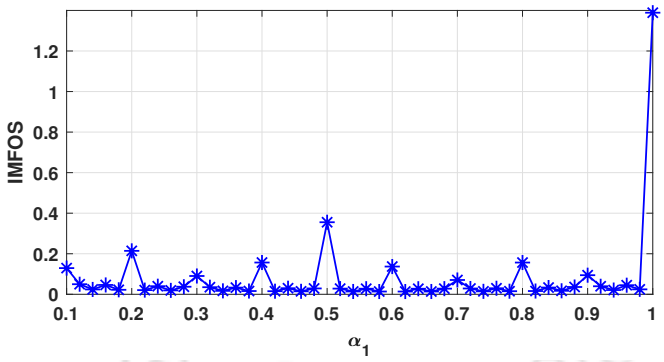

Figure 3.14: Instability measure of the endemic equilibrium point for α_1.

equilibrium point is positive.

Case-III: ($\alpha_1 = 1,\ \alpha_2 = 1,\ \alpha_4 = 1$ **and** α_3 **is varied**)

In this case, it is also seen that for all value of α_3 (0.1:0.02:1), IMFOS > 0, hence endemic equilibrium remains stable. The IMFOS values are shown in Figure 3.16

Case-IV: ($\alpha_1 = 1,\ \alpha_2 = 1,\ \alpha_3 = 1$ **and** α_4 **is varied**)

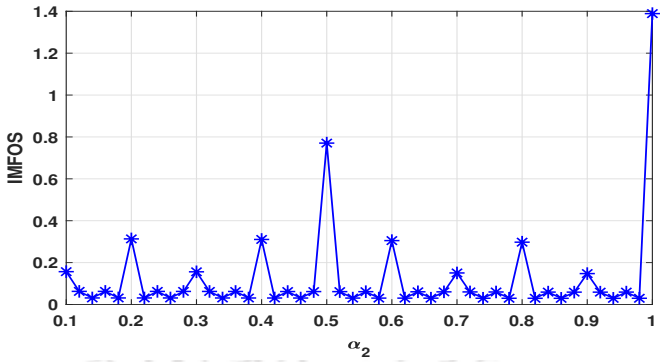

Figure 3.15: Instability measure of the endemic equilibrium point for α_2.

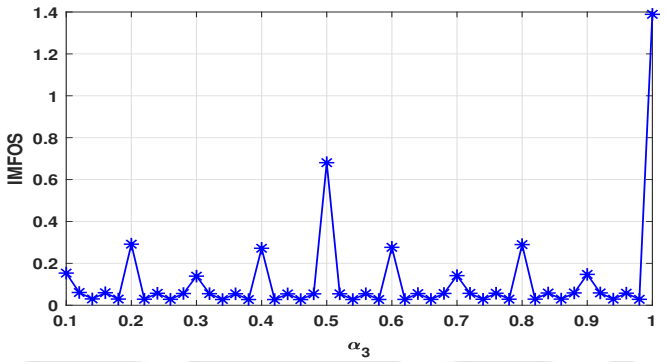

Figure 3.16: Instability measure of the endemic equilibrium point for α_3.

Parallelly, the stability of endemic equilibrium doesn't affect by the parameter α_4. The sign of IMFOS for different value of α_4 keeps positive which is displayed in Figure 3.17

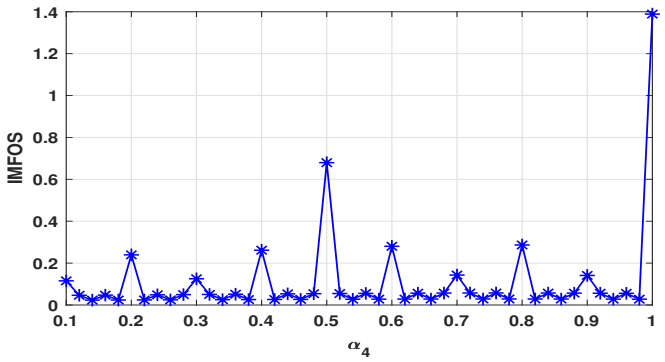

Figure 3.17: Instability measure of the endemic equilibrium point for α_4.

Therefore, no bifurcation occurs for the above cases (Case-I, Case-II, Case-III, and Case-IV).

Remark 3.11.1. *Case-I, Case-II, Case-III, and Case-IV are also analyzed similarly for* E_0.

It is observed that E_0 remains unstable for the above considered order when $R_0 > 1$.

Remark 3.11.2. *When $R_0 < 1$, an opposite scenario is observed. In each case (Case-I, Case-II, Case-III, and Case-IV), E_0 becomes stable, whereas endemic equilibrium becomes unstable.*

3.12 Conclusions

In this chapter, two new fractional-order HBV infection models with HBV DNA-containing capsids and the recycling effects of these capsids are studied for both commensurate and incommensurate orders. The novelty of this study is that we consider a HBV dynamics model taking into account the incommensurate order for the first time. So, this study is more realistic than the previous ones. In all the cases discussed in this chapter, the orders of fractional derivatives lie in the range 0 to 1. The commensurate order system (3.2.2) and the incommensurate order system (3.8.1) are numerically solved using the Adams-Bashforth Moulton method and the Implicit Product-Integration of Trapezoidal Type method, respectively. The model solutions and experimental data are compared, and it is seen from the comparison that the solutions are in good agreement. Bifurcation analysis is carried out for the incommensurate order system, considering variations in both the parameters and the fractional order. This study reveals the following findings.

1. Based on the comparison of the model solution with experimental data, the proposed model is seen to be more realistic and biologically sound.

2. Analytical and numerical results indicate that the order of fractional derivative in the sense of Caputo has no impact on the stability of the equilibrium points. In addition, it is also seen that the number of equilibrium points is independent of fractional derivative order.

3. The convergence rate of the solutions is highly influenced by the fractional orders.

4. It is observed that the infection rate increases sharply, and solution peak appears early with the increase of fractional order (α). For a lower value of α, the solution requires longer time to stabilize. This suggests that long-term memory behaviors increase the instability of the disease.

5. The fractional order corresponding to the infected hepatocytes (α_2) has the most significant influence on HBV infection. On the other hand, fractional order for the virus compartment (α_4) has negligible impact on the virus dynamics.

6. It is observed that there are two types of recovery modes of infection: biphasic and triphasic.

7. When the virus production rate (β) crosses its threshold value $\beta^*(= 0.91)$, the modified model (3.8.1) undergoes bifurcation.

CHAPTER 4

The Roles of Proliferation on HBV Infection

In this chapter, the temporal dynamics of HBV infection is investigated through two intercellular mathematical models considering proliferation of both types of hepatocytes (uninfected and infected) and recycling effect of capsids. Both models are formulated on the basis of a key finding in the existing literature: mitosis of an infected hepatocyte yields two uninfected progenies. In the first model (defined by P-model), we examine the continuous proliferation, while the second model (defined by M-model) deals with the discontinuous proliferation (happens when the total number of liver cells decreases to less than 70% of its initial number). The proposed models are calibrated with the experimental data obtained from an adult chimpanzee. Global sensitivity analysis of the model parameters is also performed for both the models. As a result, it is observed that the differences between the outcomes of continuous and discontinuous proliferations are significant and noteworthy.

4.1 Introduction

Cellular proliferation or mitosis stands as one of the pivotal biological processes influenced by this viral infection as HBV promotes cell proliferation through HBx-induced microRNA-21 in hepatocellular carcinoma [39]. In some mouse models, the HBV X protein has been found to significantly impair liver regeneration [41, 132], but has little effect in other models [133]. In the literature, a limited number of studies were dedicated to investigate the impacts of cellular proliferation of uninfected as well as infected hepatocyte during the infection. For example, in the year 2010, Hews et al. [26] introduced a HBV infection dynamics model considering the logistic growth of uninfected hepatocytes with standard incidence function, and found that the proliferation itself can affect virus replication and expression. However, it's worth noting that their model incorporated numerous assumptions. Taking into account the supposition that infected hepatocytes also undergo proliferation at a rate similar to or lower than that of healthy hepatocytes during the infection, Hews et al. [42] modified their previously proposed model given in [26]. Hews et al. [42] obtained some new outcomes, such as healthy hepatocytes can be found in chronic HBV infection only when the proliferation of infected hepatocytes is significantly impaired. However, throughout that study [42], it was assumed that infected hepatocytes proliferate to a considerable extent and generate only infected daughter cells. Dahari et al. [21] suggested that variations in proliferation between uninfected and infected hepatocytes could offer a rich explanation for the diverse patterns that are observed in the time of decline of viral loads. Based on the data collected regarding cellular proliferation of an infected hepatocyte, it is noted that three different scenarios may occur when an infected hepatocyte undergoes proliferation (mitosis), demonstrated in Figure 4.1 as

1. Results in two uninfected daughter cells.
2. Results in one uninfected and one infected daughter cell.
3. Results in two infected daughter cells.

4.2 Model formulation and analysis

In order to analyze the dynamics of HBV infection focusing on the roles of proliferation of susceptible and infected hepatocytes, a new infection dynamics model is proposed in this chapter. The liver mainly consists of hepatocytes and various types of non-parenchymal

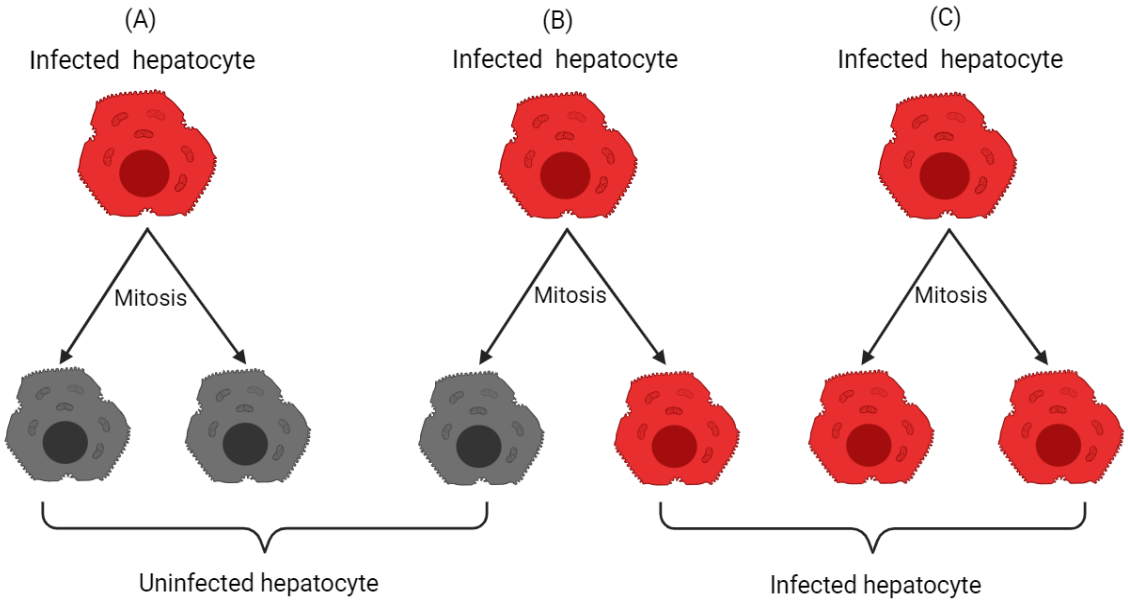

Figure 4.1: Proliferation of an infected hepatocyte results (A) two uninfected hepatocytes, (B) one uninfected and one infected hepatocytes, and (C) two infected daughter cells. This illustration is created with BioRender.com.

cells. The total number of liver cells of a healthy adult is denoted by T which contains both hepatocytes and non-parenchymal cells (cells in the liver that cannot be infected), such as Kupffer cells, hepatic stellate cells, liver sinusoidal endothelial cells and diverse types of lymphocytes. Non-parenchymal cells play crucial roles during infection, as these produce inflammatory mediators, such as cytokines, oxidative stress, microRNA, and lipid-derived metabolites (including retinoic acid and endocannabinoids), and interact directly with parenchymal cells like hepatocytes [134]. It is estimated that for an adult, the total number of liver cells (T) is 2×10^{11}, of which only 60% are virus-targeted liver cells, *i.e.*, hepatocytes, and the remaining 40% accounts for non-parenchymal cells [3, 48, 135]. The total number of hepatocytes (virus-targeted cells) is grouped into two classes in this model: (i) susceptible hepatocytes, and (ii) infected hepatocytes. In a manner akin to model (2.2.1), this model also incorporates rcDNA-containing capsids ($U(t)$) and complete virions ($V(t)$) as two distinct compartments. It is assumed that the susceptible and infected hepatocytes proliferate following the logistic growth law with proliferation rates r and ρ, respectively. In the context of liver infection, the logistic growth proves more realistic and accurate due to the fixed size of the liver for each individual. Due to the logistic growth terms, the total number of liver cells ($X(t)+Y(t)$) cannot exceed the carrying capacity of the liver (T), as expected. We consider that the infection occurs at a constant rate k. The parameter μ represents the natural death rate of susceptible hepatocytes. Accordingly, the dynamical equations

for susceptible hepatocytes ($X(t)$), infected hepatocytes ($Y(t)$), HBV capsids ($U(t)$), and viruses ($V(t)$) are described by the following reaction equations:

$$\frac{dX(t)}{dt} = rX(t)\left(1 - \frac{X(t)+Y(t)+\theta T}{T}\right) + 2\rho Y(t)\left(1 - \frac{X(t)+Y(t)+\theta T}{T}\right) - kX(t)V(t) - \mu X(t), \tag{4.2.1}$$

$$\frac{dY(t)}{dt} = kX(t)V(t) - \rho Y(t)\left(1 - \frac{X(t)+Y(t)+\theta T}{T}\right) - \delta Y(t), \tag{4.2.2}$$

$$\frac{dU(t)}{dt} = aY(t) + \gamma(1-\eta)U(t) - \eta\beta U(t) - \delta U(t), \tag{4.2.3}$$

$$\frac{dV(t)}{dt} = \eta\beta U(t) - \delta_v V(t), \tag{4.2.4}$$

where θ denotes the fraction of non-parenchymal cells. The term $rX(t)\left(1 - \frac{X(t)+Y(t)+\theta T}{T}\right)$ of equation (4.2.1) represents the fact that upon proliferation, uninfected hepatocytes always produce uninfected hepatocytes, while the second term, *i.e.*, $2\rho Y(t)\left(1 - \frac{X(t)+Y(t)+\theta T}{T}\right)$ indicates that the proliferation of an infected hepatocyte results in two uninfected hepatocytes. The remaining parameters hold the same meanings as in the model (2.2.1), described in Chapter 2.

We define the following functions:

$$f_1(X(t),Y(t),U(t),V(t)) := rX(t)\left(1 - \frac{X(t)+Y(t)+\theta T}{T}\right) + 2\rho Y(t)\left(1 - \frac{X(t)+Y(t)+\theta T}{T}\right) - kX(t)V(t) - \mu X(t), \tag{4.2.5}$$

$$f_2(X(t),Y(t),U(t),V(t)) := kX(t)V(t) - \rho Y(t)\left(1 - \frac{X(t)+Y(t)+\theta T}{T}\right) - \delta Y(t), \tag{4.2.6}$$

$$f_3(X(t),Y(t),U(t),V(t)) := aY(t) + \gamma(1-\eta)U(t) - \eta\beta U(t) - \delta U(t), \tag{4.2.7}$$

$$f_4(X(t),Y(t),U(t),V(t)) := \eta\beta U(t) - \delta_v V(t). \tag{4.2.8}$$

Clearly, the functions $f_i(X(t),Y(t),U(t),V(t))$, $i = 1,2,3,4$ are polynomial functions of $X(t), Y(t), U(t)$ & $V(t)$. The initial conditions (X_0, Y_0, U_0, V_0) and all parameters are restricted to non-negative values due to biological constraints. Each f_i is continuous and satisfies the well-known Lipschitz condition for uniqueness of solution. Hence, the initial value problems (4.2.1), (4.2.2), (4.2.3), (4.2.4) have unique solution in any interval $[0, b^*), b^* \in \mathbb{R}^+$, where $\mathbb{R}^+$ denotes the set of positive real numbers.

Based on the proliferation rates of uninfected and infected hepatocytes, two different scenarios are analyzed here. In the first case, it is assumed that the both types of liver cells

proliferate with the same rate, *i.e.*, $r = \rho$. In the second one, we consider that as compared to uninfected hepatocytes, infected hepatocytes proliferate at a lower rate, *i.e.*, $\rho < r$.

4.3 Parameter estimation and model calibration

The values of some parameters are taken from the existing literature and shown in Table 4.1. The quantity $(1-\theta)$ denotes the fraction of the total number liver cells that are hepatocytes and are the primary target of the viruses. Following the previous studies [136, 137], based on the fact that 60% of liver cells are hepatocytes, the value of θ is set to 0.4. The values of proliferation rate of infected hepatocytes (ρ) are constrained to be between 0.001 and 0.35/day [48]. The values of proliferation rate of uninfected hepatocytes (r) lie between 0.001 and 3.4/day [44]. Based on the study by Ko et al. [105], the value of η can be fixed to 0.8, implying that a smaller number of capsids are recycled. The values of other parameters are estimated. Parameter estimation involves determining the values of unknown

Table 4.1: Descriptions of model parameters. This table contains parameter values which are taken directly from existing literature.

Parameters	Descriptions	Values	Units	Sources
r	Proliferation rate of uninfected hepatocytes	$0.001 - 3.4$	day^{-1}	[48]
ρ	Proliferation rate of infected hepatocytes	$0.001 - 0.35$	day^{-1}	[44, 138]
T	Total number of liver cells	2×10^{11}	cells	[42, 139]
θ	Fraction of liver cells that cannot be infected	0.4	unitless	[48]

parameters that best fit a given model or system based on observed data. The difficulty arises from several factors like complexity of models, measurement noise, non-uniqueness, computational challenges, and the need for accurate prior knowledge. The non-uniqueness of parameter values presents a major challenge in estimation processes. Some models may have multiple sets of parameters that can produce similar outputs, leading to non-unique solutions. This ambiguity complicates the process of identifying the correct parameter values. For this, prior to estimating the model parameters, the identifiability of these parameters is examined first.

4.3.1 Identifiability analysis

Structural identifiability examines the ability of a model to identify its unknown parameters when noise-free data is provided. Only after ensuring the structural identifiability of the

unknown parameters, one can proceed with data fitting schemes to estimate their values. In order to study the structural identifiability, the proposed model (equations (4.2.1)-(4.2.4)) is written in a general form as:

$$x'(t) = f(x, p), \tag{4.3.1}$$

and the observed variables are as follows

$$y(t) = g(x, p). \tag{4.3.2}$$

Here, $x(t)$ represents the state variables, p denotes the parameter vector, and $y(t)$ corresponds to the output (derived from experimental data), also referred to as the observations. Examination of structural identifiability of ODE models through differential algebra methods can be applied using various open-source software. In this study, DAISY is used to check the structural identifiability of the proposed model. It is assumed that the model parameters $p = \{r, \rho, k, \mu, \delta, a, \gamma, \beta, \delta_v\}$ are unknown. The observed/experimental data collected from the study of Asabe et al. [100] are represented in the proposed model by the variable $U(t)$. This observed variable is expressed as

$$y(t) = U(t).$$

In terms of the observed variable $y(t)$, structural identifiability means the following: Let ϕ_1 and ϕ_2 be two distinct vectors of model parameters. The model is said to be structurally identifiable if and only if

$$y(t, \phi_1) = y(t, \phi_2) \text{ implies that } \phi_1 = \phi_2,$$

which means two identical observations result in identical sets of parameters. The first step in this method is to derive the input-output equations for the proposed model by eliminating the unobserved state variables $(X(t), Y(t), V(t))$. Due to the presence of intricate complexities in the proposed model, the associated input-output equation in terms of the variable $U(t)$ and model parameter p is obtained by using DAISY, sophisticated computational software tool. The standard ranking of the variables (input $<$ output $<$ state variable) is considered in the following manner:

$$y < \dot{y} < \ddot{y} < \cdots < X < Y < U < V < \dot{X} < \dot{Y} < \dot{U} < \dot{V} < \ddot{X} < \ddot{Y} < \ddot{U} < \ddot{V} < \cdots$$

The simulation begins with the parameter set $p = \{r, \rho, k, \mu, \delta, a, \gamma, \beta, \delta_v\}$ and the initial condition $I_0 = \{X_0, Y_0, U_0, V_0\}$. As a result, we get that the model is "AlGEBRAICALLY OBSERVABLE" and "GLOBALLY IDENTIFIABLE" from input–output data. Now, we are in a position to estimate the model parameters using the experimental data.

4.3.2 Methodology: estimation of parameters and validation

Once the proposed model is validated with experimental data, it becomes a powerful tool to analyzing the infection dynamics under various conditions. In order to validate our proposed model, the experimental data of HBV DNA from a male chimpanzee are considered. This chimpanzee was labeled as A2A007. The age and the body weight of this chimpanzee were 5.1 years and 17.7 kgs, respectively. These data have been previously published in the work of Asabe et al. [100]. In the study carried out by this group, the experiment was performed on a cohort of nine healthy adult chimpanzees following the ethical guidelines governing their use and care.

Before estimation, it is crucial to take into account the total number of experimental data. According to the study of Sontag [107], for any ODE model with p unknown parameters, $2p+1$ experimental observations are enough for identification of p parameters. The number of unknown parameters in our model stands at 10. Consequently, the value of $2p+1$ equals to 21. So, we have decided to divide the whole data set following the $2p+1$ rule to estimate the parameter values. Based on the experimental data structure of the chimpanzee A2A007, the entire duration of the experiment is divided into two sub-intervals: (i) 20-179 (21 data points), (ii) 179-346 (22 data points). The model parameters are estimated in each sub-interval minimizing the sum square error (SSE) objective function. The SSE function is defined as

$$\text{SSE} = \sum_{i=1}^{N} \left[Q_i - q(i)\right]^2, \quad N = \text{total number of experimental data}, \tag{4.3.3}$$

where model solution and experimental data are denoted by Q_i and $q(i)$, respectively. This optimization process is carried out through the utilization of the '*fminsearchbnd*' built-in MATLAB function. The upper and lower bound of the interested parameters are collected from the existing literature. The estimated values of each parameter in each time interval are shown in Table 4.2. The solution of the proposed model and the experimental data are compared in Figure 4.2A, and it is observed that the model solution exhibits an excellent agreement with the experimental data. From the bar diagram shown in Figure 4.2B, it is observed that the percentage error at each time point is less than 5% and and fall within an

acceptable range [140].

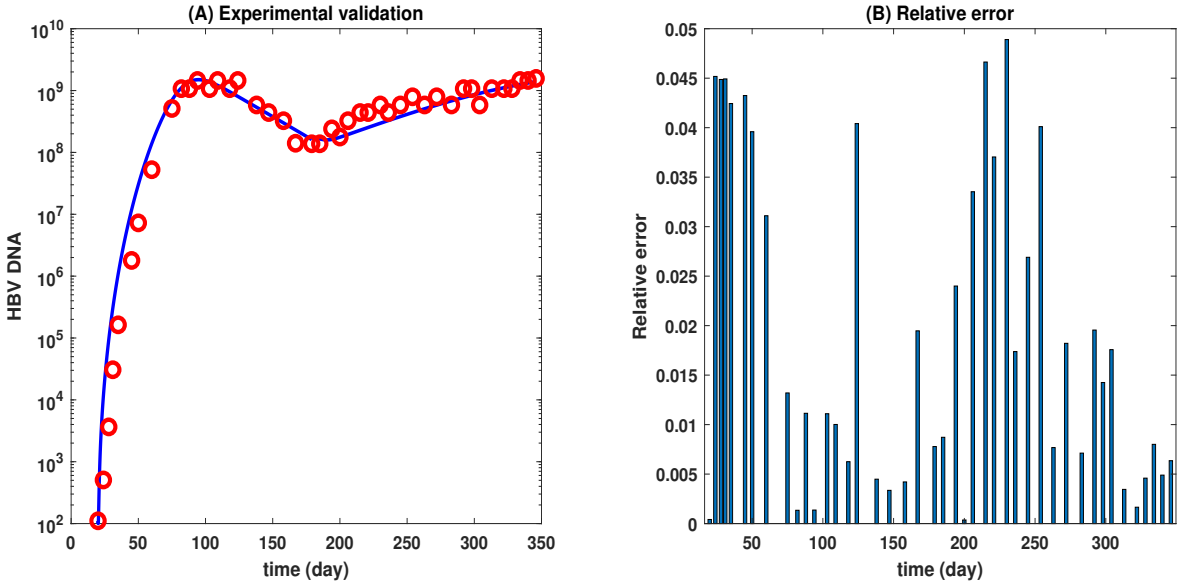

Figure 4.2: (A) Comparison of model solution with experimental data of Chimpanzee A2A007. Solid blue line represents model solution whereas red circles reflect the experiment data. (B) Relative error between model solution and experimental data.

4.4 Optimal criteria for maintaining smoothly the essential functions of liver

In the literature, many authors have proposed different types of HBV infection dynamics model and analyzed them without considering the lower bound of uninfected hepatocytes or upper bound of infected hepatocytes for survival of the patients. During liver transplantation, resections that leave 20–30% of the original liver cells are considered safe and allow the donor liver to regenerate [141, 142]. According to the experimental study by Kishi et al. [143] conducted on over 300 right lobe hepatectomy patients, it was found that liver cells remnant volumes greater than 20% are sufficient for safe resection for a healthy liver. So, it is very important to maintain a certain level of uninfected hepatocytes throughout the infection period. As per the discussion, it is assumed that a minimum 20% of the total hepatocytes (excluding the population of non-parenchymal cells) or 52% (40% non-parenchymal cells and 12% hepatocytes) with respect to entire liver size is required to maintain the critical liver functions during the infection. Any number less than 20% is lethal for the sufferer. Thus, for further study, we pay close attention to this optimum value of uninfected hepatocytes.

Table 4.2: Estimated value of parameters for the chimpanzee-A2A007.

Parameters	Time interval	
	20-179	179-346
r	0.0118	0.5953
ρ	0.0144	0.0125
k	5.12×10^{-12}	1.18×10^{-12}
a	170	165
γ	2.95	2.33
β	1.92	1.10
μ	0.01	0.01
δ	0.032	0.01
δ_v	0.10	0.104

4.5 How does the proliferation rate influence the infection?

Both uninfected and infected hepatocytes have the ability to undergo proliferation in order to compensate the deficiency of the liver cells. In this study, we mainly focus to explore the roles of proliferation of liver cells during HBV infection. The understanding of how proliferation affects chronic infections is relatively scarce compared to the extensive knowledge available for acute infection. However, the authors seek to investigate the influence of proliferation on both acute and chronic infection. To this quest, we study the impacts of proliferation from two distinct perspectives. In the first case, it is assumed that both types of hepatocytes proliferate with equal rate ($r = \rho$), and secondly that the rates differ ($r \neq \rho$). In this context, four distinct cases are discussed as follows:

- **Case-1:** Equal proliferation rate of both uninfected and infected hepatocytes in acute infection.
- **Case-2:** Different proliferation rates of uninfected and infected hepatocytes in acute infection.
- **Case-3:** Equal proliferation rate of both uninfected and infected hepatocytes in chronic infection.

- **Case-4:** Different proliferation rates of uninfected and infected hepatocytes in chronic infection.

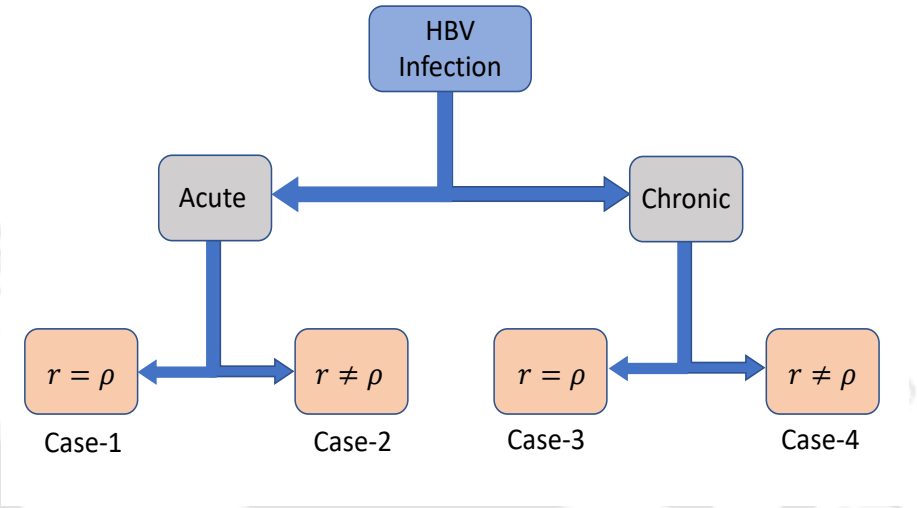

Figure 4.3: Schematic representation of four cases mentioned above.

4.5.1 Effects of proliferation in acute and chronic infection when both types of hepatocytes proliferate at same rate ($r = \rho$)

In this case, it is considered that both types of hepatocytes proliferate with same rate (r). Accordingly, the equations (4.2.1) and (4.2.2) reduce to the following forms:

$$\frac{dX(t)}{dt} = r(X(t) + 2Y(t))\left(1 - \frac{X(t) + Y(t) + \theta T}{T}\right) - kX(t)V(t) - \mu X(t), \tag{4.5.1}$$

$$\frac{dY(t)}{dt} = kX(t)V(t) - rY(t)\left(1 - \frac{X(t) + Y(t) + \theta T}{T}\right) - \delta Y(t), \tag{4.5.2}$$

where the equations (4.2.3) and (4.2.4) remain unchanged.

4.5.1.1 Steady states of the system

The steady-states of the system (equations (4.5.1), (4.5.2), (4.2.3), and (4.2.4)) are obtained by solving the following system of equations given by

$$r(X(t)+2Y(t))\left(1-\frac{X(t)+Y(t)+\theta T}{T}\right)-kX(t)V(t)-\mu X(t)=0, \tag{4.5.3}$$

$$kX(t)V(t)-rY(t)\left(1-\frac{X(t)+Y(t)+\theta T}{T}\right)-\delta Y(t)=0, \tag{4.5.4}$$

$$aY(t)+\gamma(1-\eta)U(t)-\eta\beta U(t)-\delta U(t)=0, \tag{4.5.5}$$

$$\eta\beta U(t)-\delta_v V(t)=0. \tag{4.5.6}$$

1. **Trivial or liver failure steady-state:** Clearly, $(0,0,0,0)$ is a solution of the system of equations (4.5.3)-(4.5.6). So, the model exhibits liver failure steady-state, and it is denoted by E_0.

2. **Disease-free steady-state:** By substituting $Y(t)=0$, $U(t)=0$, and $V(t)=0$ in equations (4.5.3)-(4.5.6), we obtain the non-zero value of $X(t)$ as $\frac{T(r-r\theta-\mu)}{r}$. Therefore, $E_f := \left(\frac{T(r-r\theta-\mu)}{r},0,0,0\right)$ is another steady-state. In the context of biology, this steady-state will be biologically relevant if and only if $(r-r\theta-\mu)>0$, which implies $3r>5\mu$ (putting $\theta=0.4$). This indicates that thrice of proliferation rate should be more than five-folds of the death rate of uninfected hepatocytes for existence of this steady-state.

   In terms of HBV infection dynamics, the basic reproduction number represents the average number of secondary infected hepatocytes produced by one infected hepatocyte in a completely susceptible population. In this case, basic reproduction number is denoted by the symbol R_0^E and is calculated using next-generation approach [112]. The expression of R_0^E is given by

$$R_0^E=\frac{a\eta\beta kT(r-r\theta-\mu)}{r\delta_v R_s(\delta+\mu)}, \text{ where } R_s=\eta\beta-(1-\eta)\gamma+\delta.$$

   The physical interpretation of the threshold R_s is well-explained in Chapter 2, and it is shown that the solution of the equation (4.2.3) will be bounded if $R_s>0$. Thus, for the rest of the study, we will proceed with $R_s>0$.

3. **Endemic steady-state:** In terms of Mathematics, the system has two endemic steady-states. The individual expressions of these two equilibria are not given due

to the presence of large number of terms. Instead, using the values of parameters shown in Table 4.1 and in the third column of Table 4.2, the numerical values of these two equilibria are presented below as:

(a) **First endemic steady-state (E_1):** $X_1^* = 1.40435 \times 10^9$, $Y_1^* = 8.36257 \times 10^{10}$, $U_1^* = 2.053 \times 10^{13}$, $V_1^* = 3.76024 \times 10^{12}$.

(b) **Second endemic steady-state (E_2):** $X_2^* = 3.11891 \times 10^9, Y_2^* = -3.92172 \times 10^9, U_2^* = -9.62779 \times 10^{11}, V_2^* = -1.76341 \times 10^{11}$.

It is clear that for the steady-state $(X_2^*, Y_2^*, U_2^*, V_2^*)$, the values of Y_2^*, U_2^*, V_2^* are negative. From biological perspective, this steady-state is not feasible. Therefore, the equilibrium point E_1 only exists for the set of parameter values provided in Table 4.1 and Table 4.2.

4.5.1.2 Stability analysis of equilibrium points

- **Liver failure steady-state** (E_0)

Acute liver failure (ALF) also known as fulminant hepatic failure is the loss of liver function that happens quickly, usually in a matter of days or weeks, in people who do not have any liver disease. ALF is quite uncommon. In general, the main cause of ALF is the use of drugs or the hepatitis virus infection. In literature, it is seen that chronic liver failure (CLF), which develops itself more slowly, is more common than acute liver failure. In order to study the stability of this liver failure steady-state, we first calculate the Jacobian matrix of proposed model (system of equations (4.5.1), (4.5.2), (4.2.3), and (4.2.4)) at E_0, and it is given by

$$J_{E_0} = \begin{pmatrix} r(1-\theta)-\mu & 2r(1-\theta) & 0 & 0 \\ 0 & -\delta - r(1-\theta) & 0 & 0 \\ 0 & a & -\eta\beta + (1-\eta)\gamma - \delta & 0 \\ 0 & 0 & \eta\beta & -\delta_v \end{pmatrix}. \tag{4.5.7}$$

The corresponding eigenvalues of the matrix (4.5.7) are $\{-\delta_v, -\eta\beta + (1-\eta)\gamma - \delta (= -R_s < 0), -\delta - (1-\theta)r, r(1-\theta) - \mu\}$. All eigenvalues except $(r(1-\theta)-\mu)$ are negative. The eigenvalue $(r(1-\theta)-\mu)$ will be negative if $r(1-\theta) < \mu$. Hence, liver failure steady-state will be locally asymptotically stable if $3r < 5\mu$ (taking $\theta = 0.4$, refers Table 4.1). Otherwise, E_0 becomes unstable, *i.e.*, it is found that E_0 is conditionally stable. Although Hews et al. [26] concluded that liver failure steady-state is always unstable, which does not always

follow by the existing biological evidence. For example, Oketani et al. [144] documented that HBV-related ALF can develop following an acute HBV infection or during a flare-up of chronic HBV infection, *i.e.*, the likelihood of ALF is contingent upon the patient's physical circumstances. According to the review by Garg and Madan [145], acute-on-chronic liver failure (ACLF) is classified as a distinct syndrome, and it is noted that ACLF related to HBV has specific characteristics. Until more effective treatments become available, mortality rates for this syndrome—both in the acute and chronic—are expected to remain elevated. Overall, ALF is a complex health problem with a high short-term mortality. Our results differ from those of Hews et al. [26]. Here, we become able to derive a condition $3r < 5\mu$ pertaining ALF which helps to maintain the instability of E_0 and benefits the patients. By increasing the proliferation rate, ALF can be prevented, thereby promoting patient survival. In Figure 4.4, the trajectories of both uninfected and infected hepatocytes, capsids and viruses are presented considering five different initial conditions. In this case, the value of the parameter k is considered as 1.67×10^{-13} [131] . As a result, it is observed that solutions of the system converge to the E_0 if the condition $3r < 5\mu$ satisfies.

Remark 4.5.1. *In biological terminology, the inequality $3r < 5\mu$ provides the following crucial information: if the thrice of proliferation rate is less than the five times of death rate of uninfected hepatocytes, the health condition of the patient will deteriorate day by day, and the liver will subsequently become damage permanently. In general, for all humans, the death or degradation rate of uninfected hepatocytes is almost constant. Humans have no control over it. Proliferation rate differs among individuals. So, in this circumstance, the only option to prevent liver failure is to keep the proliferation rate above a certain threshold value.*

- **Disease-free steady-state** (E_f)

The Jacobian matrix at E_f is given by

$$J_{E_f} = \begin{pmatrix} r(\theta-1)+\mu & r(\theta-1)+3\mu & 0 & -\dfrac{kT(r-\theta r-\mu)}{r} \\ 0 & -(\delta+\mu) & 0 & \dfrac{kT(r-\theta r-\mu)}{r} \\ 0 & a & -\eta\beta+(1-\eta)\gamma-\delta & 0 \\ 0 & 0 & \eta\beta & -\delta_v \end{pmatrix} \tag{4.5.8}$$

Clearly, $r(\theta-1)+\mu$ is an eigenvalue of the matrix (4.5.8), and it will be negative if $\mu < r(1-\theta)$, *i.e.*, $5\mu < 3r$ (putting $\theta = 0.4$). Other three eigenvalues are the eigenvalues of

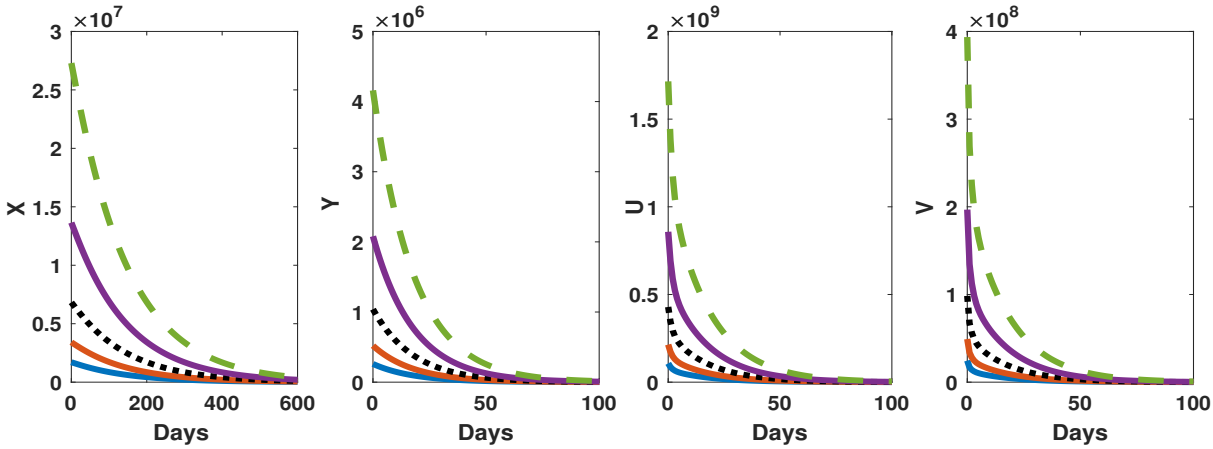

Figure 4.4: Convergence of solution to the liver failure equilibrium point for five different initial conditions. The values of other parameters are taken from both Table 4.1 and Table 4.2.

the matrix

$$\begin{pmatrix} -(\delta+\mu) & 0 & \dfrac{kT(r-\theta r-\mu)}{r} \\ a & -\eta\beta+(1-\eta)\gamma-\delta & 0 \\ 0 & \eta\beta & -\delta_v \end{pmatrix} \tag{4.5.9}$$

Let the characteristic equation of the matrix (4.5.9) be

$$\xi^3+\mathcal{A}_1\xi^2+\mathcal{A}_2\xi+\mathcal{A}_3=0,$$

where

$$\begin{aligned}
\mathcal{A}_1 &= \eta\beta+(\eta-1)\gamma+\delta_v+2\delta+\mu=R_s+\delta+\mu>0 \text{ when } R_s>0,\\
\mathcal{A}_2 &= R_s(\delta+\mu+\delta_v)+\delta_v\delta+\delta_v\mu>0 \text{ when } R_s>0,\\
\mathcal{A}_3 &= a\eta\beta\theta Tk-a\eta\beta Tk+\frac{a\eta\beta Tk\mu}{r}+\delta_v(\delta+\mu)R_s>0, \text{ when } R_s>0,\ R_0^E<1,\\
\mathcal{A}_1\mathcal{A}_2-\mathcal{A}_3 &= \frac{rR_s(\delta+\mu)(R_s+\delta+\mu)-a\eta\beta Tk(\mu+(\theta-1)r)}{r}\\
&\quad+\delta_v^2(R_s+\delta+\mu)+\delta_v(R_s+\delta+\mu)^2>0 \text{ when } R_s>0,\ R_0^E<1.
\end{aligned}$$

So, using *Routh Hurwitz* criteria [112], it is identified that the disease-free equilibrium is locally asymptotically stable when the following conditions are satisfied:

1. $5\mu < 3r$.
2. $R_s > 0$.
3. $0 < R_0^E < 1$.

The first condition $5\mu < 3r$ means that the five-fold of death rate of infected hepatocytes must be less than the thrice of proliferation rate to establish the stability. In the third condition, we consider $R_0^E > 0$ because, in order to ensure the existence of E_f biologically, one must have $(r(1-\theta) - \mu > 0)$ which implies $R_0^E > 0$. In terms of biology, if the above three criteria are met, this model suggests that patients could potentially be free from infection without any medical intervention. Hews et al. [42] also derived a similar type of condition for the stability of the disease-free equilibrium, which reveals a correlation between the proliferation rate and the death rate of infected hepatocytes. By combining our results with those obtained by Hews et al. [42], it can be concluded that the cure of the infection is strongly associated with the proliferation and death rates of both types of hepatocytes. In addition, the system is numerically solved for seven different initial conditions, and it is seen that in each instance, the system stabilizes to the disease-free steady-state as shown in Figure **??**.

Remark 4.5.2. *The stability criteria $3r < 5\mu$ for liver failure, and $3r > 5\mu$ for disease-free steady-states are complementary to each other. Therefore, when both hepatocytes proliferate at equal rate, the dynamics of the infection strongly dependent on the trade-off between the proliferation and death rates of uninfected hepatocytes.*

- **Endemic steady-state** (E_1)

Out of two endemic steady-states, E_1 become biologically feasible when $R_0^E > 1$ and $R_s > 0$ (verified numerically). Due to the presence of high complexity in the expression of this steady-state, its stability is determined numerically. To that purpose, we first calculate the well-known Jacobian matrix at the steady-state E_1, and it is given by

$$J_{E_1} = \begin{pmatrix} -12.1046 & 0.0909218 & 0 & -0.00210356 \\ 12.13 & -0.0984924 & 0 & 0.00210356 \\ 0 & 150 & -0.611 & 0 \\ 0 & 0 & 0.696 & -3.4 \end{pmatrix}. \tag{4.5.10}$$

The eigenvalues of the Jacobian matrix (4.5.10) are calculated as $\lambda_1 = -12.1936$, $\lambda_2 = -3.40902$, $\lambda_3 = -0.603852$, $\lambda_4 = -0.00761528$. It is seen that the values of all eigenvalues $\lambda_i, i = 1, 2, 3, 4$ are negative. Therefore, E_1 becomes locally asymptotically stable provided $R_0^E > 1$. This steady state reflects a chronic infection scenario where the virus persists over a prolonged period without leading to either viral clearance or progression to severe liver disease.

In order to visualize the stability of endemic equilibrium, we consider the value of $k = 3 \times 10^{-12}$ [33] and $r = \rho = 0.3$ to make the value of R_0^E is greater than unity. As a result, $R_0^E \approx 109$ is obtained. In Figure 4.5 (right y-axis plot), the concentration profile for each model compartment are displayed for ten different initial conditions and for $R_0^E \approx 109$. For each initial condition, it is seen that the solutions of the system asymptotically converge to the endemic equilibrium point E_1. On the other hand, the solutions for $R_0^E < 1$ and for the same initial conditions tend to the disease-free steady-state E_f (left y-axis in Figure 4.5) showing the instability of E_1 when $R_0^E < 1$.

4.5.1.3 Effects of proliferation rate

The proliferation rate of infected hepatocytes can vary between acute and chronic infections [50]. In this section, it is studied how hepatocyte proliferation contributes to the infection. In this quest, we set five different values of proliferation rate (r) within the realistic range, as mentioned in Table 4.1. In addition, the possible relationships between initial conditions of the patients and proliferation are also explored.

Acute infection

Figure 4.6 illustrates how the infection dynamics is influenced by the simultaneous proliferation of uninfected as well as infected hepatocyte in acute case. In this case, the values of parameters are chosen in such a way that the value of R_0^E remains below unity. As a result, it is noticed that when proliferation rate (r) is equal to 0.1 (signifies negligible proliferation), maximum liver cell becomes infected within few months. For this value of proliferation rate, the number of uninfected hepatocytes falls below the minimum requirement of the liver to function smoothly, as mentioned in Section 4.4. The number of uninfected hepatocytes increases at a fixed time as the proliferation rate increases whereas no significant change is observed for infected hepatocyte, capsid and virion compartments. Therefore, examining the profile of uninfected hepatocyte, it can be concluded that the proliferation reduces infection in acute case [48].

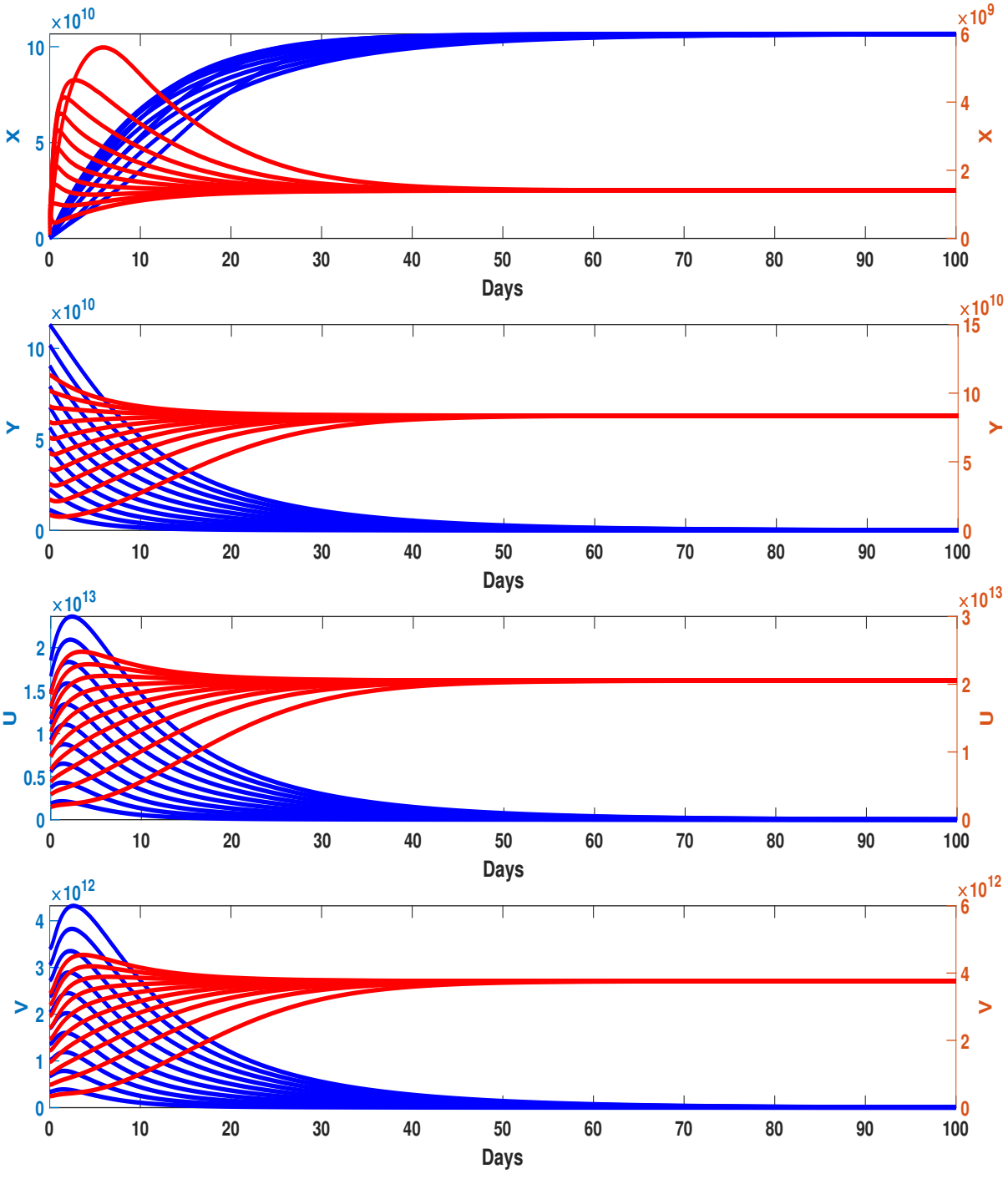

Figure 4.5: Times series of concentration of four variables ($X(t)$, $Y(t)$, $U(t)$, $V(t)$) for 10 distinct initial conditions. The left y-axis represents the solutions for $R_0^E < 1$ whereas the right y-axis shows the solutions when $R_0^E > 1$.

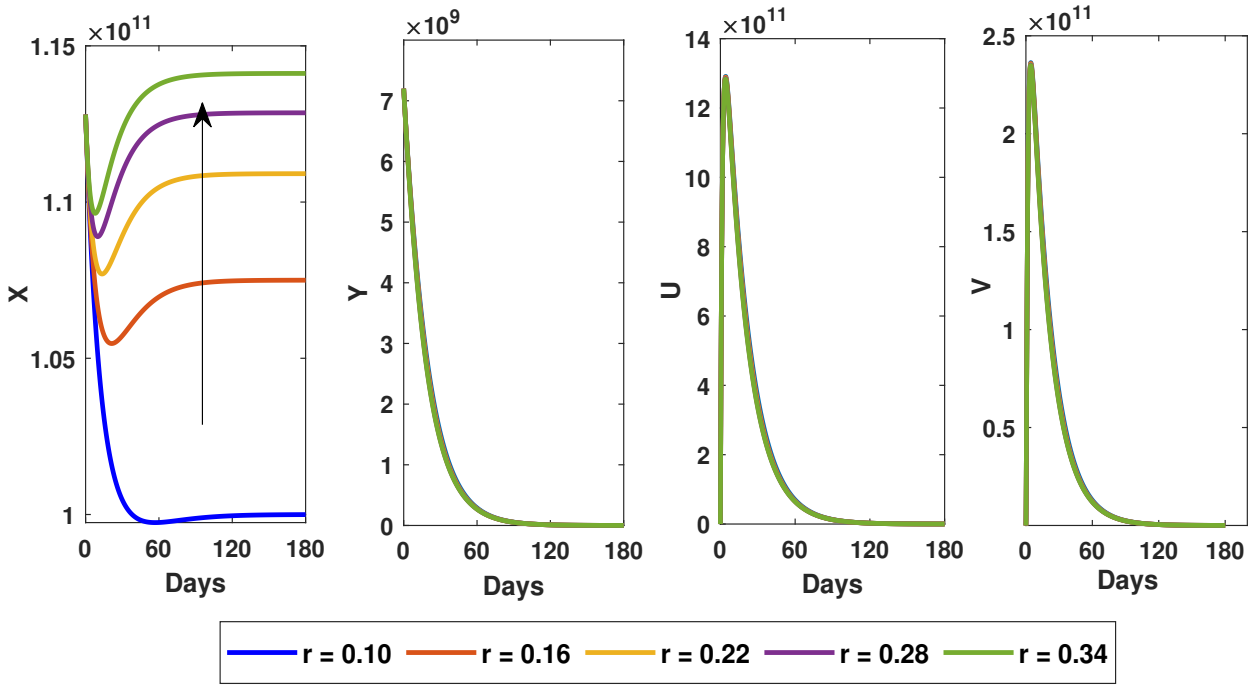

Figure 4.6: Effects of proliferation rate in acute infection. For different value of r, the solutions for infected hepatocytes, capsids and viruses remain unaffected. The arrow indicates the direction of growth of the proliferation rate (r).

Chronic infection

In the case of chronic infection, we have examined the impacts of the proliferation rate and explored the relationship between proliferation and the initial phage of the patients. The proposed model is solved for different values of proliferation rate (r) and the solutions are plotted in Figure 4.7. In acute infection, it is observed that the proliferation rate leads to negligible change in the concentration of infected hepatocytes, capsids and virus compartments (refers Figure 4.6), but in this case, the changes are substantial and considerable. Infected hepatocytes exhibit rapid changes in their profile compared to uninfected counterparts. Since the stability levels of infected hepatocytes, capsids, and viruses rise significantly with the increase in proliferation rate as depicted in the Figure 4.7, it is conspicuous that proliferation serves as a positive factor in the persistence of the infection when both hepatocytes proliferate at equal rate.

In order to elucidate the association between initial conditions of the patients and the proliferation, four different initial conditions (ic_1, ic_2, ic_3, ic_4) are considered following the smooth functional criteria of the liver outlined in the Section 4.4, and the simulation results

are presented in Figure 4.8. For all initial states, proliferation seems to play similar roles, *i.e.*, for a fixed value of r, the solutions converge to the same steady-state in spite of taking different initial conditions. The long-term behavior of the infection is solely governed by mitosis. No notable role of initial conditions of patients is observed in the chronic infection.

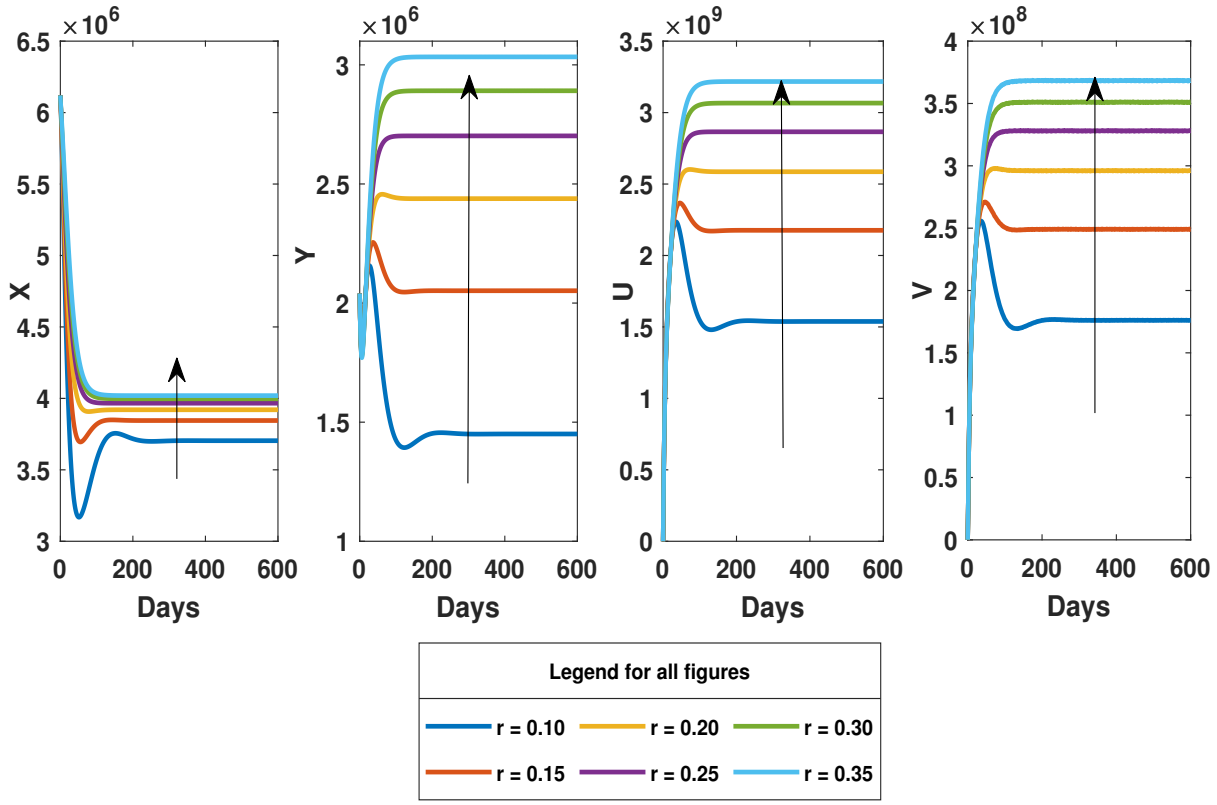

Figure 4.7: Effects of proliferation rate (r) on chronic infection. The arrows indicate the direction of growth of the proliferation rate (r).

4.5.2 Effects of different proliferation rates ($r \neq \rho$) on acute and chronic infection

In this section, it is considered that the rate at which infected hepatocytes proliferate is lower than that of healthy hepatocytes, *i.e.*, $\rho < r$ [42]. Consequently, we revisit the reaction equations corresponding to uninfected and infected hepatocytes as given in equations

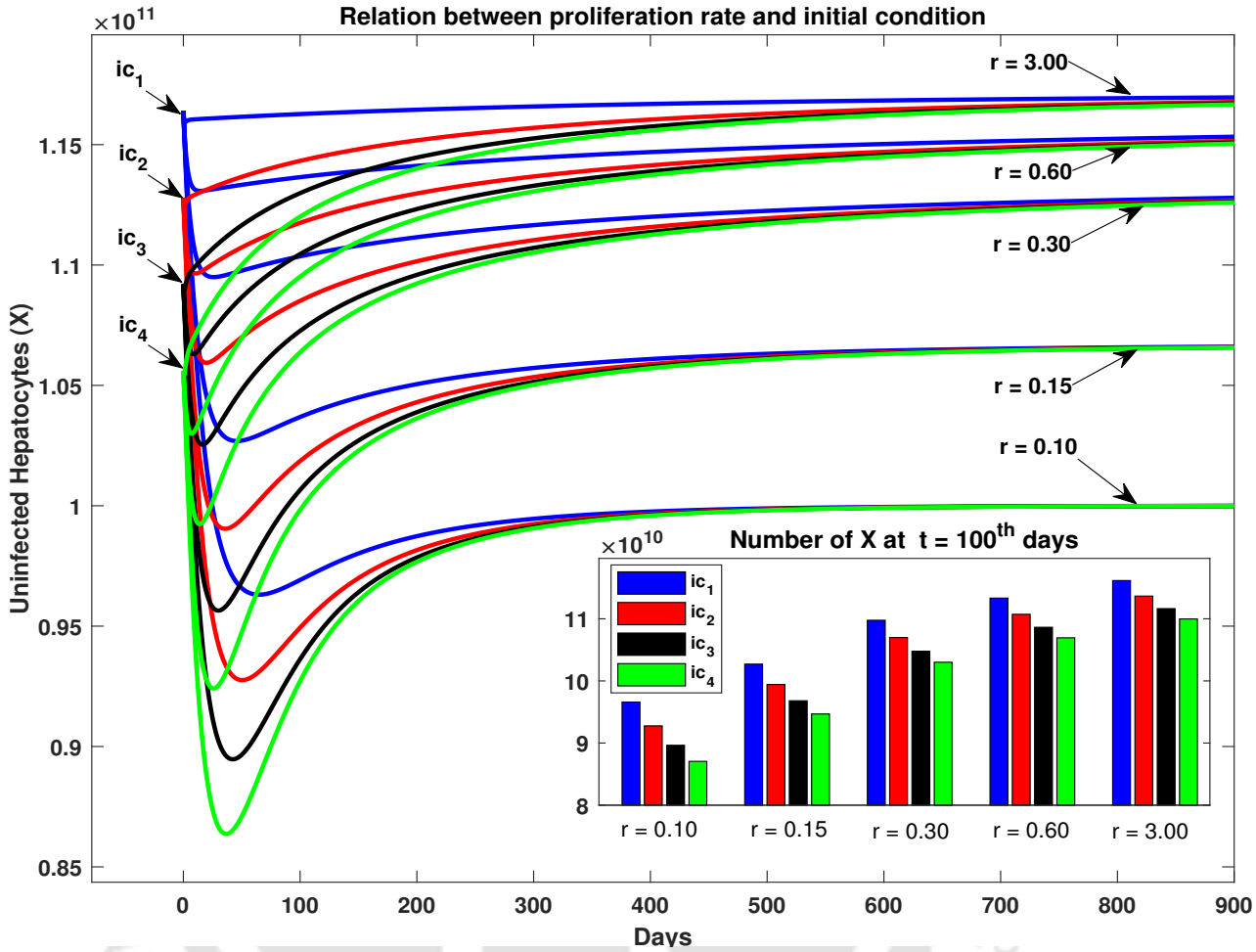

Figure 4.8: The correlation between the proliferation rate and initial conditions of the patients. Lines of the same color indicate that they correspond to the same initial condition but different value of proliferation rate. In the bar diagram, we depict the number of uninfected hepatocytes at $t = 100^{th}$ day.

(4.2.1) and (4.2.2). In Section 4.2, we have already discussed that this system of equations (equations (4.2.1), (4.2.2), (4.2.3) and (4.2.4)) possesses a unique solution. Here, we focus on exploring how variations in the proliferation rates of uninfected and infected hepatocytes affect infection dynamics in the presence of standard incidence function and capsid recycling. To this purpose, a thorough study is carried out in this direction.

4.5.2.1 Steady-states

After considering the case $r \neq \rho$, it appears that both the systems of equations (equations (4.5.1),(4.5.2), (4.2.3), (4.2.4), and equations (4.2.1),(4.2.2), (4.2.3), (4.2.4)) have the equal

number of equilibrium points. It is also seen that the expressions for the liver failure equilibrium point (E_0) and the disease-free equilibrium point (E_f), as calculated in Section 4.5.1.1, are same. However, the values of the other two equilibrium points are different. The basic reproduction number for the system of equations (equations (4.2.1),(4.2.2), (4.2.3), (4.2.4)) is calculated as

$$R_0^{\mathcal{U}} = \frac{a\eta\beta kT(r - r\theta - \mu)}{\delta_v R_s(\mu\rho + \delta r)}, \text{ where } \mathcal{U} \text{ denotes the unequal proliferation.}$$

In addition, the stability analysis is also performed for this system of equations (4.2.1),(4.2.2), (4.2.3), (4.2.4). Stability analysis/proofs are similar and directly follows from the Section 4.5.1.2, *i.e.*,

- Liver failure equilibrium point becomes locally asymptotically stable if $r(1-\theta)-\mu < 0$.
- Disease-free equilibrium point becomes locally asymptotically stable if $r(1-\theta)-\mu > 0$ and $R_0^{\mathcal{U}} < 1$.

The biological interpretation of the constraints $r(1-\theta)-\mu < 0$, and $r(1-\theta)-\mu > 0$) are explained in the Remarks 4.5.1 and Remark 4.5.2.

4.5.2.2 Acute infection

In this case, we have conducted two experiments:

- **Experiment-1:** Proliferation rate of uninfected hepatocytes (r) varies within a reasonable range ($0.001 - 3.4$) and proliferation rate of infected hepatocytes is kept fixed at $\rho = 0.25$ (average value, according to Table 4.1).
- **Experiment-2:** Proliferation rate of infected hepatocytes (ρ) varies within a reasonable range ($0.001 - 0.35$) and proliferation rate of uninfected hepatocytes is kept fixed at $r = 1.7$ (average value, according to Table 4.1).

Figures 4.9(A) and 4.9(B) display the simulation results of Experiment-1 and Experiment-2, respectively. Since the severity of the infection is generally determined by the number of uninfected hepatocytes, we only focus on the profile of uninfected hepatocyte compartment. In Experiment-1, it is observed that when uninfected hepatocytes undergo rapid proliferation, there is a significant increase in the concentration of healthy hepatocytes. Consequently, the disease gradually diminishes over time.

On the other hand, in case of Experiment-2, it is seen that if only infected hepatocytes proliferate, the number of uninfected hepatocytes convergences to the disease-free steady-state, resulting the recovery from the infection. However, for different values of ρ, we obtain almost same profile of infected hepatocytes.

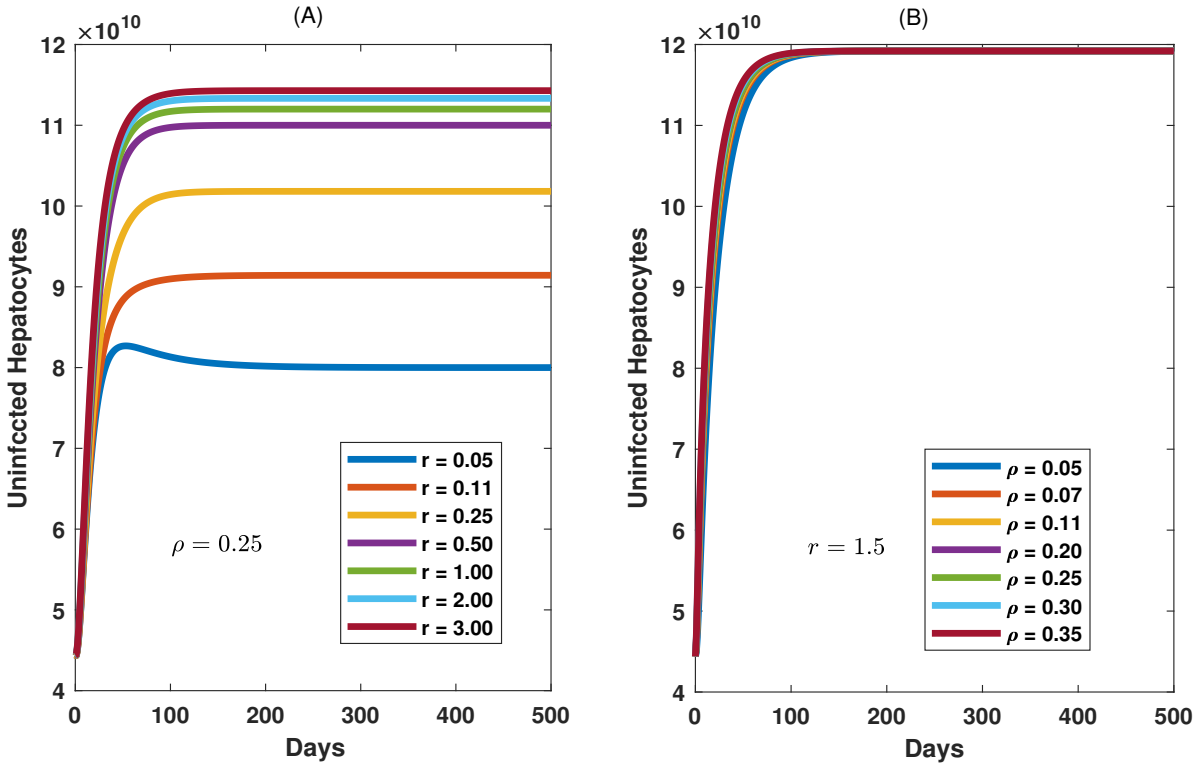

Figure 4.9: Effects of different proliferation rates on acute infection. (A) The impacts of proliferation rate of uninfected hepatocytes (r). (B) The impacts of proliferation rate of infected hepatocytes (ρ).

4.5.2.3 Chronic infection

The understanding of cellular proliferation in chronic infection is still incomplete and possibly unexplored. It also remains unclear whether the roles of proliferation in chronic infections resemble those observed in acute infections. In order to analyze the biologically plausible dynamics in chronic infection, two more experiments on proliferation are conducted in a manner similar to the acute case.

- **Experiment-3 (r: free parameter, ρ: fixed parameter):** The influences of proliferation of uninfected hepatocytes are discussed in the context of long-term infection.

In this experiment, the effects of r are studied keeping ρ fixed. In Figures 4.10(A) and 4.10(B), the temporal behavior of uninfected and infected hepatocytes are demonstrated. Compared to the outcomes of acute infection, chronic infections manifest an opposite trend on these two compartments. In this circumstance, the infection becomes more severe due to rapid proliferation of uninfected hepatocytes. Based on the Figures 4.10(A) and 4.10(B) and rigorous analysis of the proposed model, the probable reasons for these opposite trends in the profiles of liver cells can be explained by considering the fact that the rapid proliferation of uninfected hepatocytes leads to a quick increase in the population of healthy hepatocytes. Consequently, this could cause more frequent interactions between viruses and healthy cells, thereby intensifying the infection.

- **Experiment-4: (r: fixed parameter, ρ: free parameter)** In this case, we study how the proliferation of infected hepatocytes influences the outcomes of the infection. The variations in the outcomes of uninfected and infected liver cells are visualized in Figures 4.10(C) and 4.10(D). As the proliferation rate of infected hepatocytes increases, the number of uninfected hepatocytes increases while the number of infected hepatocytes decreases. Therefore, the persistence of chronic infection is closely associated with the cellular proliferation of infected hepatocytes resulting in two uninfected cells.

For a better understanding, all the results obtained so far are furnished in Table 4.3. With the increase of proliferation rates, if the number of hepatocytes increases, we put "Increase" in the corresponding cell of the Table 4.3. In case of decrease in hepatocytes, we put "Decrease". "No Notable Change" signifies that the respective compartment exhibits no notable changes.

Table 4.3: The relationship between the proliferation of both uninfected and infected hepatocytes and the dynamics of acute and chronic infections. NNC: No Notable Change.

		$r = \rho$ (increase)	$r \neq \rho$	
			r increase, ρ fixed	ρ increase, r fixed
Acute	Uninfected hepatocytes	Increase	Increase	NNC
	Infected hepatocytes	NNC	NNC	NNC
Chronic	Uninfected hepatocytes	Increase	Decrease	Increase
	Infected hepatocytes	Increase	Increase	Decrease

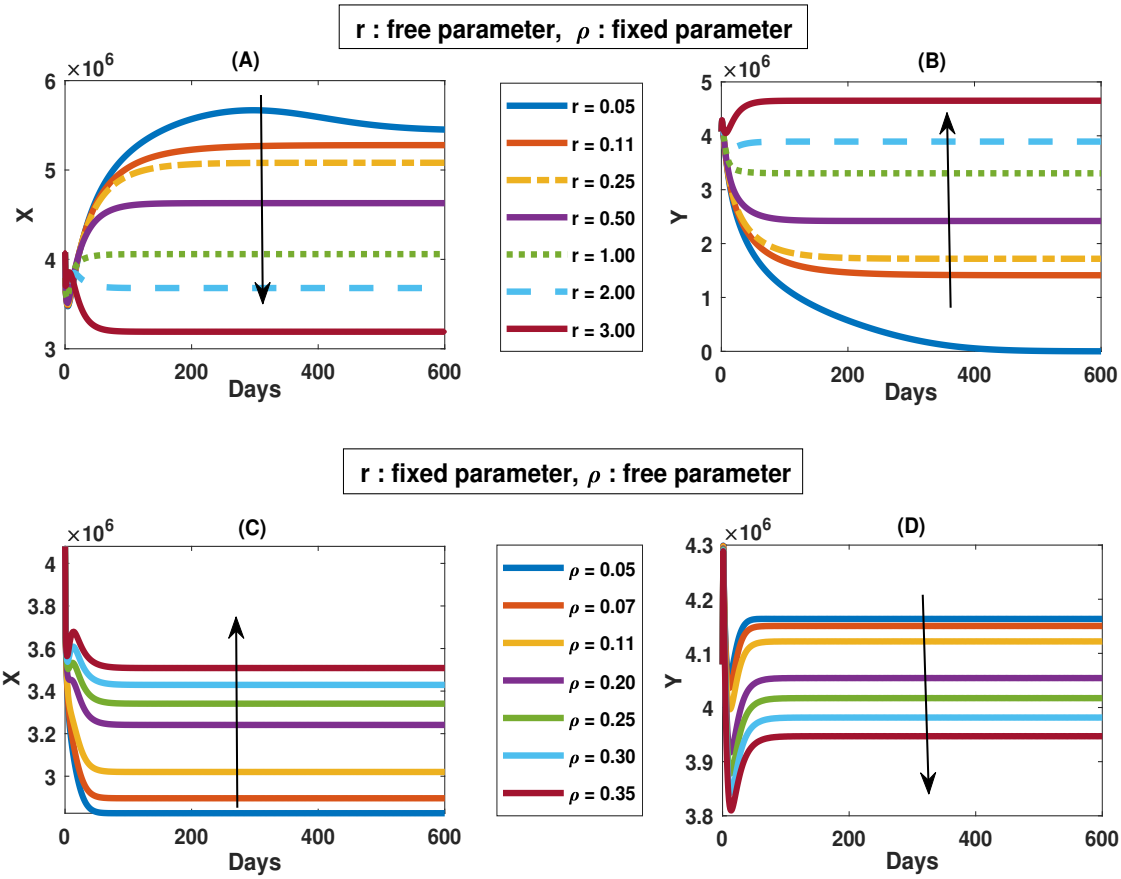

Figure 4.10: Effects of different proliferation rate ($r \neq \rho$) in chronic infection. The arrows indicate the direction of growth of the proliferation rate r or ρ.

4.6 Modified model: Proliferation is not a continuous biological process

In the proposed model (equations (4.2.1), (4.2.2), (4.2.3) and (4.2.4)), it is assumed that proliferation always occurs, *i.e.*, proliferation is a continuous biological process. In the literature, it is seen that during liver regeneration after partial resection or injury, the remaining hepatocytes rapidly multiply to restore the liver function. In response to liver damage or diseases like hepatitis or cirrhosis, compensatory hepatocyte proliferation occurs to replace damaged cells. According to a study of Miyaoka and Miyajima [146], cellular proliferation only occurs when the total number of liver cells decreases to less than 70% of its initial number, *i.e.*, cellular proliferation is not a continuous process. It is a widely accepted concept that all remnant hepatocytes actively divide to recover the original cell

count and liver mass. In order to include this phenomenon into the proposed model, those terms responsible for continuous proliferation $(rX(t)+2\rho Y(t))\left(1-\frac{X(t)+Y(t)+\theta T}{T}\right)$ in equation (4.2.1) and $\rho Y(t)\left(1-\frac{X(t)+Y(t)+\theta T}{T}\right)$ in equation (4.2.2) are replaced with $(rX(t)+2\rho Y(t))\left(1-\frac{X(t)+Y(t)+\theta T}{T}\right)H\left(0.7-\frac{X(t)+Y(t)+\theta T}{T}\right)$ and $\rho Y(t)\left(1-\frac{X(t)+Y(t)+\theta T}{T}\right)H\left(0.7-\frac{X(t)+Y(t)+\theta T}{T}\right)$, respectively, where $H(\tau)$ denotes Heaviside step function defined by

$$H(\tau)=\begin{cases}0, & \tau<0,\\ 1, & \tau\geq 0.\end{cases}$$

Here, $H\left(0.7-\frac{X(t)+Y(t)+\theta T}{T}\right)$ indicates the fact that cellular proliferation initiates only when the total liver cell count falls below 70% of its initial number. The associated modified governing equations for uninfected and infected classes are given by the following equations:

$$\begin{aligned}\frac{dX(t)}{dt}&=(rX(t)+2\rho Y(t))\left(1-\frac{X(t)+Y(t)+\theta T}{T}\right)H\left(0.7-\frac{X(t)+Y(t)+\theta T}{T}\right)\\&\quad-kX(t)V(t)-\mu X(t),\end{aligned}\tag{4.6.1}$$

$$\begin{aligned}\frac{dY(t)}{dt}&=kX(t)V(t)-\rho Y(t)\left(1-\frac{X(t)+Y(t)+\theta T}{T}\right)H\left(0.7-\frac{X(t)+Y(t)+\theta T}{T}\right)\\&\quad-\delta Y(t).\end{aligned}\tag{4.6.2}$$

Since $H(\tau)$ exhibits discontinuity at $\tau=0$, its applicability in continuous system is restricted as it fails to accurately capture an uninterrupted process. Due to this limitation in Heaviside function, $H(\tau)$ is approximated by a smooth function as follows:

$$H(\tau)\approx\frac{1}{2}\left(1+\tanh\left(\frac{\tau}{\epsilon}\right)\right),$$

where ϵ is very small in magnitude. The function $\left(1+\tanh\left(\frac{\tau}{\epsilon}\right)\right)$ provides a smooth, monotonic description of proliferation. The graphical representation of these two functions are shown in Figure 4.11. The reaction equations for capsids (equation (4.2.3)) and virus (equation (4.2.4)) classes remain unchanged since, in this context, no modification is necessary in these two compartments.

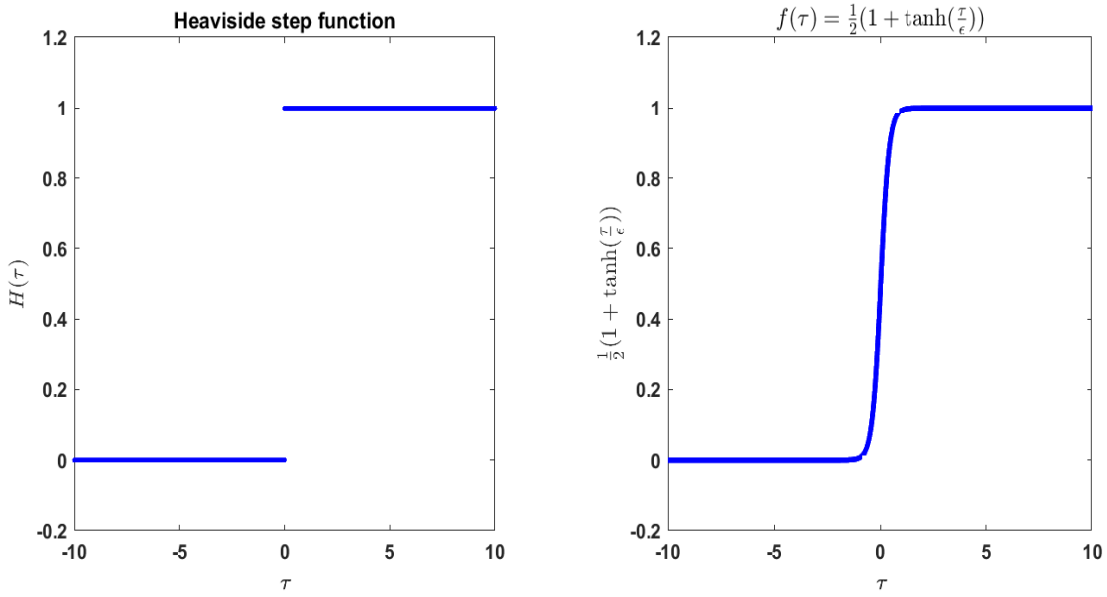

Figure 4.11: Heaviside step function and its approximation function. The value of $\epsilon = 0.4$ is used here.

4.6.1 Continuous vs discontinuous proliferation

For convenience of the discussion, the following things are defined as:

- **Continuous proliferation:** When the liver cells proliferate continuously, this process is referred to as continuous proliferation. Both the terms $rX(t)\left(1 - \dfrac{X(t)+Y(t)+\theta T}{T}\right)$ and $\rho Y(t)\left(1 - \dfrac{X(t)+Y(t)+\theta T}{T}\right)$ represent continuous proliferation of uninfected and infected hepatocytes respectively due to the genesis of these terms. This type of proliferation is crucial for enabling the replacement of old or damaged cells with new ones. In the liver, this process is vital for its regenerative capabilities, allowing it to recover from injuries and maintain its various functions. However, this continuous proliferation can lead to pathological conditions, such as cancer, where the balance between cell growth and cell death is disrupted, leading to uncontrolled cell growth.

- **Discontinuous proliferation:** Discontinuous proliferation occurs at irregular intervals. This type of proliferation typically happens in response to specific needs such as during wound healing, immune response, or periods of rapid growth. The expressions $rX(t)\left(1 - \dfrac{X(t)+Y(t)+\theta T}{T}\right) H\left(0.7 - \dfrac{X(t)+Y(t)+\theta T}{T}\right)$ and $\rho X(t)\left(1 - \dfrac{X(t)+Y(t)+\theta T}{T}\right) H\left(0.7 - \dfrac{X(t)+Y(t)+\theta T}{T}\right)$ used in the equations

(4.6.1) and (4.6.2) are termed as discontinuous proliferation because it occurs only when the number of liver cell falls below 70% of initial number.

For our convenience, we denote the system of equations ((4.2.1), (4.2.2), (4.2.3) and (4.2.4)) as P-model (primary model) and system of equations ((4.6.1), (4.6.2), (4.2.3) and (4.2.4)) as M-model (modified model). Equations (4.2.3) and (4.2.4) are common in both P-model and M-model since the incorporation of discontinuous proliferation of liver cells leaves these two equations ((4.2.3) and (4.2.4)) unchanged. Both models (P-model and M-model) are solved numerically, and the corresponding solutions are demonstrated in Figure 4.12. As a result, it is observed that despite the consideration of same values of parameters and same initial condition, there are substantial variations in the solutions. It is also noticed that in case of discontinuous proliferation, the infection becomes more severe, since the number of uninfected hepatocytes in discontinuous proliferation is significantly less than that in continuous proliferation. As the M-model is more biologically realistic than the P-model, it should serve as the basis for understanding the true infection dynamics.

4.7 Global sensitivity analysis

The purpose of sensitivity analysis is to examine how a mathematical model responds to changes in its input variables, such as model parameters, initial conditions, source functions. There are two types of sensitivity analysis: (i) local sensitivity analysis and (ii) global sensitivity analysis. Local sensitivity analysis examines the model's response when only one parameter is varied keeping all other parameters fixed. On the other hand, global sensitivity analysis investigates the model's response when all parameters are varied simultaneously. Examining GSA at a single time point $t = t_1$ does not yield a complete understanding of how a parameter behaves throughout the entire infection period. In order to gain a clear understanding of a parameter's behavior throughout the entire infection period, we perform GSA for each parameter and for each compartment over the entire time domain of interest $[0, 900]$. In this study, the method Latin Hypercube Sampling–Partial Rank Correlation Coefficient (LHS-PRCC) is applied using 1000 samples. The details about the methodology and the algorithm are well-explained in the article of Marino et al. [85]. Partial rank correlation coefficients measure the strength of the statistical relationship between each parameter and the state variable. PRCC values range from -1 to 1. The magnitude of PRCC values reflects how durable the correlation is and the sign indicates whether the correlation is positive or negative. In common practice, a parameter is considered to be insensitive if the corresponding PRCC value is close to zero. In order to study sensitiveness of each parameter,

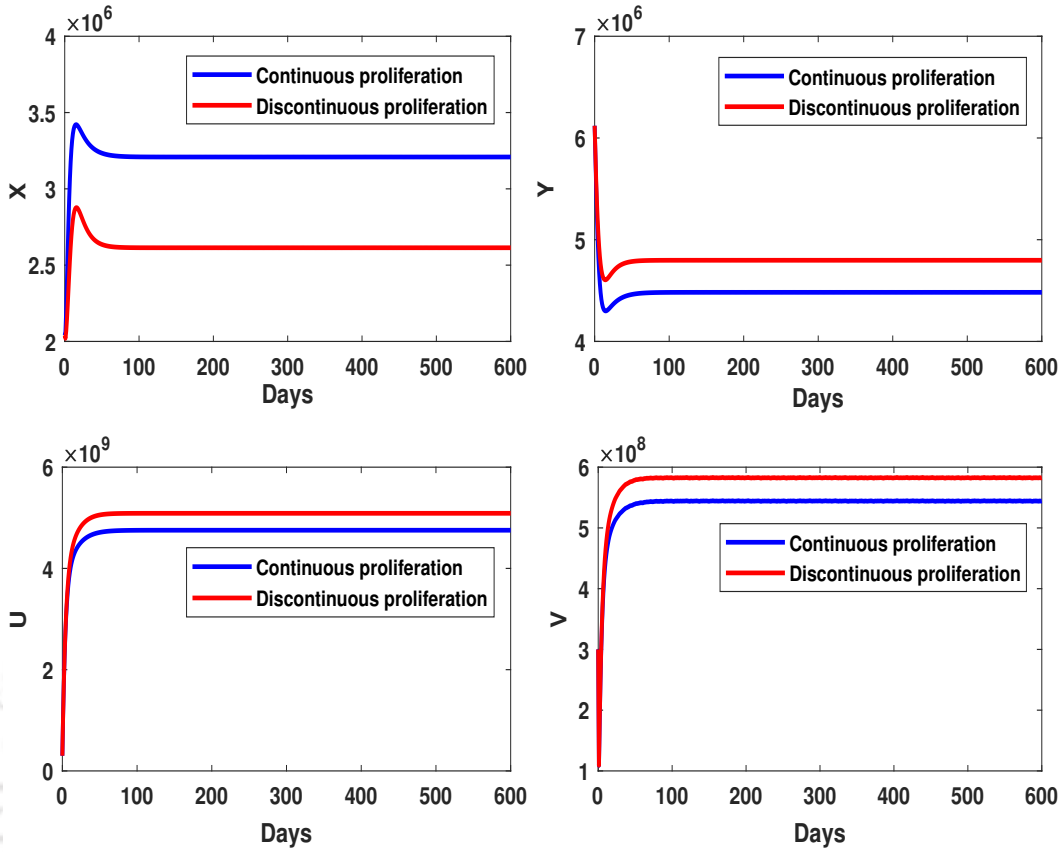

Figure 4.12: A comparison between the outcomes of continuous and discontinuous proliferation.

the GSA for both P-model and M-model are conducted here. We also investigate how the characteristics of the parameters are affected when discontinuous proliferation is taken into account.

4.7.1 Global sensitivity analysis of P-model

The long-term behaviors of the sequence of PRCC values of parameters for P-model are shown in Figure 4.13. The curves shown in Figure 4.13 are generated by plotting PRCC values at each time point. In general, these curves are called PRCC curves. For our convenience, we introduce the notation PRCC($X(t) : p$) which denotes the PRCC curve for parameter p against the model compartment $X(t)$. Based on the PRCC values, the parameters for each compartment are classified as positively sensitive, negatively sensitive, or insensitive, as listed in Table 4.4 at $t = 900^{th}$ day. Recently, Goyal et al. [48] showed that the

Table 4.4: Positively, negatively and less sensitive parameters for corresponding compartments for P-model.

Model compartments	Positively sensitive parameters	Negatively sensitive parameters	Insensitive parameters
Uninfected hepatocytes ($X(t)$)	$\delta, \delta_v, \rho, \eta$	a, k, γ, μ	β, r
Infected hepatocytes ($Y(t)$)	a, k, r, γ	$\delta, \delta_v, \rho, \eta$	β, μ
Capsids ($U(t)$)	a, k, r, γ	$\delta, \delta_v, \rho, \eta, \beta$	μ
Viruses ($V(t)$)	a, k, r, γ	$\delta, \delta_v, \rho, \eta$	μ, β

clearance of acute infection is highly associated with the production of two uninfected cells upon proliferation of an infected cell. As far as we are aware, no one has yet provided any information regarding the proliferation of infected hepatocytes in chronic infection. From Figure 4.13, it is observed that PRCC($X(t) : \rho$) always lies above the x-axis. This indicates that the proliferation of infected hepatocytes is positively correlated with uninfected hepatocytes. On the other hand, PRCC($Y(t) : \rho$), PRCC($U(t) : \rho$), PRCC($V(t) : \rho$) consistently lie below the x-axis meaning that the proliferation of infected hepatocytes shows a negative correlation with the infected hepatocytes, capsids, and viruses compartments. Therefore, GSA analysis suggests that the clearance of chronic infection is also notably influenced by the proliferation of infected cells result in two uninfected progenies. In section 4.5.2.3, the outcome of Experiment-4 also shows similar results. It is a theoretical finding. To substantiate this result, it is necessary to conduct empirical research and clinical studies.
Additionally, several other significant findings have been identified and are listed below.

1. The production rate of capsids (a) and infection rate (k) exhibit negative correlations with uninfected hepatocytes and positive correlations in other three compartments.

2. It is observed that the recycling rate of capsids enhances infection as it correlates positively with infected hepatocytes, capsids, and viruses.

3. We do not find significant impacts of virus production rate (β) on the infection in chronic phase, although it initially influences the infection.

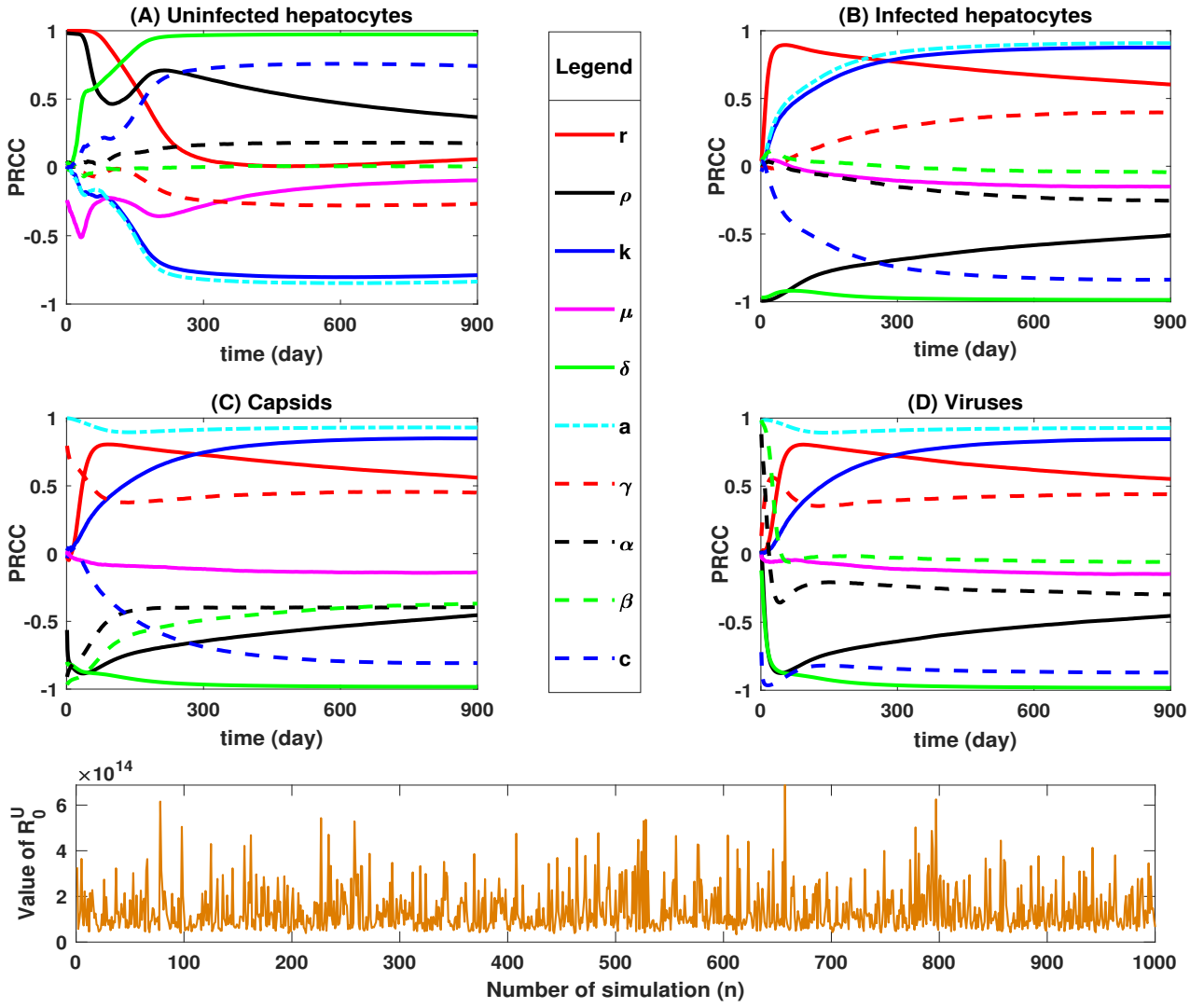

Figure 4.13: Long term behavior of the PRCC values of the model parameters for P-model. (A): On uninfected hepatocytes, (B): On infected hepatocytes, (C): On HBV capsids, (D): On Viruses. The last figure indicates the value of basic reproduction number $\left(R_0^{\mathcal{U}}\right)$ with respect to the number of simulation n.

4.7.2 Global sensitivity analysis of M-model

After incorporating the discontinuous proliferation of both uninfected and infected hepatocytes into the P-model (discussed in Section 4.6), notable changes appear in the solutions (refers Figure 4.12), even though the model parameters and initial conditions remain unchanged. This motivates to continue with further investigation. Similarly to the P-model, considering the same setup, we also examine the GSA of the M-model, and compared the

obtained results with those of the P-model. The differences between the PRCC curves for all parameters in the compartments of infected hepatocytes, capsids, and viruses are found to be insignificant. However, drastic changes are observed in the uninfected hepatocyte compartment. In Figure 4.14, the PRCC values of each parameter for the uninfected hepatocyte compartments in both the models (P-model and M-model) are depicted using bar diagram at $t = 900^{th}$ day. It is observed that for each parameter except r, the PRCC values corresponding to the P-model are higher in magnitude compared to that of the M-model. So, incorporation of discontinuous proliferation diminishes the sensitivity of the model parameters.

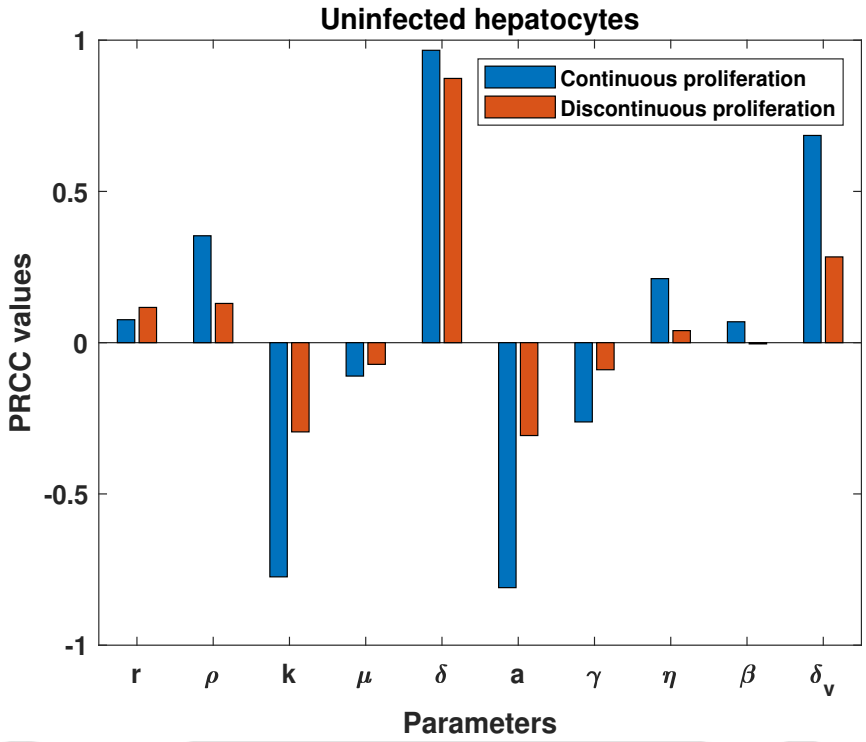

Figure 4.14: PRCC values of the parameters for the uninfected hepatocyte compartment are shown for both the P-model (blue bars) and the M-model (red bars).

4.8 Conclusions

In this paper, the effects of proliferation of uninfected as well as infected hepatocytes along with recycling of capsids on HBV infection are studied. Capsid recycling is one of the distinctive features in this model. The model solution demonstrates a strong agreement with the experimental data. The stability of the equilibrium points are established based on the value of basic reproduction number and proliferation rate. This study also addresses the consequences of both continuous and discontinuous proliferation, possibly for the first time. The global sensitivity analysis is performed to identify the most positively as well as the most negatively sensitive parameter of the proposed models. Overall, this study produces some new results, reveals rich dynamics of infection, and establishes a foundation for further research.

The followings are the key results from this study:

1. We find a biological relationship between the proliferation rate (r) and the death rate of uninfected hepatocytes (μ) for acute liver failure.

2. When both uninfected and infected hepatocytes proliferate with equal rate ($r = \rho$) in acute infection, the number of uninfected hepatocytes increases as the proliferation rate increases. At the same time, the number of infected hepatocytes decreases to zero. This suggests that during acute infection, proliferation aids the individual in a rapid recovery from the infection.

   In case of chronic infection, the severity of the infection increases if the proliferation occurs frequently.

3. When uninfected and infected hepatocytes proliferate with different rates ($r \neq \rho$), proliferation of uninfected hepatocytes cure the disease quickly where we do not find any significant contribution of proliferation of infected hepatocytes in acute case.

   On the other hand, the experiments on chronic infection indicate that the infection is highly influenced by proliferation of both types of liver cells. The proliferation of uninfected hepatocytes increases the infection whereas proliferation of infected hepatocytes decreases.

4. The difference between the solutions of continuous and discontinuous proliferation is substantial and noteworthy. It appears that discontinuous proliferation is more detrimental to a patient than continuous proliferation.

5. The global sensitivity analysis also indicates that the proliferation of infected hepatocytes acts as a negatively influential factor in the infection. Over the long term infection, the proliferation rate of infected hepatocytes shows positive correlation with uninfected hepatocytes and negative correlation with the compartments of infected hepatocytes, capsids and viruses.

CHAPTER 5

Multi-point Infection Dynamics of Hepatitis B in the Presence of Sub-Viral Particles

In this chapter, a mathematical model is proposed by incorporating the roles of SVPs and including the effects of capsid recycling. The impacts of spatial mobility of capsids, viruses, SVPs and antibodies are also taken into account in this model. Overall, this model carry unique characteristics in the context of this viral infection. This study investigates the changes in the dynamics of infection considering both single-point as well as multi-point infections as initial conditions. As a result, it is observed that SVPs can significantly enhance intracellular viral replication and gene expression by reducing the neutralization of virus particles by antibodies. The recycling of capsids substantially increases the concentration of SVPs. The experiments which are carried out on single-point as well as multi-point infections as initial conditions show that if the liver is infected at more than one point, infection propagates rapidly. The outcomes of the proposed model strongly recommend that it is imperative to consider the diffusion terms while the dynamics of this viral infection is illustrated.

5.1 Introduction

Sub-viral particles (SVPs) are non-infectious viral particles. These are predominantly composed of viral surface antigens (HBsAg) proteins that are the major components of the lipid bi-layer envelope [13]. SVPs don't contain nucleocapsid proteins and viral nucleic acids. The production of SVPs is a natural biological process. While the viruses replicate within the hepatocytes, both complete viral particles and SVPs produce simultaneously and release into the bloodstream. Generally, SVPs are found in the blood of infected individuals in two main forms: (i) spherical particles measuring 25 nm in diameter and (ii) filaments with a diameter of 22 nm, which can differ in length [53, 54]. In the literature, many authors have reported that the ratio of Dane particles to SVPs ranges from 1:10,000 to 1:100,000 [54–56], *i.e.*, a large quantity of HBsAg derived from viral particles has no effect on the reservoir of viral replication. Although, the actual reasons behind their overproduction and their exact roles in HBV pathogenesis are still not properly known [57]. The assembly and secretion pathways of SVPs are typically distinct from those used by the viral particles. Researchers are dedicated to unravel the primary causes underlying their excessive production and understand their critical functions in the development of HBV-related illnesses. In chronic HBV infection, the concentration of SVPs in the bloodstream greatly exceeds that of infectious virions. To the best of our knowledge, despite its significant overproduction, the functions of SVPs have been widely overlooked in the previous studies [3, 11, 22, 26, 27, 36, 50, 52, 58–62], leaving a gap in our knowledge about their biological importance. Recently, Cao et al. [63] demonstrated the distribution of Dane particles (virus), spherical particles, and filamentous particles using micrographs and suggested that there is a universal folding shape of HBsAg on SVPs. From the perspective of Rydell et al. [63, 64], SVPs are believed to potentially facilitate cell-to-cell spread, particularly in the presence of neutralizing antibodies. SVPs function as a disguise for the virus. As a result of this characteristic of SVPs, a substantial portion of HBV-specific antibodies produced by the host's immune system is targeted towards neutralizing SVPs, thereby helping the virus evade the immune response [64]. However, to our knowledge, this effect has not been demonstrated experimentally or in animal models so far. Although, SVPs are less efficient in blocking viral entry by binding to target cells [65]. High levels of SVPs can stimulate the immune system, leading to the production of antibodies against HBsAg. For this virus, Bruns et al. [66], and Klingmüller and Schaller [67] reported that SVP has capability to both enhance and inhibit cell attachment of the viruses. The collective evidence suggests that SVPs have some notable impacts on the advancement and perpetuation of the infection. Based on these findings, it is apparent that more elaborate studies are imperative to enhance our understanding about SVPs.

Motivated by the aforementioned discussion, in this study, we shed light on the roles of SVPs in the development of infection via a modified HBV infection dynamics model. In this framework, incorporating the diffusion effects of HBV DNA-containing capsids, virus, SVPs and antibodies, and the impacts of SVPs, we extend the previously proposed HBV infection dynamics model (2.2.1) mentioned in Chapter 2. The precise interplay between virus particles and antibodies is also focused on this work. In this model, it is considered that the capsids, viruses, SVPs and antibodies follow the Fickian diffusion that refers to the process of molecular or particle transport driven by concentration gradients, described by Fick's law of diffusion. The influences of the spatial diffusion of capsids, viruses, SVPs, and antibodies is explained from different perspectives. On the other hand, the initial conditions of the infection are another key factor that significantly affects the infection's dynamics. It is also aimed to investigate the correlations between outcomes of the infection and various types of initial conditions, such as single-origin, dual-origin, tri-origin, etc. Here,"n-origin" initial conditions indicate that the infection originates from n distinct points within the liver.

5.2 Model formulation

Incorporating the functions of SVPs and antibodies, we extend the model (2.2.1). It is believed that the diffusion of viral components plays a pivotal role in controlling and preventing the infection. The effects of spatial mobility of all viral components (rcDNA-containing capsids, viruses, SVPs) and antibodies are also taken into account to make the model more reliable and closer to reality. The extended model is formulated as follows:

5.2.1 Governing equations

The mathematical formulation of the model is as follows:

$$\frac{\partial X(x,t)}{\partial t} = \lambda - \mu X(x,t) - kV(x,t)X(x,t), \quad \text{in} \quad \Omega \times (0,\tau), \tag{5.2.1}$$

$$\frac{\partial Y(x,t)}{\partial t} = kV(x,t)X(x,t) - \delta Y(x,t), \quad \text{in} \quad \Omega \times (0,\tau), \tag{5.2.2}$$

$$\frac{\partial U(x,t)}{\partial t} = \mathcal{D}_1 \frac{\partial^2 U(x,t)}{\partial x^2} + aY(x,t) + \gamma(1-\eta)U(x,t) - \eta\beta U(x,t) - \delta U(x,t), \quad \text{in} \quad \Omega \times (0,\tau), \tag{5.2.3}$$

$$\frac{\partial V(x,t)}{\partial t} = \mathcal{D}_2 \frac{\partial^2 V(x,t)}{\partial x^2} + \eta\beta U(x,t) - g_1 A(x,t)V(x,t) - \delta_v V(x,t), \quad \text{in} \quad \Omega \times (0,\tau), \tag{5.2.4}$$

$$\frac{\partial S_v(x,t)}{\partial t} = \mathcal{D}_3 \frac{\partial^2 S_v(x,t)}{\partial x^2} + bY(x,t) - g_2 A(x,t) S_v(x,t) - \delta_{sv} S_v(x,t), \quad \text{in} \quad \Omega \times (0,\tau), \tag{5.2.5}$$

$$\frac{\partial A(x,t)}{\partial t} = \mathcal{D}_4 \frac{\partial^2 A(x,t)}{\partial x^2} + h(V(x,t) + S_v(x,t)) + r_A A(x,t)\left(1 - \frac{A(x,t)}{A_m}\right) - g_1 A(x,t) V(x,t) - g_2 A(x,t) S_v(x,t) - \delta_a A(x,t), \quad \text{in} \quad \Omega \times (0,\tau), \tag{5.2.6}$$

where $\Omega \subset \mathbb{R}$ is a connected bounded domain where viruses, cells and antibodies stay and can interact. Here, $X(x,t)$, $Y(x,t)$, $U(x,t)$, $V(x,t)$, $S_v(x,t)$ and $A(x,t)$ represent uninfected cells, infected cells, rcDNA-containing capsids, viruses, SVPs, and antibodies at the point $(x,t) \in \Omega \times (0,\tau)$, respectively. We adhere to the fact that uninfected and infected hepatocytes do not exhibit any kind of spatial movement. The corresponding spatial mobilities of capsids, viruses, SVPs, and antibodies in the liver are characterized by diffusion coefficients $\mathcal{D}_1$, $\mathcal{D}_2$, $\mathcal{D}_3$, and $\mathcal{D}_4$. The proposed model (equations (5.2.1)-(5.2.6)) is called *diffusion model* if the value of any $\mathcal{D}_i$, $i = 1,2,3,4$ is non-zero. Otherwise, this model is addressed as *non-diffusion model*. The parameter b denotes the production rate of SVPs from infected hepatocytes. In general, $b >> a$ since infection with HBV results in the production in a large number of SVPs, likely at least 1,000-fold more than virus particles [147]. It is considered that the development of antibodies is equally influenced by the presence of both virions and SVPs. The term $h(V(x,t)+S_v(x,t))$ reflects the production of antibodies whereas h denotes the production rate of antibodies following the work done by Ciupe et al. [148]. Since both virions and SVPs display the HBV-specific antigen on their surface, antibodies are equally effective in neutralizing both types, thereby providing a robust immune response against infection. The neutralizing rate of viruses is given by $g_1 A(x,t)V(x,t)$ as described in the article of Chenar et al. [149], where g_1 represents the association rate constant for antibodies reacting to viral.The SVPs are also inactivated by direct binding with antibodies, which is represented by the term $g_2 A(x,t)S_v(x,t)$ in the models [148, 150]. The parameter δ_{sv} and δ_a denote the normal decay rates of SVPs and antibodies, respectively. In the absence of viruses, we also introduce a logistic term with a maximum intrinsic growth rate r_A and a carrying capacity A_m for the maintenance of antibodies. This term ensures that the antibody population grows to a stable level, reflecting the natural homeostatic control mechanisms within the immune system.In a nutshell, the semantic representation of the above proposed model (equations (5.2.1)-(5.2.6)) are shown in the Figure 5.1.

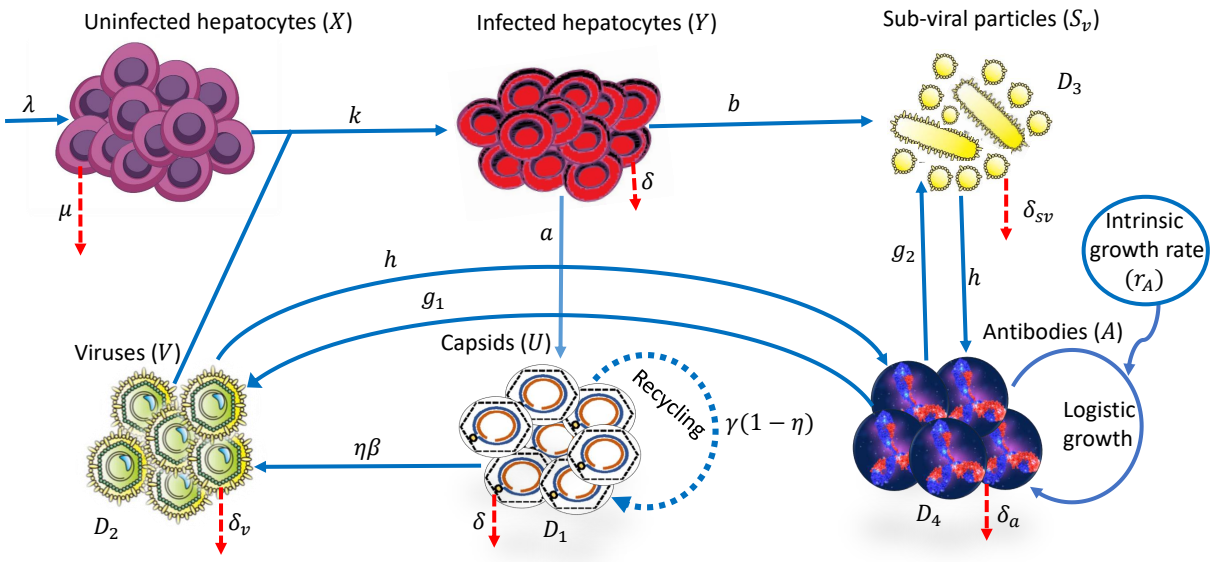

Figure 5.1: Semantic representation of the proposed model given by the system of equations (5.2.1)-(5.2.6).

5.2.2 Initial and boundary conditions

In order to close the system (equations (5.2.1)-(5.2.6)), it is essential to specify reasonable initial and boundary conditions for each compartment $(X(x,t), Y(x,t), U(x,t), V(x,t), S_v(x,t),$ and $A(x,t))$ of the proposed model. For the convenience of analysis, let L be the total length of the liver shown in Figure 5.2 and $[0, L]$ be the domain of interest. We denote $[0, L]$ as Ω. It is assumed that the infection initially starts from $x = 0$, *i.e.*, from the left side of the liver.

- **Initial conditions:**

For defining the initial conditions for each model compartment in the domain $[0, L]$, we adhere to the following biologically relevant assumptions:

1. At the point of infection (POI) $x = 0$, the concentration of uninfected hepatocytes is very low, whereas the concentration of infected hepatocytes is extremely high.

2. At the POI, the initial concentrations of HBV capsids, viruses, SVPs and antibodies are maximum and equal for all these four compartments, *i.e.*, $U_0 = V_0 = S_{v0} = A_0$.

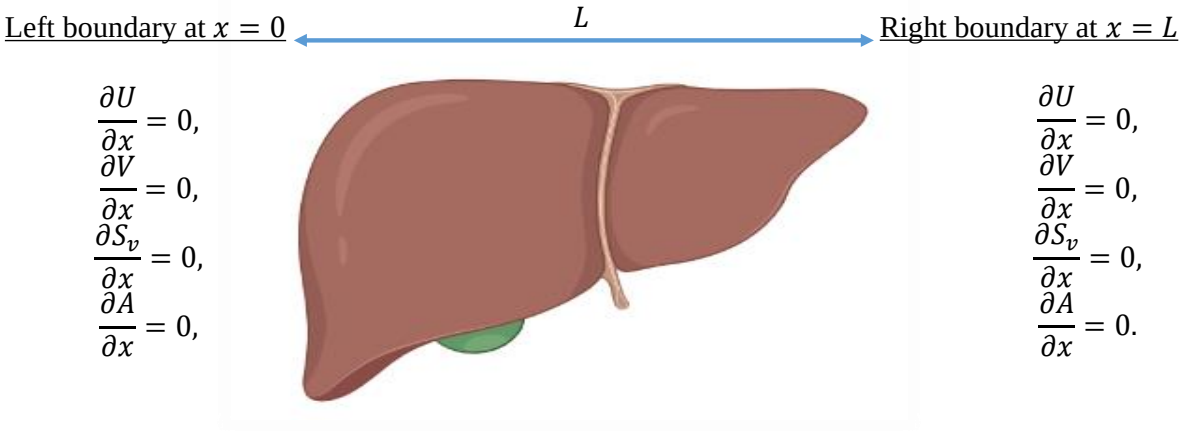

Figure 5.2: The length of the liver and the prescribed boundary conditions at $x = 0$ and $x = L$ are shown at the left and right sides of the liver, respectively. This picture of liver is taken from BioRender.com.

Following the similar approach as detailed in the article of Chaplain and Lolas [151], the respective initial conditions are formulated. In terms of mathematics, all of these initial concentrations are written as

$$\left.\begin{aligned} X(x,0) &= T\left(1-\exp\left(-\frac{x^2}{\epsilon^*}\right)\right),\ 0\le x\le L,\\ Y(x,0) &= T\exp\left(-\frac{x^2}{\epsilon^*}\right),\ 0\le x\le L,\\ U(x,0) &= U_0\exp\left(-\frac{x^2}{\epsilon^*}\right),\ 0\le x\le L,\\ V(x,0) &= V_0\exp\left(-\frac{x^2}{\epsilon^*}\right),\ 0\le x\le L,\\ S_v(x,0) &= S_{v0}\exp\left(-\frac{x^2}{\epsilon^*}\right),\ 0\le x\le L,\\ A(x,0) &= A_0\exp\left(-\frac{x^2}{\epsilon^*}\right),\ 0\le x\le L,\quad \text{with}\ \ \epsilon^*=0.01, \end{aligned}\right\} \tag{5.2.7}$$

- **Boundary conditions:**

Guided by the in vivo protocol, it is considered that the infection takes place within the liver, it is assumed that there is no-flux of capsids, viruses, SVPs and antibodies across the boundary of the liver, *i.e.*, throughout the infection, the liver acts as an impregnable fortress, forbidding the entry or exit of any external capsids, viruses, or SVPs. The end points of the

liver are denoted by $x = 0$ and $x = L$ in one-dimensional framework, shown in Figure 5.2. These imposed homogeneous Neumann boundary conditions are represented by the following equations;

$$\frac{\partial U(x,t)}{\partial x}\Big|_{x=0} = \frac{\partial V(x,t)}{\partial x}\Big|_{x=0} = \frac{\partial S_v(x,t)}{\partial x}\Big|_{x=0} = \frac{\partial A(x,t)}{\partial x}\Big|_{x=0} = 0,\ t \geq 0, \tag{5.2.8}$$

and

$$\frac{\partial U(x,t)}{\partial x}\Big|_{x=L} = \frac{\partial V(x,t)}{\partial x}\Big|_{x=L} = \frac{\partial S_v(x,t)}{\partial x}\Big|_{x=L} = \frac{\partial A(x,t)}{\partial x}\Big|_{x=L} = 0,\ t \geq 0, \tag{5.2.9}$$

where $\dfrac{\partial}{\partial x}$ denotes the outward normal derivative on the boundary of the domain $x = 0$ and $x = L$.

5.3 Non-dimensional form of the proposed model

Due to the presence of high non-linearity in the proposed model problem, the system of PDEs (equation (5.2.1)-(5.2.6)) is solved numerically. In order to do non-dimensionalization of the proposed model, the following typical scales are used:

1. Reference length scale, L, is chosen to be the total length of the liver along the x-direction. The approximate value of L is considered as $L = 13.6$ cm [152].
2. The timescale can be written as $\bar{t} = \dfrac{L^2}{\mathcal{D}_l}$, where $\mathcal{D}_l$ is the reference chemical diffusion coefficient,
3. The total number of (T) liver cells is considered as $T = 2 \times 10^{11}$ [33].
4. Initially, maximum values of concentration of capsids U_0, viruses V_0, SVPs S_{v0}, and antibodies A_0, are attained at the point of infection, $x = 0$.

By using these scales, the following non-dimensional variables and parameters are obtained as follows:

- **Dimensionless model variables:** $t^* = \dfrac{t}{\bar{t}}$, $x^* = \dfrac{x}{L}$, $Y^* = \dfrac{Y}{T}$, $X^* = \dfrac{X}{T}$, $U^* = \dfrac{U}{U_0}$, $V^* = \dfrac{V}{V_0}$, $S_v^* = \dfrac{S_v}{S_{v0}}$ and $A^* = \dfrac{A}{A_0}$.

- **Dimensionless model parameters:** $\lambda^* = \dfrac{\bar{t}\lambda}{T}$, $\mu^* = \mu\bar{t}$, $k^* = kV_0\bar{t}$, $\delta^* = \delta\bar{t}$, $a^* = \dfrac{aT\bar{t}}{U_0}$, $\gamma^* = \gamma\bar{t}$, $\beta^* = \beta\bar{t}$, $g^* = gA_0\bar{t}$, $\delta_v^* = \delta_v\bar{t}$, $b^* = \dfrac{b\bar{t}T}{S_0}$, $\delta_{sv}^* = \delta_{sv}\bar{t}$, $\delta_a^* = \delta_a\bar{t}$, $h^* = h\bar{t}$, $r_a^* = r_A\bar{t}$, $A_m^* = \dfrac{A_m}{A_0}$, $\mathcal{D}_1^* = \dfrac{\mathcal{D}_1}{\mathcal{D}_l}$, $\mathcal{D}_2^* = \dfrac{\mathcal{D}_2}{\mathcal{D}_l}$, $\mathcal{D}_3^* = \dfrac{\mathcal{D}_3}{\mathcal{D}_l}$, $\mathcal{D}_4^* = \dfrac{\mathcal{D}_4}{\mathcal{D}_l}$.

At first, the equations (5.2.1)-(5.2.6) are non-dimensionalized using the aforementioned dimensionless variables and parameters. For the sake of notational simplicity and clarity, omitting the asterisk $(*)$ from each dimensionless variable and parameter, the non-dimensional governing equations are derived as

$$\frac{\partial X}{\partial t} = \lambda - \mu X - kVX, \tag{5.3.1}$$

$$\frac{\partial Y}{\partial t} = kVX - \delta Y, \tag{5.3.2}$$

$$\frac{\partial U}{\partial t} = \mathcal{D}_1\frac{\partial^2 U}{\partial x^2} + aY + \gamma(1-\eta)U - \eta\beta U - \delta U, \tag{5.3.3}$$

$$\frac{\partial V}{\partial t} = \mathcal{D}_2\frac{\partial^2 V}{\partial x^2} + \eta\beta U - gAV - \delta_v V, \tag{5.3.4}$$

$$\frac{\partial S_v}{\partial t} = \mathcal{D}_3\frac{\partial^2 S_v}{\partial x^2} + bY - gAS_v - \delta_{sv}S_v, \tag{5.3.5}$$

$$\frac{\partial A}{\partial t} = \mathcal{D}_4\frac{\partial^2 A}{\partial x^2} + h(V+S_v) + +r_A A\left(1 - \frac{A}{A_m}\right) - gA(S_v+V) - \delta_a A. \tag{5.3.6}$$

Due to the non-dimensionalization, the domain of interest $[0, L]$ is transformed into $[0, 1]$. The initial and boundary conditions take the following form in the domain $[0, 1]$:

- **Non-dimensional form of initial conditions:**

$$\left.\begin{aligned} X(x,0) &= 1 - \exp\left(-\frac{x^2}{\epsilon^*}\right),\ 0 \le x \le 1,\\ Y(x,0) &= \exp\left(-\frac{x^2}{\epsilon^*}\right),\ 0 \le x \le 1,\\ U(x,0) &= \exp\left(-\frac{x^2}{\epsilon^*}\right),\ 0 \le x \le 1,\\ V(x,0) &= \exp\left(-\frac{x^2}{\epsilon^*}\right),\ 0 \le x \le 1,\\ S_v(x,0) &= \exp\left(-\frac{x^2}{\epsilon^*}\right),\ 0 \le x \le 1,\\ A(x,0) &= \exp\left(-\frac{x^2}{\epsilon^*}\right),\ 0 \le x \le 1. \end{aligned}\right\} \tag{5.3.7}$$

The initial conditions mentioned in equation (5.3.7) are visualized in Figure 5.3.

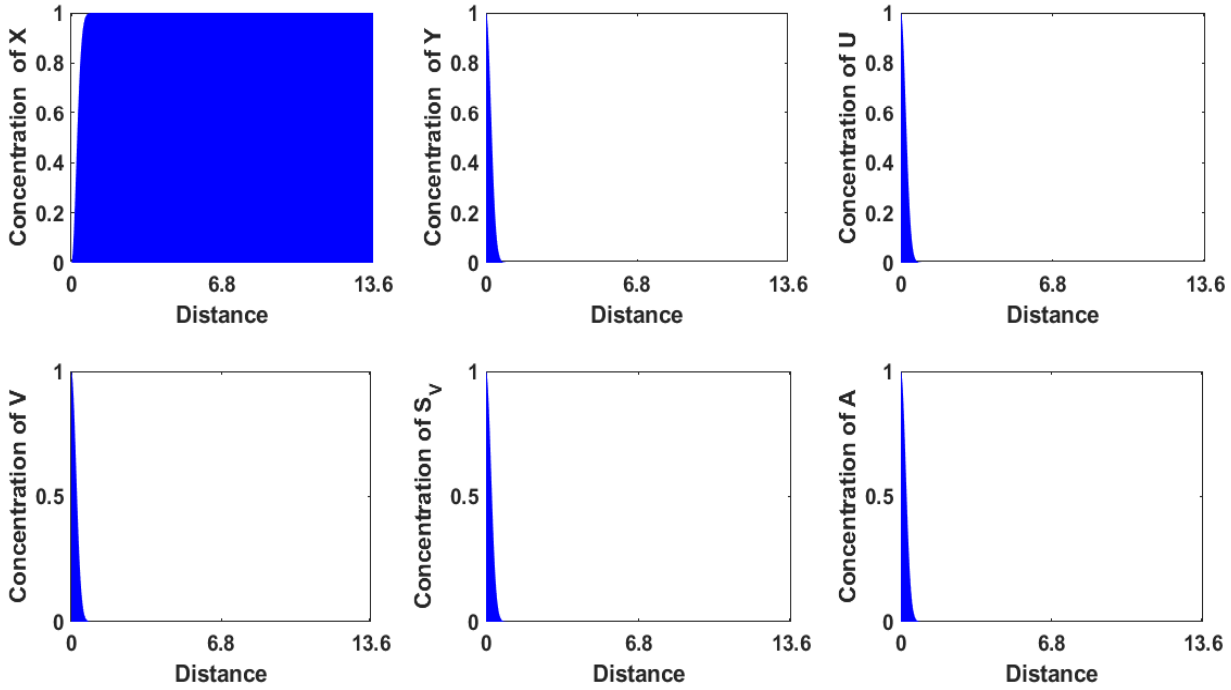

Figure 5.3: The graphical representation of all initial conditions mentioned in the equation (5.2.7).

- **Non-dimensional form of boundary conditions:**

$$\frac{\partial U}{\partial x} = \frac{\partial V}{\partial x} = \frac{\partial S_v}{\partial x} = \frac{\partial A}{\partial x} = 0 \text{ on } \partial\Omega^* \times (0, +\infty), \tag{5.3.8}$$

where $\partial\Omega^*$ represents boundary of $\Omega^* = [0, 1]$ and $(0, +\infty)$ denotes the temporal domain.

5.4 Numerical method

The computational domain $[0, 1]$ is divided into $(N - 1)$ equal sub-intervals as

$$0 = x_0 \leq x_1 \leq x_2 \leq \cdots \leq x_{i-1} \leq x_i \leq x_{i+1} \leq \cdots \leq x_{N-2} \leq x_{N-1} = 1$$

with step length $\Delta x = \dfrac{1}{(N-1)}$. Let Δt be the time step length and n be the step number to reach the final time T_f, *i.e.*, $T_f = n\Delta t$. Here, the well-known central difference scheme

for spatial derivatives and the forward scheme for temporal derivative (FTCS) is taken into account to discretize the non-dimensionalized governing equations (5.3.1)-(5.3.6). Using the following notations

$$X(i\Delta x, n\Delta t) = X_i^n,\ Y(i\Delta x, n\Delta t) = Y_i^n,$$

$$U(i\Delta x, n\Delta t) = U_i^n,\ V(i\Delta x, n\Delta t) = V_i^n,$$

$$S_v(i\Delta x, n\Delta t) = {S_v}_i^n,\ A(i\Delta x, n\Delta t) = A_i^n,$$

the corresponding discretized forms of the equations (5.3.1)-(5.3.6) at the interior nodes can be written as

$$X_i^{n+1} = X_i^n + \lambda\Delta t - \mu\Delta t X_i^n - k\Delta t V_i^n X_i^n, \tag{5.4.1}$$

$$Y_i^{n+1} = Y_i^n - \delta\Delta t Y_i^n + k\Delta t V_i^n X_i^n, \tag{5.4.2}$$

$$-p_1 U_{i-1}^{n+1} + (1+2p_1)U_i^{n+1} - p_1 U_{i+1}^{n+1} = U_i^n + a\Delta t Y_i^n + \gamma\Delta t(1-\eta)U_i^n - \eta\beta\Delta t U_i^n - \delta\Delta U_i^n, \tag{5.4.3}$$

$$-p_2 V_{i-1}^{n+1} + (1+2p_2)V_i^{n+1} - p_2 V_{i+1}^{n+1} = V_i^n + \eta\beta\Delta t U_i^n - g\Delta t A_i^n V_i^n - \delta_v\Delta t V_i^n, \tag{5.4.4}$$

$$-p_3 {S_v}_{i-1}^{n+1} + (1+2p_3){S_v}_i^{n+1} - p_3 {S_v}_{i+1}^{n+1} = {S_v}_i^n + b\Delta t Y_i^n - g\Delta t {S_v}_i^n A_i^n - \delta_{sv}\Delta t {S_v}_i^n, \tag{5.4.5}$$

$$-p_4 A_{i-1}^{n+1} + (1+2p_4)A_i^{n+1} - p_4 A_{i+1}^{n+1} = A_i^n + (h - gA_i^n)({S_v}_i^n + V_i^n) + r_A A_i^n\left(1 - \frac{A_i^n}{A_m}\right) - \delta_a\Delta t A_i^n, \tag{5.4.6}$$

where $i = 1, 2, \cdots, (N-2), n = 0, 1, 2, \cdots$. Here, $p_1 = \dfrac{\Delta t}{\Delta x^2}\mathcal{D}_1$, $p_2 = \dfrac{\Delta t}{\Delta x^2}\mathcal{D}_2$, $p_3 = \dfrac{\Delta t}{\Delta x^2}\mathcal{D}_3$, $p_4 = \dfrac{\Delta t}{\Delta x^2}\mathcal{D}_4$. Using ghost point criteria at the boundary nodes, *i.e.*, for $i = 0,$ and $i = N-1$, the discretized equations for capsids, viruses, SVPs and antibodies (5.4.3),(5.4.4), (5.4.5) and (5.4.6) take the following forms:

- **At left boundary ($x = 0$):**

$$(1+2p_1)U_0^{n+1} - 2p_1 U_1^{n+1} = U_0^n + a\Delta t Y_0^n + \gamma\Delta t(1-\eta)U_0^n - \eta\beta\Delta t U_0^n - \delta\Delta U_0^n, \tag{5.4.7}$$

$$(1+2p_2)V_0^{n+1} - 2p_2 V_1^{n+1} = V_0^n + \eta\beta\Delta t U_0^n - g\Delta t A_0^n V_0^n - \delta_v\Delta t V_0^n, \tag{5.4.8}$$

$$(1+2p_3){S_v}_0^{n+1} - 2p_3 {S_v}_1^{n+1} = {S_v}_0^n + b\Delta t Y_0^n - g\Delta t {S_v}_0^n A_0^n - \delta_{sv}\Delta t {S_v}_0^n, \tag{5.4.9}$$

$$(1+2p_4)A_0^{n+1} - 2p_4 A_1^{n+1} = A_0^n + (h - gA_0^n)(S_0^n + V_0^n) + r_A A_0^n\left(1 - \frac{A_0^n}{A_m}\right) - \delta_a\Delta t A_0^n. \tag{5.4.10}$$

- **At right boundary ($x = 1$):**

$$-2p_1U_{N-2}^{n+1} + (1+2p_1)U_{N-1}^{n+1} = U_{N-1}^n + a\Delta tY_{N-1}^n + \gamma\Delta t(1-\eta)U_{N-1}^n - \eta\beta\Delta tU_{N-1}^n - \delta\Delta U_{N-1}^n, \tag{5.4.11}$$

$$-2p_2V_{N-2}^{n+1} + (1+2p_2)V_{N-1}^{n+1} = V_{N-1}^n + \eta\beta\Delta tU_{N-1}^n - g\Delta tA_{N-1}^nV_{N-1}^n - \delta_v\Delta tV_{N-1}^n, \tag{5.4.12}$$

$$-2p_3S_{vN-2}^{n+1} + (1+2p_3)S_{vN-1}^{n+1} = S_{vN-1}^n + b\Delta tY_{N-1}^n - g\Delta tS_{vN-1}^nA_i^n - \delta_{sv}\Delta tS_{vN-1}^n, \tag{5.4.13}$$

$$-2p_4A_{N-2}^{n+1} + (1+2p_4)A_{N-1}^{n+1} = A_{N-1}^n + (h - gA_{N-1}^n)(S_{vN-1}^n + V_{N-1}^n) + r_AA_{N-1}^n\left(1 - \frac{A_{N-1}^n}{A_m}\right) - \delta_a\Delta tA_{N-1}^n. \tag{5.4.14}$$

The corresponding systems of equations for U, V, S_v and A are solved using the well-known tridiagonal matrix algorithm (TDMA).

5.5 Parameter estimation

The baseline values of some parameters are directly taken from existing literature. It is assumed that the infectious viral particles and SVPs degrade naturally with same rate, *i.e.*, $\delta_v = \delta_{sv}$. The value of volume fraction of rcDNA-containing capsids (η) in favor of virus production are considered as 0.8 throughout this study. Since, the ratio of Dane particles to SVPs ranges from 1:10,000 to 1:100,000 [54–56], it is noted that the production rate of SVPs is accounted to be at least 1000 times that of virus production rate, *i.e.*, $b = 1000a$. The diffusion coefficients $(\mathcal{D}_1, \mathcal{D}_2, \mathcal{D}_3, \mathcal{D}_4)$ are systematically varied within a realistic range to capture the diverse spectrum of viral infection dynamics. All details regarding the new parameters, such as descriptions, units, values, and their corresponding references are mentioned in Table 5.1.

5.6 Results and discussion

By applying the methodology described in Section 5.4, the dimensionless system of equations (5.3.1)-(5.3.6) is solved considering the above-mentioned initial conditions (5.3.7) and boundary conditions (5.3.8). However, for the sake of illustration, the obtained results are presented in dimensional form to provide a clear understanding of the actual biology and to facilitate comparison between different scenarios.

Table 5.1: Descriptions of model variables and parameters.

Parameters	Descriptions	Values	Units	Source
g	Binding rate of antibody and viruses or SVPs	10^{-4}	day^{-1}	[153]
h	production rate of antibodies	0.01	day^{-1}	[153]
δ_{sv}	Death rate of sub-viral particles	3.8	day^{-1}	Assumed
δ_a	Death rate of antibodies	0.15	day^{-1}	[153]
r_A	Intrinsic growth rate of antibodies	0.0365	day^{-1}	[148]
A_m	Carrying capacity of antibodies	4×10^{15}	-	[148]
$\mathcal{D}_1$	Diffusion coefficient of capsids	0.08	$\text{cm}^2\text{day}^{-1}$	-
$\mathcal{D}_2$	Diffusion coefficient of viruses	0.09	$\text{cm}^2\text{day}^{-1}$	-
$\mathcal{D}_3$	Diffusion coefficient of SVPs	0.09	$\text{cm}^2\text{day}^{-1}$	-
$\mathcal{D}_4$	Diffusion coefficient of antibodies	0.08	$\text{cm}^2\text{day}^{-1}$	-

5.6.1 Effects of diffusion

In general, the mobility of infectious virus particles inside the host plays some decisive roles in the progression and transmission of any kind of viral infection. In this section, in order to examine the relative importance of diffusion of capsids, viruses, SVPs and antibodies on HBV infection dynamics, we first consider the system in the absence of any kind of diffusion, (*i.e.*, $\mathcal{D}_1 = \mathcal{D}_2 = \mathcal{D}_3 = \mathcal{D}_4 = 0$). Subsequently, when diffusivity is imposed into the model, the values of diffusion coefficients $(\mathcal{D}_1, \mathcal{D}_2, \mathcal{D}_3, \mathcal{D}_4)$ are varied within the reliable range to explore diverse scenarios and uncover testable biological aspects. As, in this case, none of the diffusion coefficients is set to zero, we proceed to discuss the effects in the following manner:

1. The effects of diffusion on uninfected and infected hepatocytes.
2. The effects of diffusion on HBV capsids and free viruses.
3. The effects of diffusion on SVPs and antibodies.

5.6.1.1 Effects of diffusion on uninfected and infected hepatocytes

Changes in the dynamics of uninfected and infected hepatocytes are shown in the Figure 5.4. In order to visualize the concentration profiles of respective classes with respect to time

and space in a easier way, contour color plots are presented. Figure 5.4A and Figure 5.4B display the distribution pattern of uninfected hepatocytes with and without diffusivities of HBV capsids, viruses, SVPs and antibodies. Significant variations are observed in the distribution patterns. At the early stages of infection, the influence of diffusion on the uninfected hepatocyte compartment is not significant, as the concentration remains nearly uniform with time (contour lines are parallel to space-axis). However, after this initial phase, diffusion begins to exert substantial impacts. For this set of parameters, after 1330^{th} day, the distribution of uninfected hepatocytes shows a paradigm shift in the contour line (for example, contour line 2450000000). In the diffusion model, uninfected hepatocytes exhibit an almost uniform distribution along space, whereas in the non-diffusion model, they display a non-uniform pattern. In the non-diffusion model, the infection takes a considerable amount of time to spread throughout the liver.

In case of infected hepatocytes, similar kind of dynamics are observed in Figure 5.4C and Figure 5.4D as shown in uninfected hepatocytes. In the non-diffusion model, the rate of temporal changes in the concentration of infected hepatocytes is higher compared to diffusion one. In essence, the diffusion of virion components (capsids, virions, SVPs) and antibodies enhances the infection increasing the susceptibility in cells. However, both the models lead to the same steady state for both type of hepatocytes.

5.6.1.2 Effects of diffusion on HBV capsids and free viruses

The contour plots shown in Figure 5.5 delineates the concentration profiles of HBV DNA-containing capsids and viruses. For non-zero values of diffusion coefficients $\mathcal{D}_1, \mathcal{D}_2, \mathcal{D}_3, \mathcal{D}_4$, the densities of capsids and viruses demonstrate a nearly orthotropic pattern (property changes in mutually perpendicular directions) in Figure 5.5A (capsids) and Figure 5.5C (viruses). It is also observed that for same time (suppose $t = 1400^{th}$day), there are significant differences in the concentrations of capsid and virus compartments between the diffusion and non-diffusion models. In the absence of diffusion, the spread of capsids as well as virion particles occurs slowly (Figure 5.5B and Figure 5.5D). However, due to the inclusion of diffusions, viruses start to propagate rapidly throughout the liver, leading to a spatially homogeneous distribution. Therefore, diffusivities of capsids, viruses, SVPs and antibodies influence the infection pattern and its dynamics.

5.6.1.3 Effects of diffusion on SVPs and antibodies

In this section, we discuss how the spatial movements of capsids, viruses, SVPs, and antibodies affect the concentrations of non-infectious SVPs and virus-neutralizing antibodies.

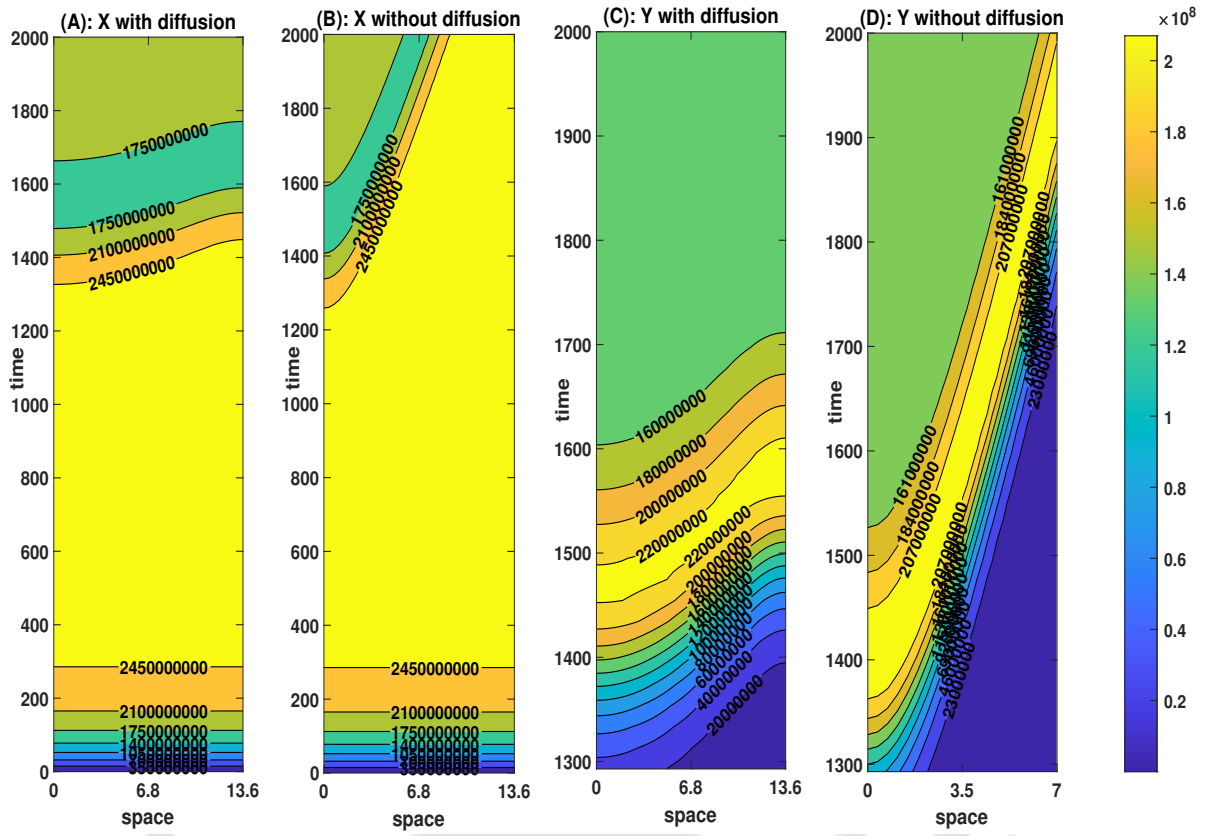

Figure 5.4: Contour color plots: The effects of diffusion on uninfected and infected hepatocytes.

In Figure 5.6A and Figure 5.6C, the values of SVPs ($S_v(x,t)$) and antibodies ($A(x,t)$) with diffusion are visualized using contour color plots. On the other hand, Figure 5.6B and Figure 5.6D shows the corresponding concentrations of SVPs and antibodies under non-diffusion conditions. Initially, it is considered in this study that the infection starts from the left side of the liver, *i.e.*, from the origin $(0,0)$ according to our $xt-$frame. There are notable changes in the concentrations of SVPs and antibodies observed exclusively on the left side of the liver, while the right side exhibits the absence of SVPs also antibodies in the non-diffusion model. The antibodies are concentrated only near the site of infection in non-diffusion model. It is quite impractical and unrealistic since antibodies have the capacity to diffuse through tissues and blood, allowing them to reach infection sites efficiently. When diffusion is taken into account, substantial variations in both sides of the liver are observed.

Contour plots shown in Figure 5.4, 5.5 & 5.6 indicate that all compartments (uninfected hepatocytes, infected hepatocytes, capsids, viruses, SVPs and antibodies) reach an endemic steady-state more rapidly in case of non-diffusion model compared to that with the diffusion.

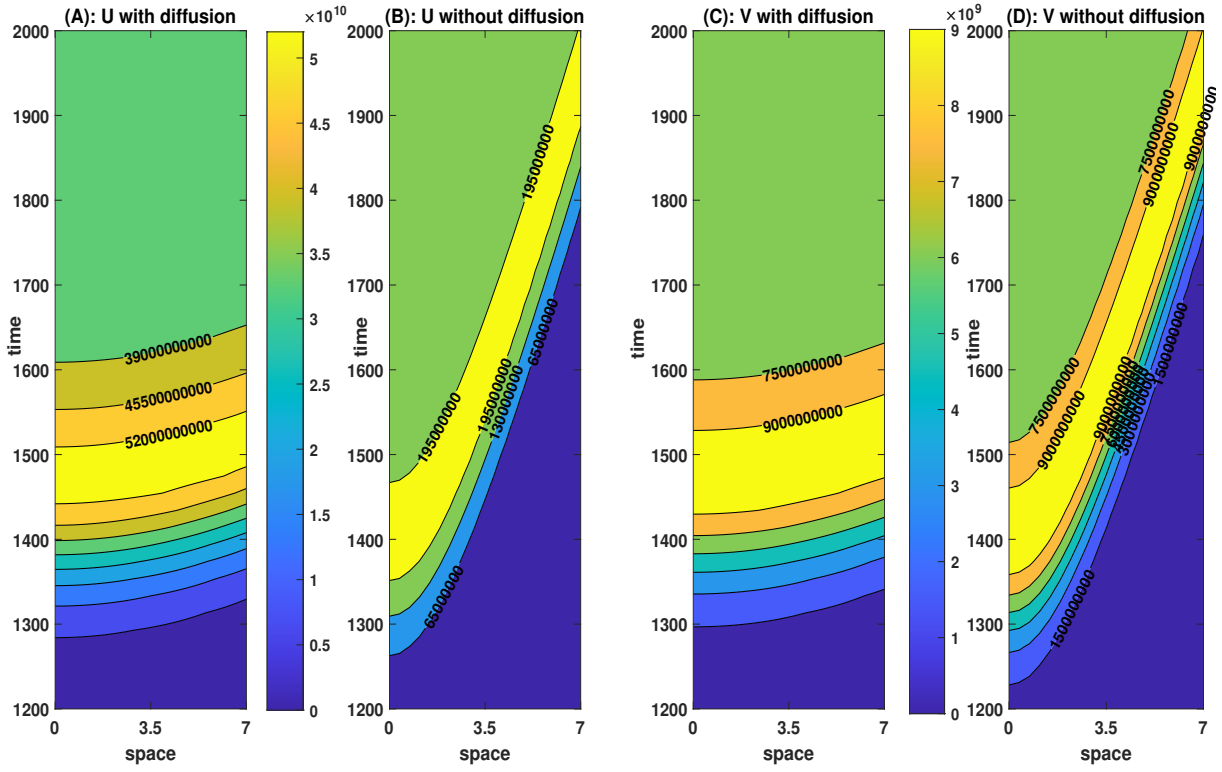

Figure 5.5: Contour color plots: The effects of diffusion on HBV capsids and infectious virus particles.

5.6.2 Effects of SVPs

SVPs are one of the intracellular viral components that weaken the host immune system. These viral elements are released from the infected hepatocytes in a large number (typically 1,000- to 100,000-fold) compared to infectious virus particles during infection period [54–56]. In this section, we investigate the effects of SVPs on virus and antibody growth dynamics throughout the liver. The system of equations (5.3.1) (5.3.6) is solved by considering the following cases: (i) in the presence of SVPs, and (ii) in the absence of SVPs. In Figure 5.7 (1-6), the result of the first case, (*i.e.*, with the SVPs) are displayed. On the other hand, the outcomes of the second case (*i.e.*, without SVPs) are depicted in Figure 5.7 (7-12). Upon comparing the solutions of both cases, notable changes are observed, particularly in the virus and antibody profiles. The snapshots of the virus and antibody compartments are captured at different positions, such as at $x = 2.5$, $x = 5$, $x = 7.5$, $x = 10$, $x = 12.5$ and $x = 13.6$,

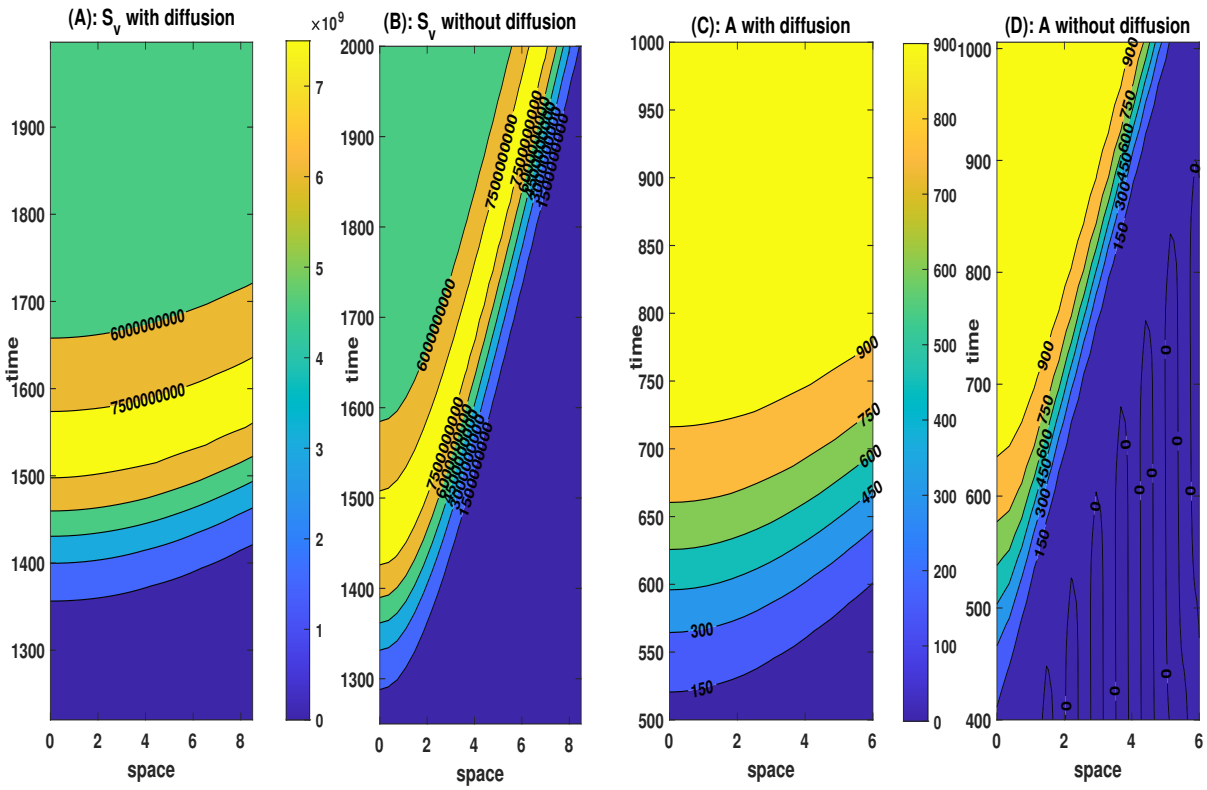

Figure 5.6: Contour color plots: The effects of diffusion on SVPs and antibodies.

and are shown in Figure 5.7 (13-18) for viruses and in Figure 5.7 (19-24) for antibodies. Due to the integration of SVPs into the model, these following critical insights are noted:

1. There is a discernible rise in the peak of virus compartment (refer to Figure 5.7 (13-18)).
2. The virus compartment is stabilized at a higher level in the presence of SVPs (refer to Figure 5.7 (13-18)).
3. The peak level for the virions compartment rises quickly due to the inclusion of SVPs (refer to Figure 5.7 (13-18)).
4. After a certain time period, substantial changes are observed in the solution for the antibody compartment (refer to Figure 5.7 (19-24)). The stability level of antibodies significantly decreases due to the presence of SVPs. The primary reason is the excessive production of SVPs which leads to the depletion of a considerable amount of antibodies, resulting in a swift decline in the concentration of antibodies.

Therefore, the above findings suggest that SVPs play some important roles in the development of this viral infection. Similar types of results have also been reported in the literature.

For example, Bruns et al. [66] found that SVPs significantly enhance intracellular viral replication and gene expression. Recently, Rydell et al. [64] confirmed that SVPs significantly reduced the neutralization of virus particles by antibodies. The removal of spherical SVPs stands as an important milestone in achieving the functional cure of HBV infection [154]. Thus, in conclusion, SVPs merit attention as a promising avenue for future therapeutic strategies targeting viral agents.

5.6.3 Effects of capsid recycling on the production of SVPs

The recycling of capsids acts as a crucial mechanism in HBV. In chapter (2), it is shown how the recycling pathway substantially augments viral concentration during HBV infection. To the best of our knowledge, we didn't find any prior documented investigation related to the interplay between capsid recycling and SVPs in the literature. The possible associations between capsid recycling and SVPs are studied here. The proposed model is solved under two distinct cases:

Case-1: with recycling ($\gamma \neq 0,\ \eta < 1$)
We incorporate the recycling effects into the proposed model through the term $\gamma(1-\eta)U(x,t)$ in equation (5.2.3). By assigning a realistic estimated value to γ, we solve the system of equations. The resulting surface plot for SVPs is depicted in Figure 5.8A.

Case-2: without recycling ($\gamma = 0,\ \eta = 1$)
In this case, the impacts of capsid recycling is ignored, *i.e.*, the simulation is done by considering $\gamma = 0$ and the corresponding profiles of SVPs are shown in Figure 5.8B.

In Figure 5.8(C)-Figure 5.8(H), the solutions of SVPs for various positions are highlighted. The trends of the solutions exhibit similarities but demonstrate significant differences in values. The extreme values for each solution vary considerably. Incorporation of recycling of capsids results in a higher peak in the solution compared to when recycling is not considered. Therefore, the recycling of capsids is implicated in enhancing the concentration of SVPs during HBV infection.

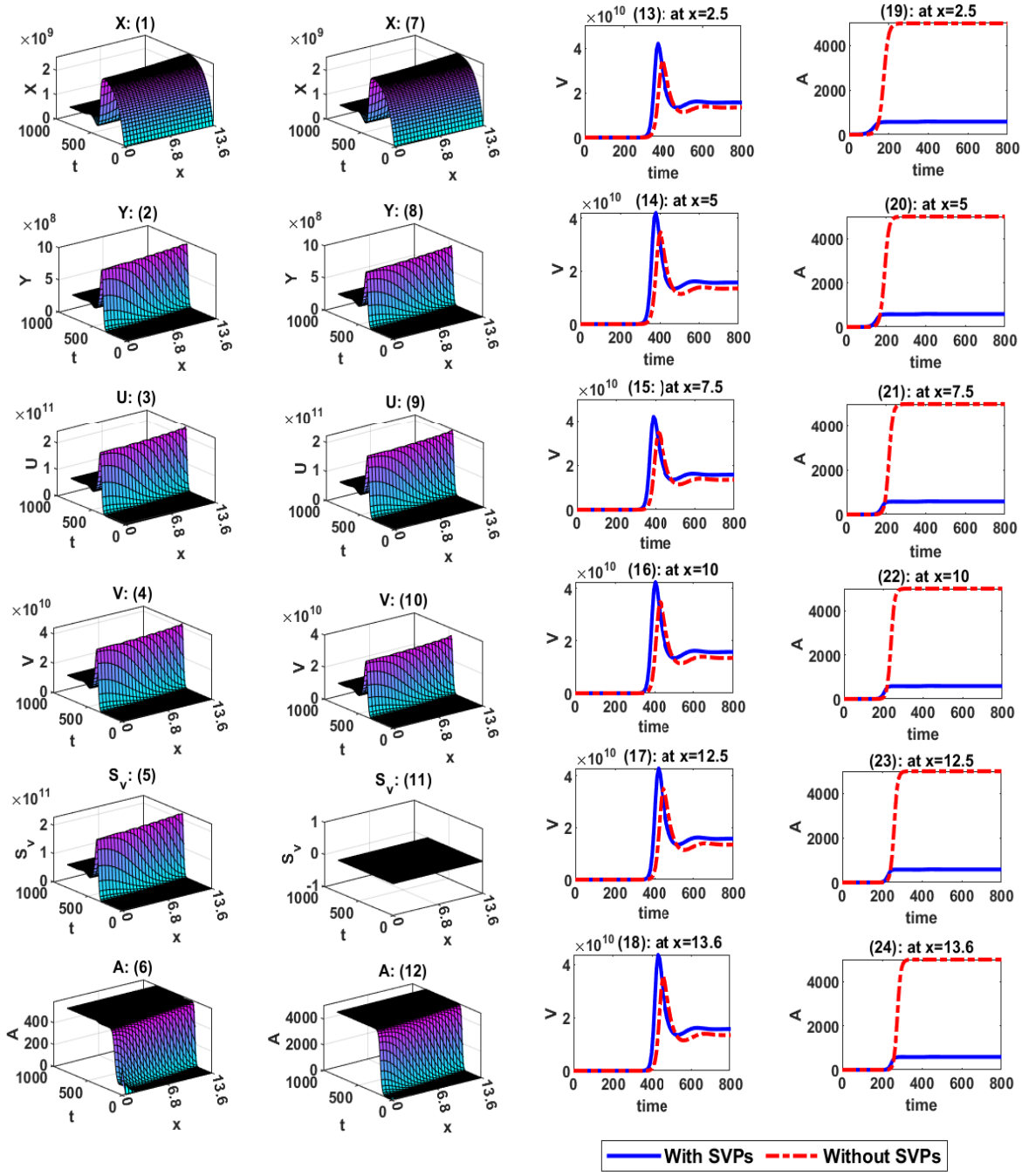

Figure 5.7: Comparisons between the virus and antibody profiles considering both the cases: with and without SVPs. Here, the blue lines illustrate the system's solution incorporating SVPs, while the red curves depict the solution without SVPs.

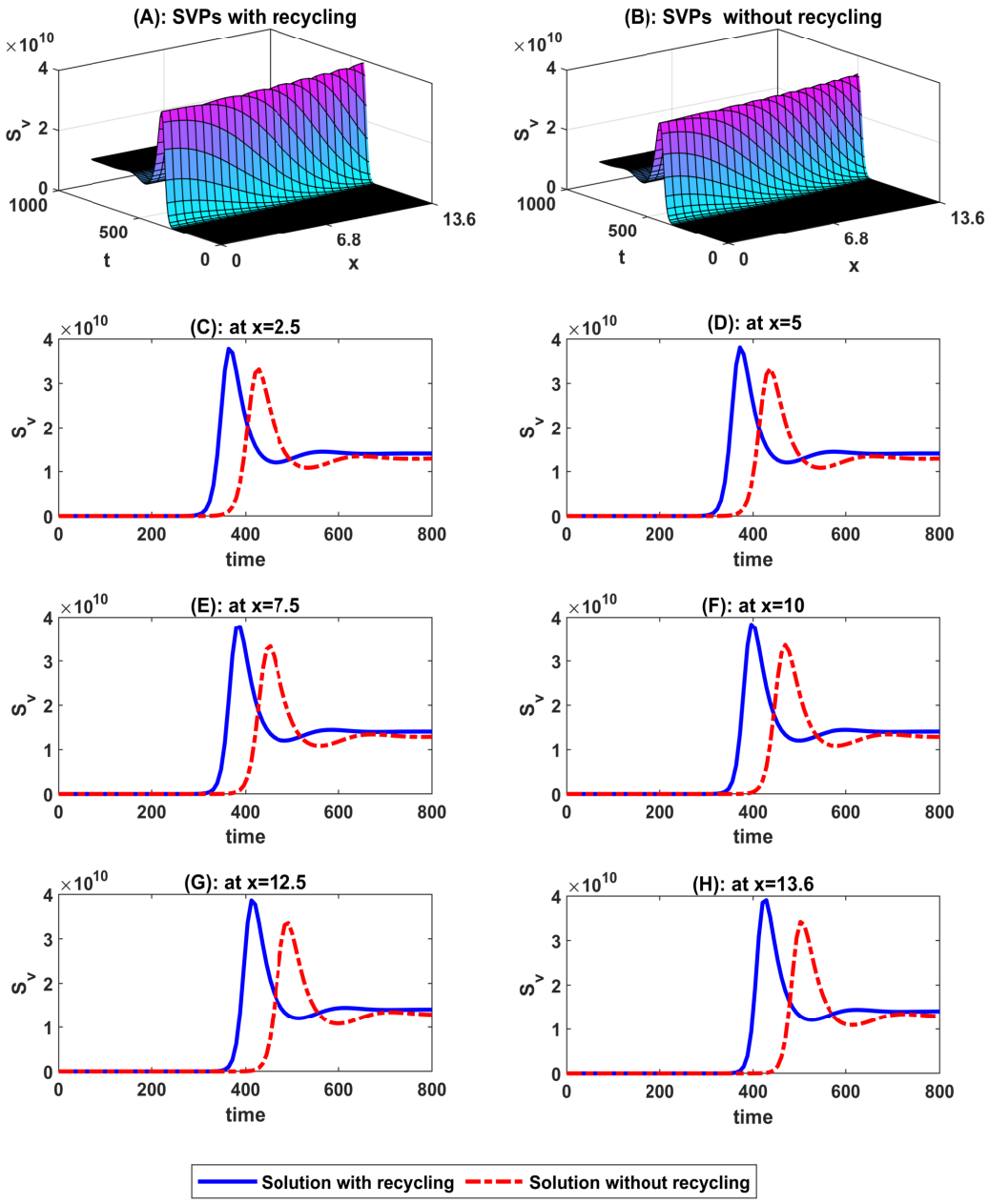

Figure 5.8: The effects of capsid recycling on SVPs. Figure 5.8 (A): surface plot of SVPs when recycling is taken into account. Figure 5.8 (B): surface plot of SVPs when recycling is not considered. Figure 5.8 (C)-Figure 5.8 (H): The comparison between the concentration of SVPs at $x = 2.5$, $x = 5$, $x = 7.5$, $x = 10$, $x = 12.5$, and $x = 15$ with respect to time.

5.7 Infection initiating from multiple points on the liver

In the preceding sections, we made the assumption that the infection initially originates only from a single point at $x = 0$ (left side). Subsequently, the corresponding initial conditions were considered as described in the equation (5.2.7). This virus predominantly infects hepatocytes which serve as the primary functional cells within the liver. However, the infection doesn't necessarily involve every hepatocyte in the liver at same time. The virus may infect hepatocytes in various parts of the liver over time [155] (Figure 5.9). In order to explore the changes in the infection dynamics, the initial conditions (equation (5.2.7)) are modified by introducing multiple points of infection. For ease of analysis and comparison across different scenarios, we categorize the solutions of the proposed model (5.3.1)-(5.3.6) as follows:

1. SWSPI: Solutions with single point of infection,
2. SWDPI: Solutions with dual points of infection,
3. SWTPI: Solutions with triple points of infection.

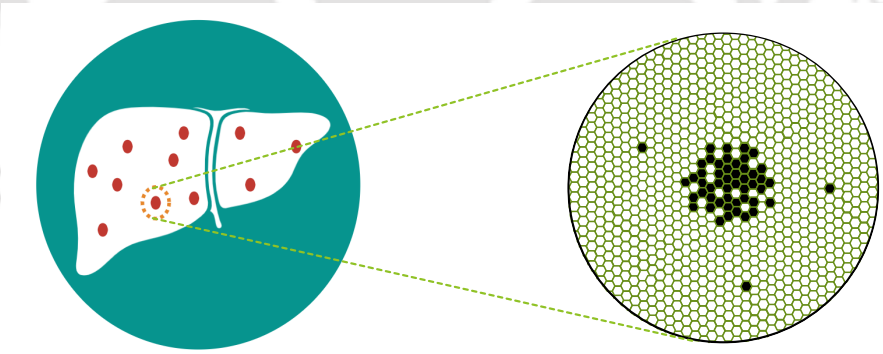

Figure 5.9: Distribution of infection in the liver during the course of HBV infection.

5.7.1 Dual-origin infection

In this case, it is assumed that the infection starts from both the ends ($x = 0$ and $x = L$) of the liver with equal severity of infection. The initial numbers of infected hepatocytes, capsids, viruses, SVPs, and antibodies are considered to be same to those observed in single point infection, however, in this case, they are equally distributed into two endpoints.

5.7.1.1 Initial conditions

In the context of dual-origin infection, the corresponding non-dimensional form of initial conditions are given as follows:

$$\left.\begin{aligned}
X(x,0) &= 1-\left\{\exp\left(-\frac{x^2}{\epsilon^*}\right)+\exp\left(-\frac{(x-1)^2}{\epsilon^*}\right)\right\},\ 0\le x\le 1,\\
Y(x,0) &= \left\{\exp\left(-\frac{x^2}{\epsilon^*}\right)+\exp\left(-\frac{(x-1)^2}{\epsilon^*}\right)\right\},\ 0\le x\le 1,\\
U(x,0) &= \left\{\exp\left(-\frac{x^2}{\epsilon^*}\right)+\exp\left(-\frac{(x-1)^2}{\epsilon^*}\right)\right\},\ 0\le x\le 1,\\
V(x,0) &= \left\{\exp\left(-\frac{x^2}{\epsilon^*}\right)+\exp\left(-\frac{(x-1)^2}{\epsilon^*}\right)\right\},\ 0\le x\le 1,\\
S_v(x,0) &= \left\{\exp\left(-\frac{x^2}{\epsilon^*}\right)+\exp\left(-\frac{(x-1)^2}{\epsilon^*}\right)\right\},\ 0\le x\le 1,\\
A(x,0) &= \left\{\exp\left(-\frac{x^2}{\epsilon^*}\right)+\exp\left(-\frac{(x-1)^2}{\epsilon^*}\right)\right\},\ 0\le x\le 1.
\end{aligned}\right\} \tag{5.7.1}$$

In Figure 5.10, this initial state of each compartment is displayed for dual origin infection.

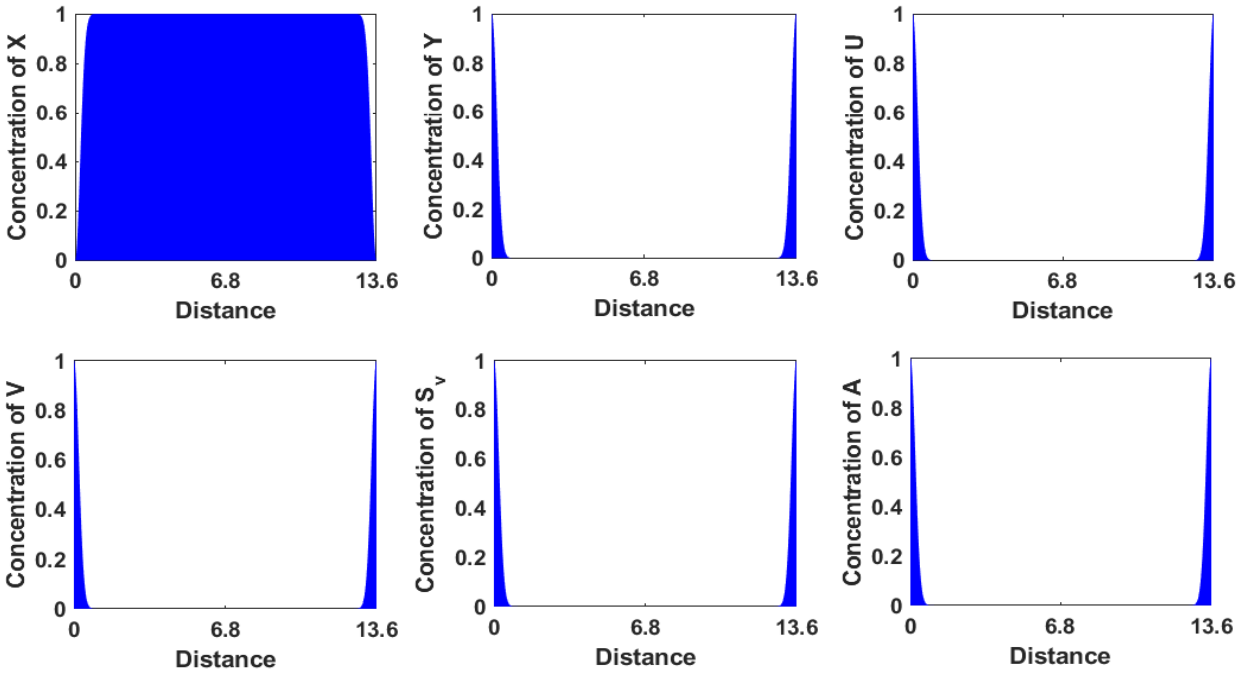

Figure 5.10: Initial conditions: The infection initiates at $x = 0$ and $x = L$ simultaneously.

5.7.2 Triple-origin infection

Here, we consider that the liver is initially infected at three distinct points: both endpoints ($x = 0$ and $x = L$) and the midpoint ($x = L/2$). Similarly, as dual-origin infection, the total number of uninfected hepatocytes, infected hepatocytes, capsids, viruses, SVPs, and antibodies mirror those in a single-point infection.

5.7.2.1 Initial conditions

$$\left.\begin{aligned}
X(x,0) &= 1 - \left\{\exp\left(-\frac{x^2}{\epsilon^*}\right) + \exp\left(-\frac{(x-0.5)^2}{\epsilon^*}\right) + \exp\left(-\frac{(x-1)^2}{\epsilon^*}\right)\right\}, \ 0 \le x \le 1,\\
Y(x,0) &= \left\{\exp\left(-\frac{x^2}{\epsilon^*}\right) + \exp\left(-\frac{(x-0.5)^2}{\epsilon^*}\right) + \exp\left(-\frac{(x-1)^2}{\epsilon^*}\right)\right\}, \ 0 \le x \le 1,\\
U(x,0) &= \left\{\exp\left(-\frac{x^2}{\epsilon^*}\right) + \exp\left(-\frac{(x-0.5)^2}{\epsilon^*}\right) + \exp\left(-\frac{(x-1)^2}{\epsilon^*}\right)\right\}, \ 0 \le x \le 1,\\
V(x,0) &= \left\{\exp\left(-\frac{x^2}{\epsilon^*}\right) + \exp\left(-\frac{(x-0.5)^2}{\epsilon^*}\right) + \exp\left(-\frac{(x-1)^2}{\epsilon^*}\right)\right\}, \ 0 \le x \le 1,\\
S_v(x,0) &= \left\{\exp\left(-\frac{x^2}{\epsilon}\right) + \exp\left(-\frac{(x-0.5)^2}{\epsilon}\right) + \exp\left(-\frac{(x-1)^2}{\epsilon}\right)\right\}, \ 0 \le x \le 1,\\
A(x,0) &= \left\{\exp\left(-\frac{x^2}{\epsilon^*}\right) + \exp\left(-\frac{(x-0.5)^2}{\epsilon^*}\right) + \exp\left(-\frac{(x-1)^2}{\epsilon^*}\right)\right\}, \ 0 \le x \le 1.
\end{aligned}\right\} \tag{5.7.2}$$

Figure 5.11 presents the initial state of each compartment for the triple-origin infection setup.

5.7.2.2 Outcomes of the infection: Comparison among SWSPI, SWDPI, and SWTPI

The proposed model is solved for different initial conditions: (i) single-origin infection (5.3.7), (ii) dual-origin infection (5.7.1), and (iii) triple-origin infection (5.7.2). In order to compare the model solutions, we obtain the solutions for uninfected hepatocytes, infected hepatocytes,

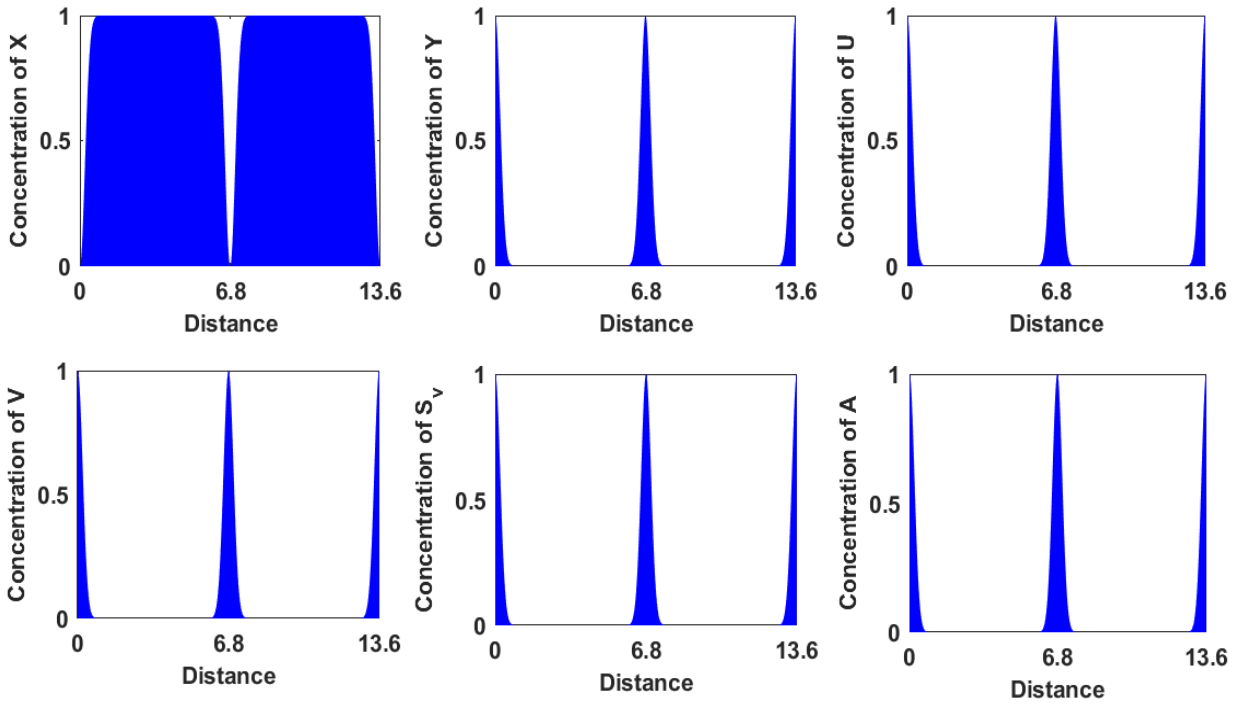

Figure 5.11: Initial conditions: The infection initiates at $x = 0$, $x = L/2$ and $x = L$ simultaneously.

viruses and SVPs by integrating along the spatial dimension as follows:

$$\bar{X}(t) = \int_{x=0}^{x=L} X(x,t)dx, \tag{5.7.3}$$

$$\bar{Y}(t) = \int_{x=0}^{x=L} Y(x,t)dx, \tag{5.7.4}$$

$$\bar{U}(t) = \int_{x=0}^{x=L} U(x,t)dx, \tag{5.7.5}$$

$$\bar{V}(t) = \int_{x=0}^{x=L} V(x,t)dx, \tag{5.7.6}$$

$$\bar{S_v}(t) = \int_{x=0}^{x=L} S_v(x,t)dx, \tag{5.7.7}$$

$$\bar{A}(t) = \int_{x=0}^{x=L} A(x,t)dx, \tag{5.7.8}$$

where $\bar{X}(t)$, $\bar{Y}(t)$. $\bar{V}(t)$, $\bar{S_v}(t)$ denotes the number of uninfected hepatocytes, infected hepatocytes, viruses and SVPs at time t, respectively. As the proposed model is solved numerically, the integrations (5.7.3), (5.7.4), (5.7.6), (5.7.7) are converted to summation, resulting in the

following expressions:

$$\bar{X}(t_j) = \sum_{i=1}^{n} X(x_n, t_j), \ \ j = 1, 2, ..., m, \tag{5.7.9}$$

$$\bar{Y}(t_j) = \sum_{i=1}^{n} Y(x_n, t_j), \ \ j = 1, 2, ..., m, \tag{5.7.10}$$

$$\bar{U}(t_j) = \sum_{i=1}^{n} U(x_n, t_j), \ \ j = 1, 2, ..., m, \tag{5.7.11}$$

$$\bar{V}(t_j) = \sum_{i=1}^{n} V(x_n, t_j), \ \ j = 1, 2, ..., m, \tag{5.7.12}$$

$$\bar{S}_v(t_j) = \sum_{i=1}^{n} S_v(x_n, t_j), \ \ j = 1, 2, ..., m, \tag{5.7.13}$$

$$\bar{A}(t_j) = \sum_{i=1}^{n} A(x_n, t_j), \ \ j = 1, 2, ..., m, \tag{5.7.14}$$

where n and m represent the number of grid points along x and t-axis, respectively. In Figure 5.12, the model solutions for uninfected hepatocytes, infected hepatocytes, viruses and SVPs are plotted and compared with each other.

- **Changes in the dynamics of uninfected hepatocytes, infected hepatocytes, viruses and SVPs**

  1. The solutions converge to the same steady-state for all three types of initial conditions (5.3), (5.7.1), (5.7.2).
  2. As the number of initial points of infection increases, the peaks of infected hepatocytes, viruses and SVPs become higher.
  3. If the liver is initially infected at multiple points, the number of infected cells increases rapidly for certain period of time from the time of infection.
  4. For a triple-point infection, the solution peaks occur earlier compared to the peaks observed in solutions derived from dual-point or single-point infections.
  5. From a long-term perspective, the severity of the infection remains the same regardless of the number of infection points.

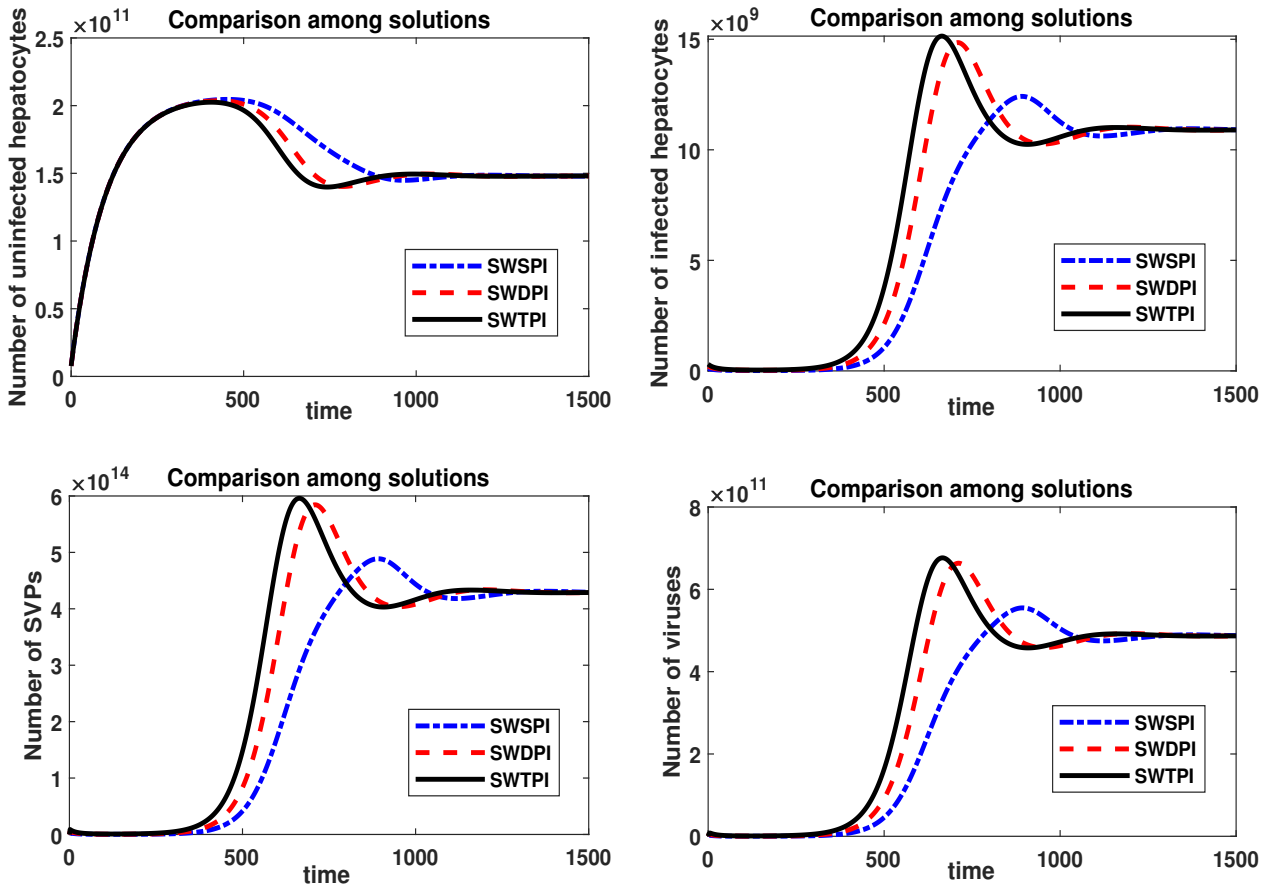

Figure 5.12: Comparison between solutions SWSPI, SWDPI and SWTPI. SWSPI: solution with single-point infection, SWDPI: solution with dual-point infection, SWTPI: solution with triple-point infection.

5.8 Conclusions

In this chapter, a novel HBV infection dynamics model is proposed including the impacts of sub-viral particles and antibodies. The diffusivity of each viral component (capsids, viruses, SVPs) and the HBV-specific antibodies are also incorporated into the model. Overall, this model carry unique characteristics in the context of HBV infection. We perform non-dimensionalization on each model equation to make them easy to use. We apply forward time and central space (FTCS) finite difference scheme to solve the proposed model numerically. Based on the experiments, this study has yielded several key findings which are as follows:

1. SVPs significantly enhance intracellular viral replication and gene expression. SVPs also reduce the neutralization of virus particles by antibodies.

2. Due to the substantial presence of SVPs within the liver, the virions compartment experiences a rapid increase and leads to a higher peak level. The stability level of virions also increases due to the incorporation of SVPs.

3. The recycling of capsids significantly enhances the concentration of SVPs.

4. Due to the diffusion of capsids, viruses, SVPs and antibodies, viruses spread rapidly throughout the liver. However, all model compartments ultimately converge to the same steady-state, regardless of whether diffusion is considered or not within the model.

5. As the number of initial points of infection increases, the peaks of infected hepatocytes, viruses and SVPs become higher and occur earlier.

6. From a long-term perspective, the severity of the infection remains the same regardless of the number of infection points.

CHAPTER 6

Exploration of Hepatitis B Virus Infection Dynamics through an Intracellular Model

In this chapter, an intracellular HBV infection dynamics model is proposed by considering several intracellular steps that are observed in the virus life cycle and can be targeted by antiviral therapy in the future. Upon comparison with experimental data, the model solutions exhibit excellent agreement. The well-known fourth-order highly accurate Runge-Kutta method is applied to numerically solve the proposed model. The effects of initial concentration of cccDNA, HBx proteins, dslDNA-containing intermediates and intracellular delay are explicitly discussed. In order to identify the most influential parameters of the model, the global sensitivity analysis of the model is also performed using widely-recognized method, Latin hypercube sampling-partial rank correlation coefficients. As a result, HBx proteins show considerable influence on the course of infection whereas intracellular delay and dslDNA-containing intermediates have no significant impact on the disease dynamics. This study also indicates that SVPs have potential to augment the infection. Furthermore, another striking result is that the recycling of capsids could play vital roles in enhancing the infection.

6.1 Introduction

Mathematical models can help understand the underlying mechanisms of disease progression and transmission. Most of the previous studies on this viral infection [22,33,72,149,156,157] have mainly focused on the cell population. By analyzing the cell population, one can get a general overview about the viral infection whereas single-cell analysis provides how individual cell responds to the viral infection [158]. In a cell population, there are various types of cells that can differ in identity, state, functions, etc. as cells are heterogeneous. The variation in DNA sequence is one of the reasons for this heterogeneity [73]. In the literature, it is observed that when cell population is considered to study any kind of viral infections, the total number of cells is generally divided into two classes: uninfected and infected cells. Due to this classification, intracellular dynamics of the infection can not be explained by those models that are designed based on the consideration of cell populations because these models assume that all infected cells share the same characteristics. By modeling intracellular processes, one can study (i) the effects of each component of the virus and parameters that are involved in the intracellular dynamics, (ii) the efficiencies and modes of action of antiviral therapies, and (iii) the influence of host factors (host DNA repair mechanism, immune system, signaling pathways, etc.) utilized by the virions throughout the various stages of the viral life cycle, etc [159]. Moreover, the consideration of intracellular mechanisms also aids in shaping treatment strategies and guiding drug development. Besides, it has been demonstrated that if intracellular interactions are neglected, it can lead to an overestimation of viral lifespan and results in inaccurate assumptions about drug efficacy and mechanisms of action [160,161]. In addition, it is important to note that intracellular dynamics models are essential to evaluate the efficacies of those drugs that target specific stages of the viral life cycle [160,162]. In 1940, Delbruck [76] considered the phage-infected E.coli cells to study the heterogeneity in virus infected cells. In that experiment, it was shown that the amount of progeny virus produced from each infected cell differs significantly. According to the studies on influenza A virus [163], foot-and-mouth disease virus (FMDV) [164], and poliovirus [165], virion levels show considerable differences between individual cells.

Nowadays, single-cell analysis has become a significant milestone in many fields, including immunology, oncology, stem cells, virology, etc. The followings are some key advantages of single-cell analysis in virology:

1. The dynamics of infection in each infected cell can be studied at the micro level.

2. The intracellular components having significant influence on viral infection can be identified.

3. One can determine the most sensitive parameter for this infection.

4. Single-cell analysis helps in designing the new antiviral therapies.

In this study, based on the biological and clinical findings about the HBV intracellular life cycle [105, 166–170], an intracellular dynamics model is proposed with some assumptions. This model includes the roles of HBx protein, the impacts of capsid recycling and the formation of double-stranded linear DNA (dslDNA)-containing capsids, etc. The model also considers the assembly of both non-infectious sub-viral particles (SVPs) and infectious virion particles. Superinfection is also taken into account. The proposed model is further extended by incorporating intracellular delay. The comparison with experimental data shows that the model solution aligns closely with the experimental data. The main objective of this study is to identify the parameters that are most positively and negatively sensitive for each compartment of the model through global sensitivity analysis. This enables us to explore synergistic effects of parameters and to suggest novel forms of combination therapy.

6.2 Model formulation

HBV is a member of the hepadnaviridae family and by virtue of its exceptional characteristics, it replicates through RNA intermediates similarly as it happens in case of retroviruses. In this way, the replication cycle of HBV is able to perpetuate the infection in hepatocytes through its unique features. HBV replication begins when the virus enters the hepatocytes through the sodium taurocholate cotransporting polypeptide receptor by receptor-mediated endocytosis [7]. Although, initially, HBV binds to heparan sulfate proteoglycans (HSPGs) with a low affinity [171]. This model does not explicitly consider the roles of NTCP and HSPGs receptors in HBV entry. Inside the hepatocytes, virus releases its core particles, *i.e.*, relaxed circular DNA (rcDNA)-containing capsids. The number of viruses produced from a single infected hepatocyte and the quantity of rcDNA-containing capsids generated from incoming viruses from extracellular space are designated by $V(t)$ and $R(t)$, respectively. It is considered that the viruses uncoat their core particles with the release rate α_1^*. The natural decay rate of rcDNA-containing capsids is denoted by δ_r. The parameter α_2^* represents the rate at which rcDNAs are converted into cccDNAs [10]. Mathematically, this biological phenomenon can be expressed by the following differential equation:

$$\frac{dR(t)}{dt} = \alpha_1^* V(t) - \alpha_2^* R(t) - \delta_r R(t). \tag{6.2.1}$$

In the next step, in order to release the viral genome, HBV nucleocapsids travel to the nucleus of hepatocytes. To overcome the high viscosity of the cytoplasm, HBV utilizes the microtubular network for efficient nuclear delivery [172]. After entering the genome into the nucleus, the rcDNAs are repaired through the host DNA repair mechanism [167] and are converted into cccDNAs which are denoted by $C(t)$. There are several evidences which show that the persistence of cccDNAs is one of the major obstacles to prevent this viral infection [168, 173]. It is also believed that cccDNAs have significant contribution in the persistence of HBV infection as these are resistant to degradation and remain in the nuclei of the infected hepatocytes even after treatment is completed [174]. Despite serological evidence of viral clearance, cccDNAs persist in individuals, contributing to the potential for viral reactivation [175]. These can also remain inside the hepatocytes for months or even years. There are different ways in which cccDNAs are lost, such as cell proliferation, cell death due to cytolytic immune response, cell cure due to non-cytolytic immune response, and natural death of infected cells [176]. In this study, only the natural decay of cccDNAs (δ_c) is taken into account. This intracellular mechanism can be formulated as follows:

$$\frac{dC(t)}{dt} = \alpha_2^* R(t) + \gamma e^{-\Lambda S_p(t)} U(t) - \delta_c C(t). \tag{6.2.2}$$

Here, the term $\gamma e^{-\Lambda S_p(t)} U(t)$ represents the recycling of rcDNA-containing capsids. The details about the recycling of capsids are discussed later. In the ensuing step, cccDNAs use the cellular transcriptional tools to produce viral RNAs including pregenomic RNAs (pgRNAs) and other messenger RNAs (mRNAs) which are the key components in the production of viral proteins [177]. In general, three subgenomic mRNAs (0.7 kb mRNA, 2.1 kb mRNA and 2.4 kb mRNA) and two gemomics mRNAs of 3.5 kb are transcribed from cccDNAs [178]. These mRNAs are heterogeneous and positively oriented [179]. The incorporation of these viral mRNAs in the model is crucial due to their pivotal roles in the viral life cycle, including the involvement of surface proteins (HBsAg) production, the activation of cccDNA through HBV X proteins (HBx), etc [180]. For ease-of-use in model formulation, we denote 3.5 kb mRNA by $R_g(t)$. As both 2.4 kb mRNA and 2.1 kb mRNA produce surface proteins, these are treated as a single compartment by $R_s(t)$. Similarly, 0.7 kb mRNA is represented by $R_h(t)$. The parameters $\lambda_{rg}, \lambda_{rs}$ and λ_{rh} reflect the transcription rates of 3.5 kb mRNA, 2.1 & 2.4 kb mRNA, and 0.7 kb mRNA, respectively. HBx proteins that are denoted by $H(t)$ are produced from 0.7 kb mRNA and prevent the cccDNA from becoming silent. HBx can also enhance the transcription rate of cccDNAs [181]. Moreover, HBx inhibits the development of immune response to HBV infection, thereby preventing apoptosis of infected hepatocytes [169, 182]. Therefore, HBx plays some important roles in HBV repli-

cation. Keeping everything in mind, these complex replication steps are demonstrated by the following system of equations:

$$\frac{dR_g(t)}{dt} = \lambda_{rg}\Phi C(t) - \mu_1 R_g(t)P(t) - \delta_{r_g}R_g(t), \tag{6.2.3}$$

$$\frac{dR_s(t)}{dt} = \lambda_{rs}\Phi C(t) + \lambda_{dsl}D_L(t) - \lambda_{s_p}R_s(t) - \delta_{r_s}R_s(t), \tag{6.2.4}$$

$$\frac{dR_h(t)}{dt} = \lambda_{rh}\Phi C(t) - \delta_{r_h}R_h(t), \tag{6.2.5}$$

where δ_{r_g}, δ_{r_s} and δ_{r_h} indicate corresponding natural decay rates of $R_g(t)$, $R_s(t)$ and $R_h(t)$. Here, Φ denotes the volume fraction of active cccDNAs. The de-silencing of cccDNAs depends on the concentration of HBx proteins [180]. Recently, Fatehi et al. [11] modeled the silencing and de-silencing mechanisms of cccDNAs in the presence of HBx proteins by the following equations:

$$\text{(A1)Silencing:} \quad \text{cccDNA} \xrightarrow{\frac{\lambda_{off}}{1+s\bar{X}}} \text{silenced cccDNA},$$

$$\text{(A2) De-silencing:} \quad \text{Silenced cccDNA} \xrightarrow{\lambda_{on}(1+s\bar{X})} \text{cccDNA},$$

where λ_{off} and λ_{on} denote the silencing and de-silencing rates of cccDNAs, respectively, and s indicates the efficiency of the available numbers of HBx proteins ($\bar{X}$) according to the model proposed by Fatehi et al. [11]. Following equations (A1) and (A2), it is considered that

$$\Phi = \left(1 - \frac{1}{\frac{1}{1-\Phi_0} + H(t)}\right) = \frac{\Phi_0 + H(t)(1-\Phi_0)}{1 + H(t)(1-\Phi_0)}.$$

Here, Φ_0 is the initial volume fraction of active cccDNAs. When the concentration of HBx proteins increases, the value of Φ also increases. If $H(t) = 0$, Φ becomes Φ_0. The dslDNA which is denoted by $D_L(t)$ can also produce surface proteins but may not be able to produce functional pgRNAs due to some mutations that are introduced when it is converted into cccDNA [170]. cccDNAs that are produced from dslDNA are functionally defective, as the non-homologous end-joining pathway is error-prone [180]. It is assumed that 2.1 and 2.4 kb mRNAs are produced from dslDNAs with production rate λ_{dsl}. The meaning of two terms $\mu_1 R_g(t)P(t)$ in equation (6.2.3) and $\lambda_{s_p}R_s(t)$ in equation (6.2.4) are explained later. As a result of translation of these mRNAs by ribosomes, viral proteins are synthesized [11]. A portion of 3.5 kb mRNAs is translated into viral polymerase ($P(t)$), while another portion is

translated into core protein ($C_p(t)$) [183]. λ_p and λ_c indicate the subsequent translation rates of the polymerase and core protein. It is considered that 0.7 kb mRNAs is translated into HBx proteins with translation rate λ_h and degrade naturally at a rate δ_h. The corresponding governing equations for polymerases, core proteins and HBx proteins are formulated as

$$\frac{dP(t)}{dt} = \lambda_p R_g(t) - \mu_1 R_g(t)P(t) - \delta_p P(t), \tag{6.2.6}$$

$$\frac{dC_p(t)}{dt} = \lambda_c R_g(t) - \mu_2 m Z(t) C_p(t) - \delta_{c_p} C_p(t), \tag{6.2.7}$$

$$\frac{dH(t)}{dt} = \lambda_h R_h(t) - \delta_h H(t), \tag{6.2.8}$$

where, δ_p and δ_{c_p} are the decay rates of polymerases and core proteins, respectively. After translation, 3.5 kb mRNAs are reverse-transcribed to viral genome DNA by viral polymerase. The pgRNA and polymerase form a 1:1 ribonucleoproteins which are generally termed as RNP complexes [184]. These are assembly competent. These RNP complexes are denoted by $Z(t)$ and μ_1 denotes the interaction rate between 3.5 kb RNA and the polymerase. The mass balance equation for RNP complexes is given by

$$\frac{dZ(t)}{dt} = \mu_1 R_g(t)P(t) - \mu_2 Z(t)C_p(t) - \delta_z Z(t). \tag{6.2.9}$$

Here, δ_z reflects the decay rate of RNP complex. In the next step, RNP complexes are encapsidated by core proteins (HBcAg) to form pgRNA-containing capsids (pgNCs) with interaction rate μ_2. In this model, it is assumed that nucleocapsids contain $m = 120$ core proteins following a T = 4 architecture. We ignore the T = 3 particles in this study because these particles occur in only 5% of cases [185, 186]. The pgNCs are also known as immature nucleocapsids and denoted by the symbol $P_g(t)$. Consider δ_{p_g} is the decay rate of pgRNA-containing capsids. Based on the existing biological studies [184], it is observed that a portion of pgRNA-containing capsids is enveloped by the surface proteins and are secreted from the infected hepatocytes as non-infectious viral particles. Mathematically, pgRNA-containing capsids adhere to the following dynamical equation:

$$\frac{dP_g(t)}{dt} = \mu_2 Z(t)C_p(t) - \beta_1 P_g(t) - \delta_{p_g} P_g(t). \tag{6.2.10}$$

The reverse-transcription is one of the key steps in this virus life cycle. Through this process, the viral RNAs are converted into the viral DNA. The pgRNA acts as a template for DNA synthesis [187]. This step is associated with a series of events involving both the host and the virus factors. After encapsidation by the core proteins, it is assumed that the viral poly-

merase reverse-transcribes the pgRNA with a rate β_1 into single-stranded DNA (ssDNA). The ssDNA-containing capsids are designated by $S(t)$ with a degradation rate δ_s. It is assumed that the double-stranded DNA-containing capsids (dsDNA) and dslDNA-containing capsids are produced from ssDNA with the same rate β_2. According to the findings of Tu et al. [170], ∼90% of nucleocapsids generates rcDNA-containing capsids after reverse-transcription, while the remaining ∼10% produce dslDNA-containing capsids. In order to determine the relative contributions of different types of rcDNA-containing capsids on cccDNA production, this model distinguishes between rcDNA ($R(t)$) generated from upcoming virus from extracellular space and newly produced rcDNAs, *i.e.*, dsDNA-containing capsids, represented by $D(t)$. Newly produced rcDNA-containing capsids can either gain an envelope of HBsAg by passing through the endoplasmic reticulum, pre-Golgi compartment, and are released as infectious virions into the blood, or can recycle back to the nucleus [105]. In the case of low level of surface proteins, rcDNA-containing capsids deliver its content to the nucleus and increase the pool of cccDNAs [188]. This process is known as the 'recycling of capsids'. Λ^{-1} denotes the average level of surface proteins ($S_p(t)$) [50]. Here, γ stands for the recycling rate of capsids. The reaction equations for ssDNA, dsDNA and dslDNA can be given by the system of equations (6.2.11)-(6.2.13).

$$\frac{dS(t)}{dt} = \beta_1 P_g(t) - \beta_2 S(t) - \delta_s S(t), \tag{6.2.11}$$

$$\frac{dU(t)}{dt} = 0.9\beta_2 S(t) - \gamma e^{-\Lambda S_p(t)} U(t) - k_2 \left(1 - e^{-\Lambda S_p(t)}\right) U(t) S_p(t) - \delta_u U(t), \tag{6.2.12}$$

$$\frac{dD_L(t)}{dt} = 0.1\beta_2 S(t) - \lambda_{dsl} D_L(t) - \delta_{d_L} D_L(t). \tag{6.2.13}$$

In equation (6.2.2) as well as in equation (6.2.12), the term $\gamma e^{-\Lambda S_p(t)} U(t)$ represents the recycling of capsids [50]. The parameters δ_u and δ_{d_L} are the natural decay rates of dsDNA and dslDNA-containing capsids, respectively.

Surface proteins are among the key components of this virus. These proteins are produced by the translation of subgenomic RNAs (2.4 kb and 2.1 kb mRNA) by ribosomes. 2.4 kb mRNAs are translated into large surface proteins whereas translation of 2.1 kb of mRNAs leads to middle and small surface proteins [189]. For simplicity, these three surface proteins are referred to as one compartment and designated by $S_p(t)$ in this model. The natural decay rate of the surface proteins is denoted by δ_{s_p}. The parameter λ_{s_p} is considered to be the mean value of production rate of surface proteins. During the infection, both complete viral particles and SVPs are produced simultaneously and released into the bloodstream. SVPs are secreted from the hepatocytes in much larger amounts compared to infectious

virions [190]. SVPs are predominantly composed of viral surface antigens (HBsAg). Mainly two types of SVPs are produced: (i) spherical particles measuring 25 nm in diameter, and (ii) filaments with a diameter of 22 nm, which can differ in length [191]. Spherical SVPs are made of 48 S (small) proteins whereas filamentous SVPs have 1:1:4 protein stoichiometry for L (large), M (medium), and S (small) surface proteins [192]. All of these SVPs are non-infectious in nature. We denote the average production rate of SVPs by η_{s_p}. Accordingly, the pertinent dynamical equation is outlined below as,

$$\frac{dS_p(t)}{dt} = \lambda_{s_p} R_s(t) - k_2 \left(1 - e^{-\Lambda S_p(t)}\right) U(t) S_p(t) - \eta_{s_p} S_p(t) - \delta_{s_p} S_p(t). \tag{6.2.14}$$

The matured capsids are released from the infected hepatocytes into the extracellular space or blood as infectious Dane particles or complete virions. The virions exit via the cell's secretory pathway by exocytosis [193] and follows the given mathematical relationship:

$$\frac{dV(t)}{dt} = k_2 \left(1 - e^{-\Lambda S_p(t)}\right) U(t) S_p(t) - \delta_v V(t), \tag{6.2.15}$$

where δ_v and k_2 characterize the death and release rates of viruses, respectively. The governing equation for SVPs can be given by

$$\frac{dS_v(t)}{dt} = \eta_{s_p} S_p(t) - \delta_{sv} S_v(t). \tag{6.2.16}$$

Here, SVPs (denoted by $S_v(t)$) are cleared at rate δ_{sv}.

6.2.1 Full dynamics model

Based on the law of mass action, the temporal change of each component of virus is formulated. The following system of equations (6.2.17) describes the intracellular dynamics of the HBV infection with the non-negative initial conditions:

$$
\left.
\begin{aligned}
\frac{dR(t)}{dt} &= \alpha_1^* V(t) - \alpha_2^* R(t) - \delta_r R(t),\\
\frac{dC(t)}{dt} &= \alpha_2^* R(t) + \gamma e^{-\Lambda S_p(t)} U(t) - \delta_c C(t),\\
\frac{dR_g(t)}{dt} &= \lambda_{rg}\Phi C(t) - \mu_1 R_g(t) P(t) - \delta_{r_g} R_g(t),\\
\frac{dR_s(t)}{dt} &= \lambda_{rs}\Phi C(t) + \lambda_{dsl} D_L(t) - \lambda_{s_p} R_s(t) - \delta_{r_s} R_s(t),\\
\frac{dR_h(t)}{dt} &= \lambda_{rh}\Phi C(t) - \delta_{r_h} R_h(t),\\
\frac{dH(t)}{dt} &= \lambda_h R_h(t) - \delta_h H(t),\\
\frac{dP(t)}{dt} &= \lambda_p R_g(t) - \mu_1 R_g(t) P(t) - \delta_p P(t),\\
\frac{dZ(t)}{dt} &= \mu_1 R_g(t) P(t) - \mu_2 Z(t) C_p(t) - \delta_z Z(t),\\
\frac{dC_p(t)}{dt} &= \lambda_c R_g(t) - \mu_2 m Z(t) C_p(t) - \delta_{c_p} C_p(t),\\
\frac{dP_g(t)}{dt} &= \mu_2 Z(t) C_p(t) - \beta_1 P_g(t) - \delta_{p_g} P_g(t),\\
\frac{dS_p(t)}{dt} &= \lambda_{s_p} R_s(t) - k_2(1 - e^{-\Lambda S_p(t)}) U(t) S_p(t) - \eta_{s_p} S_p(t) - \delta_{s_p} S_p(t),\\
\frac{dS(t)}{dt} &= \beta_1 P_g(t) - \beta_2 S(t) - \delta_s S(t),\\
\frac{dD_L(t)}{dt} &= 0.1\beta_2 S(t) - \lambda_{dsl} D_L(t) - \delta_{d_L} D_L(t),\\
\frac{dV(t)}{dt} &= k_2 \left(1 - e^{-\Lambda S_p(t)}\right) U(t) S_p(t) - \delta_v V(t),\\
\frac{dU(t)}{dt} &= 0.9\beta_2 S(t) - \gamma e^{-\Lambda S_p(t)} U(t) - k_2 \left(1 - e^{-\Lambda S_p(t)}\right) U(t) S_p(t) - \delta_u U(t),\\
\frac{dS_v(t)}{dt} &= \eta_{s_p} S_p(t) - \delta_{sv} S_v(t).
\end{aligned}
\right\} \tag{6.2.17}
$$

All the model parameters are non-negative. The system (6.2.17) is solved numerically using the fourth-order highly-accurate *Runge–Kutta* method. The description of all model variables are summarized in the Table 6.1.

Table 6.1: State variables and their biological meanings

Variables	Descriptions
$R(t)$	Number of rcDNA-containing capsids
$C(t)$	Number of cccDNAs
$R_g(t)$	Number of 3.5 kb pgRNAs
$R_s(t)$	Number of 2.4 and 2.1 kb mRNAs
$R_h(t)$	Number of 0.7 kb mRNAs
$H(t)$	Number of HBx proteins
$P(t)$	Number of Polymerases
$Z(t)$	Number of RNP complexes
$C_p(t)$	Number of Core proteins
$P_g(t)$	Number of pgRNA-containing capsids
$S_p(t)$	Number of Surface proteins
$S(t)$	Number of single-stranded DNA-containing capsids
$D(t)$	Number of newly produced double-stranded DNA-containing capsids
$D_L(t)$	Number of double-stranded linear DNA-containing capsids
$V(t)$	Number of Viruses
$S_v(t)$	Number of SVPs

6.3 Model validation

In order to validate the proposed model (6.2.17), it is extended by incorporating the effects of entecavir (ETV) that acts as a reverse-transcriptase inhibitor and blocks the production of dsDNA-containing capsids from pgRNA-containing capsids. It is assumed that the efficiency of ETV (ϵ_{ETV}) satisfies $0 < \epsilon_{ETV} \leq 1$. As a result of incorporation of ETV, the equations (6.2.10) and (6.2.11) are modified as follows:

$$\left.\begin{aligned} \frac{dP_g(t)}{dt} &= \mu_2 Z(t) C_p(t) - (1-\epsilon_{ETV})\beta_1 P_g(t) - \delta_{p_g} P_g(t), \\ \frac{dS(t)}{dt} &= (1-\epsilon_{ETV})\beta_1 P_g(t) - \beta_2 S(t) - \delta_s S(t). \end{aligned}\right\} \tag{6.3.1}$$

Experimental data of four humanized mice are collected from the work of Kitagawa et al. [194]. Each mouse was infected with HBV at 1.0×10^6 copies. On the day 53 of post-inoculation, the mice, displaying a sustained level of HBV in serum, were administered ETV

continuously for 70 days. The treatment protocol involved daily dosing of 0.02 mg/kg ETV. The efficiency of ETV, as stated in the study by Kitagawa et al. [194], is recorded as 0.97, and this value is utilized in this study. Through a thorough comparison between the model solution and the experimental data from four humanized mice (labeled as Mouse-501, Mouse-502, Mouse-503, Mouse-504), it is seen from Figure 6.1 that model solutions agree well with the respective experimental data as well as the dynamics of the infection. Therefore, this model demonstrates a close alignment with the reality and reflects a strong correspondence with the actual observations.

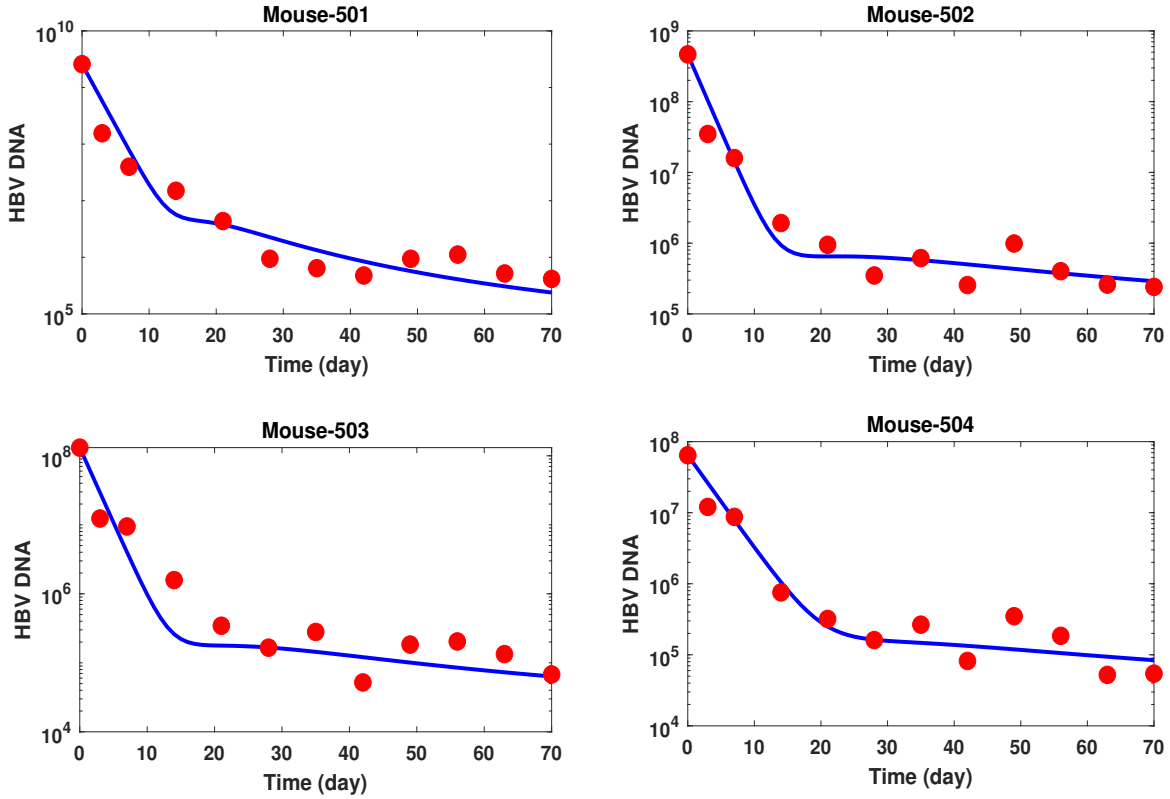

Figure 6.1: Calibration of the proposed model using experimental data collected from four humanized mice subjected to ETV treatment. Solid blue lines: model solution. Solid red circles: experimental data. Both model solutions and experimental data are presented on a logarithmic scale along the y-axis.

6.4 Results and discussion

In this study, an intracellular model of HBV infection dynamics that incorporates essential steps of the viral life cycle is proposed. The onset of the infection is assumed to be the initial

condition which is represented by

$$(R(0), C(0), R_g(0), R_s(0), R_h(0), H(0), P(0), Z(0), C_p(0), P_g(0), S_p(0), S(0), D_L(0), U(0), S_v(0), V(0)) = (0, 0, 0, 0, 0, 0, 0, 0, 0, 0, 0, 0, 0, 0, 0, V(0) \neq 0).$$

In order to study the effects of initial concentration of cccDNAs, we vary the initial concentration of cccDNAs. Otherwise, for the entire length of simulation, the stage of infection remains same. Even, same stage of infection is considered during global sensitivity analysis. According to Nowak and May [195], the lifespan of infected hepatocytes in HBV infection ranges from 10 to 100 days. So, the maximum lifespan of infected hepatocytes is considered to be 100 days to conduct the subsequent numerical experiments.

6.4.1 Effects of initial concentration of cccDNA

The existence of cccDNAs is highly associated with the persistence of infection in patients. It is thought to be a major factor for persistence of HBV infection as it is resistant to degradation and remains in the nucleus of infected cells even after treatment is completed. Due to its strong stability, cccDNAs are not lost in the course of cell division [196, 197]. Despite serological evidence of viral clearance, cccDNAs persist in individuals and act as a potential candidate for viral reactivation. It can also remain inside the hepatocytes for months or even years [198]. The effects of initial concentration of cccDNAs on all viral components are demonstrated here. The initial concentrations of cccDNAs are varied keeping the concentrations of other compartments fixed. To this purpose, five distinct initial concentrations of cccDNAs are considered. As a result, it is observed that the initial concentrations of cccDNAs significantly influence all compartments. The presence of a few copies of cccDNAs in the liver can re-initiate and blow-up the infection as shown in Figure 6.2. This small amount of cccDNAs that remains in the liver may act as a reservoir for the virus. Though a small quantity of cccDNAs may not be clinically important, but it remains as a crucial factor in the persistence and transmission of HBV infection. Although there are several approaches (e.g., inhibition of cccDNAs formation, blocking their function, or inducing their degradation) to target cccDNAs for the persistence of HBV infection, some novel antiviral strategies are needed to achieve a complete cure [199].

6.4.2 Roles of HBx proteins on HBV infection

HBx proteins contribute to the infection through various mechanisms, which have already been discussed in Section 6.2. These proteins can protect infected hepatocytes from immune-

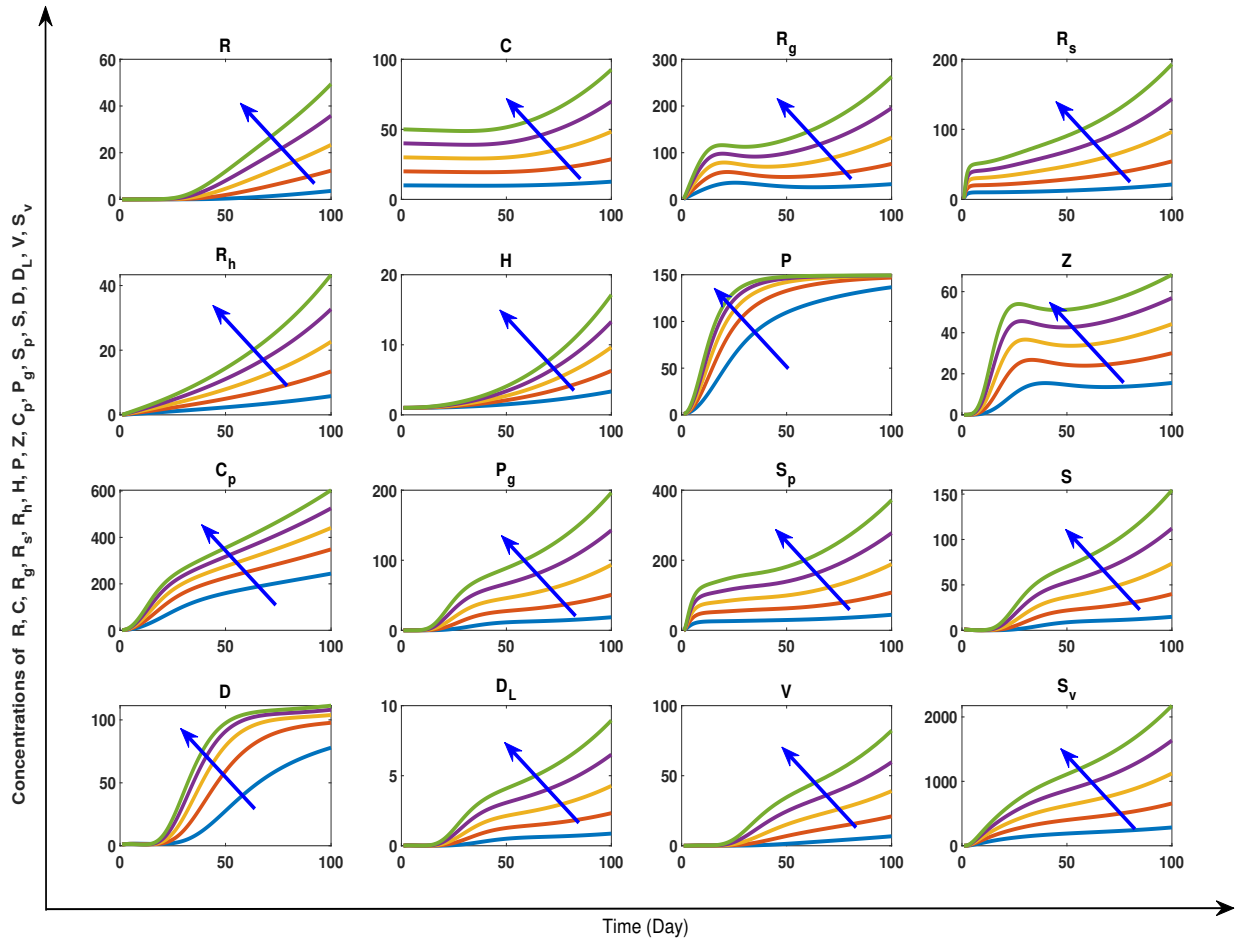

Figure 6.2: The effects of initial concentrations of cccDNAs on all components. Time and concentrations of each component are taken along the x-axis and along y-axis, respectively. Five different initial conditions ($C(0) = 10, 20, 30, 40, 50$) are considered here. The blue arrow in each subplot indicates direction of growth of the initial condition of cccDNAs.

mediated apoptosis by suppressing the immune systems in HBV infection [182], although many aspects of HBx are still unknown. Due to this, the impacts of HBx protein are incorporated in the model (6.2.17) to illustrate how it affects the intracellular components of the virus during infection. The simulation results show that the inclusion of HBx proteins substantially changes the concentration levels of model compartments. Figure 6.3 illustrates the changes in the concentration of cccDNAs and viruses, while variations in other components are presented in the supplementary material (Figure S1 and Figure S2). In Figure 6.3, it is observed that the numbers of cccDNAs and viruses increase rapidly when HBx is taken into account. Similar dynamics are also recorded for other compartments. In essence, the HBx proteins exert considerable influence on pathogenesis. Recently, Sivasudhan et al. [200]

also noted numerous pivotal functions of HBx in the persistent infection and advancement of HCC. Therefore, considering the HBx protein as a therapeutic target may provide a promising avenue for future management of HBV infection. In this regard, the antiviral agent SC75741 is identified as a good inhibitor for HBx proteins [201]. Moreover, targeting the X protein to maintain the silencing of cccDNA can be suggested as a potential therapeutic strategy [180].

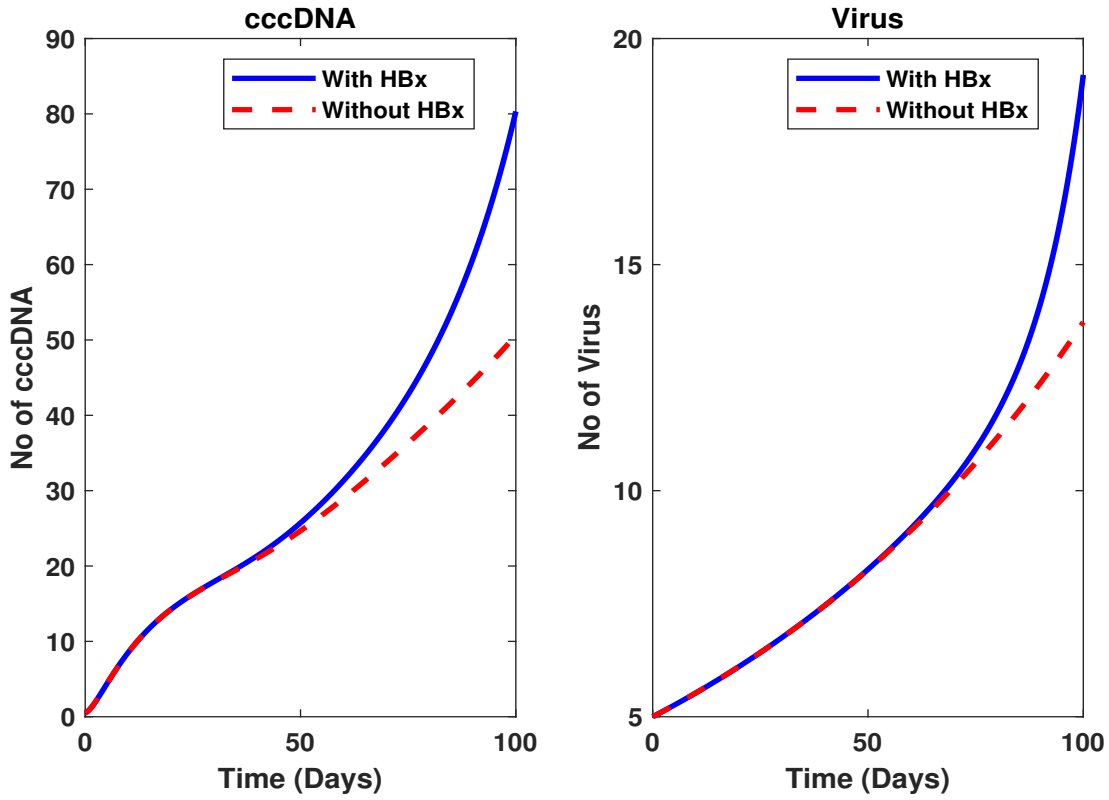

Figure 6.3: The effects of HBx protein are demonstrated. Blue solid line and red dotted line represent the solution of the system (6.2.17) with and without considering the effects of the HBx protein, respectively.

6.4.3 Impacts of intracellular delay

Time delay is seen to be an important factor in the intracellular replication process for some viruses. In comparison to an ODE model, a delay differential equation model (DDEM) typically has a much more realistic dynamics. Time delay may be responsible for the loss of stability of a steady-state and the oscillation in dynamics. In general, there are two types of delay: (i) pharmacological and (ii) intracellular. The delay between the ingestion of a drug

and its appearance within the cells is known as the pharmacological delay. The time-lapse between the infection of a host cell and the discharge of viral particles from the infected cell is known as the intracellular delay [202]. In this study, the intracellular delay is incorporated into every step of viral life cycle to make the process non-instantaneous. The DDEM is solved for different value of delay. As a result, the simulation demonstrates that the intracellular delay has very little impact on viral dynamics since there is no significant difference among the solutions. In a recent study, Murray et al. [50] also noted the limited influence of the delay on the infection dynamics.

6.4.4 Impacts of double-stranded linear DNA-containing capsids

The dslDNA-containing capsid is one of the intracellular components of the virus. It can be integrated in the host cell genome. dslDNA-containing capsids could be released as virions that contain dslDNAs or could be transported to the nucleus. dslDNA is a defective form of the viral DNA. It can produce viral surface proteins, but is unable to produce functional pgRNA due to some mutations that are introduced when it is converted into cccDNA [166]. The impacts of dslDNA-containing capsids on infection dynamics are examined in this study. In section 6.2, the roles of dslDNA to the production of 2.4 and 2.1 kb mRNAs are incorporated into the model (6.2.17) through the term $\lambda_{dsl} D_L(t)$. Keeping other parameters fixed, the system (6.2.17) is solved for different values of λ_{dsl} and the solutions are compared. No substantial change is observed in the model compartments especially in the cccDNA and virus compartments. Therefore, targeting the dslDNA containing capsids for possible future treatment options does not seem promising. Moreover, the differential equation corresponding to the dslDNA-containing capsids may be ignored in this model (6.2.17) for further analysis.

6.5 Simplification of the proposed model

For further analysis, the proposed model (6.2.17) is simplified ignoring some less important parameters and components based on some assumptions and findings discussed so far.

1. The degradation of intracellular components are much slower compared to their recruitment. Therefore, degradation rates are considered to be too small and can be ignored except for cccDNA and virus [51].

2. It is assumed that all cccDNAs are active. In this case, the volume fraction of active cccDNAs Φ is taken to be equal to 1 for further analysis. As a result, the corresponding

equations $\frac{dR_h(t)}{dt} = \lambda_{rh}\Phi C(t) - \delta_{r_h}R_h(t)$ and $\frac{dH(t)}{dt} = \lambda_h R_h(t) - \delta_h H(t)$ that enhance the number of active cccDNAs are ignored.

3. The system of equations (6.2.17) does not seem to be affected significantly by dslDNA-containing capsids, as observed in Section 6.4.4. Thus, the reaction equation corresponding to dslDNA in the dynamics model (6.2.17) is also ignored.

4. Since the other compartments of the system of equations (6.2.17) does not depend on $\frac{dS_v(t)}{dt} = \eta_{s_p}S_p(t) - \delta_{sv}S_v(t)$, (equation for SVPs) it is also not considered for further analysis.

Therefore, on the basis of these considerations, the dynamics model (6.2.17) is reduced to the following:

$$\left.\begin{aligned}
\frac{dR(t)}{dt} &= \alpha_1^* V(t) - \alpha_2^* R(t), & \frac{dC(t)}{dt} &= \alpha_2^* R(t) + \gamma e^{-\Lambda S_p(t)}U(t) - \delta_c C(t),\\
\frac{dR_g(t)}{dt} &= \lambda_{rg}\Phi C(t) - \mu_1 R_g(t)P(t), & \frac{dR_s(t)}{dt} &= \lambda_{rs}\Phi C(t) - \lambda_{s_p}R_s(t),\\
\frac{dP(t)}{dt} &= \lambda_p R_g(t) - \mu_1 R_g(t)P(t), & \frac{dZ(t)}{dt} &= \mu_1 R_g(t)P(t) - \mu_2 Z(t)C_p(t),\\
\frac{dC_p(t)}{dt} &= \lambda_c R_g(t) - \mu_2 m Z(t)C_p(t), & \frac{dP_g(t)}{dt} &= \mu_2 Z(t)C_p(t) - \beta_1 P_g(t),\\
\frac{dS(t)}{dt} &= \beta_1 P_g(t) - \beta_2 S(t), & & \\
\frac{dS_p(t)}{dt} &= \lambda_{s_p}R_s(t) - k_2\left(1 - e^{-\Lambda S_p(t)}\right)U(t)S_p(t) - \eta_{s_p}S_p(t), & & \\
\frac{dU(t)}{dt} &= \beta_2 S(t) - \gamma e^{-\Lambda S_p(t)}U(t) - k_2\left(1 - e^{-\Lambda S_p(t)}\right)U(t)S_p(t), & & \\
\frac{dV(t)}{dt} &= k_2\left(1 - e^{-\Lambda S_p(t)}\right)U(t)S_p(t) - \delta_v V(t). & &
\end{aligned}\right\} \tag{6.5.1}$$

6.5.1 Global sensitivity analysis of model parameters

Experimental data often contain inherent uncertainties. When such data are used to estimate model parameters, the accuracy of these parameters is affected. Consequently, the solutions generated by the model can become erroneous. In this case, sensitivity analysis is effective for determining the nature of parameters during the infection period. Most of the studies generally focus on local sensitivity analysis (LSA). However, LSA does not provide complete necessary information about the uncertainty and sensitivity of the concerned model parameters. In this case, global sensitivity analysis (GSA) performs better and can clearly

describe the contributions of each model parameter irrespective of the roles of other parameters. The GSA is a statistical technique, which is used to study the sensitivity of parameters of a system or of a mathematical model. Various methods are used for the global sensitivity analysis, such as Sobol indices, Fourier amplitude sensitivity test, partial rank correlation coefficient (PRCC). In this study, Latin hypercube sampling-partial rank correlation coefficient (LHS-PRCC) method is applied. This method is well-explained in the article of Marino et al. [116]. In this method, PRCC values provide relevant useful information. PRCC can also aid us in determining the most influential set of parameters to achieve specific objectives in the elimination of this disease.

6.5.2 Scatter plots: The monotonic relationship between input and output variables

In order to make better prediction on the infection dynamics and to recommend new different types of treatment strategies, it is essential to explore how the outputs of a system are influenced if the values of the associated parameters vary within biologically relevant ranges. Simulation results of the model (6.5.1) are shown by scatter plots which are presented in Figures 6.4, 6.5, and 6.6. PRCC values of all model parameters are computed with respect to dependent variables on the 90^{th} day and are visualized in Table 6.2. The positive PRCC value between a model parameter and a compartment indicates that any increase (or decrease) in the parameter's value, whether individually or simultaneously, leads to an enhancement (or reduction) in the concentration of that compartment. On the other hand, negative correlation (PRCC value negative) shows the opposite aspects. Based on the PRCC values, most positively sensitive (MPS), most negatively sensitive (MNS) and less significant parameters are identified and listed in the Table 6.3.

Global sensitivity analysis reveals several striking results. Based on the PRCC values (Table 6.2) and the outputs shown in Table 6.3, some findings are listed below.

1. The production rate of SVPs (η_{s_p}) is positively correlated with almost all viral components mentioned in the model (6.5.1) except surface proteins. This means that these particles can enhance the infection. Despite being non-infectious, SVPs can accelerate the infection [203]. Clearance of SVPs may play a key role in controlling HBV infection effectively. In this context, HBsAg release inhibitors, such as REP 2055 and REP 2139-Ca [204], and REP 2139-Mg and REP 2165-Mg [205] (both are in clinical trial), may be potentially useful components of future therapies.

2. All components except from dsDNA-containing capsids have positive correlation with

recycling rate (γ). Through this looping mechanism, newly produced capsids transport from the cytoplasm to the nucleus, thereby increasing the pool of cccDNAs. Compared to other components, the surface protein (S_p) is the most sensitive to this parameter, exhibiting PRCC value of 0.8067. Therefore, recycling enhances the infection and serves as a positive feedback loop in the infection. Long-term treatment with nucleos(t)ide analogs (NAs) can decrease the cccDNA pool in HBV-infected hepatocytes by inhibiting nucleocapsid recycling [206]. Besides, Wong et al. [207] observed that the capsid assembly modulators (CAMs) can inhibit cccDNA replenishment by disrupting capsid disassembly and nucleocapsid recycling. So, targeting capsid recycling could be an effective strategy for eradicating HBV.

3. The production rate of 3.5 kb pgRNA (λ_{rg}) is positively associated with all viral compartments considered in the model (6.5.1), implying that transcription of cccDNA is a critical step in the viral life cycle. On the other hand, transcription rate of 2.4 kb and 2.1 kb mRNA (λ_{rs}) is negatively correlated with nearly all model compartments except 2.4 kb and 2.1 kb mRNAs, surface proteins and virus. It indicates that the availability of surface proteins leads to a higher quantity of viruses, resulting enhancement of the infection. This accurately reflects the biological mechanisms of the viral infection. Hence, transcription of cccDNA should be considered while proposing any new control strategy. Disruption of cccDNAs is one of the ways to reduce the infection. Gene editing drugs, like clustered regularly interspaced short palindromic repeats-associated 9 (CRISPR/Cas9 [208]), zinc-finger nucleases (ZFNs [209]) (both are in clinical trial) may show strong potential as standalone therapy or as synergy therapy. Apart from this, in order to reduce HBV transcription, transcription inhibitors (ARC-520 [210], GSK3389404 [211]) and gene expression inhibitor (RG7834 [212]) can be considered as future options.

4. It is also observed that the production rate of polymerases (λ_p) and the production rate of core proteins (λ_c) both are sensitive (positive for some compartments and negative for others) for all model compartments. In addition, these two parameters are synchronously MPS and MNS. This kind of behavior is quite peculiar. As far as the infection is concerned, production rate of polymerase and core proteins play dual role (simultaneously MPS and MNS). This is one of the crucial findings in this study. Probably, dual role of these two parameters are noticed in this study for the first time. No one has informed about this kind of behaviors of these two parameters so far. In order to target capsid assembly, it is essential to stop the formation of capsid-like structures. In this scenario, the capsid assembly modulator drug NVR3-778 [213]

(under clinical trials) can be focused.

5. Since the production rates of ssDNA and dsDNA-containing capsids (β_1 and β_2) promote infection, nucleos(t)ide analogs (NAs) such as lamivudine (LAM), telbivudine (LDT), entecavir (ETV), adefovir dipivoxil (ADV), and tenofovir disoproxil fumarate (TDF) [206] are promising candidates for inhibiting the infection. Nowadays, these drugs are widely used due to their effectiveness.

6. Global sensitivity analysis identifies that the production rate of 3.5 kb pgRNA (λ_{rg}) behaves as the most positively influential parameter in the framework of the system delineated by equation (6.5.1). This is because it is the most positively sensitive parameter, as reflected by its high PRCC values, among the following compartments: rcDNA-containing capsids, 3.5 kb pgRNA, pgRNA-containing capsids, surface proteins, ssDNA-containing capsids, and viruses.

It is important to note that all the drugs, which are mentioned above except NAs are in clinical trial and may be considered for use in the future as monotherapy or combination therapy (CT), subject to approval by the competent authority. In this study, we do not account the functions of interferon therapy (IFN-α or Peg-IFN-α) because the proposed model does not include immune cells. Considering all these results and findings discussed so far, it is believed that the best way to control this disease as well as the best CT can be determined.

Table 6.2: List of PRCC values. As shown in the north-west box, P stands for parameters and V stands for variables. Blue and red PRCC values represent highest and lowest PRCC values of the corresponding component w.r.t model variable.

V / P	$R(t)$	$C(t)$	$R_g(t)$	$R_s(t)$	$P(t)$	$Z(t)$	$C_p(t)$	$P_g(t)$	$S_p(t)$	$S(t)$	$D(t)$	$V(t)$
α_1^*	0.7146	0.0440	-0.0084	0.0763	-0.0323	0.0281	-0.0397	0.0158	0.0685	0.0009	-0.1002	0.0190
α_2^*	-0.6844	0.0695	0.0676	0.0768	0.0117	0.0218	-0.0013	0.0678	0.0879	0.0714	0.0401	0.0823
γ	0.4304	0.7408	0.6212	0.7125	-0.0362	0.1259	0.1214	0.4856	0.8067	0.4780	-0.7547	0.4594
Λ	-0.4580	-0.7496	-0.6412	-0.7047	-0.0432	-0.0623	-0.2121	-0.4784	-0.8020	-0.5152	-0.7685	-0.4910
δ_c	-0.4108	-0.6848	-0.5533	-0.6251	-0.0719	-0.0477	-0.1634	-0.3979	**-0.8485**	-0.4042	0.6313	-0.4379
λ_{rg}	**0.8694**	0.8170	**0.9396**	0.7930	0.0056	0.2820	0.4618	**0.8776**	**0.8604**	**0.8832**	0.7692	**0.8887**
μ_1	-0.0196	-0.0122	0.0002	0.0117	**-0.9683**	-0.0338	-0.0182	-0.0078	-0.0247	-0.0166	-0.0401	-0.0254
λ_{rs}	-0.5532	**-0.8325**	-0.7335	0.0805	-0.0257	-0.1442	-0.1683	-0.5978	0.0495	-0.6078	**-0.8510**	0.5852
λ_{sp}	0.0126	0.0213	-0.0194	**-0.9032**	0.0344	0.0353	-0.0306	-0.0152	-0.0003	-0.0017	0.0464	0.2282
λ_p	-0.4967	-0.4049	**-0.8911**	-0.3980	**0.9676**	**0.9227**	**-0.9195**	-0.4958	-0.4632	-0.4791	-0.3685	-0.5258
μ_2	-0.0412	-0.0492	-0.0375	-0.0261	-0.0175	-0.3507	-0.1730	-0.0554	-0.0419	-0.0708	-0.0181	0.0194
λ_c	0.6015	0.5311	0.3926	0.4855	-0.0309	**-0.9256**	**0.9265**	0.5984	0.5979	0.6112	0.4744	0.6317
β_1	-0.0012	-0.0312	0.0121	-0.0008	-0.0451	-0.0047	0.0133	**-0.7437**	0.5540	-0.0074	-0.0318	-0.0059
η_{sp}	0.6982	**0.9162**	0.8513	**0.9001**	0.0125	0.2242	0.2595	0.7496	-0.0519	0.7479	**0.9236**	0.7310
β_2	0.0276	0.0148	0.0867	0.0324	-0.0529	-0.0640	0.0606	0.0216	0.0088	**-0.7475**	0.4520	0.0417
k_2	-0.3843	-0.7432	-0.6226	-0.7010	0.0201	-0.0470	-0.1710	-0.4766	-0.8015	-0.4813	-0.7765	-0.4356
δ_v	**-0.6996**	-0.0383	-0.0500	0.0065	0.0312	0.1229	-0.1222	-0.0488	0.0437	-0.0175	0.0967	**-0.7370**

Table 6.3: Complete list of positively correlated, negatively correlated, non-significant, most positively significant and most negatively significant parameters. The parameters that are positively correlated are arranged in monotonically decreasing order whereas those that are negatively correlated are arranged in monotonically increasing order.

Variables	Positively correlated parameters	Negatively correlated parameters	Less-sensitive parameters	Most positively sensitive parameter	Most negatively sensitive parameter
$R(t)$	$\lambda_{rg},\ \alpha_1^*,\ \eta_{sp}$ $\lambda_c,\ \gamma$	$\delta_v,\ \alpha_2^*,\ \lambda_{rs},\ \lambda_p,$ $\Lambda,\ \delta_c,\ k_2$	$\mu_1,\ \lambda_{s_p},\ \mu_2,$ $\beta_1,\ \beta_2$	λ_{rg}	δ_v
$C(t)$	$\eta_{sp},\ \lambda_{rg},$ $\gamma,\ \lambda_c$	$\lambda_{rs},\ \Lambda,\ k_2,$ $\delta_c,\ \lambda_p$	$\alpha_1^*,\ \alpha_2^*,\ \lambda_{s_p},\ \beta_1,$ $\beta_2,\ \delta_v,\ \mu_1,\ \mu_2$	η_{sp}	λ_{rs}
$R_g(t)$	$\lambda_{rg},\ \eta_{sp},$ $\gamma,\ \lambda_c$	$\lambda_p,\ \lambda_{rs},\ \Lambda,$ $k_2,\ \delta_c$	$\alpha_1^*,\ \alpha_2^*,\ \mu_1,\ \mu_2,$ $\lambda_{s_p},\ \beta_1,\ \beta_2,\ \delta_v$	λ_{rg}	λ_p
$R_s(t)$	$\eta_{sp},\ \lambda_{rg},$ $\gamma,\ \lambda_c$	$\lambda_{s_p},\ \lambda,\ k_2,$ $\delta_c,\ \lambda_p$	$\alpha_1^*,\ \alpha_2^*,\ \mu_1,\ \mu_2,\ \lambda_{rs},$ $\lambda_c,\ \beta_1,\ \beta_2,\ \delta_v$	η_{sp}	λ_{s_p}
$P(t)$	λ_p	μ_1	All other parameters	λ_p	μ_1
$C_p(t)$	$\lambda_c,\ \lambda_{rg},\ \eta_{sp}$	$\lambda_p,\ \Lambda$	All other parameters	λ_c	λ_p
$Z(t)$	$\lambda_p,\ \lambda_{rg},\ \eta_{sp}$	$\lambda_c,\ \mu_2$	All other parameters	λ_p	λ_c
$P_g(t)$	$\lambda_{rg},\ \eta_{sp},$ $\lambda_c,\ \gamma$	$\beta_1,\ \lambda_{rs},\ \lambda_p,\ \Lambda,$ $k_2,\ \delta_c$	$\alpha_1^*,\ \alpha_2^*,\ \mu_1,\ \mu_2,$ $\lambda_{sp},\ \beta_2,\ \delta_v$	λ_{rg}	β_1
$S_p(t)$	$\lambda_{rg},\ \gamma,$ λ_c	$\delta_c,\ k_2,$ $\Lambda,\ \lambda_p$	All other parameters	λ_{rg}	δ_c
$S(t)$	$\lambda_{rg},\ \eta_{sp},$ $\lambda_c,\ \gamma$	$\beta_2, \lambda_{rs},\ \Lambda,$ $k_2,\ \lambda_p,\ \delta_c$	All other parameters	λ_{rg}	β_2
$D(t)$	$\eta_{sp},\ \lambda_{rg},$ δ_c, λ_c	$\lambda_{rs},\ k_2,\ \Lambda,$ $\gamma,\ \lambda_p$	All other parameters	η_{sp}	λ_{rs}
$V(t)$	$\lambda_{rg},\ \eta_{sp},$ $\lambda_c,\ \gamma,$	$\delta_v,\ \lambda_{rs},\ \lambda_p,$ $\Lambda,\ \delta_c,\ k_2$	All other parameters	λ_{rg}	δ_v

Scatter plots for rcDNAs ($R(t)$).

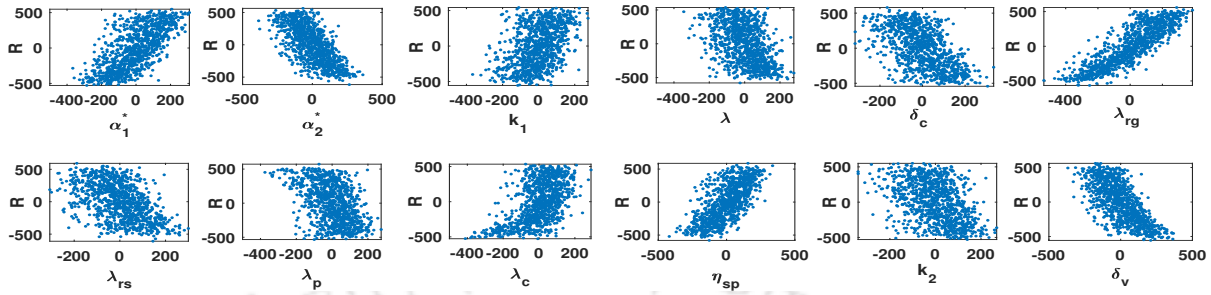

Scatter plots for cccDNAs ($C(t)$).

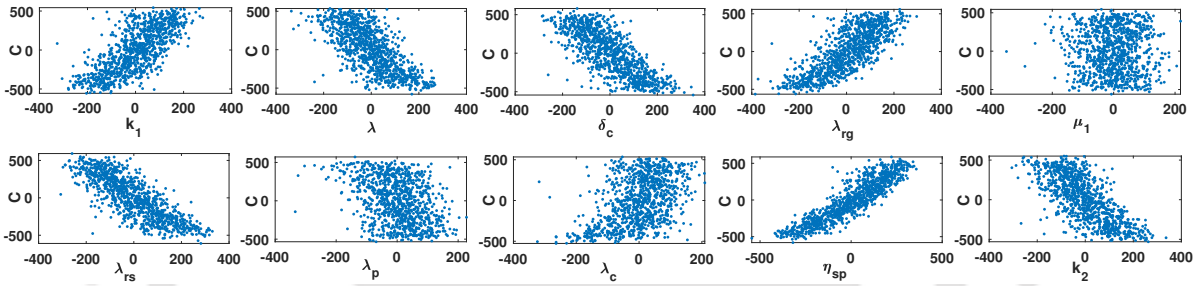

Scatter plots for 3.5 kb pgRNAs ($R_g(t)$).

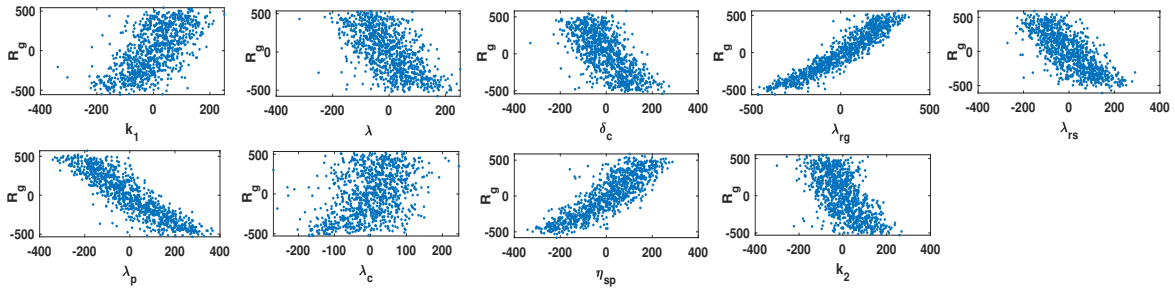

Scatter plots for 2.4 and 2.1 kb mRNAs ($R_s(t)$).

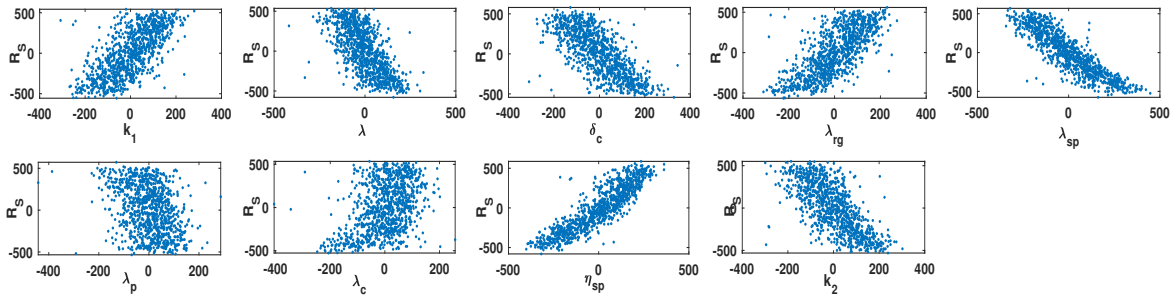

Figure 6.4: Scatter plots of rcDNAs, cccDNAs, 3.5 kb mRNAs, 2.4 and 2.1 kb mRNAs.

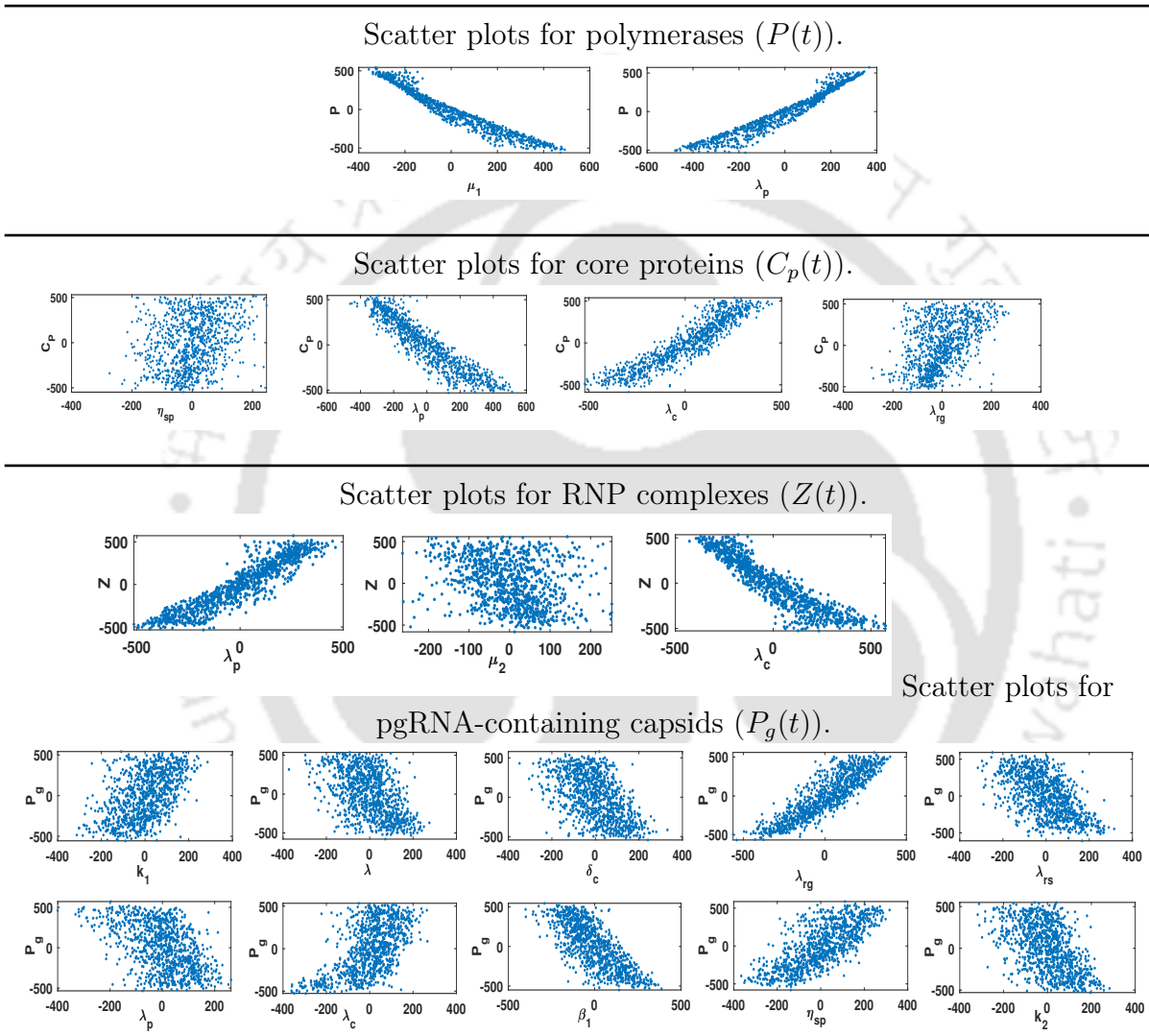

Figure 6.5: Scatter plots of polymerases, core proteins, RNP complexes, and pgRNA-containing capsids.

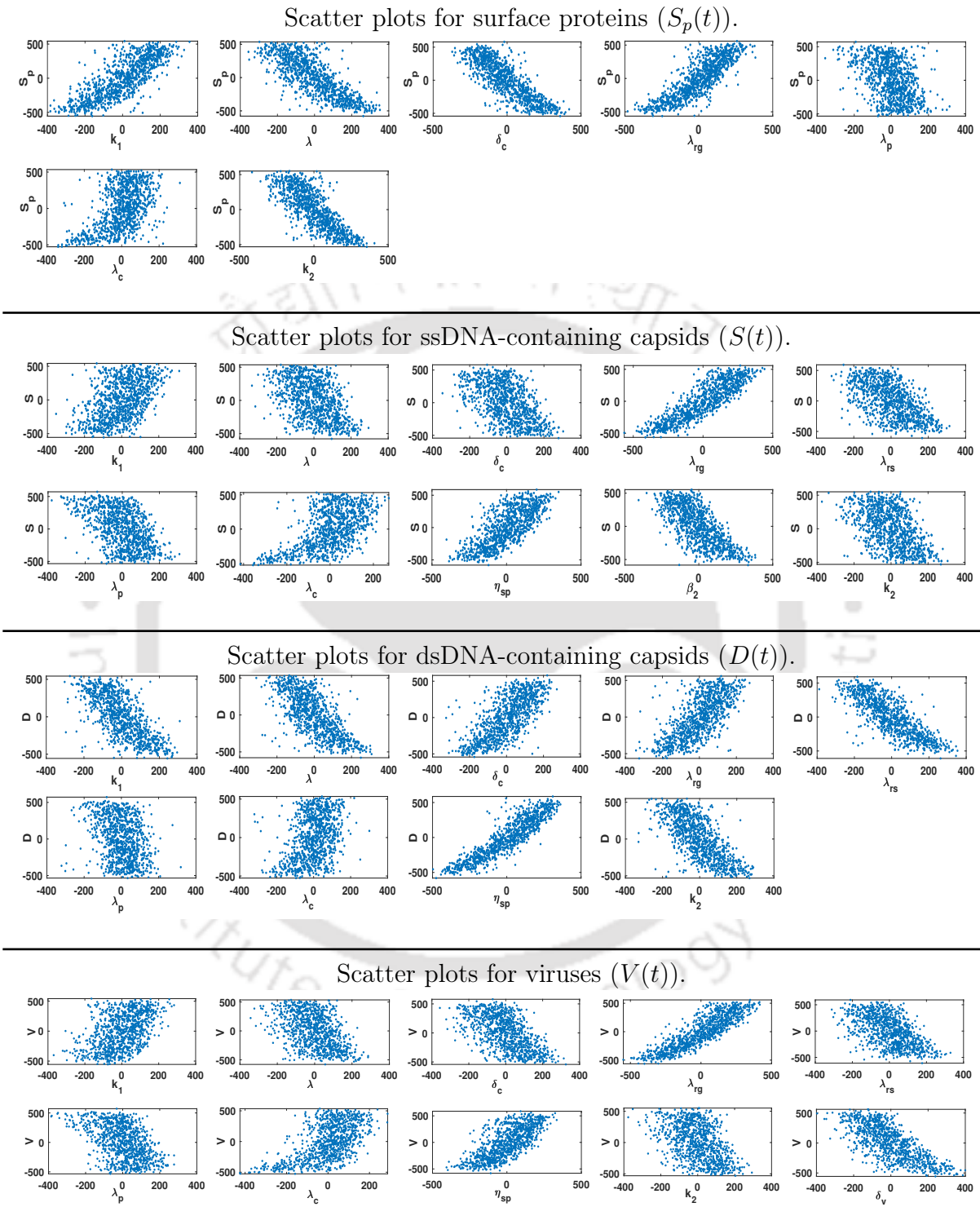

Figure 6.6: Scatter plots of surface proteins, ssDNA-containing capsids, dsDNA-containing capsids and viruses.

6.6 Conclusions

In case of viral infection, intracellular dynamics model has revealed various intrinsic biological phenomena of individual infected cell. Based on the biological and clinical findings about the HBV intracellular dynamics, this study proposes an intracellular dynamics model. The proposed model is validated with experimental data obtained from four humanized mice. The close alignment between the model's solutions and the observed data underscores the reliability and robustness of the model. In order to study the global sensitivity of the model's parameters, a sampling-based method, Latin hypercube sampling-partial rank correlation coefficient is applied. The most positively and most negatively correlated parameters for each model compartment as well as for the entire system are identified. It is also uncovered that certain parameters (λ_c, λ_p) have dual role in modulating disease dynamics since these two parameters are synchronously most positively sensitive for some compartments while being the most negatively sensitive for other some compartments. It is expected that the findings of this study add a new dimension to our understanding of the disease's progression and the factors that control the infection. The outcomes of this study lead to the following conclusions:

1. There is significant contribution of HBx proteins to the progression of HBV infection. So, targeting the HBx protein as a future antiviral therapy could be a promising strategy to control the infection. In this case, SC75741 may be considered as an antiviral agent to inhibit the functions of HBx proteins.

2. The simulation results illustrate that the intracellular delay has little effect on the infection dynamics.

3. This study indicates that dslDNA-containing capsids have no efficient bearing on the outcomes of the infection.

4. The recycling of capsids enhances the infection. The available inhibitors (e.g., capsid assembly modulators) associated with capsids recycling mechanism have been proved to be effective in reducing HBV infection.

5. The production rate of 3.5 kb pgRNA (λ_{rg}) stands out as the most positively influential/sensitive parameter in shaping the dynamics of the infection. The disruption of cccDNAs may help in reducing the infection. In addition to widely used drugs, like nucleos(t)ide analogs and interferon therapy, gene editing drugs (CRISPR/Cas9, ZFNs), gene expression inhibitor (RG7834), could be viable candidates for controlling the infection.

6. This study also indicates that SVPs have substantial impacts in the advancement of the infection. The clearance of HBsAg is a critical milestone in the achievement of functional cure. In order to do this, HBsAg release inhibitors, such as REP 2055, REP 2139-Ca, REP 2139-Mg, REP 2165-Mg, may become effective antiviral agents. All of these drugs are currently undergoing clinical trials.

CHAPTER 7

Conclusions and Future Scopes

7.1 Conclusions

This dissertation explores the dynamics of HBV infection through several intercellular models that incorporate various aspects, including the effects of capsid recycling, the roles of fractional-order derivatives, both continuous and discontinuous proliferation of uninfected and infected hepatocytes, diffusion of viral particles, and the impacts of SVPs. The influence of antibodies in the presence of SVPs is also examined. In addition to the intercellular models, this thesis considers the intracellular dynamics of HBV infection. The intracellular model is proposed based on the recent biological findings and clinical insights. The proposed models are evaluated by comparing their outcomes with experimental data for validation. In order to study the sensitivity of model parameters, sensitivity analysis is performed. Consequently, the most positively as well as most negatively sensitive parameter of the proposed models is identified.

Based on this study, it is observed that the recycling of capsids, a unique intracellular process in the life cycle of HBV, enhances the severity of infection by increasing the production of viral particles, *i.e.*, it acts as a positive feedback loop. Incorporation of capsid recycling into the model reverses the effects of volume fraction of newly produced capsids. This is one of the striking outcomes of this study that changes the usual understandings of viral

dynamics. The recycling of capsids also significantly enhances the concentration of SVPs. Therefore, in this context, available inhibitors (e.g., capsid assembly modulators) associated with capsid recycling may be recommended as effective treatment options in reducing HBV infection. On the other hand, in the presence of capsid recycling, the numerical experiments on cellular proliferation reveal some significant outcomes as follows:

- When both uninfected and infected hepatocytes proliferate at an equal rate during acute infection, the number of uninfected hepatocytes increases as the proliferation rate increases. Simultaneously, the number of infected hepatocytes decreases to zero. This suggests that, during acute infection, proliferation helps to recover from the infection. However, in the case of chronic infection, proliferation leads to an increase in the severity of the infection.

- When both types of hepatocytes proliferate at different rates in acute phase, the proliferation of uninfected hepatocytes rapidly cures the disease, while the proliferation of infected hepatocytes make no notable contribution. In contrast, experiments on chronic infection suggest that the infection is strongly influenced by the proliferation of both types of hepatocytes. The proliferation of uninfected hepatocytes exacerbates the infection, while the proliferation of infected hepatocytes reduces its severity.

It is also noted that the outcomes of the disease differ considerably between continuous and discontinuous proliferation. This highlights the importance of targeting and regulating proliferation patterns as a potential therapeutic approach to reduce the detrimental effects of HBV infection.

Beside the above observations, the abundance of SVPs in the liver causes a rapid increase in the virion compartment, resulting in a higher peak level under critical situations. SVPs significantly enhance the intracellular viral replication by reducing the neutralization of virus particles by HBV-specific antibodies. This suggests that, despite being non-infectious in nature, SVPs can accelerate the infection. The diffusion of SVPs, along with other components such as capsids, viruses, and antibodies, facilitates the rapid spread of infection across the liver. So, the clearance of SVPs may play a key role in controlling HBV infection effectively. In this context, HBsAg release inhibitors, such as REP 2055, REP 2139-Ca, REP 2139-Mg, and REP 2165-Mg (currently all in clinical trials), may serve as promising candidates for future therapies. In addition, the studies on the multi-points infection show that as the number of initial infection points increases, the peaks of the solutions for infected hepatocytes, viruses, and SVPs become higher and occur earlier. From the long-term perspective, the severity of the infection remains unchanged regardless of the number of infection points,

as the model solutions converge to the same steady-state. This is one of the most striking outcomes of this thesis.

Moreover, similar to the case of the ordinary derivative, we also examine how the dynamics change when a fractional-order derivative is considered in place of an ordinary derivative. As a result, it is seen that the fractional derivative does not make any substantial impact on the long-term dynamics of the disease as it neither alters the number of equilibrium points nor affects their stability. However, the rate of convergence of the solution is highly influenced by the order of fractional derivative. For lower values of the fractional order, the solution requires a longer time to stabilize to the steady state. For a multi-order system of FDEs, the fractional-order derivative corresponding to the infected hepatocytes has the most significant influence on the infection.

The results discussed above are derived from the intercellular dynamics model. Considering the intracellular dynamics of hepatitis B, single-cell analysis is also conducted in this dissertation, offering some biologically testable insights, such as:

- Intracellular delay and double-stranded linear DNA-containing capsids have a negligible impact on the intracellular dynamics of the infection.
- HBx proteins play a crucial role in the progression of HBV infection. Therefore, targeting HBx proteins could offer a promising therapeutic strategy for managing HBV infection in the future. Notably, the antiviral agent SC75741 has been identified as an effective inhibitor of HBx proteins.
- Among the intracellular dynamics, the production rate of 3.5 kb pgRNAs is the most influential and sensitive parameter in shaping the infection dynamics.

The findings presented in this thesis offer a broad and versatile perspective on HBV infection. From various angles, this research has provided crucial insights into the underlying mechanisms of the disease. One of the primary challenges in combating HBV infection is the lack of a 100% effective treatment. However, the results of this study highlight several key mechanisms that could be targeted in future therapeutic strategies. These findings have the potential to make significant contributions across multiple fields, including pharmacology, where people can get new ideas to propose new antiviral therapies, as well as in medical science and healthcare. Additionally, medical practitioners may gain novel insights and innovative approaches for improving patient care and treatment outcomes. The application of these findings could lead to more effective treatment options for HBV infection and promote better management of this global health challenge.

7.2 Future scopes

This dissertation primarily focuses on both intercellular and intracellular dynamics of HBV infection. It highlights the advancement and progression of mathematical models, transitioning from basic frameworks to more complex and realistic representations. These studies can be further expanded and explored in various directions in the future. A few potential avenues for future research in this area are outlined below.

7.2.1 Cost-effective treatments

An optimal treatment strategy for controlling HBV infection over a set period involves selection of the best approach to achieve both health and financial goals. This strategy is guided by an objective function, a mathematical framework designed to balance multiple competing priorities. The primary goals are to reduce the number of infected hepatocytes and lower the viral load, thereby slowing the progression of the infection. At the same time, the strategy aims to minimize the adverse side effects of drugs and the overall cost of therapy, ensuring that the treatment is both effective and sustainable. By leveraging mathematical modeling and optimization techniques, this approach provides a systematic way to design treatment protocols that address biological, patient-specific, and financial considerations. Using the intracellular dynamics model proposed in Chapter 6, an optimal therapy can be designed.

7.2.2 HBV infection dynamics with time-dependent parameter

In the context of this disease, parameters are often time-dependent, reflecting how the disease progresses and affects the patients with time. Consider the proposed model (2.2.1) discussed in Chapter 2. If we assume that every parameter of the model (2.2.1) varies with time, the following non-autonomous HBV infection dynamics model can be derived:

$$\left.\begin{aligned}
&\text{Susceptible hepatocytes :} && \frac{dX(t)}{dt} = \lambda(t) - \mu(t)X(t) - k(t)V(t)X(t),\\
&\text{Infected hepatocytes:} && \frac{dY(t)}{dt} = k(t)V(t)X(t) - \delta(t)Y(t),\\
&\text{rcDNA-containing capsids:} && \frac{dU(t)}{dt} = a(t)Y(t) + \gamma(t)(1-\eta(t))U(t) - \eta(t)\beta(t)U(t) - \delta(t)U(t),\\
&\text{Free viruses:} && \frac{dV(t)}{dt} = \eta(t)\beta(t)U(t) - \delta_v(t)V(t).
\end{aligned}\right\} \tag{7.2.1}$$

After verifying the biological criteria that a mathematical model should satisfy, the possible functional form of each parameter and its effects on infection over time can be analyzed.

7.2.3 Pattern formation

Understanding the pattern formation of HBV infection is crucial for comprehending the disease's progression and overall impact on the liver. By investigating the spatial and temporal patterns of HBV spread within liver tissues and the corresponding immune responses, researchers can gain insights into the underlying mechanisms of the infection dynamics, viral persistence, and liver damage. This knowledge is instrumental in developing targeted therapies, as it identifies specific regions within the liver that are most affected by the virus and immune-mediated injury.

7.2.4 Exploring HBV infection in a triangular domain mimicking liver geometry

Most of the previous models have considered a one-dimensional domain in analyzing the infection dynamics of this virus. The primary concern with these models lies in the inadequacy in initial conditions due to the complex three-dimensional geometric nature of the liver. A two-dimensional representation of the human liver often appears triangle. Investigation of HBV infection within a two-dimensional triangular domain framework could represent a generalization of existing models in the context of spatial domains. Considering this triangular shape of the liver, model (2.2.1) can be modified as follows:

$$\begin{aligned}
\frac{\partial X(t)}{\partial t} &= \mathcal{D}_1\left(\frac{\partial^2 X(t)}{\partial x_1^2}+\frac{\partial^2 X(t)}{\partial x_2^2}\right)+\lambda(t)-\mu(t)X(t)-kX(t)V(t),\\
\frac{\partial Y(t)}{\partial t} &= \mathcal{D}_2\left(\frac{\partial^2 Y(t)}{\partial x_1^2}+\frac{\partial^2 Y(t)}{\partial x_2^2}\right)+k(t)V(t)X(t)-\delta(t)Y(t),\\
\frac{\partial U(t)}{\partial t} &= \mathcal{D}_3\left(\frac{\partial^2 U(t)}{\partial x_1^2}+\frac{\partial^2 U(t)}{\partial x_2^2}\right)+a(t)Y(t)+\gamma(t)(1-\eta(t))U(t)-\eta(t)\beta(t)U(t)-\delta(t)U(t),\\
\frac{\partial V(t)}{\partial t} &= \mathcal{D}_4\left(\frac{\partial^2 V(t)}{\partial x_1^2}+\frac{\partial^2 V(t)}{\partial x_2^2}\right)+\eta(t)\beta(t)U(t)-c(t)V(t).
\end{aligned} \tag{7.2.2}$$

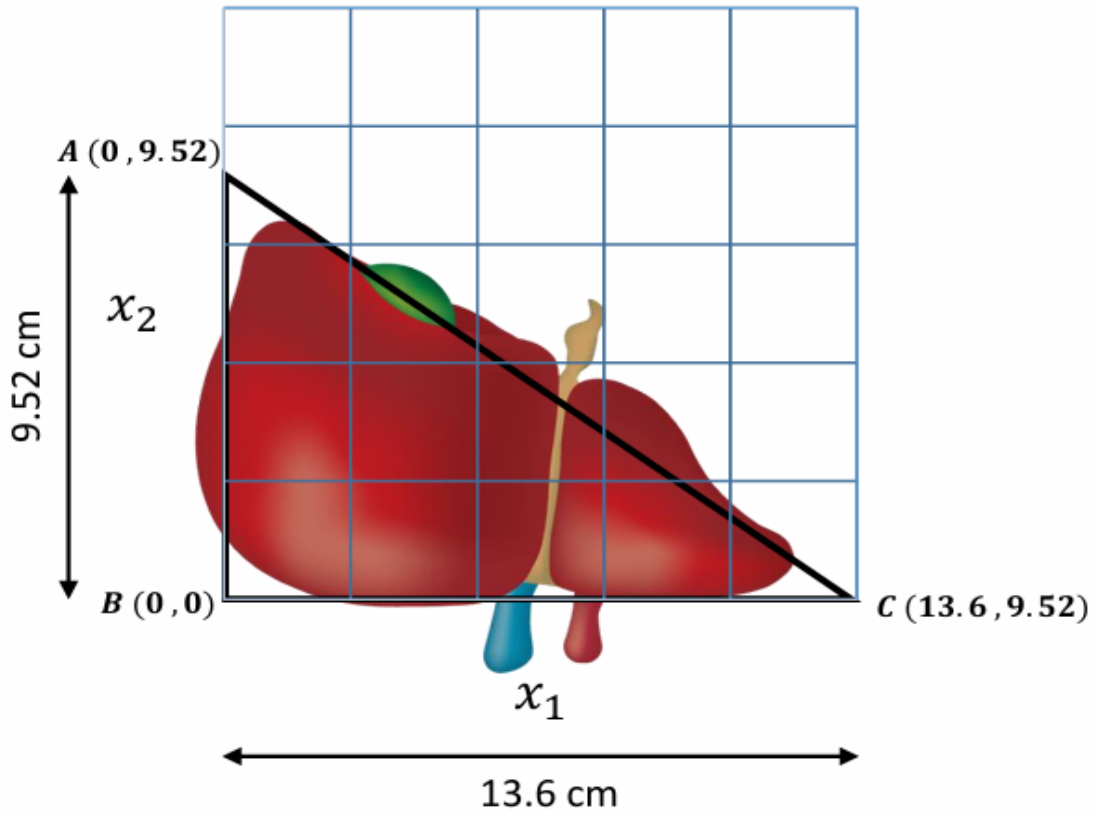

Figure 7.1: Geometrical two dimensional representation of the liver.

with initial conditions at (l_1, l_2) position

$$X(x_1,x_2,0) = X_0\left(1-\exp\left(-\frac{(x_1-l_1)^2+(x_2-l_2)^2}{\epsilon}\right)\right),\ 0\le x_1\le 13.6,\ 0\le x_2\le\left(9.52-\frac{9.52x_1}{13.6}\right),$$
$$Y(x_1,x_2,0) = Y_0\exp\left(-\frac{(x_1-l_1)^2+(x_2-l_2)^2}{\epsilon}\right),\ 0\le x_1\le 13.6,\ 0\le x_2\le\left(9.52-\frac{9.52x_1}{13.6}\right),$$
$$U(x_1,x_2,0) = U_0\exp\left(-\frac{(x_1-l_1)^2+(x_2-l_2)^2}{\epsilon}\right),\ 0\le x_1\le 13.6,\ 0\le x_2\le\left(9.52-\frac{9.52x_1}{13.6}\right),$$
$$V(x_1,x_2,0) = V_0\exp\left(-\frac{(x_1-l_1)^2+(x_2-l_2)^2}{\epsilon}\right),\ 0\le x_1\le 13.6,\ 0\le x_2\le\left(9.52-\frac{9.52x_1}{13.6}\right), \tag{7.2.3}$$

where we took $\epsilon = 0.01$, and boundary conditions are

$$\left.\frac{\partial X}{\partial x_i}\right|_{AB} = \left.\frac{\partial Y}{\partial x_i}\right|_{AB} = \left.\frac{\partial U}{\partial x_i}\right|_{AB} = \left.\frac{\partial V}{\partial x_i}\right|_{AB} = 0, \quad t\ge 0, \quad i = 1,2, \tag{7.2.4}$$

$$\left.\frac{\partial X}{\partial x_i}\right|_{BC} = \left.\frac{\partial Y}{\partial x_i}\right|_{BC} = \left.\frac{\partial U}{\partial x_i}\right|_{BC} = \left.\frac{\partial V}{\partial x_i}\right|_{BC} = 0, \quad t \geq 0, \quad i = 1, 2, \tag{7.2.5}$$

and

$$\left.\frac{\partial X}{\partial x_i}\right|_{CA} = \left.\frac{\partial Y}{\partial x_i}\right|_{CA} = \left.\frac{\partial U}{\partial x_i}\right|_{CA} = \left.\frac{\partial V}{\partial x_i}\right|_{CA} = 0, \quad t \geq 0, \quad i = 1, 2. \tag{7.2.6}$$

We have planned to study the infection dynamics using the model (7.2.2) in the following two ways:

- Case-1: Consider all parameters as constant
- Case-2: Consider all parameters to be time-varying

Bibliography

[1] Hepatitis B, https://www.who.int/news-room/fact-sheets/detail/hepatitis-b, 9 April 2024.

[2] S. A. Whalley, J. M. Murray, D. Brown, G. J. Webster, V. C. Emery, G. M. Dusheiko, A. S. Perelson, Kinetics of acute hepatitis B virus infection in humans, The Journal of Experimental Medicine 193 (7) (2001) 847–854.

[3] S. M. Ciupe, R. M. Ribeiro, P. W. Nelson, G. Dusheiko, A. S. Perelson, The role of cells refractory to productive infection in acute hepatitis B viral dynamics, Proceedings of the National Academy of Sciences 104 (12) (2007) 5050–5055.

[4] R. M. Ribeiro, A. Lo, A. S. Perelson, Dynamics of hepatitis B virus infection, Microbes and Infection 4 (8) (2002) 829–835.

[5] I. Gentile, G. Borgia, Vertical transmission of hepatitis B virus: challenges and solutions, International Journal of Women's Health 6 (2014) 605–611.

[6] H. C. Huang, C. C. Chen, W. C. Chang, M. H. Tao, C. Huang, Entry of hepatitis B virus into immortalized human primary hepatocytes by clathrin-dependent endocytosis, Journal of Virology 86 (17) (2012) 9443–9453.

[7] H. Yan, G. Zhong, G. Xu, W. He, Z. Jing, Z. Gao, Y. Huang, Y. Qi, B. Peng, H. Wang, et al., Sodium taurocholate cotransporting polypeptide is a functional receptor for human hepatitis B and d virus, eLife 1 (2012) e00049.

[8] B. Rabe, D. Glebe, M. Kann, Lipid-mediated introduction of hepatitis B virus capsids into nonsusceptible cells allows highly efficient replication and facilitates the study of early infection events, Journal of Virology 80 (11) (2006) 5465–5473.

[9] S. Lewin, T. Walters, S. Locarnini, Hepatitis B treatment: rational combination chemotherapy based on viral kinetic and animal model studies, Antiviral Research 55 (3) (2002) 381–396.

[10] H. Guo, D. Jiang, T. Zhou, A. Cuconati, T. M. Block, J. T. Guo, Characterization of the intracellular deproteinized relaxed circular DNA of hepatitis B virus: an intermediate of covalently closed circular DNA formation, Journal of Virology 81 (22) (2007) 12472–12484.

[11] F. Fatehi, R. J. Bingham, E. C. Dykeman, N. Patel, P. G. Stockley, R. Twarock, An intracellular model of hepatitis B viral infection: An in silico platform for comparing therapeutic strategies, Viruses 13 (1) (2021) 11.

[12] C. Saraceni, J. Birk, A review of hepatitis B virus and hepatitis C virus immunopathogenesis, Journal of Clinical and Translational Hepatology 9 (3) (2021) 409–418.

[13] G. M. Prifti, D. Moianos, E. Giannakopoulou, V. Pardali, J. E. Tavis, G. Zoidis, Recent advances in hepatitis B treatment, Pharmaceuticals 14 (5) (2021) 417.

[14] C. A. Philips, R. Ahamed, J. K. Abduljaleel, S. Rajesh, P. Augustine, Critical updates on chronic hepatitis B virus infection in 2021, Cureus 13 (10) (2021) e19152.

[15] L. L. Stein, R. Loomba, Drug targets in hepatitis B virus infection, Infectious Disorders-Drug Targets 9 (2) (2009) 105–116.

[16] N. Paul, S. H. Han, Combination therapy for chronic hepatitis B: current indications, Current Hepatitis Reports 10 (2011) 98–105.

[17] C. K. Hui, H. Y. Zhang, S. Bowden, S. Locarnini, J. M. Luk, K. W. Leung, Y. H. Yueng, A. Wong, F. Rousseau, K. Y. Yuen, et al., 96 weeks combination of adefovir dipivoxil plus emtricitabine vs. adefovir dipivoxil monotherapy in the treatment of chronic hepatitis B, Journal of Hepatology 48 (5) (2008) 714–720.

[18] R. Siqueira de Mello, V. Fernandes Arnaud-Sampaio, L. Ferreira Maciel, V. de Sá, T. Glaser, H. Ulrich, C. Lameu, Complex diseases demand novel treatment strategies: understanding drug combination, Drug Combination Therapy 4 (2) (2022) 6.

[19] C. Panda, Telbivudine plus tenofovir in combination therapy in patients with chronic hepatitis B infection–an indian experience., The Journal of the Association of Physicians of India 61 (11) (2013) 785–788.

[20] J. M. Ntaganda, Effects of combination of therapies on chronic hepatitis B virus through resolution of an optimal control problem using comparative of direct method and Pontryagin's maximum principle, International Journal of Computing Science and Mathematics 13 (3) (2021) 301–310.

[21] H. Dahari, E. Shudo, R. M. Ribeiro, A. S. Perelson, Modeling complex decay profiles of hepatitis B virus during antiviral therapy, Hepatology 49 (1) (2009) 32–38.

[22] M. A. Nowak, S. Bonhoeffer, A. M. Hill, R. Boehme, H. C. Thomas, H. McDade, Viral dynamics in hepatitis B virus infection, Proceedings of the National Academy of Sciences 93 (9) (1996) 4398–4402.

[23] D. Wodarz, Hepatitis C virus dynamics and pathology: the role of CTL and antibody responses, Journal of General Virology 84 (7) (2003) 1743–1750.

[24] L. Min, Y. Su, Y. Kuang, Mathematical analysis of a basic virus infection model with application to HBV infection, The Rocky Mountain Journal of Mathematics 38 (5) (2008) 1573–1585.

[25] S. A. Gourley, Y. Kuang, J. D. Nagy, Dynamics of a delay differential equation model of hepatitis B virus infection, Journal of Biological Dynamics 2 (2) (2008) 140–153.

[26] S. Hews, S. Eikenberry, J. D. Nagy, Y. Kuang, Rich dynamics of a hepatitis B viral infection model with logistic hepatocyte growth, Journal of Mathematical Biology 60 (4) (2010) 573–590.

[27] S. Eikenberry, S. Hews, J. D. Nagy, Y. Kuang, The dynamics of a delay model of HBV infection with logistic hepatocyte growth, Mathematical Biosciences and Engineering 6 (2009) 1–17.

[28] G. Huang, W. Ma, Y. Takeuchi, Global properties for virus dynamics model with Beddington–DeAngelis functional response, Applied Mathematics Letters 22 (11) (2009) 1690–1693.

[29] X. Wang, Y. Tao, X. Song, Global stability of a virus dynamics model with Beddington–DeAngelis incidence rate and CTL immune response, Nonlinear Dynamics 66 (2011) 825–830.

[30] Y. Ji, L. Min, Y. Zheng, Y. Su, A viral infection model with periodic immune response and nonlinear CTL response, Mathematics and Computers in Simulation 80 (12) (2010) 2309–2316.

[31] K. Wang, A. Fan, A. Torres, Global properties of an improved hepatitis B virus model, Nonlinear Analysis: Real World Applications 11 (4) (2010) 3131–3138.

[32] F. F. Chenar, Y. Kyrychko, K. Blyuss, Mathematical model of immune response to hepatitis B, Journal of Theoretical Biology 447 (2018) 98–110.

[33] J. M. Murray, R. H. Purcell, S. F. Wieland, The half-life of hepatitis B virions, Hepatology 44 (5) (2006) 1117–1121.

[34] K. Manna, S. P. Chakrabarty, Chronic hepatitis B infection and HBV DNA-containing capsids: Modeling and analysis, Communications in Nonlinear Science and Numerical Simulation 22 (1-3) (2015) 383–395.

[35] J. Danane, A. Meskaf, K. Allali, Optimal control of a delayed hepatitis B viral infection model with HBV DNA-containing capsids and CTL immune response, Optimal Control Applications and Methods 39 (3) (2018) 1262–1272.

[36] T. Guo, H. Liu, C. Xu, F. Yan, Global stability of a diffusive and delayed HBV infection model with HBV DNA-containing capsids and general incidence rate, Discrete & Continuous Dynamical Systems-B 23 (10) (2018) 4223–4242.

[37] S. Liu, R. Zhang, On an age-structured hepatitis B virus infection model with HBV DNA-containing capsids, Bulletin of the Malaysian Mathematical Sciences Society 44 (3) (2021) 1345–1370.

[38] B. Song, Y. Zhang, Y. Sang, L. Zhang, Stability and hopf bifurcation on an immunity delayed HBV/HCV model with intra-and extra-hepatic coinfection and saturation incidence, Nonlinear Dynamics 111 (15) (2023) 14485–14511.

[39] P. Damania, B. Sen, S. B. Dar, S. Kumar, A. Kumari, E. Gupta, S. K. Sarin, S. K. Venugopal, Hepatitis B virus induces cell proliferation via HBx-induced microRNA-21 in hepatocellular carcinoma by targeting programmed cell death protein4 (PDCD4) and phosphatase and tensin homologue (PTEN), PLOS ONE 9 (3) (2014) e91745.

[40] B. K. Wu, C. C. Li, H. J. Chen, J. L. Chang, K. S. Jeng, C. K. Chou, M. T. Hsu, T. F. Tsai, Blocking of G1/S transition and cell death in the regenerating liver of hepatitis B virus X protein transgenic mice, Biochemical and Biophysical Research Communications 340 (3) (2006) 916–928.

[41] Z. Dong, J. Zhang, R. Sun, H. Wei, Z. Tian, Impairment of liver regeneration correlates with activated hepatic nkt cells in HBV transgenic mice, Hepatology 45 (6) (2007) 1400–1412.

[42] S. Hews, S. Eikenberry, J. D. Nagy, T. Phan, Y. Kuang, Global dynamics and implications of an HBV model with proliferating infected hepatocytes, Applied Sciences 11 (17) (2021) 8176.

[43] A. Carracedo Rodriguez, M. Chung, S. M. Ciupe, Understanding the complex patterns observed during hepatitis B virus therapy, Viruses 9 (5) (2017) 117.

[44] T. C. Reluga, H. Dahari, A. S. Perelson, Analysis of hepatitis C virus infection models with hepatocyte homeostasis, SIAM Journal on Applied Mathematics 69 (4) (2009) 999–1023.

[45] C. Seeger, W. S. Mason, HBV replication, pathobiology and therapy: Unanswered questions (2016).

[46] L. Allweiss, T. Volz, K. Giersch, J. Kah, G. Raffa, J. Petersen, A. W. Lohse, C. Beninati, T. Pollicino, S. Urban, et al., Proliferation of primary human hepatocytes and prevention of hepatitis B virus reinfection efficiently deplete nuclear cccDNA in vivo, Gut 67 (3) (2018) 542–552.

[47] M. Lutgehetmann, T. Volz, A. Köpke, T. Broja, E. Tigges, A. W. Lohse, E. Fuchs, J. M. Murray, J. Petersen, M. Dandri, In vivo proliferation of hepadnavirus-infected hepatocytes induces loss of covalently closed circular DNA in mice, Hepatology 52 (1) (2010) 16–24.

[48] A. Goyal, R. M. Ribeiro, A. S. Perelson, The role of infected cell proliferation in the clearance of acute HBV infection in humans, Viruses 9 (11) (2017) 350.

[49] T. Tu, B. Zehnder, J. M. Wettengel, H. Zhang, S. Coulter, V. Ho, M. W. Douglas, U. Protzer, J. George, S. Urban, Mitosis of hepatitis B virus-infected cells in vitro results in uninfected daughter cells, JHEP Reports 4 (9) (2022) 100514.

[50] J. M. Murray, A. Goyal, In silico single cell dynamics of hepatitis B virus infection and clearance, Journal of Theoretical Biology 366 (2015) 91–102.

[51] J. Nakabayashi, The intracellular dynamics of hepatitis B virus (HBV) replication with reproduced virion "re-cycling", Journal of Theoretical Biology 396 (2016) 154–162.

[52] S. M. Ciupe, N. K. Vaidya, J. E. Forde, Early events in hepatitis B infection: the role of inoculum dose, Proceedings of the Royal Society B 288 (1944) (2021) 20202715.

[53] P. Gripon, I. Cannie, S. Urban, Efficient inhibition of hepatitis B virus infection by acylated peptides derived from the large viral surface protein, Journal of Virology 79 (3) (2005) 1613–1622.

[54] W. H. Gerlich, Medical virology of hepatitis B: how it began and where we are now, Virology Journal 10 (1) (2013) 1–25.

[55] L. Luckenbaugh, K. Kitrinos, W. Delaney IV, J. Hu, Genome-free hepatitis B virion levels in patient sera as a potential marker to monitor response to antiviral therapy, Journal of Viral Hepatitis 22 (6) (2015) 561–570.

[56] J. Hu, K. Liu, Complete and incomplete hepatitis B virus particles: formation, function, and application, Viruses 9 (3) (2017) 56.

[57] T. Garcia, J. Li, C. Sureau, K. Ito, Y. Qin, J. Wands, S. Tong, Drastic reduction in the production of subviral particles does not impair hepatitis B virus virion secretion, Journal of Virology 83 (21) (2009) 11152–11165.

[58] J. M. Murray, S. F. Wieland, R. H. Purcell, F. V. Chisari, Dynamics of hepatitis B virus clearance in chimpanzees, Proceedings of the National Academy of Sciences 102 (49) (2005) 17780–17785.

[59] H. Dahari, A. Lo, R. M. Ribeiro, A. S. Perelson, Modeling hepatitis C virus dynamics: Liver regeneration and critical drug efficacy, Journal of Theoretical Biology 247 (2) (2007) 371–381.

[60] K. Wang, W. Wang, Propagation of HBV with spatial dependence, Mathematical Biosciences 210 (1) (2007) 78–95.

[61] J. Nakabayashi, A. Sasaki, A mathematical model of the intracellular replication and within host evolution of hepatitis type B virus: Understanding the long time course of chronic hepatitis, Journal of Theoretical Biology 269 (1) (2011) 318–329.

[62] J. Danane, K. Allali, Mathematical analysis and treatment for a delayed hepatitis B viral infection model with the adaptive immune response and DNA-containing capsids, High-throughput 7 (4) (2018) 35.

[63] J. Cao, J. Zhang, Y. Lu, S. Luo, J. Zhang, P. Zhu, Cryo-em structure of native spherical subviral particles isolated from HBV carriers, Virus Research 259 (2019) 90–96.

[64] G. E. Rydell, K. Prakash, H. Norder, M. Lindh, Hepatitis B surface antigen on subviral particles reduces the neutralizing effect of anti-HBs antibodies on hepatitis B viral particles in vitro, Virology 509 (2017) 67–70.

[65] N. Chai, H. E. Chang, E. Nicolas, Z. Han, M. Jarnik, J. Taylor, Properties of subviral particles of hepatitis B virus, Journal of Virology 82 (16) (2008) 7812–7817.

[66] M. Bruns, S. Miska, S. Chassot, H. Will, Enhancement of hepatitis B virus infection by noninfectious subviral particles, Journal of Virology 72 (2) (1998) 1462–1468.

[67] U. Klingmüller, H. Schaller, Hepadnavirus infection requires interaction between the viral pre-S domain and a specific hepatocellular receptor, Journal of Virology 67 (12) (1993) 7414–7422.

[68] P. Wu, H. Zhao, Dynamical analysis of a nonlocal delayed and diffusive HIV latent infection model with spatial heterogeneity, Journal of the Franklin Institute 358 (10) (2021) 5552–5587.

[69] P. Wu, X. Wang, Z. Feng, Spatial and temporal dynamics of SARS-CoV-2: Modeling, analysis and simulation, Applied Mathematical Modelling 113 (2023) 220–240.

[70] H. Miao, M. Jiao, et al., Dynamics of a diffusive HBV infection model with capsids, two delays, and cell-to-cell transmissions, Discrete Dynamics in Nature and Society 2023 (1) (2023) 7738415.

[71] R. Xu, Z. Ma, An HBV model with diffusion and time delay, Journal of Theoretical Biology 257 (3) (2009) 499–509.

[72] K. Wang, W. Wang, S. Song, Dynamics of an HBV model with diffusion and delay, Journal of Theoretical Biology 253 (1) (2008) 36–44.

[73] A. Raj, S. A. Rifkin, E. Andersen, A. Van Oudenaarden, Variability in gene expression underlies incomplete penetrance, Nature 463 (7283) (2010) 913–918.

[74] A. A. Cohen, N. Geva-Zatorsky, E. Eden, M. Frenkel-Morgenstern, I. Issaeva, A. Sigal, R. Milo, C. Cohen-Saidon, Y. Liron, Z. Kam, et al., Dynamic proteomics of individual cancer cells in response to a drug, Science 322 (5907) (2008) 1511–1516.

[75] N. Navin, J. Kendall, J. Troge, P. Andrews, L. Rodgers, J. McIndoo, K. Cook, A. Stepansky, D. Levy, D. Esposito, et al., Tumour evolution inferred by single-cell sequencing, Nature 472 (7341) (2011) 90–94.

[76] M. Delbrück, The burst size distribution in the growth of bacterial viruses (bacteriophages), Journal of Bacteriology 50 (2) (1945) 131–135.

[77] M. L. Suvà, I. Tirosh, Single-cell RNA sequencing in cancer: lessons learned and emerging challenges, Molecular Cell 75 (1) (2019) 7–12.

[78] C. A. Tibbitt, J. M. Stark, L. Martens, J. Ma, J. E. Mold, K. Deswarte, G. Oliynyk, X. Feng, B. N. Lambrecht, P. De Bleser, et al., Single-cell RNA sequencing of the T helper cell response to house dust mites defines a distinct gene expression signature in airway Th2 cells, Immunity 51 (1) (2019) 169–184.

[79] Y. Zhou, Z. Liu, J. D. Welch, X. Gao, L. Wang, T. Garbutt, B. Keepers, H. Ma, J. F. Prins, W. Shen, et al., Single-cell transcriptomic analyses of cell fate transitions during human cardiac reprogramming, Cell Stem Cell 25 (1) (2019) 149–164.

[80] J. M. Heffernan, R. J. Smith, L. M. Wahl, Perspectives on the basic reproductive ratio, Journal of the Royal Society Interface 2 (4) (2005) 281–293.

[81] J.-J. E. Slotine, W. Li, et al., Applied nonlinear control, Vol. 199, Prentice hall Englewood Cliffs, NJ, 1991.

[82] L. Perko, Differential equations and dynamical systems, Vol. 7, Springer Science & Business Media, 2013.

[83] I. M. Sobol', On sensitivity estimation for nonlinear mathematical models, Matematicheskoe Modelirovanie 2 (1) (1990) 112–118.

[84] I. M. Sobol, Global sensitivity indices for nonlinear mathematical models and their monte carlo estimates, Mathematics and Computers in Simulation 55 (1-3) (2001) 271–280.

[85] S. Marino, I. B. Hogue, C. J. Ray, D. E. Kirschner, A methodology for performing global uncertainty and sensitivity analysis in systems biology, Journal of Theoretical Biology 254 (1) (2008) 178–196.

[86] G. J. McRae, J. W. Tilden, J. H. Seinfeld, Global sensitivity analysis—a computational implementation of the Fourier amplitude sensitivity test (FAST), Computers & Chemical Engineering 6 (1) (1982) 15–25.

[87] X. Miao, Hongyu Xia, A. S. Perelson, H. Wu, On identifiability of nonlinear ODE models and applications in viral dynamics, SIAM review 53 (1) (2011) 3–39.

[88] G. Bellu, M. P. Saccomani, S. Audoly, L. D'Angiò, DAISY: a new software tool to test global identifiability of biological and physiological systems, Computer Methods and Programs in Biomedicine 88 (1) (2007) 52–61.

[89] N. Meshkat, C. E. Z. Kuo, J. DiStefano III, On finding and using identifiable parameter combinations in nonlinear dynamic systems biology models and COMBOS: a novel web implementation, PLOS ONE 9 (10) (2014) e110261.

[90] R. Dong, C. Goodbrake, H. A. Harrington, G. Pogudin, Differential elimination for dynamical models via projections with applications to structural identifiability, SIAM Journal on Applied Algebra and Geometry 7 (1) (2023) 194–235.

[91] I. Podlubny, Fractional differential equations: an introduction to fractional derivatives, fractional differential equations, to methods of their solution and some of their applications, elsevier, 1998.

[92] A. Kilbas, Theory and applications of fractional differential equations, North-Holland Mathematics Studies 204 (2006).

[93] M. K. Beshtokov, To boundary-value problems for degenerating pseudoparabolic equations with Gerasimov–Caputo fractional derivative, Russian Mathematics 62 (10) (2018) 1–14.

[94] W. Lin, Global existence theory and chaos control of fractional differential equations, Journal of Mathematical Analysis and Applications 332 (1) (2007) 709–726.

[95] K. Diethelm, Monotonicity of functions and sign changes of their caputo derivatives, Fractional Calculus and Applied Analysis 19 (2) (2016) 561–566.

[96] B. K. Lenka, S. Banerjee, Sufficient conditions for asymptotic stability and stabilization of autonomous fractional order systems, Communications in Nonlinear Science and Numerical Simulation 56 (2018) 365–379.

[97] J. Diogo Dias, N. Sarica, C. Neuveut, Early steps of hepatitis B life cycle: From capsid nuclear import to cccDNA formation, Viruses 13 (5) (2021) 757.

[98] C. L. Thio, M. Taddese, Y. Saad, K. Zambo, R. M. Ribeiro, T. Grudda, M. S. Sulkowski, R. K. Sterling, Y. Zhang, E. D. Young, et al., Hepatitis B e antigen-negative single hepatocyte analysis shows transcriptional silencing and slow decay of infected cells with treatment, The Journal of Infectious Diseases 228 (9) (2023) 1219–1226.

[99] J. Summers, P. M. Smith, A. L. Horwich, Hepadnavirus envelope proteins regulate covalently closed circular DNA amplification, Journal of Virology 64 (6) (1990) 2819–2824.

[100] S. Asabe, S. F. Wieland, P. K. Chattopadhyay, M. Roederer, R. E. Engle, R. H. Purcell, F. V. Chisari, The size of the viral inoculum contributes to the outcome of hepatitis B virus infection, Journal of Virology 83 (19) (2009) 9652–9662.

[101] R. Bellman, K. J. Åström, On structural identifiability, Mathematical Biosciences 7 (3-4) (1970) 329–339.

[102] S. Vajda, K. R. Godfrey, H. Rabitz, Similarity transformation approach to identifiability analysis of nonlinear compartmental models, Mathematical Biosciences 93 (2) (1989) 217–248.

[103] L. Denis-Vidal, G. Joly-Blanchard, An easy to check criterion for (un) indentifiability of uncontrolled systems and its applications, IEEE Transactions on Automatic Control 45 (4) (2000) 768–771.

[104] X. Xia, C. H. Moog, Identifiability of nonlinear systems with application to HIV/AIDS models, IEEE Transactions on Automatic Control 48 (2) (2003) 330–336.

[105] C. Ko, A. Chakraborty, W. M. Chou, J. Hasreiter, J. M. Wettengel, D. Stadler, R. Bester, T. Asen, K. Zhang, K. Wisskirchen, et al., Hepatitis B virus genome recycling and de novo secondary infection events maintain stable cccDNA levels, Journal of Hepatology 69 (6) (2018) 1231–1241.

[106] X. Chen, L. Min, Y. Zheng, Y. Kuang, Y. Ye, Dynamics of acute hepatitis B virus infection in chimpanzees, Mathematics and Computers in Simulation 96 (2014) 157–170.

[107] Sontag, For differential equations with r parameters, $2r + 1$ experiments are enough for identification, Journal of Nonlinear Science 12 (2003) 553–583.

[108] Hepatitis B, https://www.hepb.org/what-is-hepatitis-b/what-is-hepb/facts-and-figures, 2024.

[109] T. Tu, J. M. Block, S. Wang, C. Cohen, M. W. Douglas, The lived experience of chronic hepatitis B: a broader view of its impacts and why we need a cure, Viruses 12 (5) (2020) 515.

[110] O. Diekmann, J. A. P. Heesterbeek, J. A. Metz, On the definition and the computation of the basic reproduction ratio R_0 in models for infectious diseases in heterogeneous populations, Journal of Mathematical Biology 28 (4) (1990) 365–382.

[111] P. Van den Driessche, J. Watmough, Reproduction numbers and sub-threshold endemic equilibria for compartmental models of disease transmission, Mathematical Biosciences 180 (1-2) (2002) 29–48.

[112] M. Martcheva, An Introduction to Mathematical Epidemiology, Vol. 61, Springer, 2015.

[113] T. Kajiwara, T. Sasaki, Y. Takeuchi, Construction of Lyapunov functionals for delay differential equations in virology and epidemiology, Nonlinear Analysis: Real World Applications 13 (4) (2012) 1802–1826.

[114] J. Nakabayashi, The intracellular dynamics of hepatitis B virus (HBV) replication with reproduced virion "re-cycling", Journal of Theoretical Biology 396 (2016) 154–162.

[115] O. Sakaguchi, Assessing hepatitis B viral kinetics using an inducible nuclear pore blockade (2023).

[116] S. Marino, I. B. Hogue, C. J. Ray, D. E. Kirschner, A methodology for performing global uncertainty and sensitivity analysis in systems biology, Journal of Theoretical Biology 254 (1) (2008) 178–196.

[117] R. J. B. McKay, M. D., W. J. Conover., A comparison of three methods for selecting values of input variables in the analysis of output from a computer code, Technometrics 21 (2) (1979) 239–245.

[118] N. Gul, R. Bilal, E. A. Algehyne, M. G. Alshehri, M. A. Khan, Y. M. Chu, S. Islam, The dynamics of fractional order hepatitis B virus model with asymptomatic carriers, Alexandria Engineering Journal 60 (4) (2021) 3945–3955.

[119] M. Lucas, U. Karrer, A. Lucas, P. Klenerman, Viral escape mechanisms–escapology taught by viruses, International Journal of Experimental Pathology 82 (5) (2001) 269–286.

[120] N. Attia, A. Akgül, D. Seba, A. Nour, Reproducing kernel hilbert space method for the numerical solutions of fractional cancer tumor models, Mathematical Methods in the Applied Sciences 46 (7) (2023) 7632–7653.

[121] H. Khan, Y. Li, A. Khan, A. Khan, Existence of solution for a fractional-order Lotka-Volterra reaction-diffusion model with Mittag-Leffler kernel, Mathematical Methods in the Applied Sciences 42 (9) (2019) 3377–3387.

[122] J. K. Popović, M. T. Atanacković, A. S. Pilipović, M. R. Rapaić, S. Pilipović, T. M. Atanacković, A new approach to the compartmental analysis in pharmacokinetics: fractional time evolution of diclofenac, Journal of Pharmacokinetics and Pharmacodynamics 37 (2010) 119–134.

[123] L. Cardoso, F. Dos Santos, R. Camargo, Analysis of fractional-order models for hepatitis B, Computational and Applied Mathematics 37 (4) (2018) 4570–4586.

[124] W. Pan, T. Li, S. Ali, A fractional order epidemic model for the simulation of outbreaks of Ebola, Advances in Difference Equations 2021 (2021) 1–21.

[125] S. Wieland, Hepatitis B virus pathogenesis, in: 13th International Symposium on Viral Hepatitis and Liver Disease, Washington, DC, 2009.

[126] P. A. Naik, J. Zu, K. M. Owolabi, Global dynamics of a fractional order model for the transmission of HIV epidemic with optimal control, Chaos, Solitons & Fractals 138 (2020) 109826.

[127] J. Danane, K. Allali, Z. Hammouch, Mathematical analysis of a fractional differential model of HBV infection with antibody immune response, Chaos, Solitons & Fractals 136 (2020) 109787.

[128] S. Simelane, P. Dlamini, A fractional order differential equation model for hepatitis B virus with saturated incidence, Results in Physics 24 (2021) 104114.

[129] K. Diethelm, S. Siegmund, H. Tuan, Asymptotic behavior of solutions of linear multi-order fractional differential systems, Fractional Calculus and Applied Analysis 20 (5) (2017) 1165–1195.

[130] R. Garrappa, Numerical solution of fractional differential equations: A survey and a software tutorial, Mathematics 6 (2) (2018) 16.

[131] S. M. Ciupe, R. M. Ribeiro, P. W. Nelson, A. S. Perelson, Modeling the mechanisms of acute hepatitis B virus infection, Journal of Theoretical Biology 247 (1) (2007) 23–35.

[132] B.-K. Wu, C.-C. Li, H.-J. Chen, J.-L. Chang, K.-S. Jeng, C.-K. Chou, M.-T. Hsu, T.-F. Tsai, Blocking of g1/s transition and cell death in the regenerating liver of hepatitis B virus X protein transgenic mice, Biochemical and Biophysical Research Communications 340 (3) (2006) 916–928.

[133] A. J. Hodgson, V. V. Keasler, B. L. Slagle, Premature cell cycle entry induced by hepatitis B virus regulatory hbx protein during compensatory liver regeneration, Cancer Research 68 (24) (2008) 10341–10348.

[134] W. Seo, W. I. Jeong, Hepatic non-parenchymal cells: Master regulators of alcoholic liver disease?, World Journal of Gastroenterology 22 (4) (2016) 1348.

[135] Z. Kmiec, Cooperation of liver cells in health and disease: with 18 tables (2001).

[136] E. Kuntz, H. D. Kuntz, Systemic diseases and the liver, Hepatology Textbook and Atlas: History· Morphology Biochemistry· Diagnostics Clinic· Therapy (2008) 837–850.

[137] S. Sherlock, J. Dooley, Chapter 3: Biopsy of the liver, Sherlock S, Dooley J. Diseases of the liver and biliary system. 11th ed. Oxford, UK: Blackwell Science Ltd (2002) 37–44.

[138] H. Dahari, J. E. Layden-Almer, E. Kallwitz, R. M. Ribeiro, S. J. Cotler, T. J. Layden, A. S. Perelson, A mathematical model of hepatitis C virus dynamics in patients with high baseline viral loads or advanced liver disease, Gastroenterology 136 (4) (2009) 1402–1409.

[139] O. Ogoke, J. Oluwole, N. Parashurama, Bioengineering considerations in liver regenerative medicine, Journal of Biological Engineering 11 (2017) 1–16.

[140] E. T. Lofgren, Visualizing results from infection transmission models: A case against "confidence intervals", Epidemiology 23 (5) (2012) 738–741.

[141] S. Gruttadauria, V. Parikh, D. Pagano, F. Tuzzolino, D. Cintorino, R. Miraglia, M. Spada, G. Vizzini, A. Luca, B. Gridelli, Early regeneration of the remnant liver volume after right hepatectomy for living donation: a multiple regression analysis, Liver Transplantation 18 (8) (2012) 907–913.

[142] A. Guglielmi, A. Ruzzenente, S. Conci, A. Valdegamberi, C. Iacono, How much remnant is enough in liver resection?, Digestive Surgery 29 (1) (2012) 6–17.

[143] Y. Kishi, E. K. Abdalla, Y. S. Chun, D. Zorzi, D. C. Madoff, M. J. Wallace, S. A. Curley, J. N. Vauthey, Three hundred and one consecutive extended right hepatectomies: evaluation of outcome based on systematic liver volumetry, Annals of Surgery 250 (4) (2009) 540–548.

[144] M. Oketani, H. Uto, A. Ido, H. Tsubouchi, Management of hepatitis B virus-related acute liver failure, Clinical Journal of Gastroenterology 7 (2014) 19–26.

[145] P. Garg, K. Madan, Acute-on-chronic liver failure due to hepatitis B, Frontiers in Gastroenterology 2 (2023) 1016915.

[146] Y. Miyaoka, A. Miyajima, To divide or not to divide: revisiting liver regeneration, Cell Division 8 (2013) 1–12.

[147] R. Prange, Host factors involved in hepatitis B virus maturation, assembly, and egress, Medical Microbiology and Immunology 201 (4) (2012) 449–461.

[148] S. M. Ciupe, R. M. Ribeiro, A. S. Perelson, Antibody responses during hepatitis B viral infection, PLOS Computational Biology 10 (7) (2014) e1003730.

[149] F. F. Chenar, Y. Kyrychko, K. Blyuss, Mathematical model of immune response to hepatitis B, Journal of Theoretical Biology 447 (2018) 98–110.

[150] K. S. Huang, Y. C. Shyu, C. L. Lin, F. B. Wang, Mathematical analysis of an HBV model with antibody and spatial heterogeneity, Mathematical Biosciences and Engineering 17 (2) (2019) 1820–1837.

[151] M. A. Chaplain, G. Lolas, Mathematical modelling of cancer invasion of tissue: dynamic heterogeneity., Networks Heterog. Media 1 (3) (2006) 399–439.

[152] K. Islam, Role of ultrasonography to detect liver size, Ultrasound in Medicine and Biology 45 (2019) S96. doi:10.1016/j.ultrasmedbio.2019.07.320.

[153] A. Meskaf, K. Allali, Y. Tabit, Optimal control of a delayed hepatitis B viral infection model with cytotoxic T-lymphocyte and antibody responses, International Journal of Dynamics and Control 5 (2017) 893–902.

[154] A. Vaillant, HBsAg, subviral particles, and their clearance in establishing a functional cure of chronic hepatitis B virus infection, ACS Infectious Diseases 7 (6) (2020) 1351–1368.

[155] A. Vaillant, Transaminase elevations during treatment of chronic hepatitis B infection: Safety considerations and role in achieving functional cure, Viruses 13 (5) (2021) 745.

[156] A. Goyal, Modeling reveals no direct role of the extent of HBV DNA integrations on the outcome of infection, Journal of Theoretical Biology 526 (2021) 110793.

[157] Q. Li, F. Lu, G. Deng, K. Wang, Modeling the effects of covalently closed circular DNA and dendritic cells in chronic HBV infection, Journal of Theoretical Biology 357 (2014) 1–9.

[158] L. Brandt, S. Cristinelli, A. Ciuffi, Single-cell analysis reveals heterogeneity of virus infection, pathogenicity, and host responses: HIV as a pioneering example, Annual Review of Virology 7 (1) (2020) 333–350.

[159] S. M. Ciupe, J. M. Conway, Incorporating intracellular processes in virus dynamics models, Microorganisms 12 (5) (2024) 900.

[160] J. Guedj, H. Dahari, L. Rong, N. D. Sansone, R. E. Nettles, S. J. Cotler, T. J. Layden, S. L. Uprichard, A. S. Perelson, Modeling shows that the NS5A inhibitor daclatasvir has two modes of action and yields a shorter estimate of the hepatitis C virus half-life, Proceedings of the National Academy of Sciences 110 (10) (2013) 3991–3996.

[161] L. Rong, A. S. Perelson, Mathematical analysis of multiscale models for hepatitis C virus dynamics under therapy with direct-acting antiviral agents, Mathematical Biosciences 245 (1) (2013) 22–30.

[162] E. F. Cardozo, D. Ji, G. Lau, R. F. Schinazi, G. F. Chen, R. M. Ribeiro, A. S. Perelson, Disentangling the lifespans of hepatitis C virus-infected cells and intracellular vRNA replication-complexes during direct-acting anti-viral therapy, Journal of Viral Hepatitis 27 (3) (2020) 261–269.

[163] F. S. Heldt, S. Y. Kupke, S. Dorl, U. Reichl, T. Frensing, Single-cell analysis and stochastic modelling unveil large cell-to-cell variability in influenza A virus infection, Nature Communications 6 (1) (2015) 1–12.

[164] X. Xin, H. Wang, L. Han, M. Wang, H. Fang, Y. Hao, J. Li, H. Zhang, C. Zheng, C. Shen, Single-cell analysis of the impact of host cell heterogeneity on infection with foot-and-mouth disease virus, Journal of Virology 92 (9) (2018) e00179–18.

[165] M. B. Schulte, R. Andino, Single-cell analysis uncovers extensive biological noise in poliovirus replication, Journal of Virology 88 (11) (2014) 6205–6212.

[166] T. Tu, H. Zhang, S. Urban, Hepatitis B virus DNA integration: in vitro models for investigating viral pathogenesis and persistence, Viruses 13 (2) (2021) 180.

[167] A. L. Marchetti, H. Guo, New insights on molecular mechanism of hepatitis B virus covalently closed circular DNA formation, Cells 9 (11) (2020) 2430.

[168] L. Allweiss, M. Dandri, The role of cccDNA in HBV maintenance, Viruses 9 (6) (2017) 156.

[169] J. Lucifora, S. Arzberger, D. Durantel, L. Belloni, M. Strubin, M. Levrero, F. Zoulim, O. Hantz, U. Protzer, Hepatitis B virus X protein is essential to initiate and maintain virus replication after infection, Journal of Hepatology 55 (5) (2011) 996–1003.

[170] T. Tu, M. A. Budzinska, N. A. Shackel, S. Urban, HBV DNA integration: molecular mechanisms and clinical implications, Viruses 9 (4) (2017) 75.

[171] A. Schulze, P. Gripon, S. Urban, Hepatitis B virus infection initiates with a large surface protein–dependent binding to heparan sulfate proteoglycans, Hepatology 46 (6) (2007) 1759–1768.

[172] K. Döhner, C. H. Nagel, B. Sodeik, Viral stop-and-go along microtubules: taking a ride with dynein and kinesins, Trends in Microbiology 13 (7) (2005) 320–327.

[173] F. Zoulim, New insight on hepatitis B virus persistence from the study of intrahepatic viral cccDNA, Journal of Hepatology 42 (3) (2005) 302–308.

[174] A. Zhu, X. Liao, S. Li, H. Zhao, L. Chen, M. Xu, X. Duan, HBV cccDNA and its potential as a therapeutic target, Journal of Clinical and Translational Hepatology 7 (3) (2019) 258.

[175] B. Werle-Lapostolle, S. Bowden, S. Locarnini, K. Wursthorn, J. Petersen, G. Lau, C. Trepo, P. Marcellin, Z. Goodman, W. E. Delaney IV, et al., Persistence of cccDNA during the natural history of chronic hepatitis B and decline during adefovir dipivoxil therapy, Gastroenterology 126 (7) (2004) 1750–1758.

[176] K. A. Lythgoe, S. F. Lumley, L. Pellis, J. A. McKeating, P. C. Matthews, Estimating hepatitis B virus cccDNA persistence in chronic infection, Virus Evolution 7 (1) (2021) veaa063.

[177] M. Levrero, T. Pollicino, J. Petersen, L. Belloni, G. Raimondo, M. Dandri, Control of cccDNA function in hepatitis B virus infection, Journal of Hepatology 51 (3) (2009) 581–592.

[178] T. M. Block, H. Guo, J. T. Guo, Molecular virology of hepatitis B virus for clinicians, Clinics in Liver Disease 11 (4) (2007) 685–706.

[179] R. J. Lamontagne, S. Bagga, M. J. Bouchard, Hepatitis B virus molecular biology and pathogenesis, Hepatoma Research 2 (2016) 163.

[180] M. Nassal, HBV cccDNA: viral persistence reservoir and key obstacle for a cure of chronic hepatitis B, Gut 64 (12) (2015) 1972–1984.

[181] A. Decorsière, H. Mueller, P. C. Van Breugel, F. Abdul, L. Gerossier, R. K. Beran, C. M. Livingston, C. Niu, S. P. Fletcher, O. Hantz, et al., Hepatitis B virus X protein identifies the smc5/6 complex as a host restriction factor, Nature 531 (7594) (2016) 386–389.

[182] M. A. Feitelson, B. Bonamassa, A. Arzumanyan, The roles of hepatitis B virus-encoded x protein in virus replication and the pathogenesis of chronic liver disease, Expert Opinion on Therapeutic Targets 18 (3) (2014) 293–306.

[183] E. B. Lewellyn, D. D. Loeb, The arginine clusters of the carboxy-terminal domain of the core protein of hepatitis B virus make pleiotropic contributions to genome replication, Journal of Virology 85 (3) (2011) 1298–1309.

[184] J. Hu, K. Liu, Complete and incomplete hepatitis B virus particles: formation, function, and application, Viruses 9 (3) (2017) 56.

[185] N. Patel, S. J. White, R. F. Thompson, R. Bingham, E. U. Weiß, D. P. Maskell, A. Zlotnick, E. C. Dykeman, R. Tuma, R. Twarock, et al., HBV RNA pre-genome encodes specific motifs that mediate interactions with the viral core protein that promote nucleocapsid assembly, Nature Microbiology 2 (8) (2017) 1–10.

[186] R. Yang, Y. H. Ko, F. Li, R. K. Lokareddy, C. F. D. Hou, C. Kim, S. Klein, S. Antolínez, J. F. Marín, C. Pérez-Segura, et al., Structural basis for nuclear import of hepatitis B virus (HBV) nucleocapsid core, Science Advances 10 (2) (2024) eadi7606.

[187] J. Hu, C. Seeger, Hepadnavirus genome replication and persistence, Cold Spring Harbor Perspectives in Medicine 5 (7) (2015) a021386.

[188] J. Hu, Hepatitis B virus virology and replication, Hepatitis B Virus in Human Diseases (2016) 1–34.

[189] S. Datta, S. Chatterjee, V. Veer, R. Chakravarty, Molecular biology of the hepatitis B virus for clinicians, Journal of Clinical and Experimental Hepatology 2 (4) (2012) 353–365.

[190] S. Tsukuda, K. Watashi, Hepatitis B virus biology and life cycle, Antiviral Research 182 (2020) 104925.

[191] W. H. Gerlich, Medical virology of hepatitis B: how it began and where we are now, Virology Journal 10 (2013) 1–25.

[192] J. M. Short, S. Chen, A. M. Roseman, P. J. G. Butler, R. A. Crowther, Structure of hepatitis B surface antigen from subviral tubes determined by electron cryomicroscopy, Journal of Molecular Biology 390 (1) (2009) 135–141.

[193] C. Lambert, T. Doring, R. Prange, Hepatitis B virus maturation is sensitive to functional inhibition of ESCRT-III, Vps4, and γ2adaptin, Journal of Virology 81 (17) (2007) 9050–9060.

[194] K. Kitagawa, K. S. Kim, M. Iwamoto, S. Hayashi, H. Park, T. Nishiyama, N. Nakamura, Y. Fujita, S. Nakaoka, K. Aihara, A. Perelson, L. Allweiss, M. Dandri, K. Watashi, Y. Tanaka, S. Iwami, Multiscale modeling of HBV infection integrating intra- and intercellular viral propagation for analyzing extracellular viral markers, PLOS Computational Biology 20 (3) (2024) e1011238.

[195] R. M. M.A. Nowak, Viral Dynamics, Oxford university Press, Oxford, 2000.

[196] S. Locarnini, Molecular virology of hepatitis B virus, in: Seminars in liver disease, Vol. 24, Copyright© 2004 by Thieme Medical Publishers, Inc., 333 Seventh Avenue, 2004, pp. 3–10.

[197] D. Glebe, Recent advances in hepatitis B virus research: a german point of view, World Journal of Gastroenterology 13 (1) (2007) 8.

[198] C. Balsano, A. Alisi, Viral hepatitis B: established and emerging therapies, Current Medicinal Chemistry 15 (9) (2008) 930–939.

[199] J. Lucifora, U. Protzer, Attacking hepatitis B virus cccDNA–the holy grail to hepatitis B cure, Journal of Hepatology 64 (1) (2016) S41–S48.

[200] E. Sivasudhan, N. Blake, Z. Lu, J. Meng, R. Rong, Hepatitis B viral protein hbx and the molecular mechanisms modulating the hallmarks of hepatocellular carcinoma: a comprehensive review, Cells 11 (4) (2022) 741.

[201] Y. Hamadalnil, H. N. Altayb, In silico molecular study of hepatitis B virus X protein as a therapeutic target, Journal of Biomolecular Structure and Dynamics 42 (8) (2024) 4002–4015.

[202] P. W. Nelson, J. D. Murray, A. S. Perelson, A model of HIV-1 pathogenesis that includes an intracellular delay, Mathematical Biosciences 163 (2) (2000) 201–215.

[203] H. W. Lee, J. S. Lee, S. H. Ahn, Hepatitis B virus cure: targets and future therapies, International Journal of Molecular Sciences 22 (1) (2020) 213.

[204] M. Al-Mahtab, M. Bazinet, A. Vaillant, Safety and efficacy of nucleic acid polymers in monotherapy and combined with immunotherapy in treatment-naive bangladeshi patients with HBeAg+ chronic hepatitis B infection, PLOS ONE 11 (6) (2016) e0156667.

[205] M. Bazinet, V. Pântea, G. Placinta, I. Moscalu, V. Cebotarescu, L. Cojuhari, P. Jimbei, L. Iarovoi, V. Smesnoi, T. Musteata, et al., Safety and efficacy of 48 weeks REP 2139 or REP 2165, tenofovir disoproxil, and pegylated interferon alfa-2a in patients with chronic HBV infection naïve to nucleos(t)ide therapy, Gastroenterology 158 (8) (2020) 2180–2194.

[206] W. Leowattana, T. Leowattana, Chronic hepatitis B: New potential therapeutic drugs target, World Journal of Virology 11 (1) (2022) 57.

[207] G. L. Wong, E. Gane, A. S. Lok, How to achieve functional cure of HBV: Stopping NUCs, adding interferon or new drug development?, Journal of Hepatology 76 (6) (2022) 1249–1262.

[208] D. Stone, K. R. Long, M. A. Loprieno, H. S. D. S. Feelixge, E. J. Kenkel, R. M. Liley, S. Rapp, P. Roychoudhury, T. Nguyen, L. Stensland, et al., CRISPR-Cas9 gene editing of hepatitis B virus in chronically infected humanized mice, Molecular Therapy-Methods & Clinical Development 20 (2021) 258–275.

[209] N. D. Weber, D. Stone, R. H. Sedlak, H. S. De Silva Feelixge, P. Roychoudhury, J. T. Schiffer, M. Aubert, K. R. Jerome, AAV-mediated delivery of zinc finger nucleases targeting hepatitis B virus inhibits active replication, PLOS ONE 9 (5) (2014) e97579.

[210] M. F. Yuen, I. Schiefke, J. H. Yoon, S. H. Ahn, J. Heo, J. H. Kim, H. Lik Yuen Chan, K. T. Yoon, H. Klinker, M. Manns, et al., RNA interference therapy with ARC-520 results in prolonged hepatitis B surface antigen response in patients with chronic hepatitis B infection, Hepatology 72 (1) (2020) 19–31.

[211] K. Han, J. Cremer, R. Elston, S. Oliver, S. Baptiste-Brown, S. Chen, D. Gardiner, M. Davies, J. Saunders, R. Hamatake, et al., A randomized, double-blind, placebo-controlled, first-time-in-human study to assess the safety, tolerability, and pharmacokinetics of single and multiple ascending doses of GSK3389404 in healthy subjects, Clinical Pharmacology in Drug Development 8 (6) (2019) 790–801.

[212] S. Menne, S. Wildum, G. Steiner, M. Suresh, K. Korolowicz, M. Balarezo, C. Yon, M. Murreddu, X. Hong, B. V. Kallakury, et al., Efficacy of an inhibitor of hepatitis B virus expression in combination with entecavir and interferon-α in woodchucks chronically infected with woodchuck hepatitis virus, Hepatology Communications 4 (6) (2020) 916–931.

[213] M. F. Yuen, K. Agarwal, E. J. Gane, C. Schwabe, S. H. Ahn, D. J. Kim, Y. S. Lim, W. Cheng, W. Sievert, K. Visvanathan, et al., Safety, pharmacokinetics, and antiviral effects of ABI-H0731, a hepatitis B virus core inhibitor: a randomised, placebo-controlled phase 1 trial, The Lancet Gastroenterology and Hepatology 5 (2) (2020) 152–166.

Status of the works communicated/published:

- **Rupchand Sutradhar, Durga Charan Dalal**, Cytoplasmic Recycling of rcDNA-containing Capsids Enhances HBV Infection, *Nonlinear Dynamics*, 112 (14) (2024) 12641–12666, **(Published)**.
- **Rupchand Sutradhar, Durga Charan Dalal**, Fractional-order models of hepatitis B virus infection with recycling effects of capsids, *Mathematical Methods in the Applied Sciences*, 46 (14) (2023) 15599-15625, **(Published)**.
- **Rupchand Sutradhar, Durga Charan Dalal**, The Roles of Continuous and Discontinuous Proliferations on Hepatitis B Virus Infection, **(Under revision)**.
- **Rupchand Sutradhar, Gopinath Sadhu, Durga Charan Dalal**, Multi-point Infection Dynamics of Hepatitis B in the Presence of Sub-Viral Particles, **(Under preparation)**.
- **Rupchand Sutradhar, Durga Charan Dalal**, Exploration of Hepatitis B Virus Infection Dynamics through an Intracellular Model, **(Under revision)**.

Conferences & Workshops Attended:

- Third International Conference on Applications of Mathematics to Nonlinear Sciences (AMNS-2023), May 25-28, 2023, Pokhara, Nepal.
- Research and Industrial Conclave, May 2023, Students Academic Board, Indian Institute of Technology Guwahati, Guwahati, India.
- Five Day International Workshop on "Application of Mathematical Modeling in Engineering and Science", April 18-22, 2023, Department of Mathematics, SKIT, Jaipur, Rajasthan, India.
- Lecture Series on "Nonlinear Dynamics and Applications", February 13-16, 2023, Department of Mathematics, Indian Institute of Technology Indore, India.
- 3rd International Workshop on Numerical and Analytical Techniques in Engineering Problems (IWNATEP-2023), January 30-February 1, 2023, Department of Mathematics, SRMIST, Kuttankulathur, Tamilnadu, India.
- 2nd Lecture Series on Mathematical Modeling in Biology, October 15-16, 2022, Bangladesh Society for Mathematical Biology (BSMB).

- International FDP on Mathematical Modeling of Bio-systems with Special Focus on Epidemiology, August 21–27, 2022, Mizoram University, India.
- 38th Annual Conference of Ramanujan Mathematical Society, December 22-24, 2023, Department of Mathematics, Indian Institute of Technology Guwahati, India.
- 2nd International Conference on Nonlinear Dynamics and Applications, February 21-23, 2024, Department of Mathematics, Sikkim Manipal Institute of Technology, India.